The University Of Sheffield.

Functional Role of the Chemokine Receptor XCR1 and its Bioengineered Ligand in Oral Squamous Cell Carcinoma (OSCC)

By:
Amir Zaki Abdullah Zubir

A thesis submitted in partial fulfilment of the requirements for the degree of Doctor of Philosophy

The University of Sheffield
Faculty of Medicine, Dentistry and Health
Department of Oral & Maxillofacial Pathology
School of Clinical Dentistry

March 2018

DECLARATION

I declare that this thesis is an original report of my research and was composed by myself, that the work contained herein is my own except where explicitly stated otherwise in the text. Any reproduction or usage of the content or images from this thesis requires permission from the author. This thesis, in its entirety or in parts, has never been previously submitted at this University or any other institution.

TABLE OF CONTENTS

LIST OF FIGURES

LIST OF TABLES

LIST OF APPENDICES

LIST OF ABBREVIATIONS

×g	Gravitational force
α	Alpha
α-SMA	Alpha-smooth muscle actin
β	beta
µL	micro litre
AA	Amino acid
ABC	Avidin-biotin complex
Akt/PKB	Akt/Protein Kinase B
AM	Acetoxymethyl
ANOVA	Analysis of variance
ANOVA	Analysis of variance
APC	Antigen presenting cell
APS	Ammonium persulphate
ATAC	Activation-induced, T cell-derived, and Chemokine-related molecule
B. stearothermophilus	*Bacillus stearothermophilus*
B2M	β-2-microglobulin
bp	Base pairs
BSA	Bovine serum albumin
Ca^{2+}	Calcium ion
$CaCl_2$	Calcium chloride
CAF	Cancer-associated fibroblast
CBM	CARD11-BCL10-MALT1
cDNA	Complementary deoxyribonucleic acid
CLM	Cell loading media
CNBr	Cyanogen bromide
Conc.	Concentration
CV	Column volume
DC	Dendritic cell
DMSO	Dimethyl sulfoxide
DNA	Deoxyribonucleic acid
dNTP	Deoxynucleotide triphosphate
DsbA	Disulphide oxidoreductase
E. coli	*Escherichia coli*
ECM	Extracellular matrix
EDTA	Ethylenediaminetetraacetic acid
EMT	Epithelial-mesenchymal transition
EndoMT	Endothelial to mesenchymal transition
ERK	Extracellular signal-regulated kinases
FAK	Focal adhesion kinase
FAK	Focal adhesion kinase
FCS	Foetal calf serum
FDC	Follicular dendritic cells
FFPE	Formalin-fixed paraffin-embedded
FPLC	Fast protein liquid chromatography

FRC	Fibroblastic reticular cell
FSP-1	Fibroblast specific protein-1
GAG	Glycosaminoglycan
GPCR	G-protein coupled receptor
GST	Glutathione-S-transferase
H&E	Haematoxylin and eosin
H_2O	Water
H_2O_2	Hydrogen peroxide
HDX	Hydrogen-deuterium exchange
HEV	High endothelial venule
His-tag	Histidine-tag
hLtn	Human lymphotactin
HPLC	High performance liquid chromatography
HPV	Human papilloma virus
HRP	Horse radish peroxidase
IB	Inclusion body
IDA	Industrial denatured alcohol
IF	Immunofluorescence
IgG	Immunoglobulin G
IHC	Immunohistochemistry
IMAC	Immobilized metal affinity chromatography
IP_3	Inositol triphosphate
IPTG	Isopropyl β-D-thiogalactopyranosidase
kDa	Kilo Dalton
L	Litre
M	Molar
MALDI-MS	Matrix-assisted laser desorption/ionization mass spectrometer
MAPK	Mitogen-activated protein kinases
MBP	Maltose binding protein
MEM	Membrane desalting buffer
MET	Mesenchymal-epithelial transition
Mg^{2+}	Magnesium ion
min	Minute
mL	Millilitre
mM	Milli-molar
MMP	Matrix metalloproteinase
MRC	Marginal reticular cell
mRNA	Messenger ribonucleic acid
MSA	Multiple sequences alignment
MTS	3-(4,5-dimethylthiazol-2-yl) -5-(3-carboxymethoxyphenyl) -2-(4-sulfophenyl) -2H-tetrazolium, inner salt
MWCO	Molecular weight cut-off
NAF	Normal activated fibroblast
NF-κB	Nuclear factor kappa-light-chain-enhancer of activated B cells
ng	nano-gram
NK	Natural killer

nm	nano-metre
nM	nano-molar
NMR	Nuclear Magnetic Resonance
NOESY-NMR	Nuclear Overhauser Effect Spectroscopy-Nuclear Magnetic Resonance
NOF	Normal oral fibroblast
NusA	Nutilization substance A
^{o}C	degree Celsius
OCCL	Oral cancer cell line
OD	Optical density
OSCC	Oral squamous cell carcinoma
PBS	Phosphate buffered saline
PCR	Polymerase chain reaction
PDGF-R	Platelet derived growth factor receptor
pI	Isoelectric pH
PI	Propidium iodide
Pre-cDC	Precursor conventional dendritic cell
PTX	Pertussis toxin
qPCR	Qualitative polymerase chain reaction
RNA	Ribonucleic acid
ROI	Region of interest
RP-HPLC	Reverse phase high performance liquid chromatography
rpm	revolution per minute
RT	Reverse transcription
RT	Room temperature
SASP	Senescence-associated secretory phenotype
SA-βgal	Senescence-associated β-galactosidase
SCM-1	Single C-Motif-1
SD	Standard deviation
SDS	Sodium dodecyl sulphate
SDS-PAGE	Sodium dodecyl sulphate-polyacrylamide gel electrophoresis
SE-HPLC	Size exclusion high performance liquid chromatography
SEM	Standard error mean
SFM	Serum free media
SFK	Src Family Kinase
siRNA	Short interfering RNA
SS	Subcapsular sinus
SUMO	Small ubiquitin-related modifier
TEMED	Tetramethylethylenediamine
TEOM	Tissue-engineered oral mucosa
TEV	Tobacco-etch virus
TGF-β	Transforming growth factor-β
TOF	Time of flight
TPM	Transmembrane protein
TrxA	Thioredoxin
U6 snRNA	Small nuclear RNA

v/v	volume per volume
VEGF	Vascular endothelial growth factor
w/v	weight per volume
WT	Wild type

for amino acids abbreviation, refer to **Appendix 16**.

ACKNOWLEDGEMENT

Firstly, I am sincerely grateful and thankful to my supervisors, Dr, Syed Ali Khurram and my co-supervisor, Dr. Tuck Seng Wong and Dr. Simon Whawell for their support throughout my study years. Their guidance and word of wisdom in every aspect of the research project made my PhD experience endurable.

I was fortunate to be able to do an interdisciplinary project, in School of Clinical Dentistry and in Chemical & Biological Engineering department, providing me a unique experience for my Ph.D. Many thanks to those who provide me technical assistance, especially to Brenka and Jason. I would like to thank everyone within the iBio Science group who directly or indirectly help me during my 4 years of my study. Not to forget Ali's research group, enriching my experience as a PhD researcher; and to Tuck's PhD students, I cherished the time we exchange wisdom and make a part of your team. Special thanks to my dearest colleagues – Ben for the afternoon lunches, Priyanka for being a dear friend, and Saima a best quirky friend you can have. Long-standing friend, Areeg the invaluable friend in the department. I also would like to extend my utmost gratitude to the Malaysian students in the department: Zulfahmi, Zulaiha, and Amalina. You guys make me feels at home far from home.

I would like to thank Majlis Amanah Rakyat (MARA) for the financial assistance, giving me the opportunity to do this Ph.D.

And finally, to the loving memory of my parents, Saliam and Abdullah Zubir. Without your love and compassion, I will not be where I am today. I cherished our time together. I missed you both so much.

ABSTRACT

Introduction: XCR1 is a chemokine receptor that is activated by the chemokine lymphotactin (hLtn) and has been shown to play an important role in oral squamous cell carcinoma (OSCC) and a few other cancers. hLtn is a metamorphic protein which interconverts between two distinct protein conformations in physiological conditions, where one has the canonical chemokine fold while the other forms a dimer. Due to the complexity, the mechanism of action and precise role of each hLtn conformation in context of cancer is unknown.

Aim: Examine the role of XCR1 and its ligand hLtn in OSCC as well as understanding the function of different hLtn conformations in the disease.

Methods: Immunohistochemistry was performed on primary and metastatic OSCC tissue sections. Autocrine regulation of XCR1 by hLtn of oral cancer cell lines (OCCL) was investigated using qPCR and flow cytometry. Additionally, the role of tumour microenvironment on XCR1 expression was also investigated using an indirect co-culture of fibroblasts (inactive, stimulated, cancer-associated and senescent) with OCCL. Recombinant hLtn variants were designed, produced and purified. The activity of the variants was determined using intracellular calcium flux and functional assays including proliferation, adhesion (collagen I and IV, and fibronectin) and cell migration/chemotaxis assays to study the effect of bioengineered hLtn variants on OCCL.

Results: XCR1 and hLtn expression was seen in basal epithelial cells in normal oral mucosa *ex vivo* and both were upregulated in primary and metastatic carcinoma. Exposure of OCCL (H357 and SCC4) to hLtn *in vitro* cause a decrease in XCR1 expression. Conditioned media from cancer-associated fibroblasts but not myofibroblasts upregulated the expression of XCR1 and hLtn mRNA in OCCL. Interestingly, senescent fibroblasts downregulate the expression of XCR1 and hLtn in SCC4 cells. hLtn CC3 mutant, with the canonical chemokine fold was highly functional and facilitated proliferation and migration through XCR1. The W55D mutant dimer caused minimal cell proliferation suggesting possible receptor dimerization.

Conclusions: These findings confirm that XCR1 and hLtn are expressed in both primary and metastatic OSCC *ex vivo*. XCR1 expression regulation by its ligand hLtn and crosstalk with fibroblasts are novel findings suggesting a close association with tumour microenvironment. A novel method was used to produce and purify hLtn variants which stimulated OCCL proliferation, adhesion and migration. These discoveries confirm and build upon previous studies and suggest that the hLtn/XCR1 axis may have a bigger role in OSCC biology than originally envisaged.

CHAPTER 1

LITERATURE REVIEW

CHAPTER 1: LITERATURE REVIEW

1.1 Oral Cancer

Cancer usually involves mutation of normal cells because of DNA damage. In normal cells, mutation or damage to the DNA is detected and the cell programmed to undergo apoptosis or cell death. In case of cancer cells, the damage or mutations are irreversible leading to uncontrolled division and proliferation through alteration of normal survival signals.

Oral cancer accounted for 3% of all cancer cases in 2015 in the United Kingdom and 2% of cancer death in 2016 (Cancer Research UK, accessed 2018), an increase of 1% from 2012 data. It has a higher incidence in developing countries due to a wider range of risk factors (de Camargo Cancela *et al.*, 2010). Oral cancer has a poor prognosis as it usually diagnosed at a late stage (Warnakulasuriya, 2009). The incidence of oral and oropharyngeal cancer is highest in East Asia, South Asia and Southeast Asia (Warnakulasuriya, 2009).

The precise cause or pathogenesis of oral cancer is not completely understood. Several factors might increase the risk and are highly associated with the disease; including tobacco and alcohol consumption (McLaughlin *et al.*, 1988; Hashibe *et al.*, 2013), and human papillomavirus (HPV) (Chaturvedi *et al.*, 2011, 2013). Statistically, oral cancer incidence is higher in the elderly with more cases in the male population than female (information obtained from Cancer Research UK website). High dietary consumption of vegetables and fruits decreases the risk of oral cancer (Levi *et al.*, 1998; Llewellyn *et al.*, 2004). In addition, some studies show an increased risk in immunocompromised patients such as those undergoing haematopoietic stem-cell transplantation (Elad *et al.*, 2010). Poor oral hygiene (Oji and Chukwuneke, 2012) and a weakened immune system (Sathiyasekar *et al.*, 2016) also associated to contribute for oral cancer development.

Oral cavity and oropharyngeal cancers mainly occur in the tongue, tonsil, oropharynx and other sites such as vestibule, buccal mucosa (the lining of the lips and cheeks), hard palate, soft palate, gingiva (gums), lips and floor of the mouth. Most of these cancers are oral squamous cell carcinoma (OSCC) and are derived from epithelial cells in the lining of the mouth (**Figure 1.1**).

OSCC usually invades and destroys tissue in the immediate vicinity and spreads from the primary site, usually through the cervical lymph nodes following the path of

drainage (Silva *et al.*, 2011). Metastasis in lymph nodes is associated with an almost 50% reduction in 5-year survival (Vartanian *et al.*, 2004).

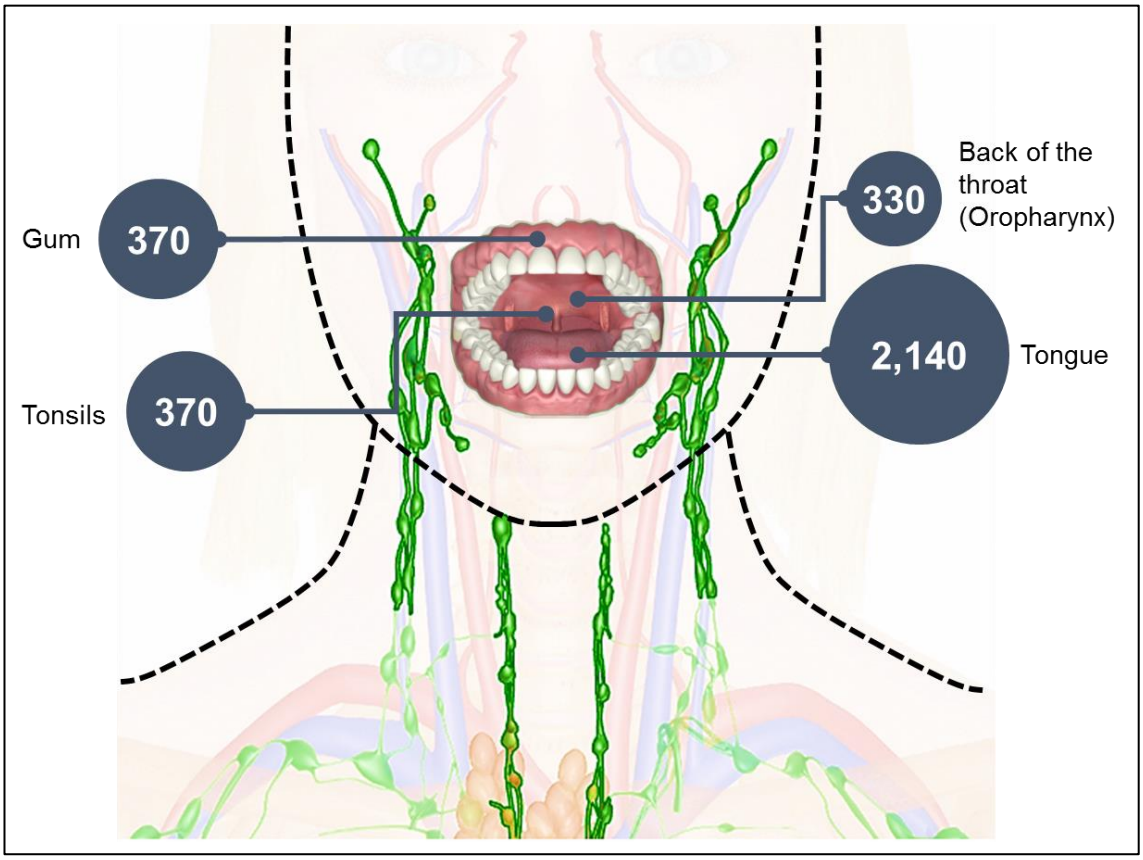

Figure 1.1: Prone sites for oral squamous cell carcinoma development. Most of the incidence originated from the tongue. Oral cancer spread is generally to the regional lymph nodes through lymphatic vessel. Almost a third of lymph nodes in human is situated in the head and neck region. The incidence rate (person per year) was obtained from Cancer Research UK website (Accessed in 2018). The image was acquired and modified from http://www.innerbody.com/image/mouth.html)).

1.2 Tumour Microenvironment

In recent years, tumour microenvironment research has become the focus to study how cancer cells grow and interact. Reactive stroma or the stroma of tumour microenvironment is fundamentally different from the normal tissue stroma. Studies of tumour progression have shown that cancer cells are not the only drives but also the tumour microenvironment through genetic and epigenetic studies (You and Jones, 2012; Baxter *et al.*, 2014). The complexity of tumour microenvironment comprises of a network of multiple cells, signalling molecules, extracellular matrix (ECM) and soluble factors which contributes as the driving force of tumour progression (Cukierman and Bassi, 2012). The multiple cells that make up the tumour microenvironment are inflammatory cells, endothelial cells, pericytes and fibroblasts (Joyce and Pollard, 2009). Cancer-associated fibroblasts (CAF) has been shown to promote tumour growth (De Veirman *et al.*, 2014; Shiga *et al.*, 2015; Deying *et al.*, 2017), progression (Shimoda, Mellody and Orimo, 2010; Bremnes *et al.*, 2011) and migration (Erdogan *et al.*, 2017) through paracrine signalling (van Zijl, Krupitza and Mikulits, 2011; Karagiannis *et al.*, 2012).

1.2.1 Tumour

Tumour formation is linked with uncontrollable growth of cells. In this context, the word tumour and cancer can sometimes be used interchangeably, while in definition, it is different. A tumour can be either benign or malignant. A benign tumour does not progress into a highly invasive tumour and invade other tissue from their initial site. Even so, uncontrollable tumour growth of cell can overcrowd the tissue area causing some health problems. The increase in size can increase its surrounding pressure resulting in applied pressure to neighbouring organ causing discomfort, pain and problem. This physical change in the cavity that are not enclosed by hard structure, such as bone, permit a flexible tumour expansion. Unfortunately, differ to tumour growth in the brain, continuous increase in size is not permitted due to cranial space restriction and the additional unnecessary pressure provided by tumour expansion can be quite fatal.

The progression of normal cell to cancer involves several pathological changes and processes. The first stage is dysplasia where cytological appearance is no longer normal, forming an abnormal tissue. These changes include the variable size and shape of the nucleus, increased staining of the nuclear, increase nuclear and cytoplasmic size ratio, increase cell mitotic activity, and lack of cytoplasmic features that are associated with normal differentiated cell of the tissue. In dysplasia, the relative number of various

type of cells seen in normal tissue are no longer observed. This stage is the transitional state between benign and to the premalignant tumour.

The pre-malignant tumour or carcinoma *in -situ* is the stage where the abnormal cells are only at the site at which it is first formed. This is the precursor of cancer before it spreads to nearby normal tissue. Once all the conditions are acquired, the abnormal cell develops to become cancerous and can become malignant or invasive. At this stage the cells have the potential to spread not only to adjacent tissue area but also other parts of the body using the circulatory system.

1.2.2 Reactive Stroma of the Tumour

Reactive stroma of the tumour consists of the immune cells, endothelial cells making up the capillaries, activated fibroblasts, basement membrane and extracellular matrix (ECM). Fibroblasts are the dominant component in the tumour stroma and studies have shown these to be a notable factor influencing cancer growth, progression and metastasis (Kalluri, 2016). Different terms are used for fibroblast association in a certain environment such as in cancer, it is termed cancer-associated fibroblasts (CAF) or 'activated' fibroblast.

1.2.2.1 Fibroblast

The fibroblast is the most versatile and extensively studied cell-type in biology *in vitro* due to its easy isolation and culture handling. They are resilient, survive stress and can grow from post-mortem human tissue. This gives fibroblast its plasticity. Resting or quiescent fibroblasts are defined as a non-epithelial, non-endothelial, non-immune cell with a mesenchymal-like cells lineage that are usually found in the interstitial stroma. It displays a spindle-shape morphology with noticeable actin cytoskeleton and vimentin filaments (Kalluri and Zeisberg, 2006).

The quiescent fibroblast can be 'activated' and become specialised fibroblast known as myofibroblast or normal activated fibroblasts (NAFs). It was first observed in wound healing where they migrated to the wound area and generated extracellular matrix (ECM) providing scaffold for tissue regeneration (Räsänen and Vaheri, 2010). Transformation to myofibroblast gives the fibroblast the phenotype of contractile stress

fibres such as α-SMA and FN-EDA 1 (Tomasek *et al.*, 2002). Furthermore, myofibroblast can proliferate, migrate, secrete soluble factors (TGF-β1, cytokines, chemokines, matrix-metalloproteinase (MMP), etc.) and ECM (collagen I, III and IV, and fibronectin, etc.) and to assist in matrix re-modelling during wound healing. After the healing process is complete, the myofibroblast undergoes reprogramming to revert to quiescent fibroblast or apoptosis. This reversible phenotype process is not well understood but it is assumed that most fibroblast undergo the latter, a programmed cell death or nemosis to restore the population of resident fibroblast (Tomasek *et al.*, 2002).

1.2.2.2 Cancer-Associated Fibroblast

Fibroblasts in tumour stroma remain in an 'activated' state, where they express soluble factors and ECM like those found by myofibroblasts. There are several terms of fibroblasts used for tumour stroma, but a widely known terminology is cancer associated fibroblasts (CAF) (Kalluri, 2016). CAF are distinguishable from normal fibroblasts phenotypically, functionally, as well as in different expression profiles of ECM components and growth factors (Kalluri and Zeisberg, 2006).

Several markers were identified to characterize a CAF including α-SMA, fibroblast activation gene (FAP), tenascin-C, platelet derived growth factor receptor (PDGF-R), periostin, vimentin, desmin and fibroblast specific protein-1 (FSP-1) (Shiga *et al.*, 2015; Kalluri, 2016). α-SMA expression is often identified with CAF (Busch and Landberg, 2015). CAF has demonstrated a heterogeneity within its population where a study identified a unique population expressing FSP-1 with lack expression of α-SMA and PDGF-R (Sugimoto *et al.*, 2006). TGF-β can induce the phenotypic features of CAF *in vitro* during wound healing and organ fibrosis by mediating fibroblast activation (Dumont and Arteaga, 2000).

The origin of CAF and its underlying mechanisms are still unclear. It was considered to originate from resident fibroblasts, adipocytes, epithelial cells (via epithelial-mesenchymal transition (EMT)), endothelial cells (via endothelial-mesenchymal transition (EndoMT)) and even from hematopoietic stem cells (Shiga *et al.*, 2015). CAF has shown to play a role in tumour development in breast (Aboussekhra, 2011), pancreas (von Ahrens *et al.*, 2017)), oral cancer (Li *et al.*, 2015; N.-N. Lin *et al.*, 2017) and bone metastasis (Prajapati and Lambert, 2016).

1.2.2.3 Senescence fibroblast

When cells undergo the state of arrest growth in response to oncogenic events, this incident is termed cellular senescence. It was firstly demonstrated in human fibroblasts of embryonic lung tissues where the proliferation rate ceased after replicative passaging (Ogrunc and d'Adda di Fagagna, 2011). Several factors can be associated to cellular senescence including epigenetic abnormalities, stress-induced premature ageing, telomere shortening, genomic damage, mitogen and proliferation-associated signals, and activation of tumour suppressors (Campisi, 2013; Wang, Cai and Chen, 2017). Growth arrest is the hallmark of cellular senescence with permanent cell cycle arrest at G1 phase, although still metabolically active (Herbig *et al.*, 2004). The senescent cells growth is permanently arrested unlike quiescence cells and its proliferative capability cannot be reverted.

Cell senescence display a tumour suppressive mechanism by preventing the cells undergoing neoplastic transformation (Campisi, 2013). The senescent cells secrete numerous cytokines, proteases, growth factors and a collection of proteins, also known as senescence-associated secretory phenotype (SASP) which can influence surrounding cells and can contribute to ageing (Rodier and Campisi, 2011). Some studies have shown that senescent fibroblasts can enhance pro-metastatic phenotypes (Wang *et al.*, 2017) and promote tumorigenesis (Krtolica *et al.*, 2001; Ruhland *et al.*, 2016).

Currently, the mechanism underlying cell senescence phenotype in terms of its trigger and maintenance is poorly understood. Therefore, there are limited amount of suitable marker and also lack of specificity targeting senescence cells (Althubiti *et al.*, 2014). Senescence-associated β-galactosidase (SA-βgal) activity is the most common marker to identify senescent cells in culture and tissue (Debacq-Chainiaux *et al.*, 2009). p16 has been identified to be a senescent marker (Coppé *et al.*, 2011) although not in all senescent cells (Haferkamp *et al.*, 2009).

1.2.3 Lymph nodes

Lymph nodes form a part of the lymphatic system with an ovoid or kidney shape organ, playing an important role in immune system (**Figure 1.2**). The nodes primarily reside by B and T lymphocytes, as well as other leukocytes. This organ is crucial for proper functioning immune system by filtering foreign particles and sometimes cancer

cells. Not to be compared to kidney and liver, lymph nodes do not have the capability as a detoxifying function but more as a checkpoint populated with leukocytes to scrutinize the circulatory system from any invaders or foreign particles.

The highly organized structure of the lymph node is designed to assist the interactions between the cell of the immune system and the foreign invader. Fluids from surrounding tissue are drained into the lymph node through the afferent lymph vessels including the antigen-presenting cells (APC). The fluid will be circulated out of the lymph node through efferent lymphatic vessel after its journey around subcapsular sinus (SS) and the trabecular sinuses towards the medulla through the cortex (Harwood and Batista, 2010). It is well compartmentalised to accommodate inflammatory cells.

In cancer, the lymph node is highly associated with cancer metastasis. Cancer dissemination into distant parts is usually through vascular or lymphatic vessel although the mechanism is poorly understood. This organ is a useful predictor of patient survival where it is use to be the key parameters to determine the disease progression and treatment options (Morton *et al.*, 2006). A specific chemokine has been shown to be the drive for cancer metastasis to lymph node such as in melanoma through CCL1/CCR8 (Das *et al.*, 2013).

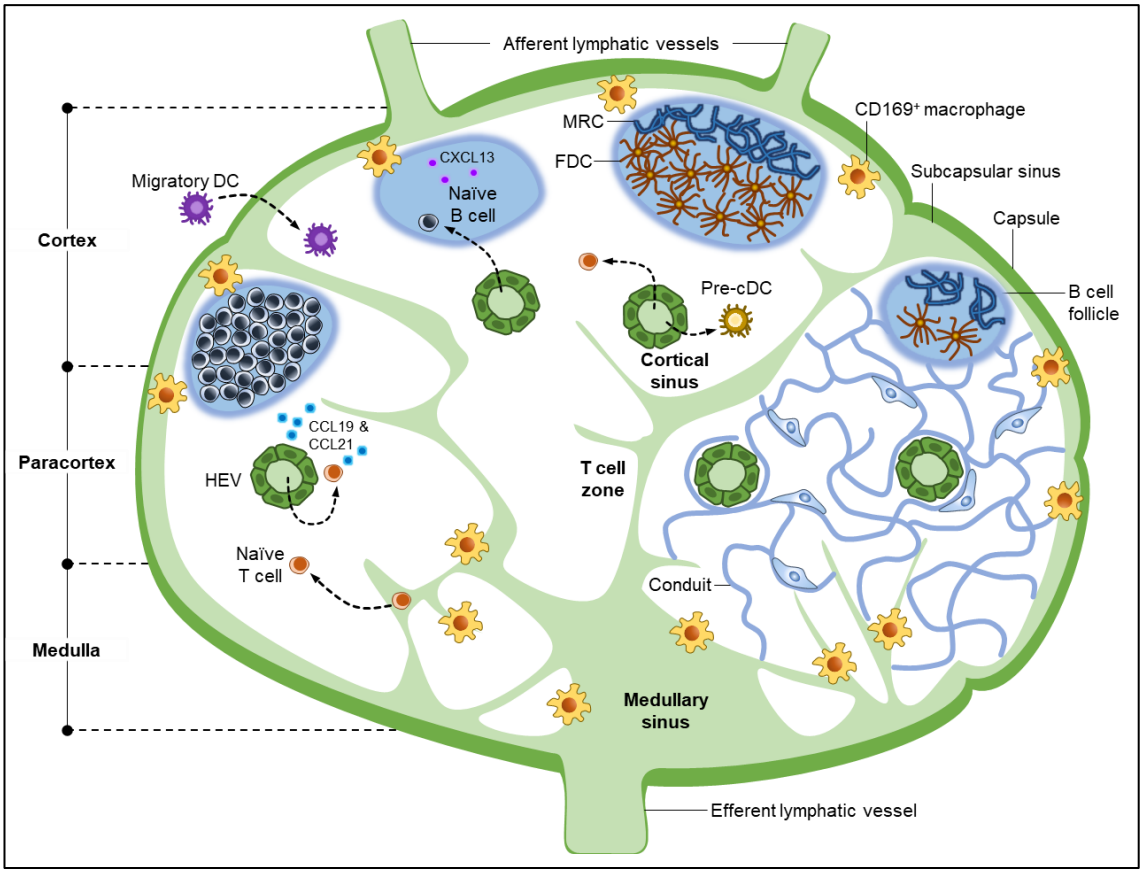

Figure 1.2: Lymph node organisation and immune cells entry. The lymph node is bean-shaped lymphoid organs encapsulated by a collagenous structure. The main structure is subdivided into three major sections: the medulla, the paracortex and the cortex. Naïve lymphocytes enter the organ either through afferent lymphatic vessel or high endothelial venules (HEVs), and exit via cortical or medullary sinuses, and efferent lymphatic vessels. Additionally, the dendritic cells (DCs) can enter the organ through the subcapsular sinus. The cortex comprises mostly of tightly packed B cells and follicular dendritic cells (FDCs) where they can arrange to form B cell follicles or germinal centres. In contrast, the paracortex regions comprise mostly of T cells, in T cell zone and fibroblastic reticular cells (FRCs), forming a network guiding the lymphocytes and DCs in the lymph nodes. MRC, marginal reticular cell; pre-cDC, precursor conventional DC. The image was reproduced and adapted from Girard, Moussion and Förster (2012).

1.3 Metastasis

A cancer which is not infiltrative and remains localised is called benign. A tumour is termed malignant when it shows infiltration and invasion into the structures surrounding the primary tumour. Metastatic tumours develop when malignant cancer cells spread to other parts of the body either by the lymphatic or the blood circulation. In OSCC, metastasis is facilitated by epithelial-mesenchymal transition (EMT) which allows the epithelial cells to acquire a more mesenchymal phenotype enabling them more motility and migration. The tissue extracellular matrix (ECM) plays an important role in cancer spread. The matrix environment is active with numerous interactions occurring at this site such as cell signalling and transport of nutrients. It also functions in cell support by interaction with integrin receptors (Juliano and Haskill, 1993). In tumour environment, factors such as matrix-metalloproteinase (Kessenbrock, Plaks and Werb, 2010), chemokines (Sheu *et al.*, 2008) and cancer-associated fibroblast (Junttila and de Sauvage, 2013) further facilitate the survival and growth of cancer cells.

Cancer cells are thought to intravasate into the blood or lymphatic vessels allowing access to local and systemic circulation which facilitates metastasis (see **Figure 1.3**). However, the factors contributing to intravasation of cancer cells are unknown. Tumour micro-environment comprises of stromal fibroblasts, endothelial cells lining blood and lymphatic vessels, and inflammatory cells which are important in cancer cell proliferation, adhesion, migration and invasion suggesting it may have in important role in metastasis.

In local invasion, cancer cells undergo EMT as well as mesenchymal-epithelial transition (MET) to detach from the site of origin (Hagman *et al.*, 2013). MET allows the cancer cells to re-associate with extracellular matrix (ECM) and anchors them to the new site. Mostly, cancer cells show immortality and unlimited division potential recruiting some proteins and factors to initiate angiogenesis, sustaining their growth and survival.

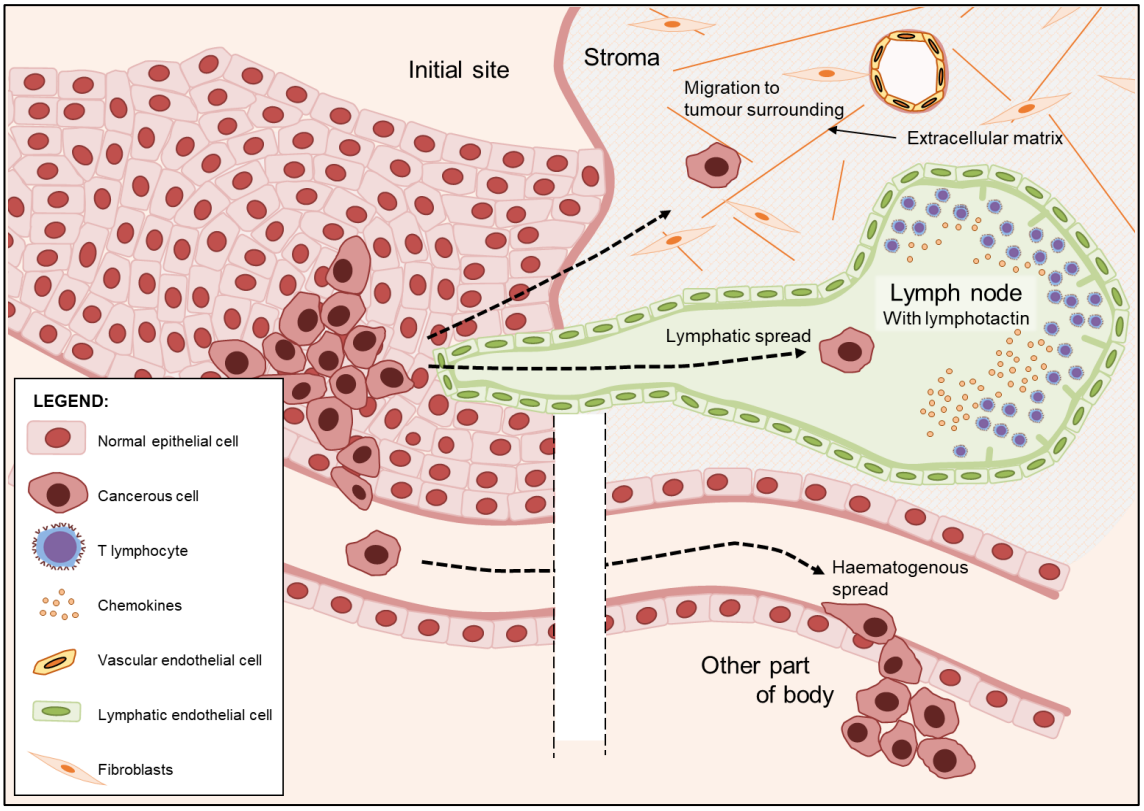

Figure 1.3: Concept of metastasis. Possible route of cancer spread (– – – →) which is either through lymphatic vessel (lymphatic spread) or blood vessels (haematogenous spread). The cancer grows from the tissue of origin and invades neighbouring tissue or spreads to distant sites.

1.3.1 Theories of Metastasis

The exact signals triggering cancer metastasis are not well understood. Paget originally proposed the “seed and soil” theory where the metastasized cancer cell (the seed) circulates in the blood or lymphatic system until it finds a suitable location in the human body (the soil) and starts to form cancer there (Fokas *et al.*, 2007). The most common site for metastasis to occur is in bone as it always undergoing constant remodelling (Hadjidakis and Androulakis, 2006; Rucci, 2008). It also serves as a latent location for cancer cells to stay dormant before they start to spread later in life.

The ‘chemoattractant’ theory of metastasis revolves around chemokines and their ability to attract cells expressing chemokine receptors. Recently, it has been reported that some cancer cells acquire upregulated expression of specific chemokine receptors (Müller *et al.*, 2001; Khurram *et al.*, 2010, 2014; Kim *et al.*, 2012; Gantsev *et al.*, 2013) which allows cancer cell movement along a chemotactic gradient hence facilitating metastasis. Lymph nodes with activated lymphocytes, macrophages and

endothelial cells are a rich source for chemokines and this has been proposed to attract the receptor expressing epithelial cells to the lymph node interior resulting in metastasis (Alitalo and Detmar, 2012; Karaman and Detmar, 2014). However, the specific mechanism of this transmigration of tumour cells from lymphatic circulation into lymph nodes is not well understood.

1.4 Chemokines

Chemokines are chemo-attractant cytokines, which can attract cells expressing the receptive receptor along a concentration gradient of the chemokine in a process called chemotaxis (see **Figure 1.4**). Chemotaxis is sensitive as it can be activated by a chemokine concentration as low as 1 nM in normal physiological conditions (Fox, Nakayama, *et al.*, 2015).

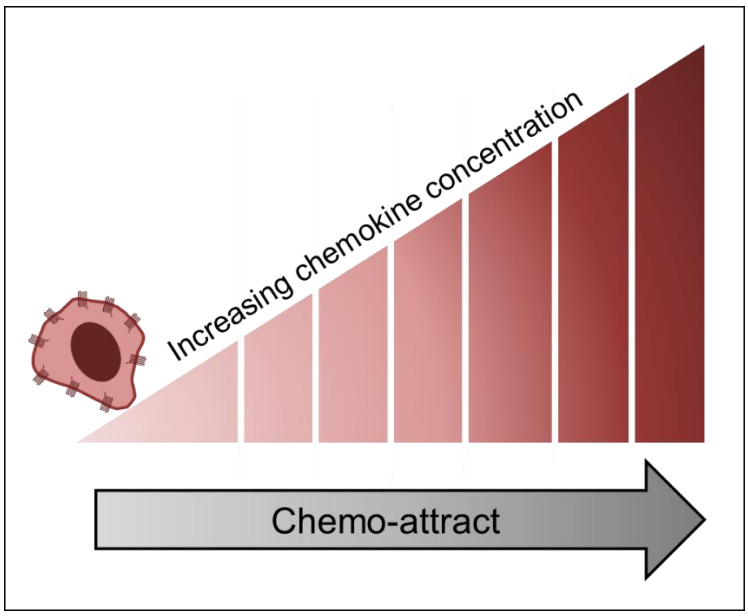

Figure 1.4: Chemotaxis. The receptive cell expressing chemokine receptor responds to chemokine concentration gradient. It can be either move towards to (chemo-attract) or away (chemo-repel) by the chemokine.

Chemokines are small proteins with a molecular mass of 8 – 10 kDa. Their distinctive characteristic is the conserved cysteine residue, which separates the chemokines into four different groups (see **Figure 1.5**). The structure consists of three antiparallel β-sheets and N-terminal α-helix which are joined by two disulphide bridges.

At least 50 chemokines have been identified in human and are divided into four subfamilies based on the position of the conserved cysteine near the N-terminal (Balkwill, 2012).

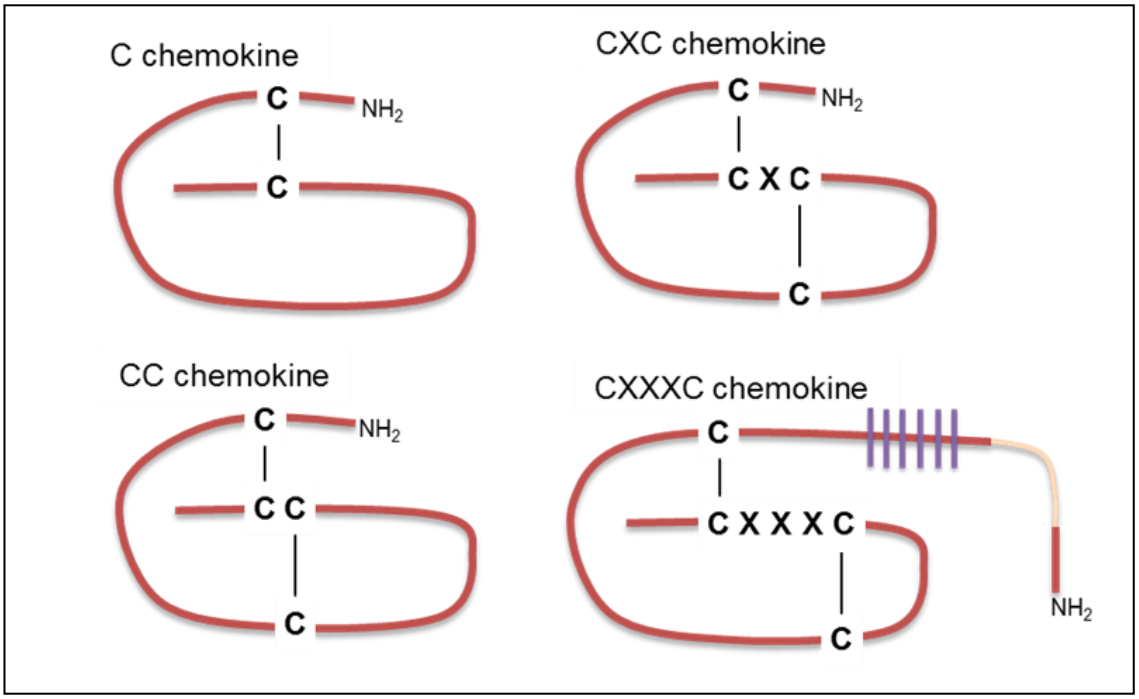

Figure 1.5: The chemokine super-families. The structure is distinguished by the distinct location of the cysteine residues. Denoted by '**X**' in the picture can be substituted to any other amino acid except cysteine. The cysteine residues form disulphide bonds holding the protein structure together. All super-families contain chemokine signature of two disulphide bridge except for C chemokine. CX3C chemokine contains a mucin-like region (**purple**) allowing it to be membrane-bound or soluble protein.

Most chemokines belong to the CXC and CC families. The C chemokine family has only two known members. This group is unique as it only has one disulphide bridge compared to conventional chemokines with at least two disulphide bridges in the structure. CX3C chemokines are the fourth group in the family with fractalkine being the only member. It can exist as either membrane-anchored protein or as glycoprotein unbounded protein (Bazan *et al.*, 1997; Tripp *et al.*, 2001; Meyer dos Santos *et al.*, 2011).

1.5 Chemokine Receptors

Chemokine receptors are also known as G-protein coupled receptors. This type of receptor is embedded in the cell membrane with the N-terminus on the extracellular aspect of the cell membrane and 7-transmembrane α-helices structure that comprise three outer and inner loops (**Figure 1.6**). The C-terminal resides in the cytoplasm are connected to a heterotrimeric G-protein; comprising three different bodies: α, β and γ.

Although there are nearly 50 chemokines identified, not all activate one specific chemokine receptor (see **Table 1.1**). Some receptors are shared between several chemokines and some of the chemokines can activate several chemokine receptors within the family (Zlotnik, Yoshie and Nomiyama, 2006). For example, in humans, the chemokine receptor CX3CR1 can only be activated by CX3CL1 (fractalkine). XCR1 can be activated by XCL1 and XCL2 but both have similar structure and differ by two amino acids.

To date, 18 chemokine receptors have been reported (Zweemer *et al.*, 2014) with six CXCR chemokine receptors, one XCR chemokine receptor, one CX3CR chemokine receptor and 10 CCR chemokine receptors (see **Figure 1.7**). Additionally, four atypical receptor (ACKR1 – 4) have the same structure as the chemokine receptor, although the ligand binding unable to activate the classical signalling pathway (Bonecchi and Graham, 2016). Some of the chemokines share the same chemokine receptor or vice versa, providing a biased signalling with additional of atypical receptor contributing to the complexity of understanding them (Steen *et al.*, 2014). The complex organisation and functions of chemokines and the receptors have been shown to be closely related to their evolutionary perspective (Zlotnik and Yoshie, 2012) (**Figure 1.8**). The phylogeny analysis amongst the chemokine receptor has shown that XCR1 are closely related to CXCR4, a well-known chemokine receptor in pathology.

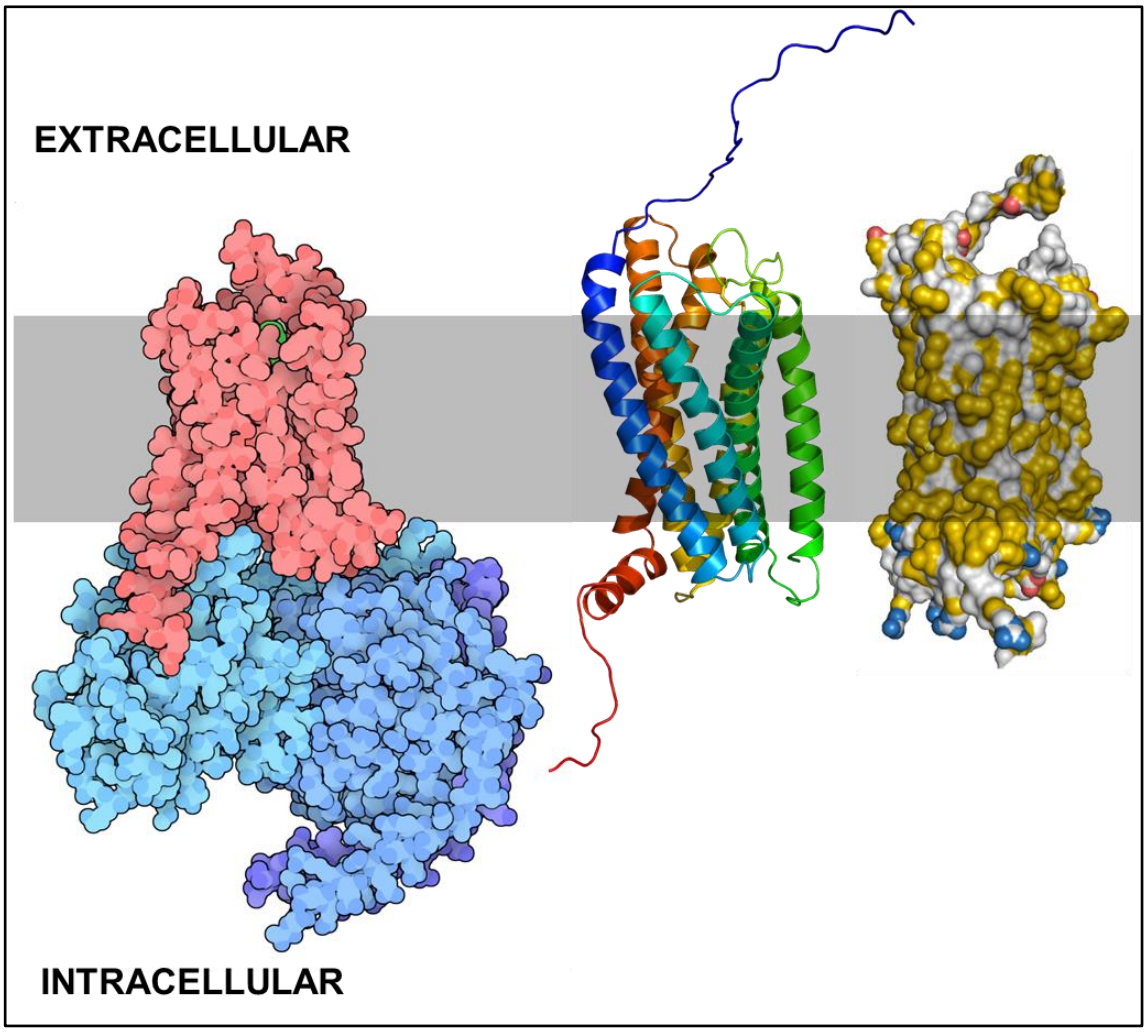

Figure 1.6: The typical structure of chemokine receptor, a class of G-protein coupled receptor (GPCR). **(Left)** Typical transmembrane receptor structure (**reddish pink**) shown attached to a GPCR (**blue-cyan**) (image was obtained from RCSB PDB-101 website). **(Middle)** A typical chemokine receptor backbone showing a seven-helical transmembrane protein (7-TPM) domain of the cell membrane. The image is the predictive protein structure of XCR1 receptor created using RaptorX software (http://raptorx.uchicago.edu/). **(Right)** XCR1 receptor with its surface shown. The image was produced using Pymol.

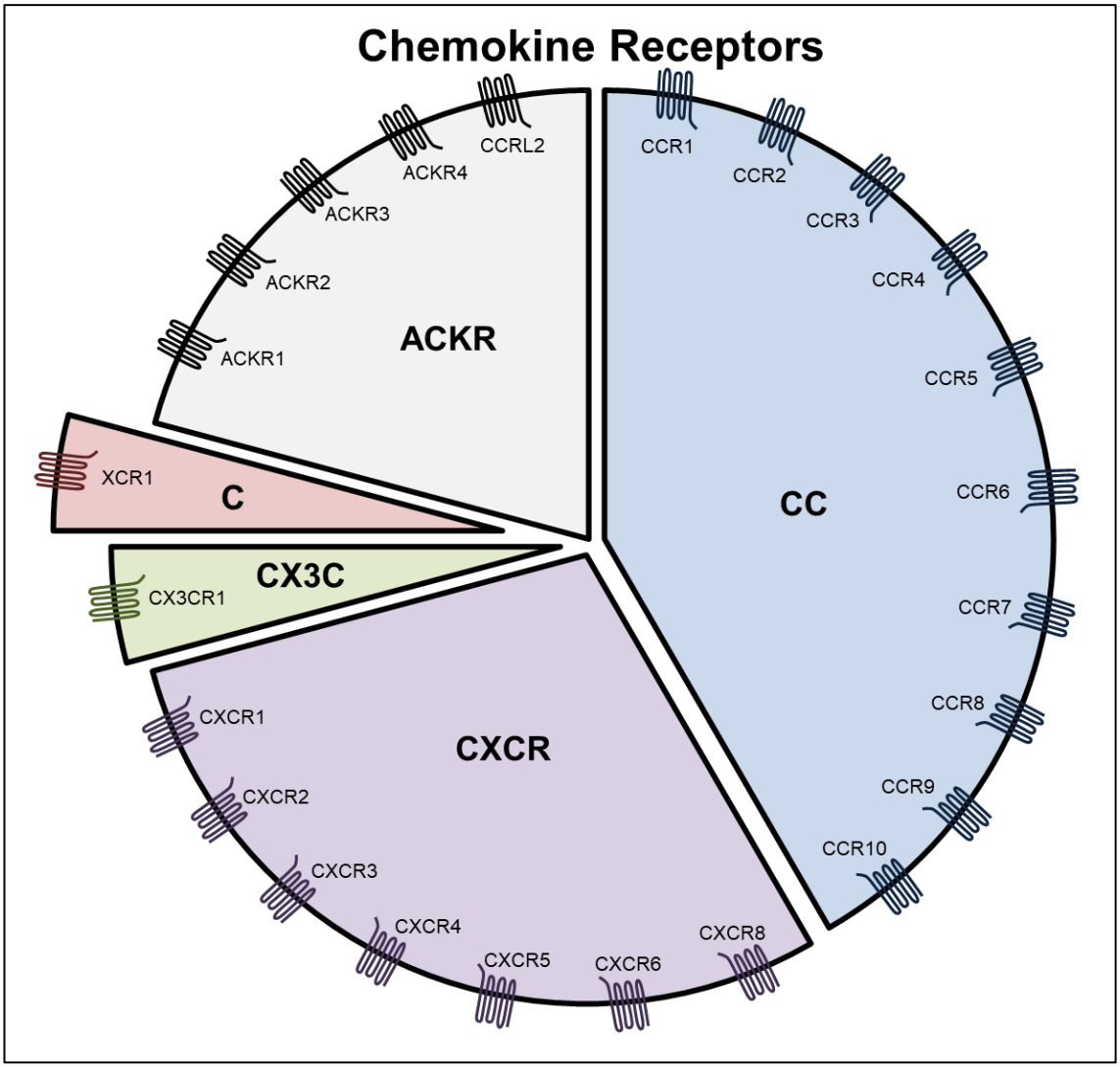

Figure 1.7: The chemokine receptors based on the family classification. **Blue** – **CC** chemokine; **purple** – **CXC** chemokine; **green** – **CX3C** chemokine; and **red** – **C** chemokine. Additionally, there is a small family of atypical chemokine receptor (**ACKR**) (in **grey**), a unified member by their incapability to initiate canonical chemokine signalling upon receptor activation. The receptor family classification is solely associated to the subfamily of its chemokine as there is no distinguishable identification between the receptors. Note that there is no CXCR7, as this has been re-classified to ACKR3. The other ACKRs were also reclassified to DARC (ACKR1), D6 (ACKR2) or CCX-CKR (ACKR4).

Table 1.1: Chemokine receptors and their respective ligands (in human).

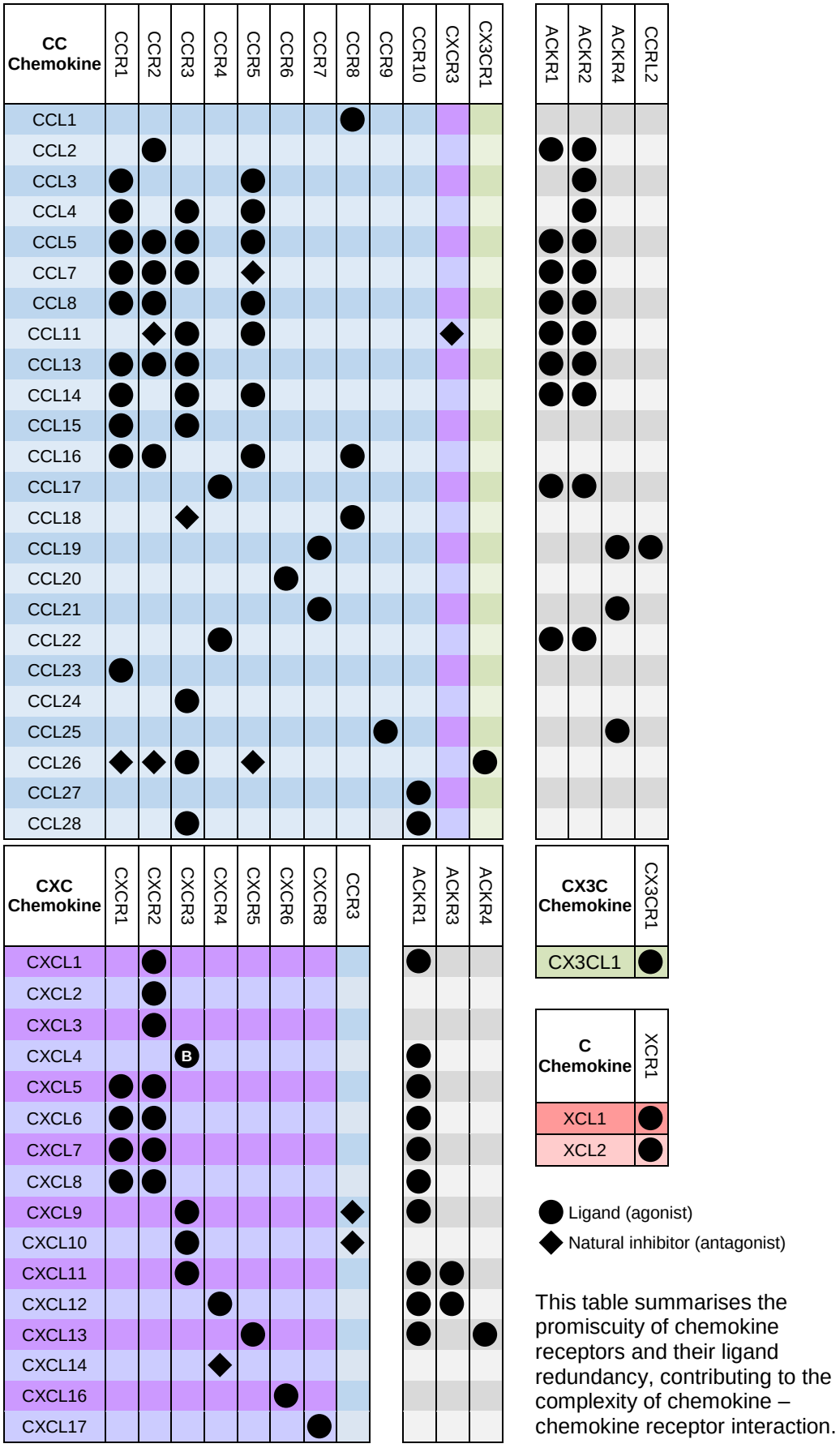

This table summarises the promiscuity of chemokine receptors and their ligand redundancy, contributing to the complexity of chemokine – chemokine receptor interaction.

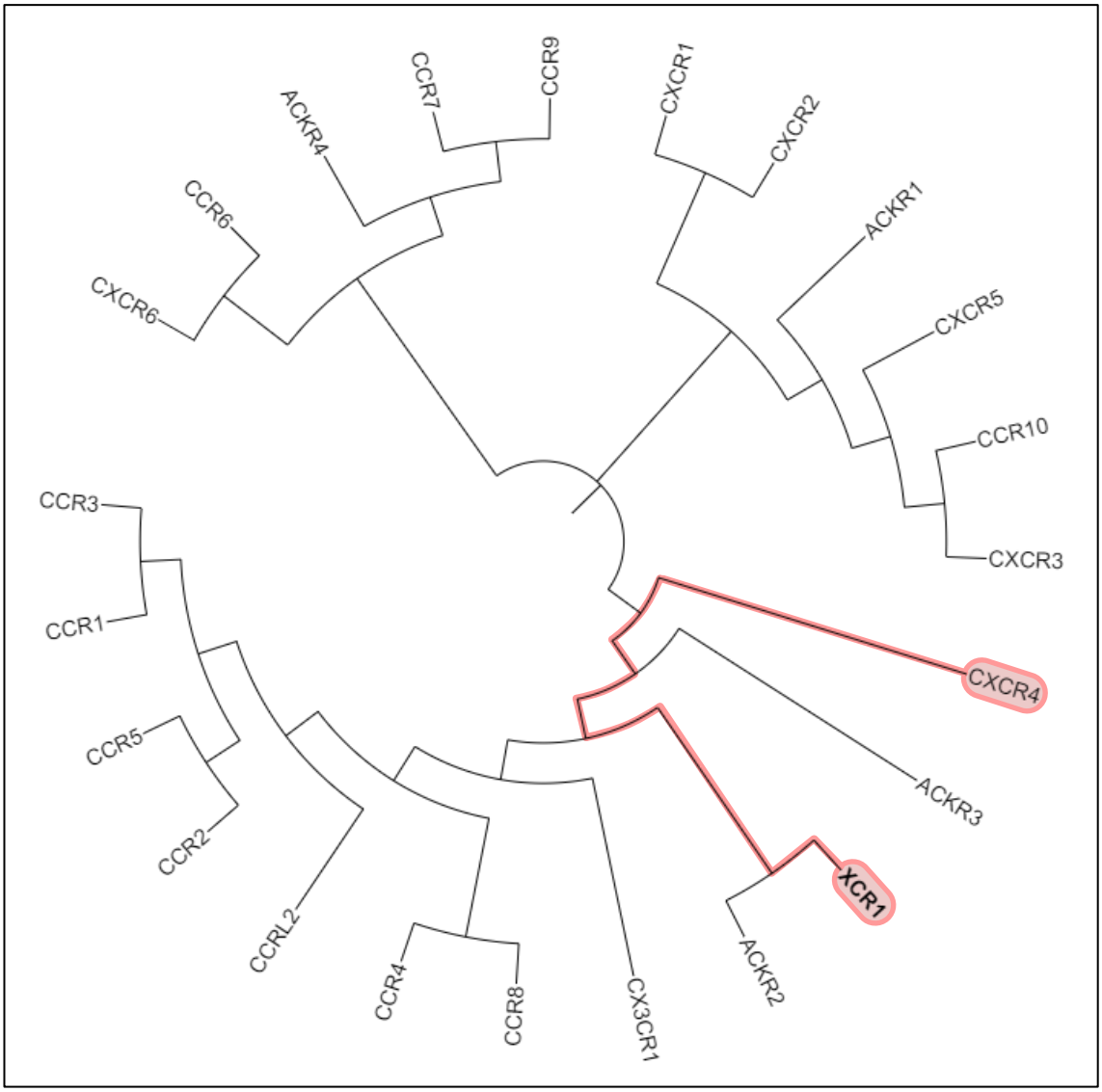

Figure 1.8: Phylogeny tree (in circular mode) of all chemokine receptors including the atypical chemokine receptors. The analysis shows that the XCR1 is closely related to CXCR4 (highlighted in **red**), the intensively studied chemokine receptor that is involved in many pathologies.

1.6 Functions of Chemokines and Chemokine Receptors

Chemokines are involved in many biological processes. Their most common function is to mediate leukocyte trafficking in the immune response. The signalling mediates adhesion and migration of cells expressing the chemokine receptor. They are also involved in homeostasis (Zlotnik, Burkhardt and Homey, 2011) and with both autocrine (Menten *et al.*, 2002; Tamgüney, Van Snick and Fickenscher, 2004; Kroeze *et al.*, 2012) and paracrine signalling (Gortz *et al.*, 2002; Heinrich *et al.*, 2013). Chemokines have also been found to be expressed during human transplant rejection (Segerer *et al.*, 2001). CXC chemokines have also been shown to play an important role in chronic inflammation (Hannelien *et al.*, 2012).

Chemokines can promote neovascularization and tumour angiogenesis (Keeley, Mehrad and Strieter, 2011). CXCL1 to CXCL8 except CXCL4 (ligands for CXCR2), CCL2 (ligand for CCR2), CCL11 (ligand for CCR3) and CCL16 (ligand for CCR1) are pro-angiogenic chemokines with only four related chemokine receptors. Chemokines are also indirectly involved in organogenesis, making new lymph nodes during development and in cancer tissue (Gantsev *et al.*, 2013).

Chemokines also play a role in other pathologies such as diabetes where monocytes have been shown to increase inflammatory cytokines and chemokines production significantly by high glucose induction (Shanmugam *et al.*, 2003) and CXCL10 expression resulting in failure of insulin-producing cells (Antonelli, Ferrari, Corrado, *et al.*, 2014). In autoimmune disease, recruitment of Th1 lymphocytes by CXCL10 increases production of interferon-γ and tumour necrosis factor-α, stimulating other cells producing the chemokine hence creating a high feedback loop (Antonelli, Ferrari, Giuggioli, *et al.*, 2014). High levels of chemokine expression are also seen in cardiovascular disease where they contribute to vascular destruction and plaque development (Ross *et al.*, 2012; Yao *et al.*, 2014).

A summary of general signal transduction for chemokine receptor when activated by its ligand can be found in **Figure 1.9**.

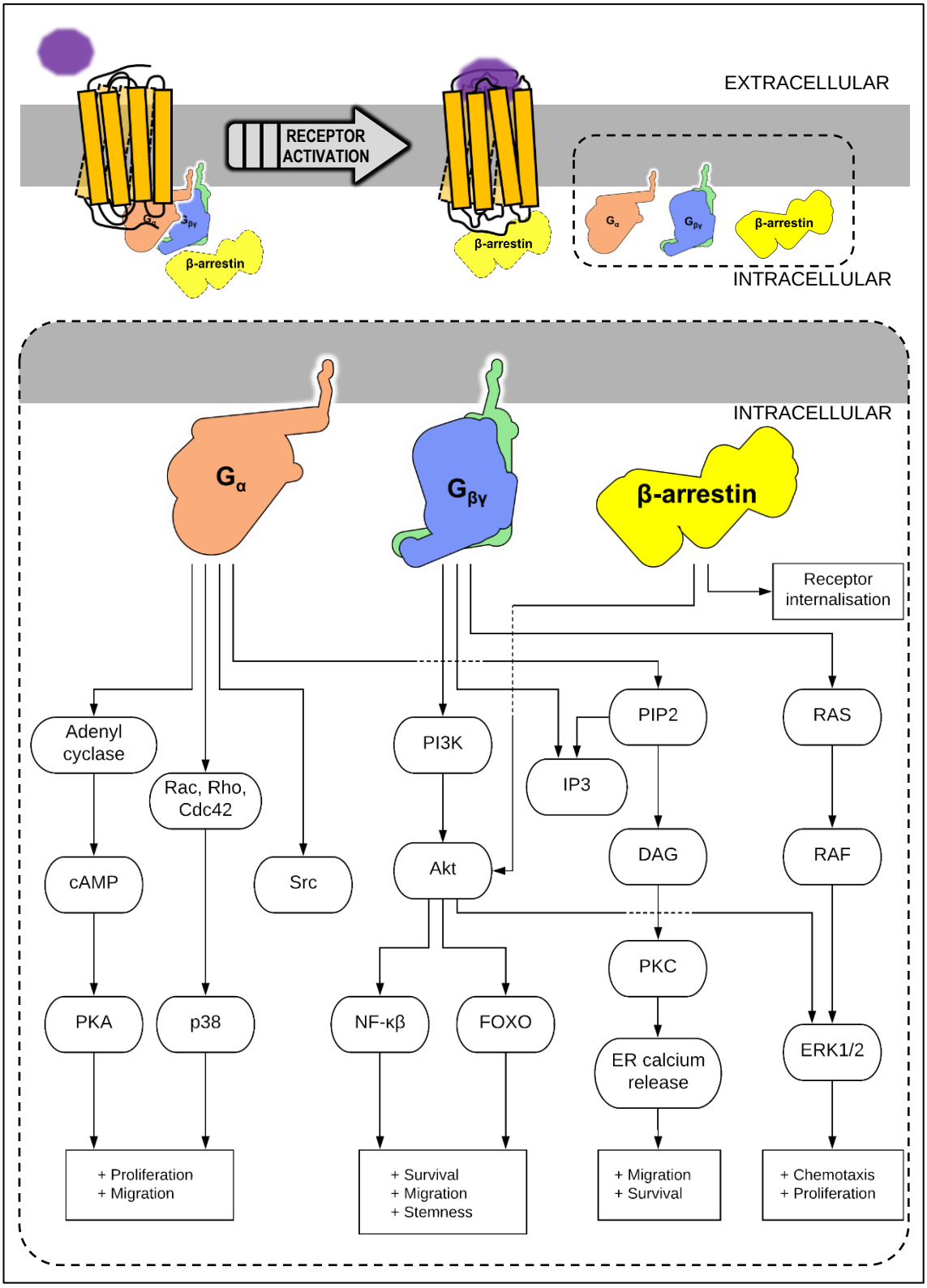

Figure 1.9: Downstream signalling of chemokine receptor upon activation by its ligand. Receptor transduction is closely related to cytokine signalling, although this information is generalised to normal cell compared to the complicated chemokine-chemokine receptor system associated with cancer pathology. The image at the top shows the activation of the chemokine receptor by its ligand (in **purple**) and the signalling pathways of the endogenous ligands (G_{α}, $G_{\beta\gamma}$ complex, and β-arrestin protein).

1.7 Chemokines and Chemokine Receptors in Tumour Biology

Chemokines and their receptors are involved in cancer-related inflammation (Mantovani *et al.*, 2010). Although they recruit leukocytes to counter cancer cells, they can also have pro-cancer functions by controlling leukocyte infiltration, assisting angiogenesis, promoting cancer cell growth and survival, subverting the anti-tumour response and facilitating metastasis (Slettenaar and Wilson, 2006). This role is further supported by the fact that epithelial cancer cells can acquire higher levels of chemokine receptors compared to their normal counterparts. Increased chemokine expression in the cancer microenvironment influences the activity of the cancer cells including cell migration, adhesion, proliferation and invasion. The summary of chemokine and chemokine receptor involved in different types of cancer cells can be found in **Table 1.2**.

Tumour development can be promoted by stimulation of angiogenesis. CXCR4 positive cells usually metastasize to distant organs and induce angiogenesis by interaction with CXCL12 in oesophageal and gastric cancer (Hannelien *et al.*, 2012). Although, other CXC chemokines have angiostatic effects and they attract anti-tumoral T lymphocyte, which reduces tumour growth.

Chemokines have been shown to promote metastasis (Sarvaiya *et al.*, 2013). The concentration gradient of CXCL12 promoted breast cancer cells movement and invasion similar to that seen in lymphocytes. Muller *et al.* (2001) showed the importance of CXCR7 and CCR7 in breast cancer invasion *in vivo*. Blood vessels consist of an endothelial cell lining that is separated from the tissue by a basal membrane and have been shown to express chemokine receptor (Murdoch, Monk and Finn, 1999) and release chemokines (Hillyer and Male, 2005; Speyer and Ward, 2011; Monnier *et al.*, 2012) which may induce adhesion and transmigration of cancer cells. It would be interesting to know if the endothelial cells express XCR1 receptor and produce hLtn for lymphocyte recruitment or cancer cell attachment.

Table 1.2: Chemokine receptors and chemokines expression in different types of cancer. **Annotation**: (n = *Number of positive cases*/Number of cases examined); [S] indicates obtained from serum or ascitic fluid; [B.MET] indicates bone metastasis; NA indicates data not available or not informed in the paper.

Type of cancer	Chemokine receptors and Chemokines		References
	Primary tumour	Metastasis	
Breast cancer	CXCR4 (n=12[1], *83*/182[2], *63*/103[3], *113*/200[4]), CXCR7 (n=*68*/80[5], *43*/103[3]), CCR4, CCR5, CCR6 (n=*72*/207[6]) CCR7 (n= n=*111*/200[4], *89*/207[6]), CCR10 (n=*63*/89[7]), CX3CR1 (n=*105*/202[8]), XCR1 (n=10[9]), CXCL12 (n=*71*/182[2], *86*/103[3], *38*/100[4]), CCL2[10], CCL5 (n=*36*/72[11]), CCL19 (n=*101*/207[6])	CXCR4 (n=*62*/100[4])), CCR7 (n=*77*/100[4]), CCR10 (n=*59*/68)[7], CXCL12 n=*55*/100[4]), CCL5 (n=*26*/47[10]), CCL21 (n=*68*/100[4])	[1] Müller *et al.*, (2001), [2] Sun *et al.*, (2014), [3] Schrevel *et al.*, (2012), [4] Y. Liu *et al.* (2010), [5] Yuan *et al.*, (2017), [6] Cassier *et al.* (2011), [7] H. Lin *et al.* (2017), [8] Jamieson-Gladney *et al.* (2011), [9] Yang *et al.* (2017), [10] (J. Wang *et al.*, 2015), [11] Araujo *et al.* (2018)
Cervical cancer	CXCR4 (n=*110*/174[1]), CCR7 (*102*/174[1]), ACKR1 (n=*168*/227[2]), ACKR2 (n=*162*/227[2]), ACKR3 (n=34[3]), ACKR4 (n=179/227[2]), CXCL8 (n=*61*/108[4]), CCL19 (n=*55*/62[5])	CXCR4 (n=*32*/35[1]), CCR7 (n=*31*/35[1]), ACKR1 (n=*14*/33), ACKR2 (n=*21*/33[2]), ACKR4 (n=*20*/33[2]), CXCL8 (n=*27*/43 [4])	[1] (Kodama *et al.*, 2006), [2] Hou *et al.* (2013), [3] Tang, Xia and Xi (2016), [4] Yan *et al.* (2017), [5] Zhang *et al.* (2017)
Lung cancer	CXCR1[13], CXCR2[13] (n=262[1]), CXCR4 (n=76/110[2], *62*/154[3]), CCR2 (n=*39*/65[5]), CCR7 (24/40[6]), CCR9 (n=39[7]), XCR1 (n=5[8]), ACKR3 (n=*21*/35[9]), CXCL1[10], CXCL5 (n=75[11]), CXCL8 (n=*56*/70[12], *49*/120[13]), CXCL12 (n=*47*/150[3]), CXCL14 (n=*24*/35[9]), CCL2 (*107*/134[5]), CCL19[10], CCL21 (n=*48*/100[4]), CCL25 (n=39[7]), CCL4[14], XCL1 (n=5[8])	CXCR4 (n=*56*/76[2], *16*/44[3], *62*/100[4]), CCR7 (n=*77*/100[4], *47*/120[13], *19*/24[6]), XCR1 (n=5[8])[B.MET], CXCL8 (n=*22*/27[12], *36*/72[13]), CXCL12 (n=*20*/42[3], *55*/100[4]), CCL19 (n=*55*/120[13]), CCL21 (n=*68*/100[4], *25*/120[13]), XCL1 (n=5[8])[B.MET]	[1] Saintigny *et al.* (2013), [2] Bi *et al.* (2017), [3] Wagner *et al.* (2009), [4] Y. Liu *et al.* (2010), [5] Zhang *et al.* (2013), [6] Yu *et al.* (2017), [7] Gupta *et al.* (2014), [8] T. Wang *et al.* (2015), [9] Choi *et al.* (2015), [10] Acharyya *et al.* (2012), [11] Wu *et al.* (2017), [12] Hosono *et al.* (2017), [13] Liu *et al.* (2015), [14] Cheng *et al.*, (2016)
Lymphoid leukaemia	CCR3, CCR4, CCR7, CCL18	-	Balkwill (2012)

Lymphoma	CCR3[1], CCR4[2], CCR10[3], CCL17[4]	-	[1] Kleinhans *et al.* (2003), [2] Kumai *et al.* (2015), [3] Notohamiprodjo *et al.* (2005), [4] Peh, Kim and Poppema (2001)
Melanoma	CXCR2, CXCR4 (n=*31*/71[1], *25*/30[2]), CCR7 (n=*18*/30[2]), CCR10 (n=*31*/40[3]), CCL27 (n=*18*/40[3]), CCL28, CXCL1, CXCL8, CXCL12 (n=*6*/30[2])	CCR7 (n=*16*/19[2]), CXCL12 (n=11/19[2])	Balkwill (2012), [1] Scala *et al.* (2005), [2] van den Bosch *et al.* (2013), [3] Simonetti *et al.* (2006)
Oral or/and oropharyngeal cancer	CXCR1, CXCR2 (n=*47*/85 [1]), CXCR4 (n=*24*/40 [2], *54*/60 [3]), CCR6 (n=4[4]), CCR7 (n=4[4], *56*/60 [3], 56/85 [5] *54*/90 [6]), XCR1 (n=10 [7]), ACKR3 (n=*30*/35[8]), CXCL9 (n=*46*/50[9]), CXCL11 (n=*25*/35 [9]), CXCL12 (n=*25*/40 [2]), CCL2[S10], CCL3 (n=*40*/98[10]) CCL21 (n=NA [5]) XCL1 (n=10 [7])	CXCR4 (n=*65*/77[3]), CCR7 (n=*73*/77[3], 4[4]), CCL3 (n=*13*/30[10])	[1] Qian *et al.* (2014), [2] Xia *et al.* (2012), [3] Al-Jokhadar *et al.* (2017). [4] Chen *et al.* (2013), [5] Shang, Liu and Shao, (2009), [6] Tsuzuki *et al.* (2006), [7] Khurram *et al.* (2010), [8] Xia *et al.* (2011), [9] Chang *et al.* (2013), [10] Ding *et al.* (2014)
Ovarian cancer	CXCR4 (n=*26*/44[1], *241*/241[2]), XCR1 (n=*55%*/NA [3]), CXCL12 (n=*40*/44[1], *199*/289[1]), XCL1 & XCL2 (n=NA [3])	CXCR4 [4]	[1] Jiang *et al.* (2006), [2] Popple *et al.* (2012), [3] Kim *et al.* (2012), [4] Balkwill (2012)
Pancreatic cancer	CXCR1 (n= *40*/65 [1]), CXCR4 (n=*34*/60[2]), CCR4 (n=*66*/75[3]), CCR6 (n=25[4]), CX3CR1 (n=*56*/104[5]), CXCL12 (n=*52*/60[2]), CCL20 (n=25[4]), CX3CL1 (n=*70*/104[5])	CXCR4 (n=*28*/35[2]), CX3CR1 (n=*34*/69[5]), CX3CL1 (n=*44*/69[5])	Balkwill (2012), [1] Chen, L. et al (2015), [2] J. Zhang *et al.* (2017), [3] Cheng *et al.* (2017), [4] Rubie *et al.* (2010), [5] Celesti *et al.* (2013)
Stomach cancer	CXCR2 (n=*82*/116[1], *200*/357[2]), CXCR4 (n=*40*/50[3], 30/93[4]), CCR4 (n=*79*/103[5]), CCR7 (n=25/93[4], *42*/64[6]), CXCL1 (n=*66*/116[1]), CXCL12 (n=*45*/50[3])	CXCR2 (n=*4*/8), CXCR4 (n=*33*/36[3], *7*/10[4]), CCR7 (n=*6*/10[4], *35*/39[6]), CXCL12 (n=*34*/36[3])	[1] Cheng *et al.* (2011), [2] Z. Wang *et al.* (2015), [3] Ying *et al.* (2012), [4] (Arigami *et al.*, 2009), [5] Yang *et al.* (2015), [6] Mashino *et al.* (2002)

1.8 Chemokine – Chemokine Receptors in Oral Cancer

Investigating biomarkers in saliva is potentially a useful tool for early detection of oral cancer (Prasad and McCullough, 2013). Saliva contains chemokines and the levels are highly elevated in the presence of cancer. OSCC can also be linked to inflammation where chronic inflammation impacts wound healing regulation allowing progression to cancer (Feller, Altini and Lemmer, 2013).

Chemokines and chemokine receptors showed higher expression in oral cancer cell lines (OCCL) compared to normal oral epithelial cells (Khurram *et al.*, 2010, 2014). Some studies have shown that chemokines in lymph nodes can attract cancer cells from the lymphatic circulation into the lymph node interior (Wiley *et al.*, 2001; Mashino *et al.*, 2002).

Most documented studies are in relation of chemokine and oral cancer progression are on CXCR4 receptor and its ligand CXCL12. CXCR4 expression is higher in metastatic oral cancer cells and clinical tissue (Delilbasi *et al.*, 2004) while the ligand is only expressed in cancer but not normal oral cells (Uchida *et al.*, 2003). CXCL12 increases invasiveness and motility of CXCR4-positive cells (Ishikawa *et al.*, 2006). The CXCL12/CXCR4 ligand-receptor interaction activates Src Family Kinase (SFK), extracellular signal-regulated kinases- ½ (ERK1/2) and Akt/Protein Kinase B (Akt/PKB) signalling (Uchida *et al.*, 2003) as well as nuclear factor kappa-light-chain-enhancer of activated B cells (NF-κB) pathway through CARD11-BCL10-MALT1 (CBM) complex (Rehman and Wang, 2009).

Other chemokines such as CXCL1 show cytoplasmic expression in OCCL and activate the CXCR2 receptor to promote tumour angiogenesis, leukocyte infiltration and lymph node metastasis (Shintani *et al.*, 2004). This chemokine is also produced by vascular endothelial growth factor (VEGF)-stimulated endothelial cells which induces invasion of CXCR2-positive oral cancer cells (Warner *et al.*, 2008). Also, ACKR3 (previously known as CXCR7) has also seen to be expressed in OSCC but not in normal epithelia however its ligand CXCL11 and CXCL12 have a moderate and high expression respectively in dysplasia and OSCC (Xia *et al.*, 2011).

Oral cancer cells also showed increase mRNA expression of CCR5 receptor when stimulated with CCL5 and increase the migration and production of matrix metalloproteinase-9 (MMP-9) (Chuang *et al.*, 2009). Overexpression of CCR7 is seen highly associated with cervical lymph node metastasis where it facilitates higher

adhesion to lymph nodes, hence assisting metastasis (Shang, Liu and Shao, 2009). Additionally, the paper also shown a positive CCR7 expression in OSCC tissue and cell lines although no expression was detected in normal oral mucosa (Shang, Liu and Shao, 2009).

In summary, chemokines and chemokine receptors appear to have an important role in oral cancer progression, but the mechanism is not well understood as some of the other more prevalent cancer. This suggests a specificity of chemokine receptor expression in certain types of cancer.

1.9 Studies of XCR1 and hLtn in oral cancer

A recent study showed XCR1 expression outside the immune system for the first time with expression in inflamed oral epithelial cells and oral cancer cells (see **Figure 1.10**) (Khurram *et al.*, 2010). In addition, hLtn expression was found in epithelium adjacent to OSCC, invasive OSCC islands, metastatic tumour in the lymph nodes as well as in stroma (see **Figure 1.11**).

hLtn expression was seen in both primary and metastatic tumours being present in the infiltrating leukocytes and the tumour stroma. hLtn and XCR1 expression was also seen in a range of OCCL at both the mRNA and protein level. However, the stimulus for hLtn release from epithelial cells remains unknown. There are only a few reported studies of hLtn and XCR1 receptor interaction in the context of cancer pathogenesis and spread. This is possibly due to the unique structure of the C chemokine itself which is not well established and researched as other chemokine families. This thesis will focus on of hLtn and its variant structures as well as their relationship with its receptor in oral cancer.

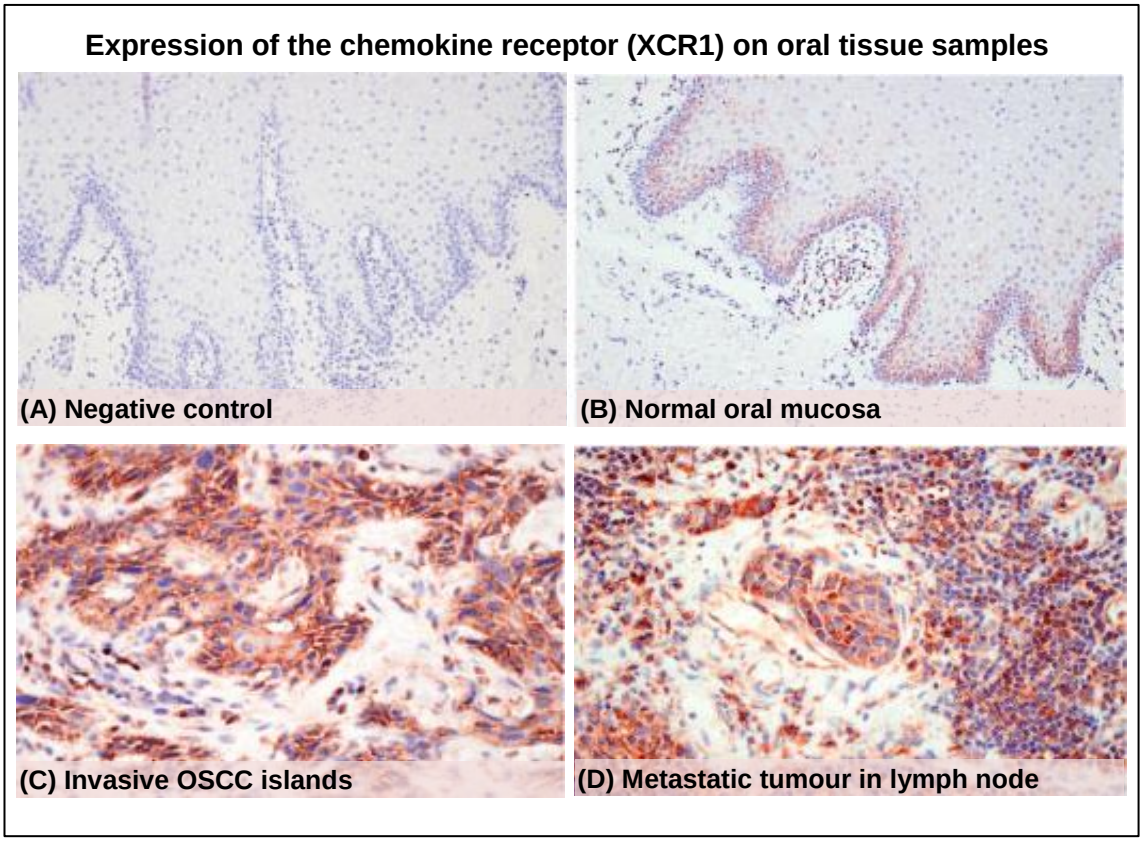

Figure 1.10: Immunohistochemistry showing XCR1 expression in oral tissue samples. **(A)** Isotype (negative) control, **(B)** Normal mucosa, **(C)** Invasive OSCC islands, and **(D)** Metastatic tumour in lymph node (image taken with permission from Khurram et al. (2010)).

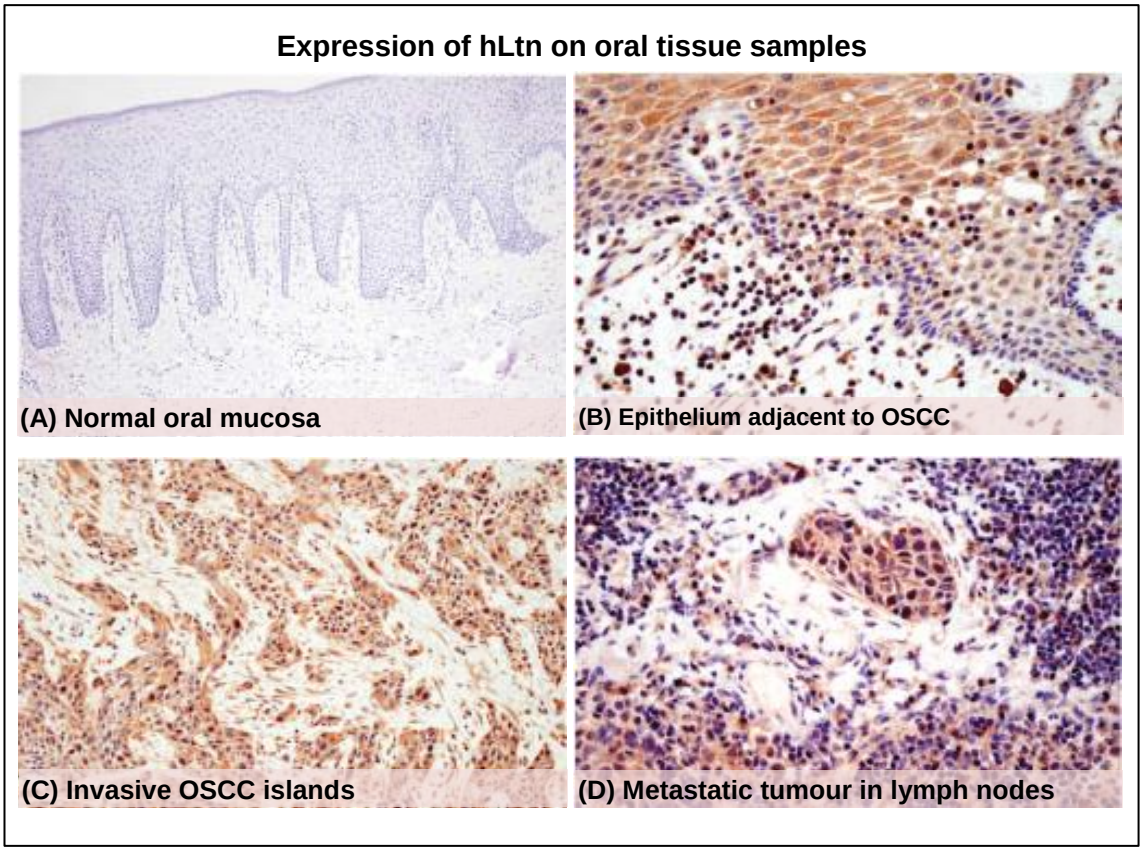

Figure 1.11: Immunohistochemistry showing hLtn expression in oral tissue samples. **(A)** Normal oral mucosa, **(B)** Normal mucosa adjacent to OSCC, **(C)** Invasive OSCC islands, and **(D)** Metastatic tumour in lymph node (image taken with permission from Khurram et al. (2010)).

1.10 XCR1

1.10.1 Discovery

XCR1 is a chemokine receptor that is only activated by hLtn, either XCL1 or XCL2 (Yoshida *et al.*, 1998). This was discovered by testing several known chemokine receptors as well as orphan receptors with only one of them inducing calcium mobilization by hLtn (Shan *et al.*, 2000). It is also known as GPR5 as it belongs to the G-protein coupled receptor family.

1.10.2 Structure

XCR1 is a transmembrane receptor spanning across the cell membrane and comprising of seven-transmembrane α-helix structure with three intra- and extra-cellular loops (see **Figure 1.12**). The N-terminus is located outside the cell and it is usually glycosylated. The C-terminus tail is lipoylated to the cell membrane by S-palmitoylation, attachment of palmitic acid to a specific cysteine residue via thioester linkage. The receptor is made up of 333 amino acids (see **Figure 1.13**).

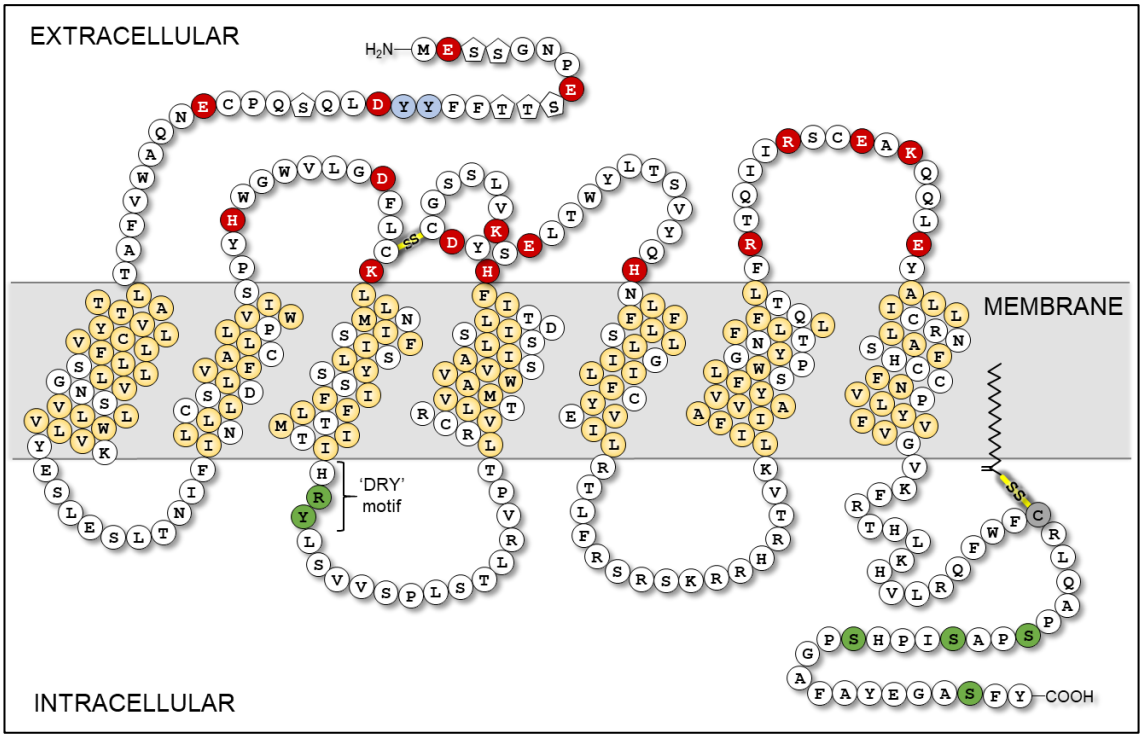

Figure 1.12: Depiction of XCR1 chemokine receptor amino acids in two-dimensional arrangement. The structure consists of extracellular N-terminus and intracellular C-terminus tail with three both extracellular and intracellular loops. The negatively charge extracellular amino acid residues (in **red**) have the potential to orientate the docking of the highly positively charge ligand based on their positioning for ligand-receptor binding. Additionally, there is a possibility of a post-translation modification of the N-terminal amino acid residues such as O-glycosylation (in pentagon) and tyrosine sulfation (in **blue**). The transmembrane residues largely consist of hydrophobic amino acids (in **orange**). The intracellular amino acids (in **green**) at the C-terminal tail and the 'DRY' motif (commonly found motif in chemokine receptors) are the possible residues that involves in receptor desensitization through β-arrestin signalling cascade. The C-terminal tail is attached to the phospholipid bilayer through membrane raft.

```
        10         20         30         40         50         60
MESSGNPEST TFFYYDLQSQ PCENQAWVFA TLATTVLYCL VFLLSLVGNS LVLWVLVKYE

        70         80         90        100        110        120
SLESLTNIFI LNLCLSDLVF ACLLPVWISP YHWGWVLGDF LCKLLNMIFS ISLYSSIFFL

       130        140        150        160        170        180
TIMTIHRYLS VVSPLSTLRV PTLRCRVLVT MAVWVASILS SILDTIFHKV LSSGCDYSEL

       190        200        210        220        230        240
TWYLTSVYQH NLFFLLSLGI ILFCYVEILR TLFRSRSKRR HRTVKLIFAI VVAYFLSWGP

       250        260        270        280        290        300
YNFTLFLQTL FRTQIIRSCE AKQQLEYALL ICRNLAFSHC CFNPVLYVFV GVKFRTHLKH

       310        320        330
VLRQFWFCRL QAPSPASIPH SPGAFAYEGA SFY
```

Figure 1.13: XCR1 chemokine receptor protein sequence. Highlighted in yellow is the transmembrane α-helix sequence

Although the protein sequence of XCR1 is known, the exact arrangement on the cell membrane has not been described. The sequence alignment shares the same trait of that in G protein-coupled receptor with similar length of transmembrane protein and ~13% identical amino acids position identified (see **Figure 1.14**). When the sequence is aligned with known XCR1 protein sequences of other species such as mouse and rat, ~69% and ~67% of the amino acids are conserved respectively and ~62% for both species alignments to human (see **Figure 1.15**). Kroczek and Henn (2012) reported antigen cross-presentation of mouse XCR1 receptor activated by hLtn suggesting that the receptor activation is less species specific but more structure dependant. Among all chemokine receptors, XCR1 is the only one that shows this unique functional characteristic

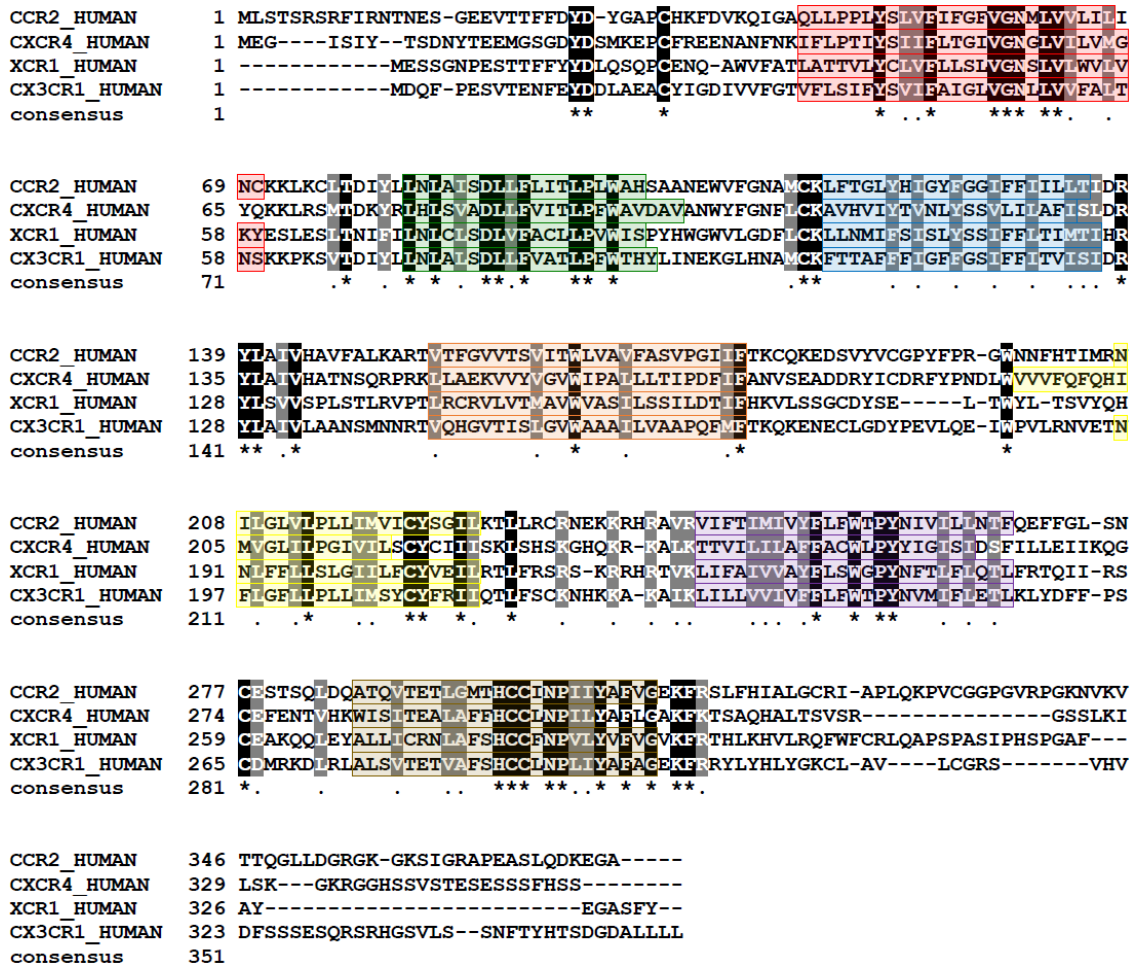

Figure 1.14: Multiple sequence alignment (MSA) between selected chemokine receptors families (CCR2, CXCR4, XCR1 and CX3CR1). Shaded in **black** indicating similar identity (*) of amino acid residues between the receptors while shaded grey is strongly similar residues (.). Highlighted in colours are the transmembrane α-helix sequence. Consensus: (*) similar identity, and (:) strongly similar. Alignment was performed using Clustal Omega and BOXSHADE. The information on the protein was obtained from UniProt database.

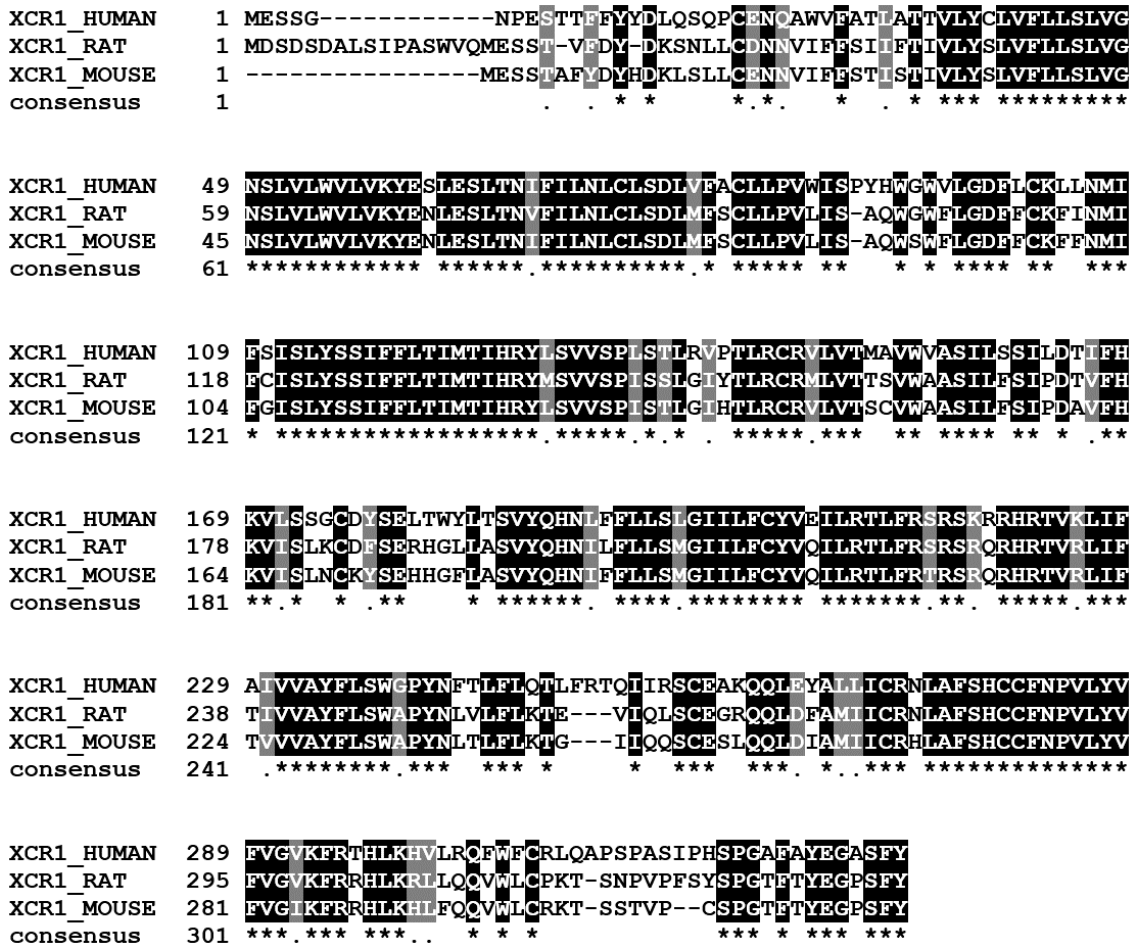

Figure 1.15: Comparison of XCR1 receptor between rat, human and mouse. Shaded in **black** indicating similar identity (*) of amino acid residues between the XCR1 receptors of selected species while shaded grey is strongly similar residues (.). Alignment was performed using Clustal Omega and BOXSHADE. The information on the protein was obtained from UniProt database.

1.10.3 Expression

XCR1 is highly expressed on T-cell lymphocytes mainly CD4+ and CD8+ T-cells (Hedrick *et al.*, 1997). The mRNA is strongly expressed in placenta and weakly in spleen and thymus (Yoshida *et al.*, 1998). Recently, XCR1 has been shown to be expressed in dendritic cells in lymph nodes involved in antigen cross presentation (Kroczek and Henn, 2012). XCR1 receptor expression has also been shown in normal oral mucosa and in OSCC (Khurram *et al.*, 2010). Higher *in vitro* and *in vivo* expression was seen in oral cancer cells and OSCC compared to normal (Khurram *et al.*, 2010).

Recently, XCR1 expression has been reported in epithelial ovarian carcinoma (Kim *et al.*, 2012) and breast cancer (Gantsev *et al.*, 2013) with up regulation of XCR1 receptor on the cancer cell surface. This is similar to some other chemokine receptors which have been reported to be upregulated in cancer cells to assist survival and growth. For example, overexpression of CXCR2 with CXCL1 and CXCL2 (the ligands) in breast cancer primes tumour survival at metastatic sites (Acharyya *et al.*, 2012) and migration to sites of metastasis appears to involve CXCR4 with elevated expression in 23 different types of cancer (Balkwill, 2004b). It appears that the XCR1 receptor may also play a similar role in cancer although it is not known whether or not all type of cancer cells express XCR1. For example, (Khurram *et al.*, 2010) found out that most OCCL express the receptor with variable levels of expression in a range of cell lines but Kim *et al.* (2012) showed that not all epithelial ovarian carcinoma express XCR1. Better understanding of XCR1 expression on epithelial cancer cells is needed to help characterise the role of XCR1 in other cancers.

1.11 hLtn (XCL1 & XCL2)

1.11.1 Discovery

The hLtn protein was first discovered during cytokine-producing profiling of mouse progenitor-T cell library (Kelner *et al.*, 1994). It was found that this cytokine was similar to CC and CXC chemokines and only attracted lymphocytes but not monocytes. Hence, it was named lymphotactin. It was also found to be produced in activated CD8+ activated and progenitor T-cells with abundance in spleen and thymus.

The human counterpart of this chemokine, human lymphotactin (hLtn) was discovered by three independent groups who named it **ATAC** (Activation-induced, T cell-derived, and Chemokine-related molecule) (Muller *et al.*, 1995), **SCM-1** (Single C-Motif-1) (Yoshie *et al.*, 1995) and human **lymphotactin** (Kennedy *et al.*, 1995). The gene is located on chromosome 1q23 in humans (Muller *et al.*, 1995).

Most of the previous studies focus on XCL1 rather than the second member of C chemokine family, XCL2 which is situated at chromosome 1q24 (NCBI, Gene ID: 6846). This protein has the same length and amino acids sequence to XCL1. The only sequence difference is the 7^{th} and 8^{th} amino acids which does not influence the protein structure. XCL2 has slightly higher affinity towards heparin even though the structure is very similar (Fox, Nakayama, *et al.*, 2015). This is probably due to the presence of two basic amino acids Arginine and Histidine at the 7^{th} and 8^{th} position providing basic residue which important in protein – GAG interaction (Hileman *et al.*, 1998).

1.11.2 Structure

hLtn belongs to the C-chemokine family which only has one disulphide bridge interconnected by Cys^{11} – Cys^{48}. As a result, the structure is somewhat unstable allowing it to interconvert between two different conformations (Peterson *et al.*, 2004).

hLtn has a molecular weight of 10 kDa (mature hLtn) or 12 kDa (with signal peptide). It has the basic structure of a chemokine, with three anti-parallel β-sheets and C-terminal α-helix (see **Figure 1.16**). The protein structure contains 15 basic amino acids making it a positively charged protein with a hydrophobic core and containing 114 amino acids overall (see **Figure 1.17**). Proteolytic cleavage removes the signal peptide located on Gly^{21} – Val^{22} leaving the mature hLtn with 93 amino acids (Peterson *et al.*, 2004).

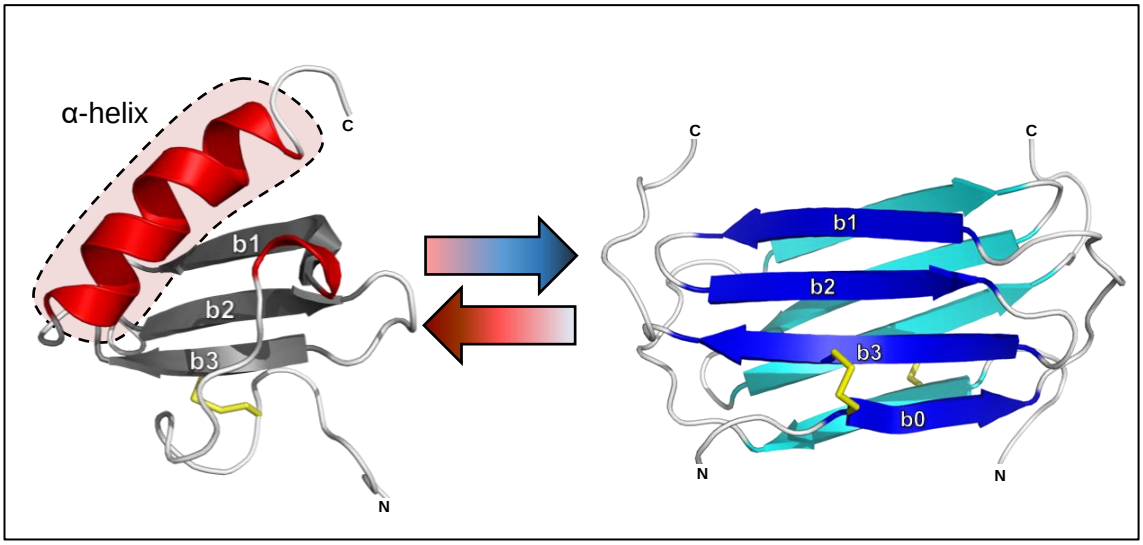

Figure 1.16: hLtn structure in physiological conditions. The canonical chemokine-fold for hLtn (left) and the novel dimeric four β-sheets structure (right) that was identified using nuclear magnetic resonance (NMR). The image was reproduced from Sun et al. (2011) using Pymol.

```
        10         20         30         40         50
MRLLILALLG ICSLTAYIVE GVGSEVSDKR TCVSLTTQRL PVSRIKTYTI

        60         70         80         90        100
TEGSLRAVIF ITKRGLKVCA DPQATWVRDV VRSMDRKSNT RNNMIQTKPT

       110
GTQQSTNTAV TLTG
```

Figure 1.17: Human lymphotactin sequence. Total of 114 amino acids including signal peptide (1-21 AA) highlighted in grey and mature protein sequence in yellow (22-114 AA) (sequence obtained from Uniprot_P47992).

Kuloglu *et al.* (2001) investigated the solution structure of hLtn and found that it has a monomeric structure but with some evidence suggesting it also exists as a dimer. The structure is salt and temperature dependent (Kuloglu *et al.*, 2002). It was also found that hLtn has two completely different, reversible protein conformations. The chemokine-like fold is monomeric and predominates at higher salt concentrations and at 10^{o}C temperature. The novel dimeric structure can be found at lower salt concentrations and at a temperature of 40^{o}C. Interestingly, both are distributed equally in physiological conditions (temperature 37^{o}C) (see **Figure 1.18**) and the conversion rate is ~1/s (Volkman, Liu and Peterson, 2009). It was suggested that this is due to the significant ionic strength required to hold the chemokine-fold. Molecular dynamic simulation also shows the importance of the salt concentration and temperature in the protein structure (Formaneck, Ma and Cui, 2006). The temperature dependence of ion-protein is sensitive to the local sequence especially at the C-terminal tail (Ma and Cui, 2006). It has been suggested that ionic charges in salt holds tryptophan of the α-helix structure pack together, conserving the structure (Lakemond *et al.*, 2000; Raghuraman and Chattopadhyay, 2006). Volkman, Liu and Peterson (2009) speculated that Arg^{23} and Arg^{43} hold the key to both structures' conversion by charge repulsion. But this only explains structural changes when considering the salt concentration. In the temperature scenario, dissociation of bonds holding the hydrophobic core is a probable explanation. Ala^{49}, Ala^{53} and Val^{59} provide a hydrophobic pocket for tryptophan and hold the α-helix structure and the β-sheet together. High energy breaks the bond that holds the structure. Nevertheless, it is difficult to explain how this can be translated *in vivo* and how physiological conditions allowing equal distribution of both hLtn forms.

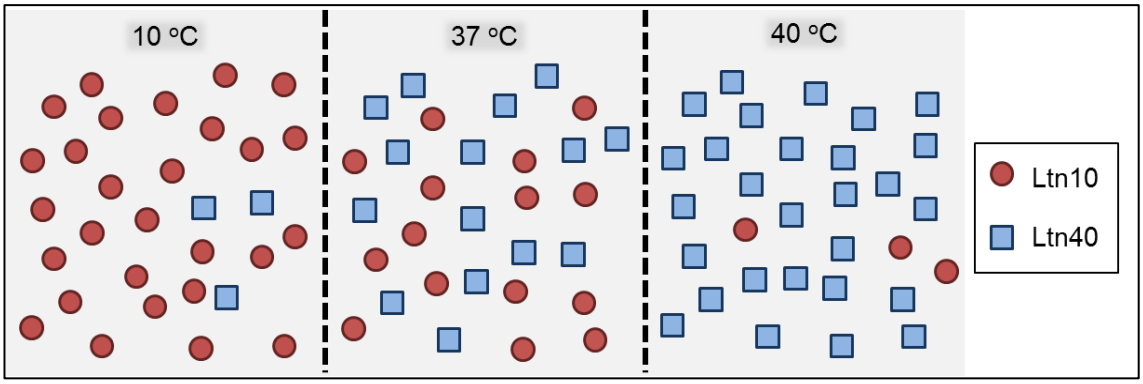

Figure 1.18: Distribution of hLtn forms at different temperatures. At low temperature, hLtn exists mostly in the canonical-chemokine fold (left) while a dimeric form exists at high temperatures 40°C (right). The structures are in equilibrium at 37°C (physiological condition, middle).

The conformation change between two protein structures in hLtn is a two-step process with no intermediary stable species (Tyler *et al.*, 2011). Some suggest that conformational change requires a "bridge" between the two structures (Sauer *et al.*, 2000). Other proteins such as the Mad2 spindle checkpoint protein and chloride intracellular channel 1 (CLIC1) are known to demonstrate the ability to switch between different fold (Bryan and Orban, 2010). Yet both are not as unique as hLtn as they form a stable intermediate variant while hLtn can interconvert without an intermediate. A model simulation shows that interconversion between two different protein conformations lies in the conserved local contacts that allow the reversible change (Camilloni and Sutto, 2009). Furthermore, the rearrangement is freely reversible with no effect from repeated temperature titrations (Tuinstra *et al.*, 2007). Organic acids abrupt the disulphide bridge result in loss of tertiary and secondary structure as well as cold denaturation where the wild type hLtn is the most sensitive compared to the mutant variants (Sun *et al.*, 2011).

Kroczek and Henn (2012) reported cross-species activation of hLtn and XCR1. The study was performed using hLtn to activate XCR1 receptor in the mouse. By comparing the structure for several species (see **Figure 1.19**), 20 amino acids are shown to be conserved across species. This illustrates that hLtn activation of XCR1 may be related to the structure rather than specific amino acid sites on the protein. Further investigation of cross-presentation may elucidate further this theory.

(Dorner *et al.*, 1997) identified that almost 40% of hLtn is O-linked glycosylated and the remaining are terminally sialylated. Others also report that some of the hLtn

population is partially folded (Marcaurelle *et al.*, 2001). hLtn can still activate Ca^{2+} signalling and chemotaxis without the presence of glycosylation but the biological activity is slightly reduced (Dong *et al.*, 2005). This confirms that hLtn is functional even in unglycosylated form. Furthermore, producing hLtn using mammalian or insect cells will produce less yield and time consuming compared to *E. coli* while maintaining glycosylation.

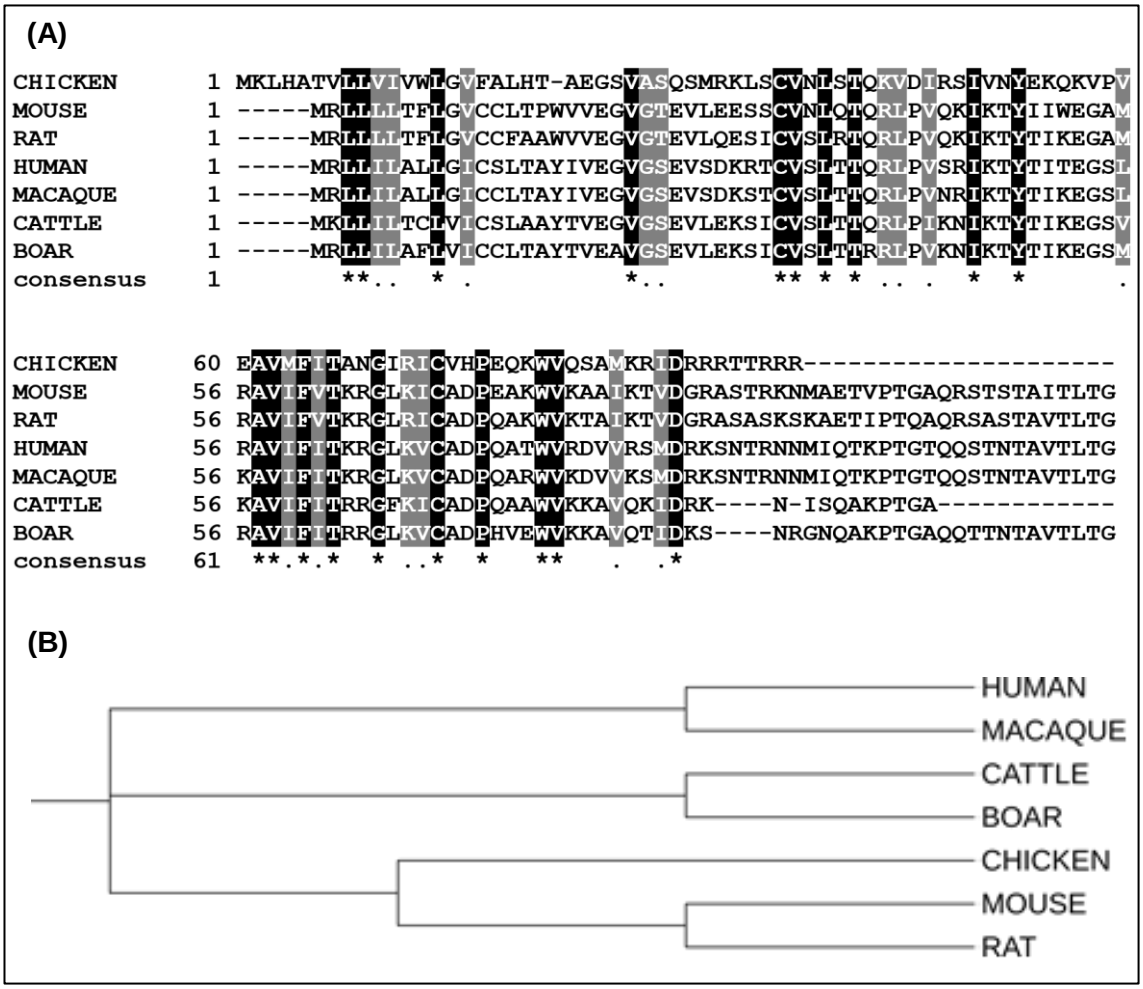

Figure 1.19: Comparison of hLtn (XCL1) in several species. **(A)** Alignment of XCL1 in different species). Shaded in **black** indicating similar identity (*) of amino acid residues between the receptors while shaded grey is strongly similar residues (.). All contains 114 amino acids (including signal peptide) except for bovine and chicken (only 97 amino acids), and boar (110 amino acids). **(B)** Taxonomy of hLtn between the species. The protein sequences were obtained from UniProt website and the multiple sequence alignment (MSA) was performed using Clustal Omega and Boxshade.

1.11.3 Expression

hLtn is primarily expressed in spleen and lung tissue (Kelner *et al.*, 1994; Yoshida *et al.*, 1999) but the specific cells expressing hLtn in these tissues have not been reported. Mostly, hLtn expression can be seen in activated CD8+ T-cells (Muller *et al.*, 1995), progenitor T-cells (Kelner *et al.*, 1994), natural killer (NK) cells (Hedrick *et al.*, 1997), neutrophils (Huang *et al.*, 2001) and lymphocytes to induce chemotaxis as part of the immune response.

hLtn can also be expressed in non-lymphoid cells. Recently, the expression was reported in synovial fluid of patient with meniscal tears in their knee (Nair *et al.*, 2015). Human intestinal mast cells also express multiple chemokines including hLtn due to its immunoregulatory role (Feuser *et al.*, 2012). The synovial fluid of patients with rheumatoid arthritis has also been shown to contain hLtn indicating that hLtn play a role in the immune response and chronic inflammatory conditions outside the lymphoid system (Blaschke *et al.*, 2003).

1.11.4 Functions

hLtn or XCL1 is a chemotactic chemokine which only attracts leukocytes and T-cells. hLtn binds with high affinity to glycosaminoglycan (GAG) which is important for the interaction with lymphocytes *in vivo* (Peterson *et al.*, 2004).

Some studies suggest a role for hLtn in allograft rejection (Wang *et al.*, 1998). The level of mRNA is highly upregulated in the transplant area whilst none is detectable in isografts. This suggests that hLtn is an immune system mediator, recruiting lymphocytes during organ rejection.

1.12 hLtn and XCR1 in Tumour Biology

The first recorded involvement of hLtn and XCR1 in tumour biology was by Khurram *et al.* (2010). In this study, normal oral epithelial cell was shown to express XCR1 receptor as well as cancer cells. This was also the first time that XCR1 receptor expression was demonstrated outside the immune system and inflammatory cells. Oral cancer cell lines were also shown to contain hLtn mRNA and cytoplasmic protein.

Six years ago, (Kim *et al.*, 2012) showed that primary and metastatic human epithelial ovarian carcinoma cells express XCR1 receptor while the normal ovarian epithelial cells do not. It was also demonstrated that XCR1 receptor expression induced pro-metastatic behaviour in the cells. This suggests a role for the XCR1 receptor in facilitating metastasis.

XCR1 was also found to be expressed in breast cancer which contributes to lymphoid neo-organogenesis (Gantsev *et al.*, 2013). Müller *et al.* (2001) performed a screening of chemokine receptor expression and found no XCR1 expression in breast cancer cells and normal primary mammary epithelial cells except for malignant melanoma cells. This indicates that XCR1 is not necessarily expressed by all breast cancer cell lines. Even in OSCC, although, a range of all oral cancer cell lines express XCR1, the level varies widely (Khurram *et al.*, 2010).

OCCL contain cytoplasmic hLtn but the stimulus of secretion is not known (Khurram *et al.*, 2010). It would be interesting to investigate factors that induce release of hLtn from cancer cells. This will allow an understanding of the mechanism in relation to metastasis.

1.13 hLtn (XCL1) Variants

To study both hLtn functional structures, stable production of mutant variants is required. This would allow the hLtn10 and hLtn40 variants to remain locked in the designed state even at different temperature and physiological conditions.

1.13.1 hLtn10 variant

The first paper on the production of mutant hLtn10 was published in 2007 (Tuinstra *et al.*, 2007). The paper proposed the addition of a second disulphide bridge, which wild-type hLtn lacks in order to hold the protein structure into its canonical chemokine-fold. By comparing hLtn to a CC chemokine, CCL15 (see **Figure 1.20**), CC1 and CC3 mutant sequences were acquired. Both were tested for chemokine functional activity.

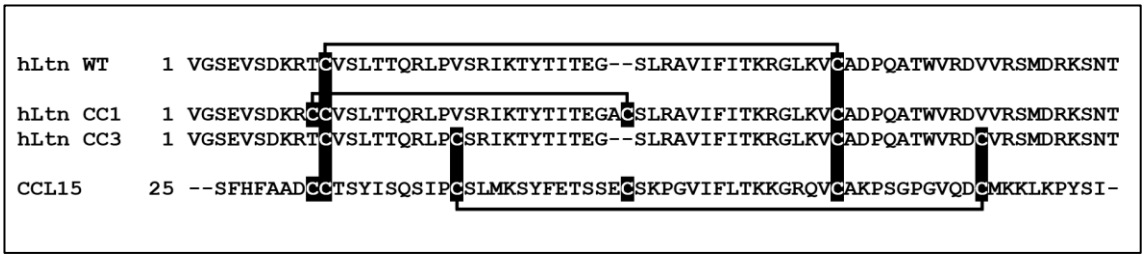

Figure 1.20: Sequence alignment for initial hLtn10 variant structure validation. The sequences were compared against a CC chemokine (CCL15) with three disulphide bridges to predict the placement of the second disulphide bond for hLtn to create the canonical chemokine fold. The CC1 mutant is based on the first disulphide alignment to CCL15, while the CC3 mutant disulphide is based on the additional unusual third disulphide bridge present in CCL15. The sequences were obtained from UniProt website and the MSA performed using ClustalOmega and Boxshade. The image was reproduced from Tuinstra *et al.* (2007).

The CC1 mutant has a cysteine addition at location T10C and Ala-Cys dipeptide insertion between Gly^{32} and Ser^{33}. hLtn lacks disulphide connection between the N-terminal and the 30s loop compared to other chemokine family. Tuinstra *et al.* (2007) suggested that this locks the protein into hLtn10 conformation but may also restrict its biological function and mobility as it lacks cysteine on the 30s loop. A second design of hLtn10 variant was also constructed, CC3 by overlapping it with the third disulphide

bridge location of CCL15. The overlaid structure proposed hLtn mutation at V21C and V59C (see **Figure 1.21**). Both hLtn10 mutants retain their structure even when introduced to extreme temperature (hLtn40 conditions). Ca^{2+} flux activation was studied to determine functionality, with CC1 and CC3 both showing the same EC50 value (half maximal effective concentration) compared to the wild-type (normal hLtn).

XCR1 is activated by hLtn but the mechanism is yet not fully understood. Some researchers suggest that N-terminus is important for receptor activation while others suggest the C-terminus is equally important for activation *in vivo* (Tuinstra *et al.*, 2007). Tuinstra *et al.* (2007) showed that the N-terminus is important in XCR1 activation. Experiment was performed using truncated mutant protein where the first Valine of the mature hLtn sequence was replaced or the N-terminus has an additional resulting in no Ca^{2+} flux activation. Thus, the authors suggest that the C-terminus does not have a role in XCR1 activation. The variant that showed no response lacks the α-helix structure and adopts the hLtn40 conformation. However, Hedrick *et al.* (1997) reported that the truncated C-terminal hLtn is inactive and suggested it is likely to be important *in vivo*. This suggests that hLtn can behave rather differently *in vivo*. Some of the experiments reported in literature were performed using commercial hLtn lacking the first Valine indicating that this was functionally active *in vitro* (Khurram *et al.*, 2010). These first Valine may thus not be essential, but the activity may be less compared to hLtn with 93 amino acids. This remains to be elucidated.

Tuinstra *et al.* (2007) replaced all the methionine residues in the hLtn sequence to accommodate the purification and cleavage process during protein production using cyanogen bromide (CnBr). Although it did not cause any major alteration to the protein structure, it is usually ideal to keep the protein sequence changes to a minimum to allow close resemblance to the natural form. Furthermore, although it was also reported that CC1 and CC3 both have the canonical chemokine-fold and activity, the paper only provides detail of the CC3 construct and not the other construct. This is probably due to the mutation applied where CC3 structure has more resemblance to the wild type hLtn which its 30s loop of the structure is not restricted.

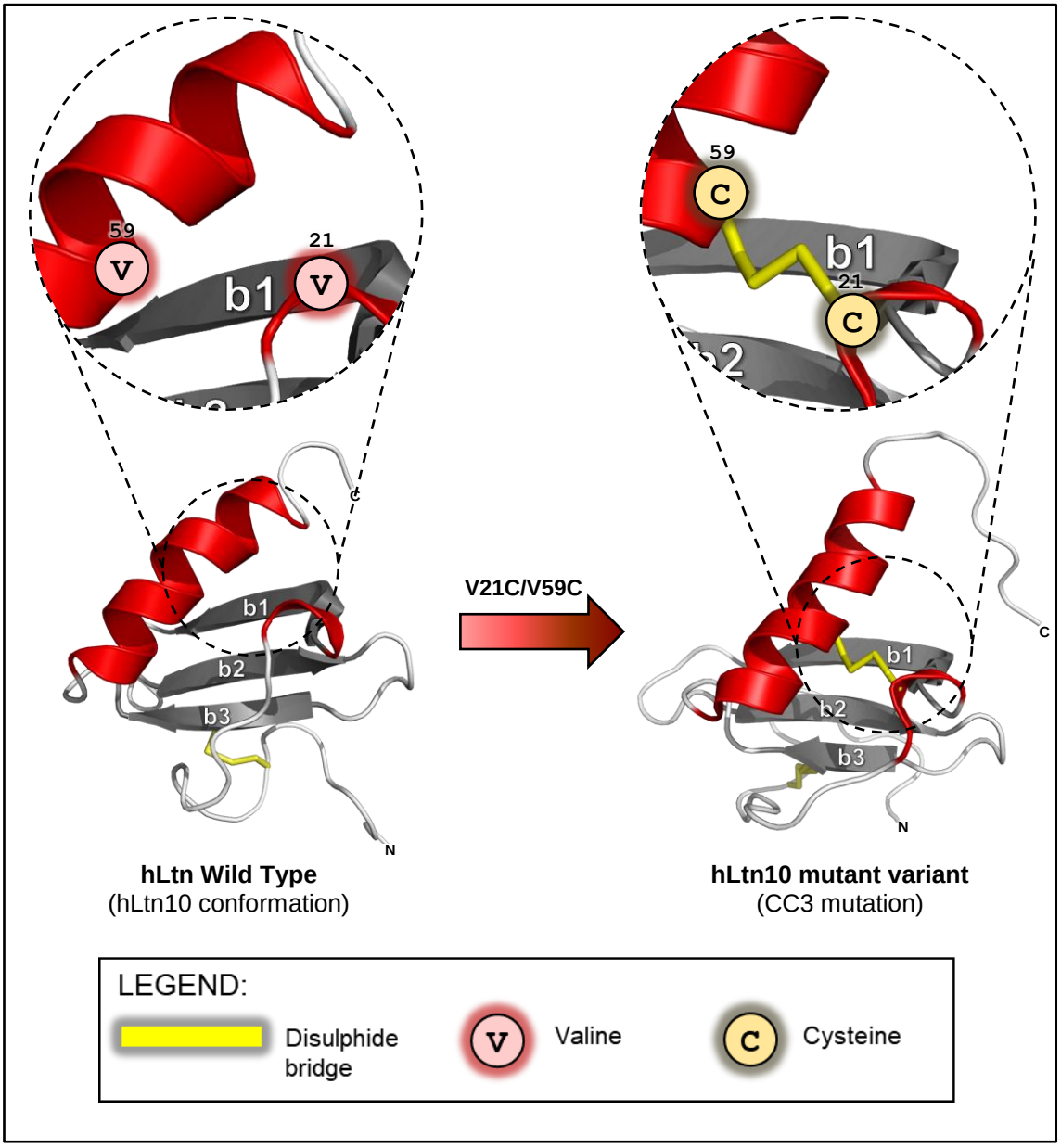

Figure 1.21: hLtn10 mutant variant. Conversion of hLtn structure (left) to hLtn10 mutant variant (right) performed by adding an extra disulphide bridge, where Val^{21} and Val^{59} are both replaced by cysteine. The image was inspired from Sun et al. (2011) and created using Pymol. The protein structure files (ID: 1J9O and 2HDM) were obtained from PDB website.

1.13.2 hLtn40 variant

To create hLtn40 variant, changing the only tryptophan in the sequence, Trp^{55} to aspartic acid (Asp) removes the α-helix structure that holds the hydrophobic core of the protein, allowing it to form the novel four β-sheets structure (see **Figure 1.22**) (Tuinstra *et al.*, 2008). Due to their proximity, Ala^{49}, Ala^{53} and Val^{59} together with Trp^{55} create a hydrophobic pocket, holding the α-helix structure in canonical chemokine-fold.

In hLtn40, the N-terminus forms a new β-sheet structure, denoted as β0-sheet. While β1, β2 and β3 sheets still exist in the conformation, they undergo some changes. The β-sheets are slightly longer in hLtn40 and the β2-sheet is shifted forming an anti-parallel β-sheet connection with the β1 and β3 strands (see **Figure 1.23**). Furthermore, the 30s and 40s loop of hLtn40 is shorter. This structure replaces virtually all the tertiary interactions in hLtn10 with different tertiary and quaternary contacts in hLtn40. Furthermore, the hydrophobic core region hidden in hLtn10 is exposed in hLtn40. This leads to dimer formation in solution. The Lys^{25} and Glu^{31} of hLtn40 stabilize the dimer by hydrophobic and electrostatic interaction (see **Figure 1.24**). In addition, the hLtn40 β2 strand seems to rotate 180^{o} during this conversion. The R groups of Val^{37}, Phe^{39} and Thr^{41} that are buried in the hydrophobic core of hLtn10 structure are completely solvent-exposed in hLtn40. Val^{37} and Phe^{39} contribute to the hydrophobic core of the monomer form and are essential in stabilising the canonical chemokine-fold.

The hLtn40 variant has a high affinity for heparin (Tuinstra *et al.*, 2008). This is important *in vivo* as glycosaminoglycans (GAGs) are a highly abundant component in the ECM and on the cell surface. A class of GAG, heparin/heparan (HSGAG) plays a role in biological activities such as cell adhesion (Sasisekharan, Raman and Prabhakar, 2006). GAGs provide a platform for cell adhesion and interacts with the cell through cell-substratum adhesion and hyaluronate in GAGs contributes to appropriate cell movement. The hLtn10 mutant can activate XCR1 in the presence of heparin whereas both the hLtn40 and wild type hLtn are unable to do so (Tuinstra *et al.*, 2008). This raises the question of the role of the ECM *in vivo* or whether other molecules may be required to allow hLtn-XCR1 association. Also, heparin may be key as it provides hLtn with a tendency to remain in hLtn40 structure *in vivo*. Furthermore, while the active chemokine-fold polymerizes and binds to the cell surface GAG (Hoogewerf *et al.*, 1997), the wild type hLtn and hLtn10 variant have less or no affinity towards it (Tuinstra *et al.*, 2008).

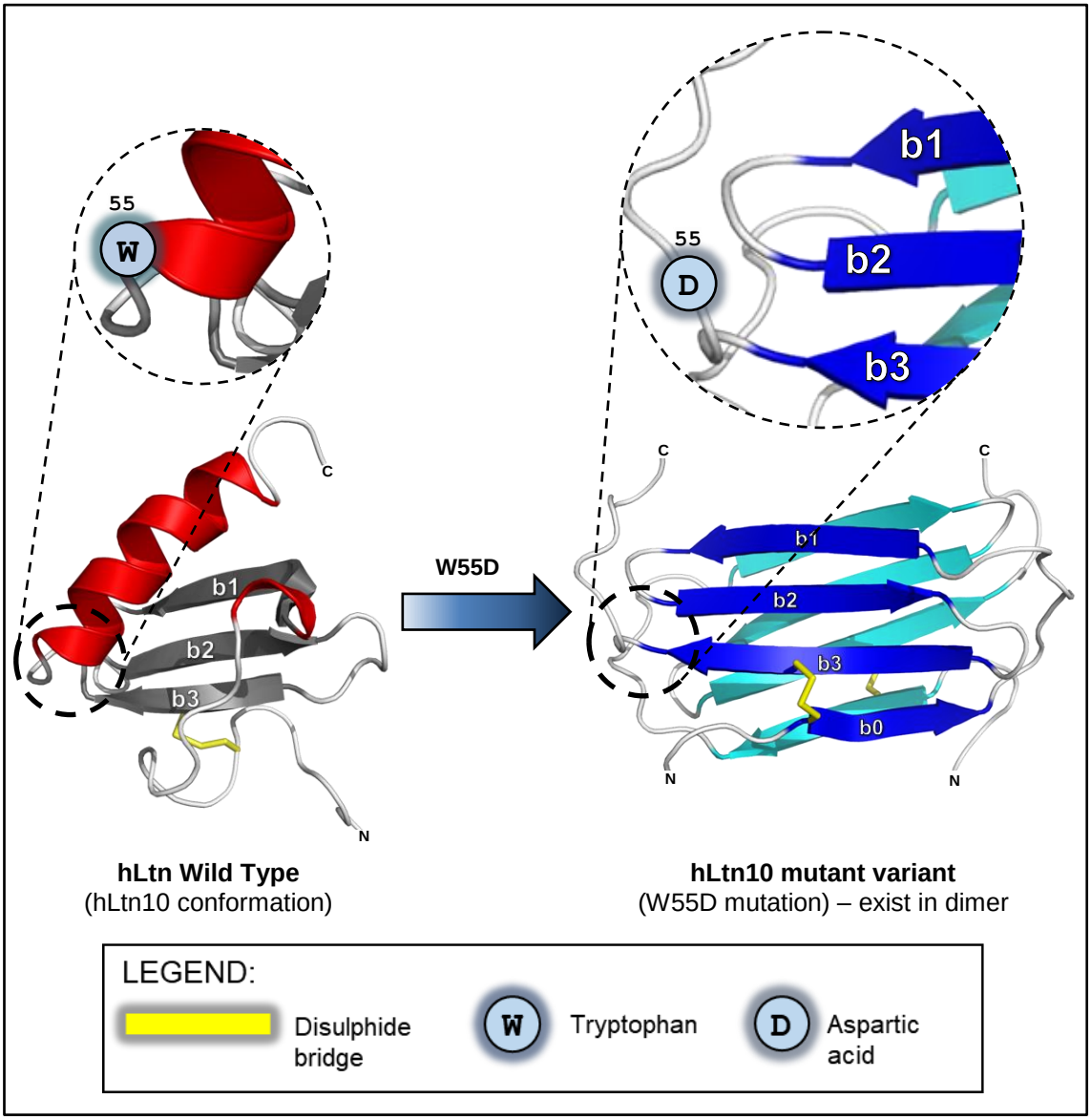

Figure 1.22: hLtn40 mutant variant. Conversion of hLtn structure (left) to hLtn40 mutant variant (right) is achieved by substituting tryptophan (W) to aspartic acid (D) in the α-helix structure on position 55th amino acid. Tryptophan residue is responsible for holding the α-helix structure of canonical hLtn fold. The image was inspired from Sun et al. (2011) and created using Pymol. The protein structure files (ID: 1J9O and 2JP1) were obtained from PDB website).

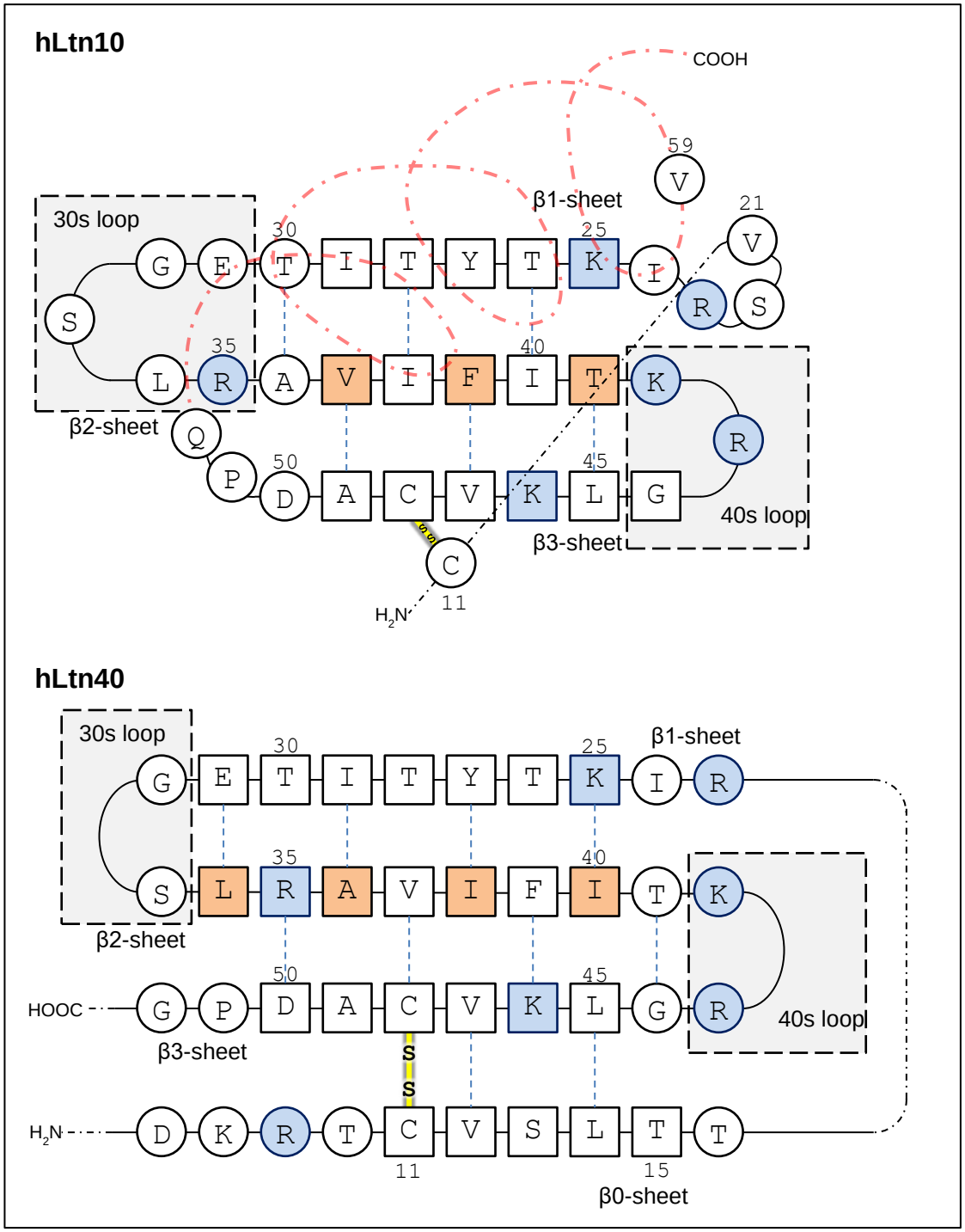

Figure 1.23: Comparison of the β-sheets structure for hLtn10 (top) and hLtn40 (bottom) of wild type conformation. Amino acids in square boxes (□) are the one that involve in β-sheet. Blue dotted-lines (-----) are the hydrogen bonds forming between the β-sheets. Amino acids in **blue** are basic while in **orange** are the residues that contribute to the structure hydrophobic core. The image was reproduced and adapted from Kuloglu *et al.* (2002) .

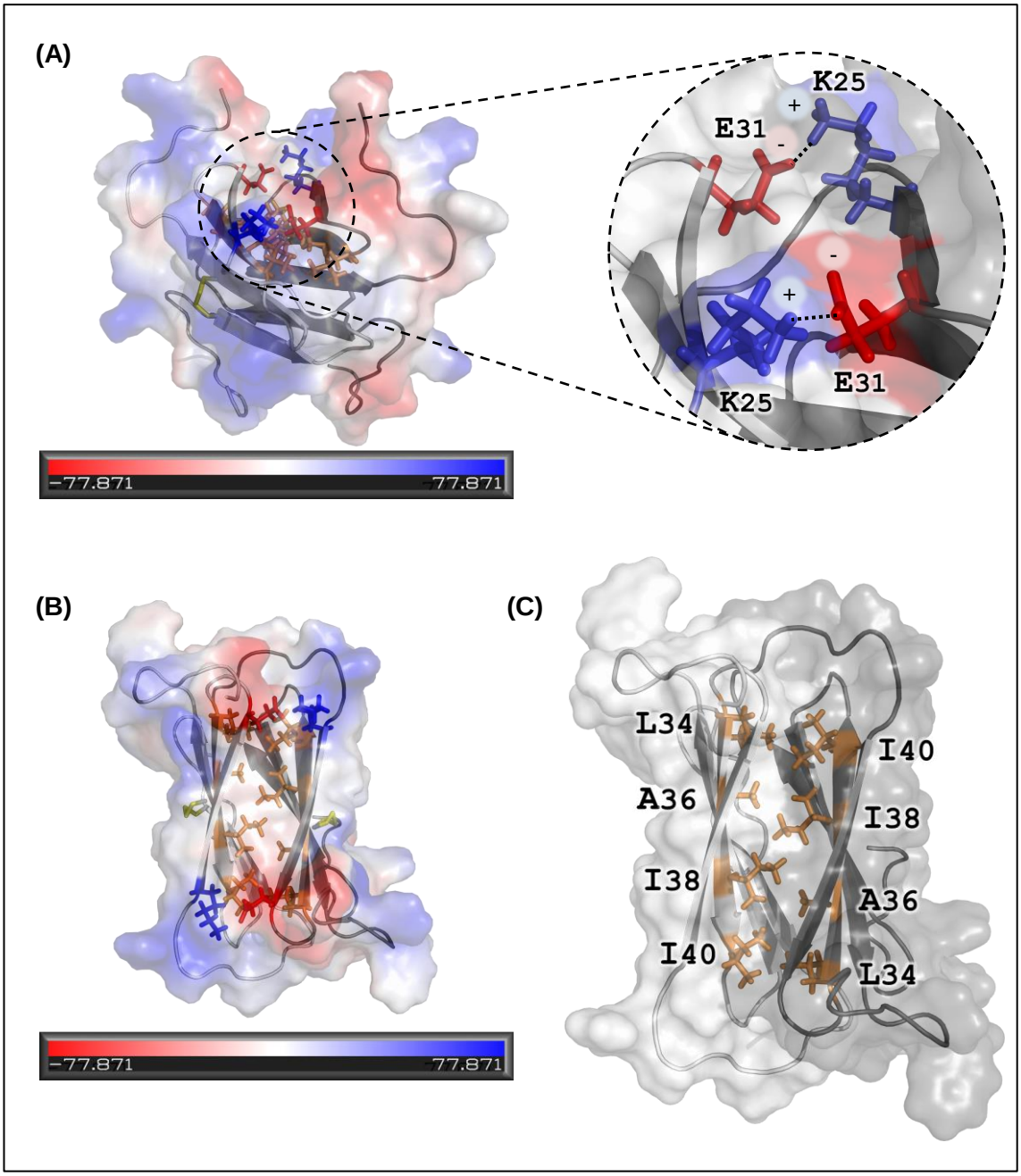

Figure 1.24: Hydrophobic and electrostatic stabilization of hLtn40 dimer. The image on the left is the dimer presented with the surface electrostatic potential. **(A)** Side view of protein dimer. Lys^{25}, a basic amino acid (R group in **blue**) and Glu^{31}, an acidic amino acid (R group in **red**) (shown in sticks) are solvent exposed, forming a salt bridge (combination of electrostatic interaction and hydrogen bonding with water). **(B)** Aerial view of the protein dimer displaying **(C)** the hydrophobic contacts (in **orange**) forming the dimer core (Leu^{24}, Ala^{36}, Ile^{38}, Ile^{40}) with white and grey surface shade. In monomer, the responsible R groups are solvent exposed, resulting in a totally different hydrophobic core contacts (refer **Figure 1.23**). The image was created using Pymol and the protein structure file (ID: 2JP1) was obtained from PDB website.

1.14 Studies on hLtn

There are several studies on hLtn in relation to its use in potential as a therapeutic agent. (Cairns *et al.*, 2001) stated that transforming myeloma cells to express hLtn, reduces their growth. By transfecting hLtn-expressing myeloma cells into nude (immune system inhibited) and BALB/c (laboratory-bred) mice, tumour growth was reduced. hLtn recruits $CD4^+$ and $CD8^+$ T-cell as well as neutrophils to the tumour sites as part of the antitumor response and this may explain these findings.

A study by Fossum *et al.* (2015) used a XCL1-fusion protein to target influenza virus. The DNA vaccines encodes a dimeric XCL1-hemagglutinin fusion protein vaccibodies targeting XCR1 expressing dendritic cells to induce T-cell responses. Guzzo *et al.* (2013) discovered that hLtn inhibits HIV-1 virus entry to host cells at an early stage, although it requires the hLtn40 variant structure for the blockade. HIV-1 virus usually mimics surface receptors on the cell surface to allow fusion and entry (Wilen *et al.*, 2012). The possible explanation is that the dimer is blocking the activation of XCR1 as the receptor is found to be novel co-receptor for XCR1 (Shimizu *et al.*, 2009).

hLtn also has potential as an antimicrobial agent (Nguyen and Vogel, 2012; Nagata, Nishiyama and Ikazaki, 2013). By using Nuclear Overhauser Effect Spectroscopy-Nuclear Magnetic Resonance NOESY-NMR, the dimer interface is observed to have clusters of high positively charged surface that can interact with bacterial membranes.

Recently, cytomegalovirus was discovered to express vXCL1 (v denotes virus) with 96 amino acids and which can be used by the virus to hide from immune system (Geyer *et al.*, 2014). The structure is similar to hLtn and can be detected 13 hours after infection. The vXCL1 can attract CD4(-) XCR1-expressing dendritic cells and subvert the immune response.

CXCL10 and hLtn were recently adapted to form a fusokine, a fusion of two cytokines for therapeutic potential (Sanchez-Lugo *et al.*, 2015) to increase the bioavailability and therapeutic potential of the chemokines. The result showed higher chemotactic effect compared to individual chemokines alone in attracting CXCR3 expressing tumour cells. Although it is not known whether the fusokine can attract XCR1 expressing cells as well.

1.15 Aims and Hypotheses of the Study

hLtn and XCR1 have shown to be involved in oral cancer progression and may play a role in local spread and lymph node metastasis. Also, due to its metamorphic properties, we want to further understand the contribution of each hLtn conformation in cancer pathogenesis.

The overall aim of this study is to investigate further the roles of hLtn and XCR1 in OSCC in the context of the tumour microenvironment. Ultimately, the aim to produce a functional hLtn variant mutants with locked conformation and study their effect on the behaviour on oral cancer cell lines. The specific aims of each chapter are listed below:

1) **Chapter 2: *Ex Vivo* Expression of XCR1 and hLtn in Oral Cancer Tissues and Lymph Nodes**
   - ❖ To investigate and quantify the *ex vivo* expression of XCR1 receptor and hLtn and to compare expression between primary tumour and metastatic deposits and correlate with clinicopathological features.

2) **Chapter 3: Regulation of XCR1 and hLtn (XCL1) Expression in Oral Cancer Cell Lines by hLtn & Conditioned Media from Oral Fibroblasts**
   - ❖ To determine the role of hLtn in regulation of the XCR1 receptor in OCCLs.
   - ❖ To understand the role of fibroblasts, in context of tumour microenvironment on the expression of XCR1 and hLtn in OCCLs.

3) **Chapter 4: Design and Production of Recombinant hLtn Variants**
   - ❖ To design and produce functional hLtn variants (WT, CC3 and W55D mutant).

4) **Chapter 5: The Effect of Recombinant hLtn on the Behaviour of Oral Cancer Cell Lines**
   - ❖ To study the effect of hLtn and each locked conformation of hLtn on the behaviour of OCCLs in range of effects (proliferation, adhesion and migration).

CHAPTER 2

EX VIVO EXPRESSION OF XCR1 AND hLtn IN ORAL CANCER TISSUES AND LYMPH NODES

CHAPTER 2: EX VIVO EXPRESSION OF XCR1 AND hLtn IN ORAL CANCER TISSUES AND LYMPH NODES

2.1 INTRODUCTION

XCR1 and hLtn expression has been shown to be present in normal and cancerous tissue. In case of oral mucosa, the expression is seen in the basal layer of normal epithelium, whereas expression is more diffuse in primary oral squamous cell carcinoma (OSCC) and metastatic deposits (Khurram *et al.*, 2010). Due to the proximity and OSCC preference for lymphatic spread, metastasis is usually to lymph nodes. XCR1 mRNA expression has been shown in normal placenta, spleen and thymus tissue (Yoshida *et al.*, 1998). While in lung (T. Wang *et al.*, 2015), breast (Yang *et al.*, 2017), and ovary (Kim *et al.*, 2012), XCR1 receptor is present only in cancerous tissue. While for hLtn, expression in tissue only has been shown in OSCC (Khurram *et al.*, 2010) but none has been reported in other cancers. The literature is heavily focussed on the receptor but not on the ligand hLtn. This chapter further investigated the expression of XCR1 receptor and its ligand in primary and metastatic OSCC, and reactive lymph node. Literatures suggest that like other chemokines, spatial expression of XCR1 by tumour cells and hLtn in lymph node may contribute to lymphatic spread.

2.2 AIM

The aim of this chapter is to investigate and quantify the *ex vivo* expression of XCR1 receptor and hLtn and to compare expression between primary tumour and metastatic deposits and correlate with clinicopathological features.

2.3 MATERIALS AND METHODS

2.3.1 Materials

List of detailed information of the materials (reagents, kits, equipment, software and miscellaneous) used in the chapter can be found in **Appendix 1-5**.

2.3.2 Tissue cohort

Tissue samples were identified using the local pathology database and retrieved from the archive (ethical approval reference 07/H1309/150) (**Table 2.1**). A cohort of 15 samples was chosen including five primary oral tumours with matched metastatic lymph nodes and, five reactive lymph nodes.

Table 2.1: Clinicopathological data of the patient tissue cohort

	Tumour
Total number of patients	5
Sex	
Men	3
Women	2
Age: median [range]	66 [40-72]
Tumour grade	
Well	-
Moderate	2
Poor	3
Tumour size (mm)	26 [9-50]
Tumour invasion depth (mm)	8 [2-27]
Lymphovascular invasion	2
Perineural invasion	3

2.3.3 Haematoxylin and Eosin (H&E) Staining

Principle: Haematoxylin is a basic dye that has the affinity to stain acidic or basophilic structures purplish blue. DNA in the nucleus, and RNA in ribosomes and in the rough endoplasmic reticulum are both acidic, thus haematoxylin binds to them and stains them purple. Eosin is an acidic solution (negatively charged) which stains basic or acidophilic structures red or pink. Cytoplasm contains many proteins, which are basic allowing eosin to bind to these proteins and stains them pink (**Figure 2.1**). Under optical microscopy, the observation of tissue can be described as the following: erythrocytes are cherry red; collagen is pale pink; cytoplasm is reddish pink and nuclei are bluish purple.

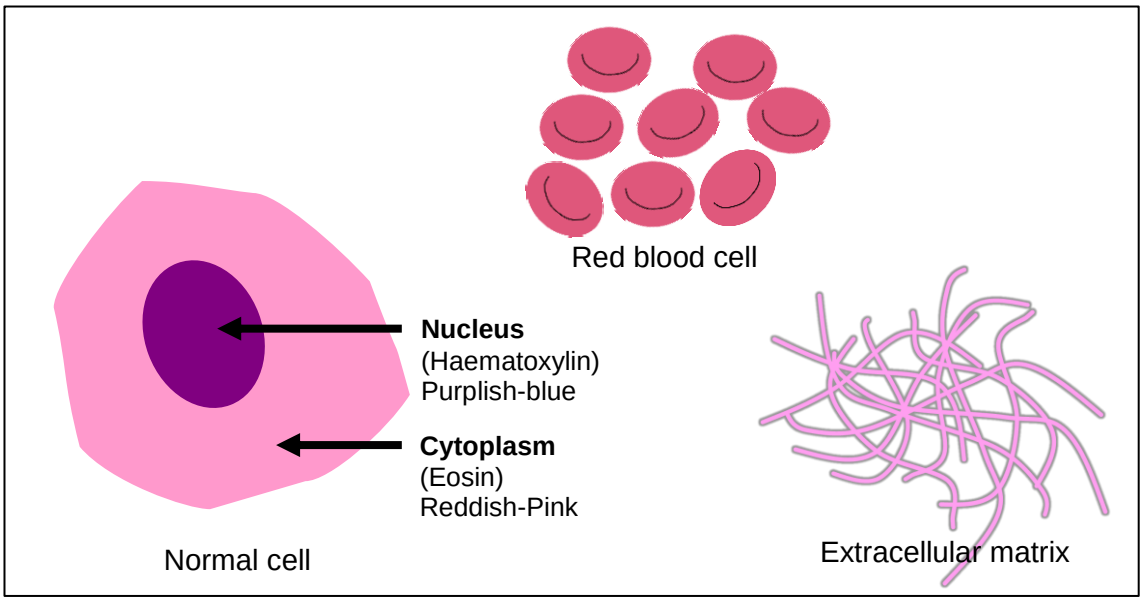

Figure 2.1: Explanation of H&E staining.

Procedure: 5 µm thick sections from FFPE (formalin-fixed paraffin-embedded) tissue blocks were mounted on SuperFrost® Plus microscope slide (Thermo Scientific, Paisley) and heated in an oven at 65°C for 15 minutes to allow the tissue to bind to the slide surface. Xylene was used to deparaffinise the tissue slides and ethanol to dehydrate the FFPE tissue. The sections were stained using a Leica ST4040 machine with setting 45 seconds per solution as in **Table 2.2**. The tissue was covered in mounting media DPX (Cat#: 44581; Sigma-Aldrich, Dorset, UK) and glass cover slips used to cover the tissue. The slides analysed using a widefield light microscope attached with camera. Images were obtained using Cell^D software (Olympus, Essex, UK).

Table 2.2: Iteration washing step for haematoxylin & eosin (H&E) staining.

No		Solution	Function
1		Xylene	Deparaffinise the FFPE Intermediate clearing solvent
2		Xylene	
3		Xylene	
4		99% IDA	Dehydrate tissue section
5		99% IDA	
6		70% IDA	
7		Distilled water	Tissue hydration
8		Distilled water	
9		Harris' haematoxylin (Shandon)	Stain nucleus
10		Harris' haematoxylin (Shandon)	
11		Harris' haematoxylin (Shandon)	
12		Harris' haematoxylin (Shandon)	
13		Running tap water	To remove residual haematoxylin
14		0.1% (v/v) acid alcohol	To remove the haematoxylin that does not attach
15		Running tap water	To remove residual acid alcohol
16		Scott's Tap Water Substitute	To intensify the blue colour from the haematoxylin stain
17		Running tap water	To remove residual Scott's tap water
18		Eosin Y – aqueous (Shandon)	Stain cytoplasm
19		Eosin Y – aqueous (Shandon)	
20		Eosin Y – aqueous (Shandon)	
21		Running tap water	To remove residual eosin
22		99% IDA	Dehydrate the tissue section
23		99% IDA	
24		99% IDA	
25		Xylene	Intermediate clearing solvent
26		Xylene	
27		Xylene	
28		Xylene	

2.3.4 Immunohistochemistry (IHC) Staining by Precipitation

Principle: IHC is a technique to investigate the distribution and spatial localization of specific protein of interest in tissue. The technique uses an antibody to target the epitope of the protein of interest. Biotinylated secondary antibody is used which binds to the primary antibody raised to recognise specific epitope of the animal used to produce the primary antibody. Avidin-biotin complex is added to further enhance the signal detection. For the enzyme substrate, peroxidase is added in conjunction of the chromogen used for optical identification of the antibody location on tissue section attachment. The mechanism of the staining is summarised in **Figure 2.2** below.

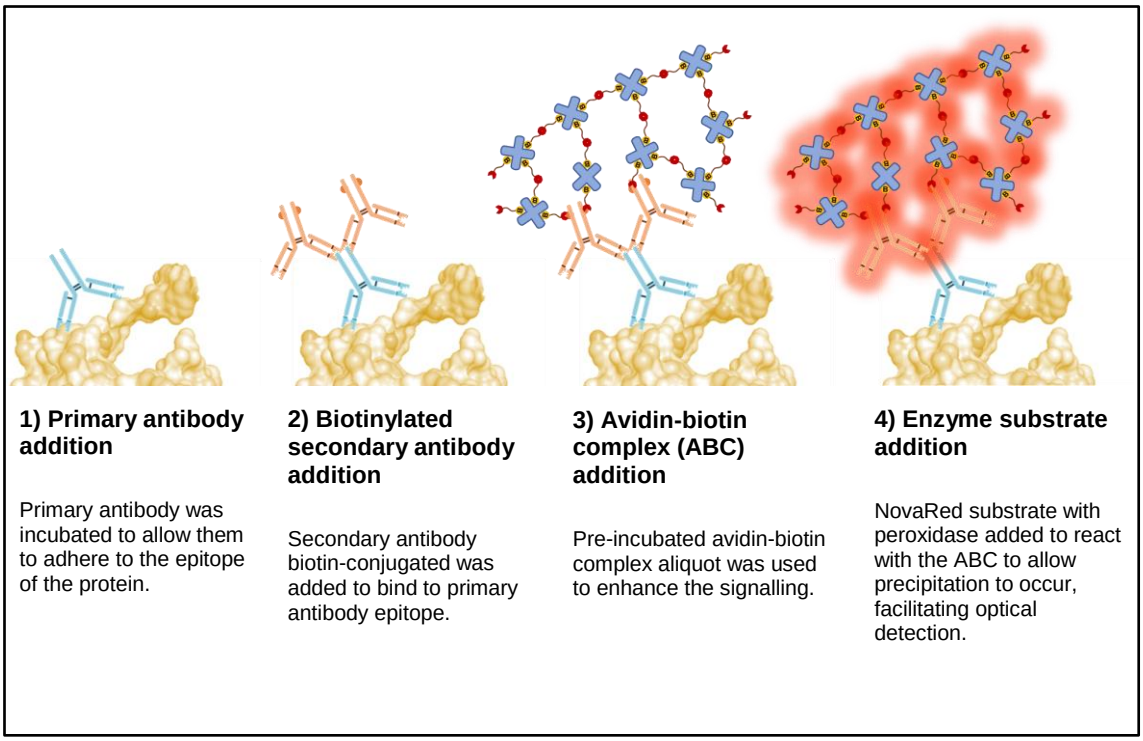

Figure 2.2: Illustration of steps involved in IHC.

Procedure: 5 µm thick tissue sections were treated with xylene to remove wax and then in ethanol for 5 min twice each. Hydrogen peroxide (2%) in methanol was used to block endogenous peroxidase for 20 minutes. Heat-induced antigen retrieval (HIAR) was performed by submerging the slides in 10 mM sodium citrate buffer (pH 6.0) and heating for 8 min at maximum power in a microwave. Non-specific protein binding was blocked by incubating the tissue section for 30 min with 100% serum (goat serum for antibodies raised in rabbit and horse serum for antibodies raised in mouse). Polyclonal anti-human XCR1 antibody (Cat#: LS-A158; LS-Bio, Nottingham, UK) (concentration 10 µg/mL) and monoclonal anti-human XCL1 antibody (Cat#: LS-B5938; LS-Bio, Nottingham, UK) (concentration 20 µg/mL) were placed onto the respective slides overnight at 4°C. For

negative control and blocking, goat serum was used for XCR1 and horse serum for XCL1. The excess primary antibody was tipped, and the residual was washed off twice. All the washing steps were performed with PBS. Secondary antibody from Vectastain® Elite® ABC-HRP Kit with Peroxidase was incubated for 30 minutes in respective treated slides; rabbit IgG (Cat#: PK-6101, Vectastain, UK) for XCR1 while mouse IgG (Cat#: PK-6102, Vectastain, UK) was used for XCL1. Avidin-biotin complex (ABC) solution was prepared 30 minutes before application onto the slides in accordance with the manufacturer's instruction (VectorStain Elite ABC kit, 2 drops solution A + 2 drops solution B per 5 ml PBS). The slides were washed twice for 5 min each and the tissues were left in ABC solution for another 30 minutes. The slides were washed twice before incubated with Vector NovaRed peroxidase (HRP) substrate (Cat#: SK-4800, Vector Laboratories, UK) solution mix. The reaction was stopped with distilled water after 5 min or as soon as colour developed. Counterstaining was performed with haematoxylin and dehydrated before mounting the slides was mounted in DPX mounting media (Cat#: 44581; Sigma-Aldrich, Dorset, UK) before analysis under light microscope. The images were taken using Cell^D software using light microscope (Olympus, Essex, UK).

2.3.5 Immunohistochemistry Quantification

IHC stained tissue was scanned using TissueFAXS Slide Loader 120 Histo (Wien, Austria). The analysis was performed using HistoQuest Analysis Software by Tissue Gnostics Imaging Solution (Vienna, Austria) to quantify the percentage of positive cell expression and the mean intensity stains of the positive expressing cells. Six regions of interests (ROIs) per slide of equal size were selected covering a total area of 0.3 mm^2 in each tumour section of primary and metastatic tumour as well as for their stromal region for analysis. The average percentage of positive cells were calculated by the software based on the threshold of NovaRed intensity level set by the user (information is available in **Appendix 6**).

2.3.6 Statistical Analysis

Paired Student's t-test was used to identify the significance of the mean expression of the specimen.

2.4 RESULTS

2.4.1 Histological Analysis of XCR1 and hLtn of Oral Cancer Tissue Sample.

In normal oral epithelium, the XCR1 expression was predominantly seen in the basal layer (**Figure 2.3**). Expression can also be seen in lymphocytes in the superficial connective tissue. A similar trend was seen for hLtn expression. The basal cell staining pattern in normal epithelium suggests that XCR1 might be expressed by progenitor/stem cells as these reside in the basal layer of normal oral tissue. Staining for hLtn was somewhat different and only seen focally and not throughout the oral epithelial basal layer. Other than that, some fibroblasts population, patrolling lymphocytes and endothelial cells in the connective tissue was also stained with XCR1 and a weaker stain for hLtn.

In primary oral squamous cell carcinoma (OSCC), XCR1 staining was seen in throughout the carcinoma epithelium with greater intensity in the basal compartment and areas of invading OSCC islands (**Figure 2.4**). Notably, the XCR1 staining was seen throughout the epithelium layer, not confined in the basal layer like in normal oral epithelium. Similarly, hLtn staining was also seen in the epithelium and the invasive epithelial islands. Expression of both XCR1 and hLtn by the same cells suggests a possible autocrine signalling mechanism in OSCC. Lymphocytes in the connective tissue are positively stained for XCR1 and hLtn. Similar staining seen by endothelial cells, although they have a weaker hLtn stain. Compared to the underlying connective tissue of normal oral mucosa, the fibroblast cells in the 'reactive stroma' stained with XCR1 and hLtn with a noticeable intensity.

In the case of metastatic OSCC in the lymph node, the tumour cells showed strong staining for XCR1 and hLtn (**Figure 2.5**). The representative sample showed that the metastatic carcinoma populated the central region of the node and spread outward to the peripheral cortex. Lymphocytes and the endothelial cells in the metastatic node also showed XCR1 and hLtn expression, as well as the fibroblasts in the reactive stroma (see **Appendix 7**).

(A) H&E (100×)

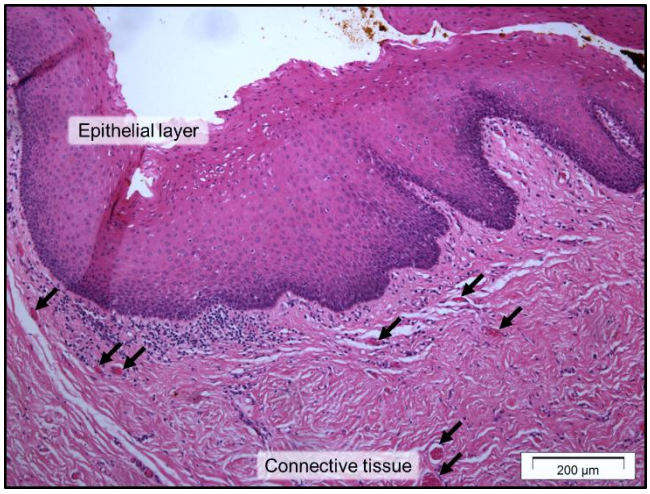

(B) XCR1 (100×)

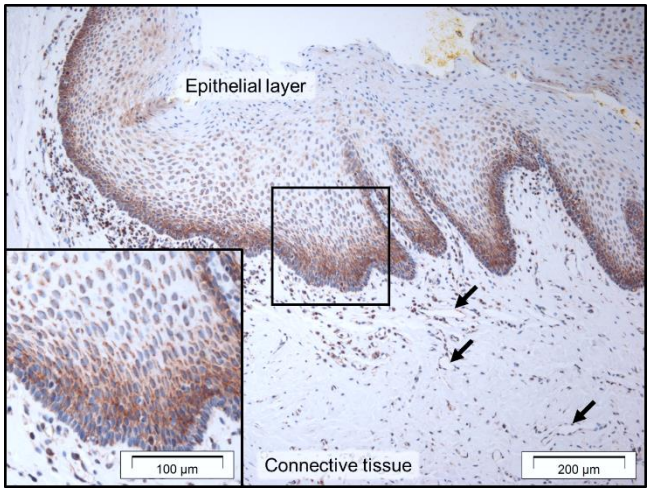

(C) XCR1 (200×)

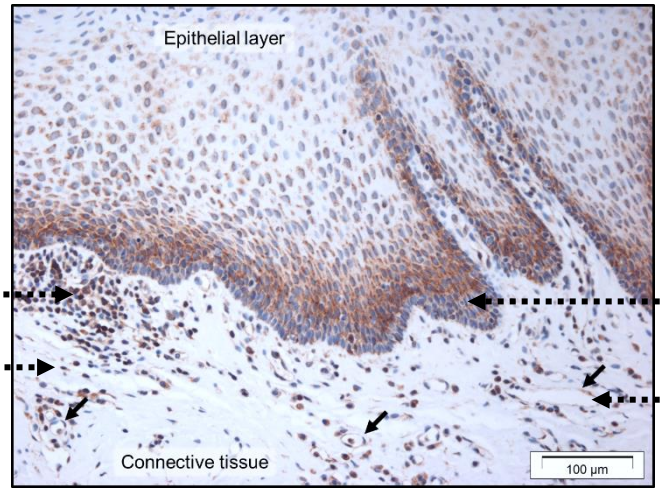

(D) XCR1 (400×)

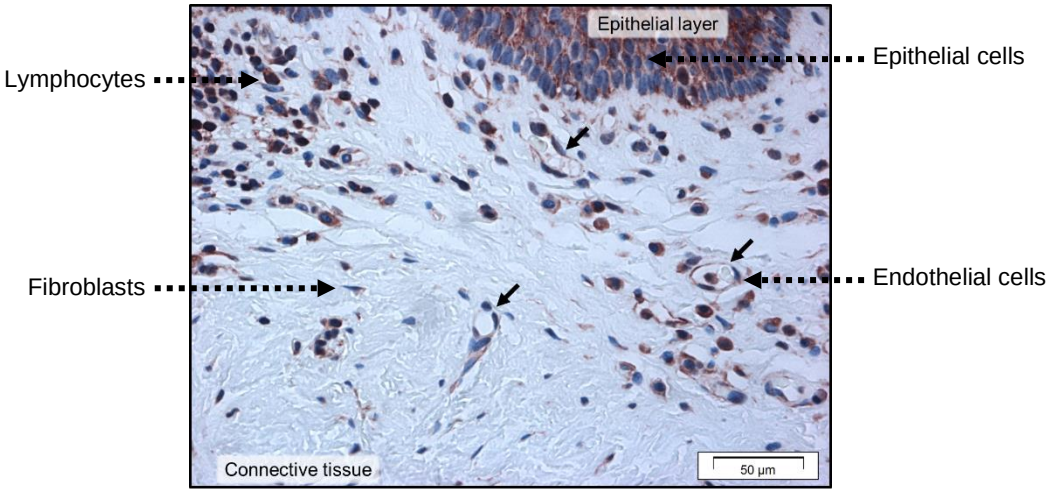

(E) hLtn (100×)

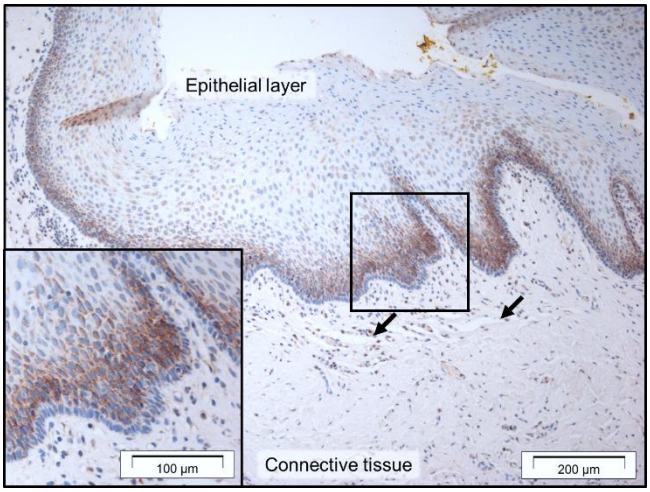

(F) hLtn (200×)

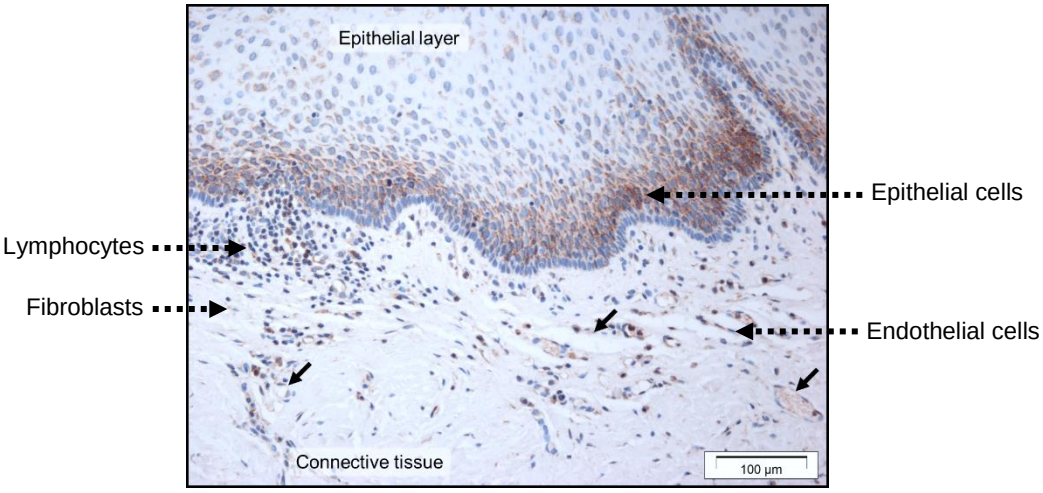

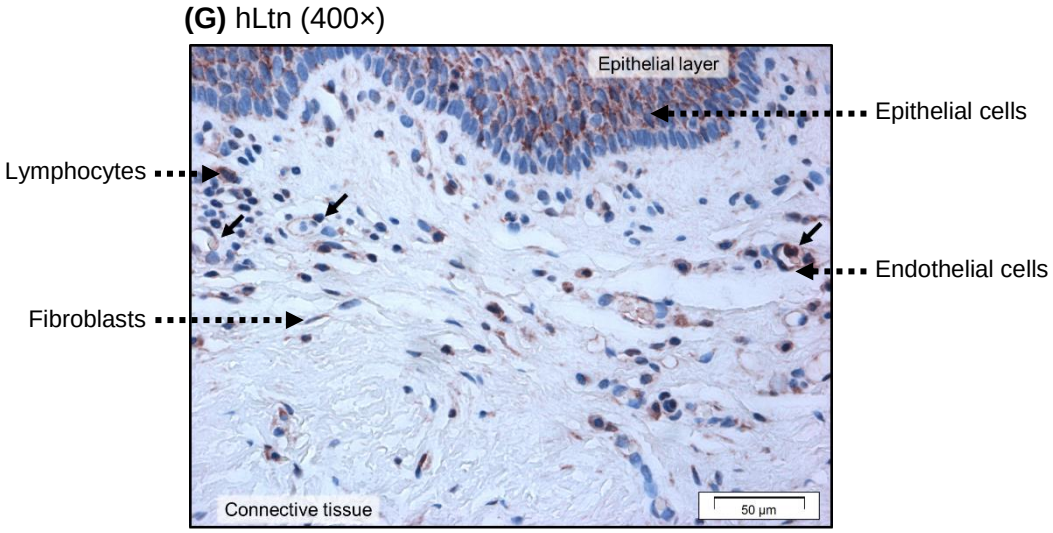

Figure 2.3: Normal oral mucosa (representative photomicrograph). **(A)** H&E staining at 100× magnification, **(B, C, D)** XCR1 staining at 100×, 200× and 400× magnification respectively, and **(E, F, G)** hLtn staining at 100×, 200× and 400× magnification respectively. XCR1 and hLtn staining is seen in the basal oral epithelium. In the superficial connective tissue layer, lymphocytes and endothelial cells are positively stained with XCR1 and hLtn, although the latter is weakly stained. Some fibroblasts show weak XCR1 and hLtn staining. The angled arrow indicates a blood/lymph vessel.

(A) H&E (100×)

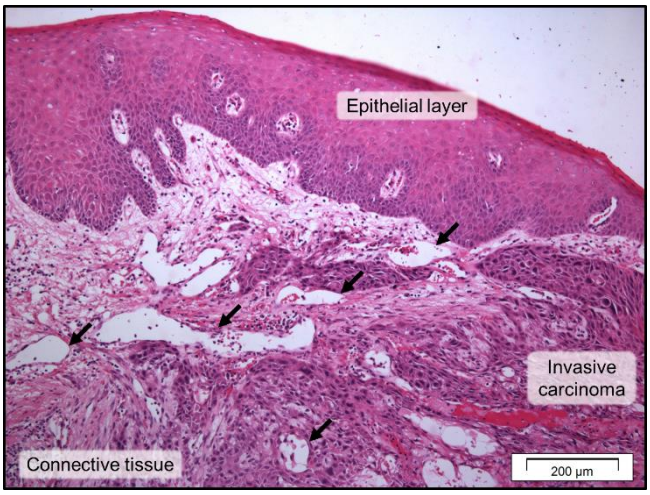

(B) XCR1 (100×)

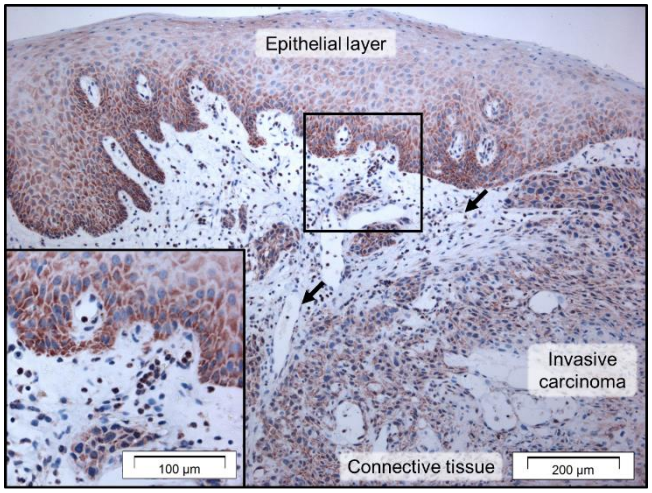

(C) XCR1 (200×)

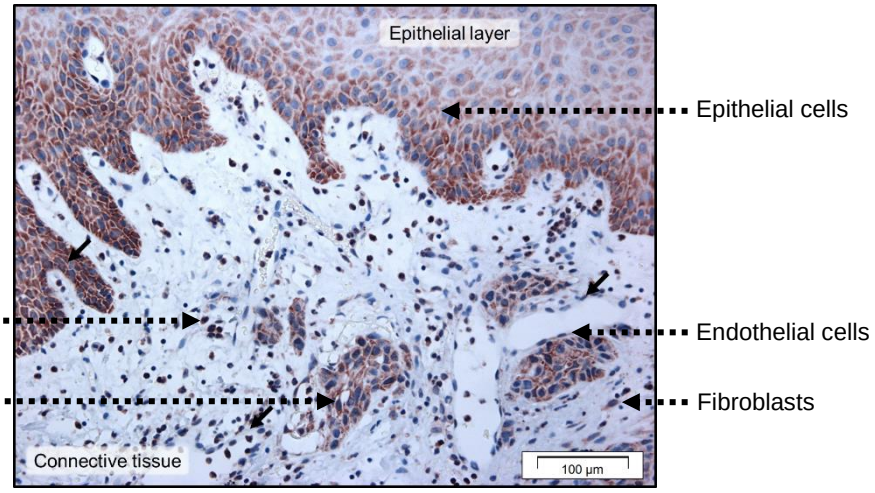

(D) XCR1 (400×)

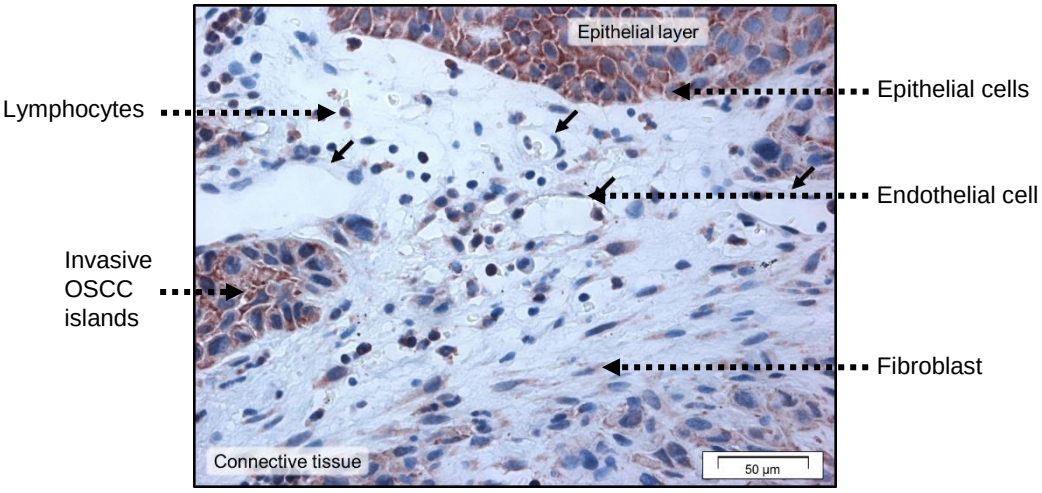

(E) hLtn (100×)

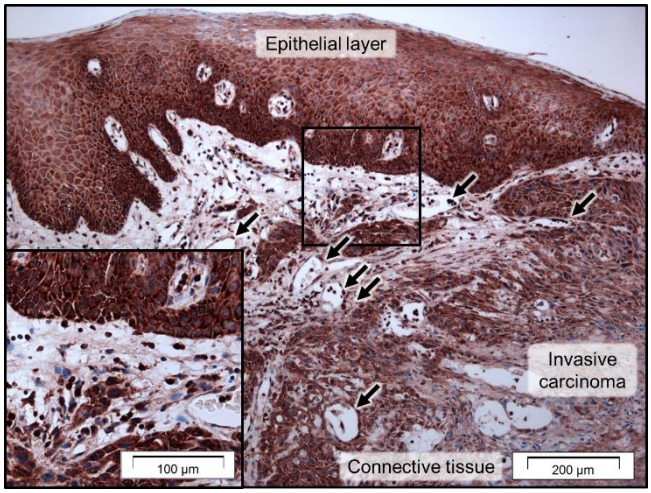

(F) hLtn (200×)

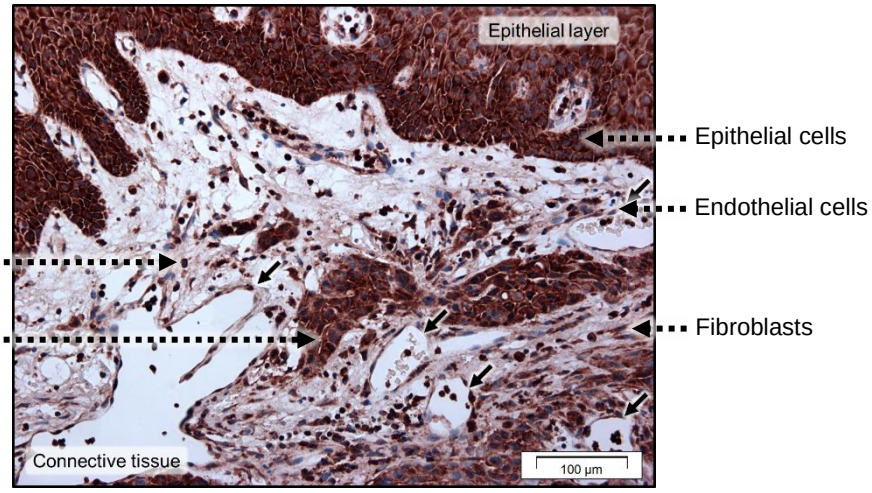

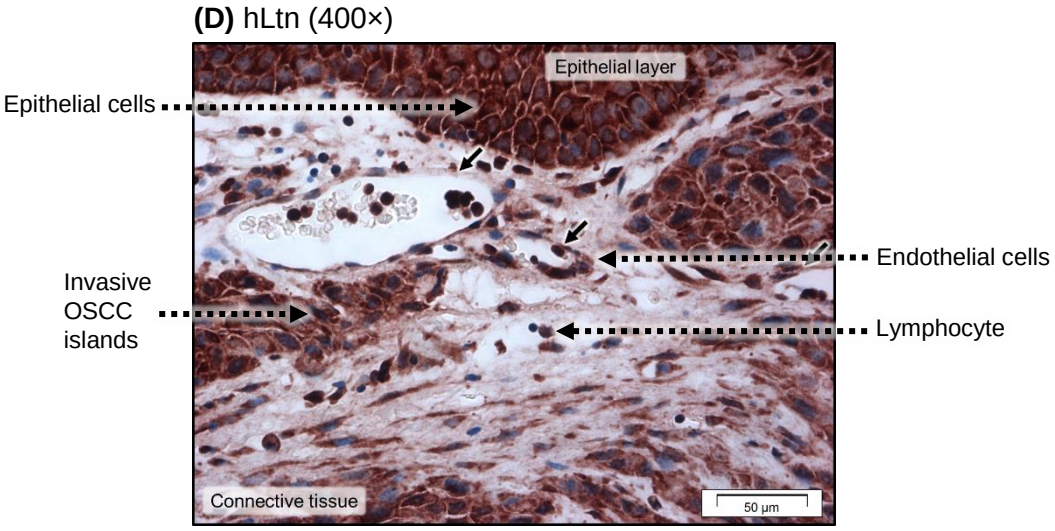

Figure 2.4: Primary oral squamous cell carcinoma with invasive carcinoma to the underlying connective tissue (representative photomicrograph). **(A)** H&E staining at 100× magnification, **(B, C, D)** XCR1 staining at 100×, 200× and 400× magnification respectively, and **(E, F, G)** hLtn staining at 100×, 200× and 400× magnification respectively. XCR1 staining is seen throughout the oral epithelium and invasive carcinoma and not just the basal layer. Strong hLtn staining is also seen throughout the epithelium as well by the invasive carcinoma. Lymphocytes and endothelial cells also show XCR1 (weak for endothelial cells) and hLtn staining within the connective tissue. A noticeable population of fibroblasts also stain for XCR1 and hLtn. The angled arrow indicates a blood/lymph vessel.

(A) H&E (100×)

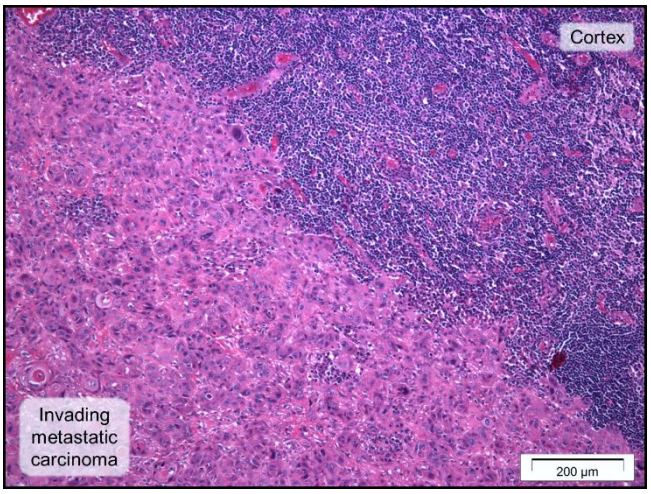

(B) XCR1 (100×)

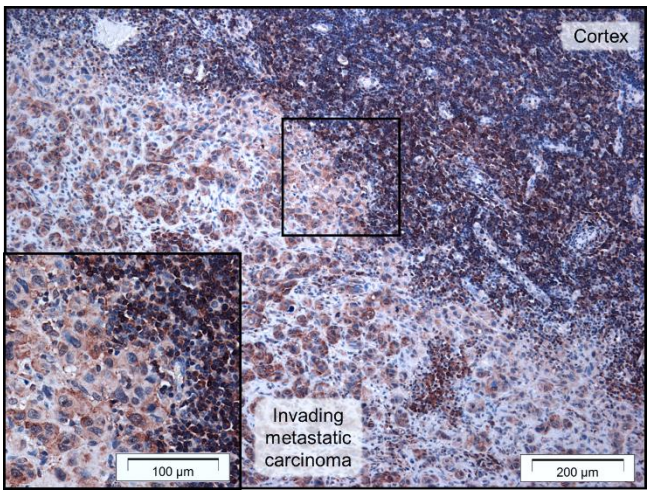

(C) XCR1 (200×)

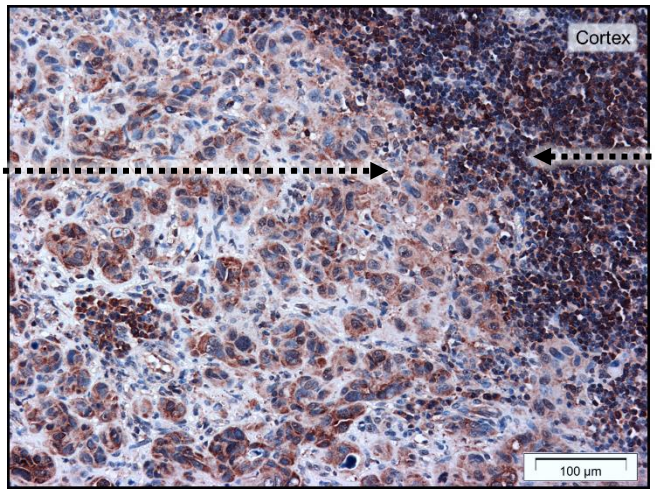

(D) XCR1 (400×)

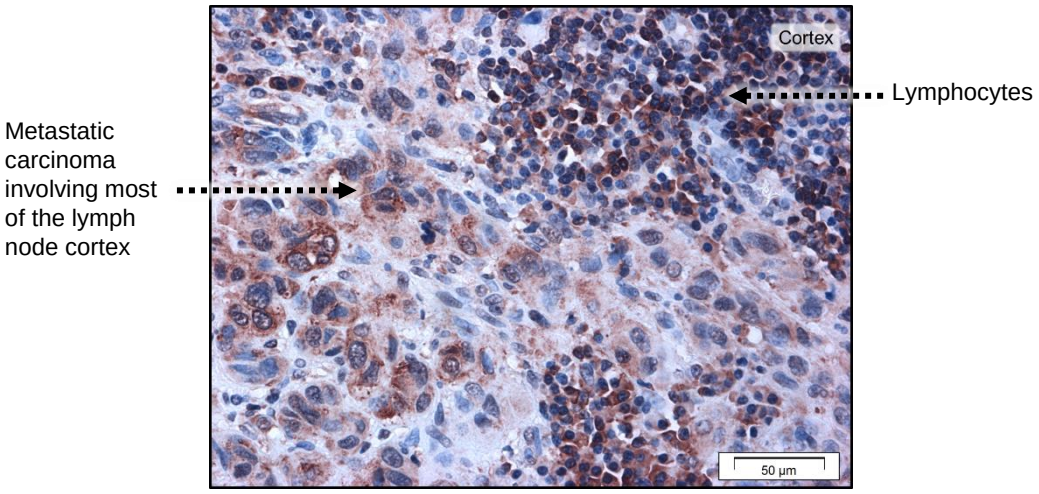

(E) hLtn (100×)

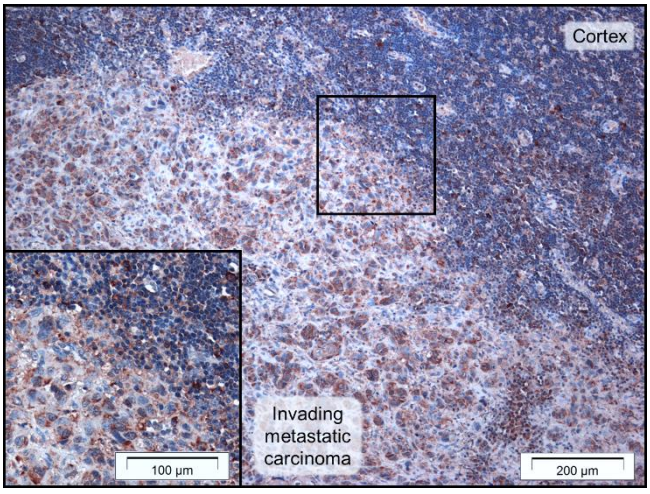

(F) hLtn (200×)

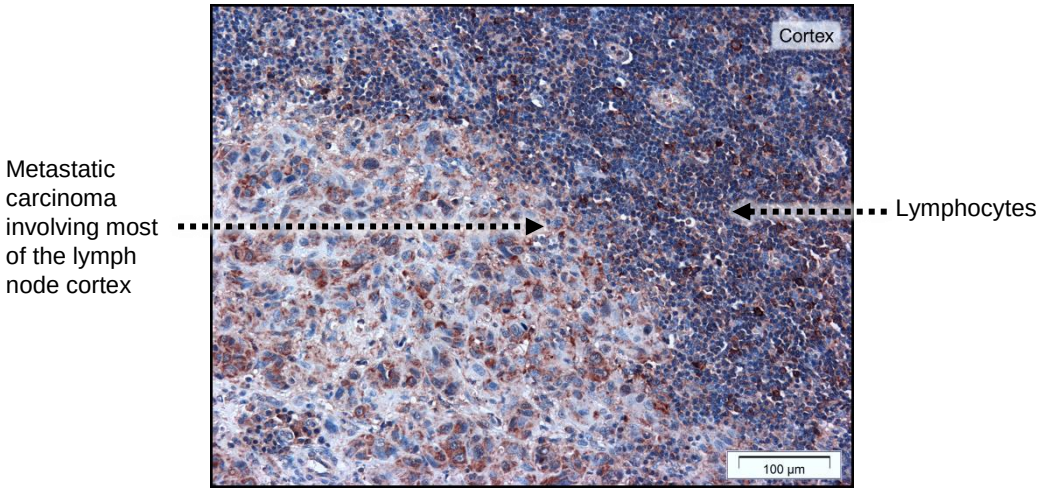

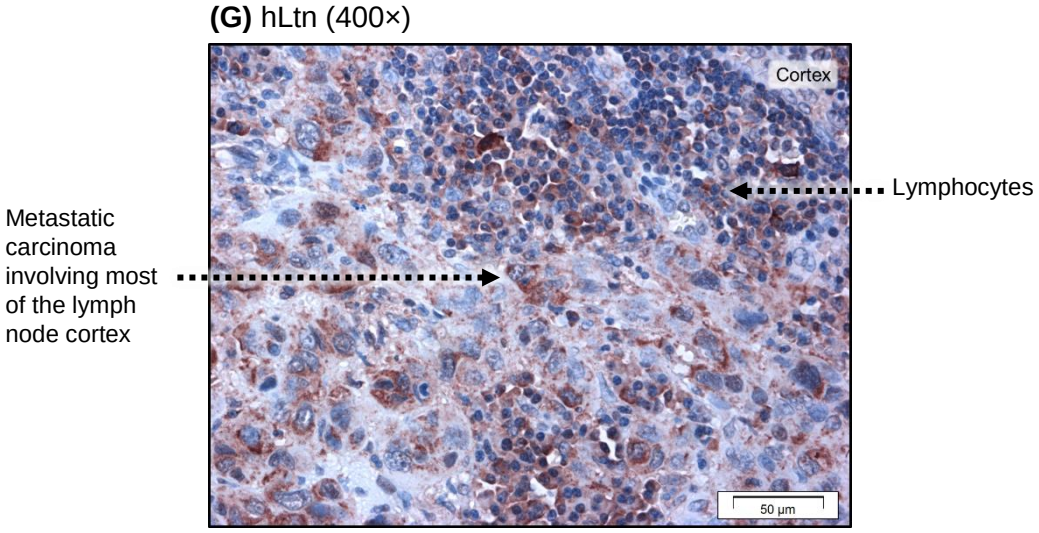

Figure 2.5: Metastatic carcinoma in the lymph node where the invading carcinoma spreading outwards to the outer cortex (representative photomicrograph). **(A)** H&E staining at 100× magnification, **(B, C, D)** XCR1 staining at 100×, 200× and 400× magnification respectively, and **(E, F, G)** hLtn staining at 100×, 200× and 400× magnification respectively. The XCR1 and hLtn staining is seen the metastatic carcinoma and the lymphocytes. hLtn stain pattern distribution is weaker by lymphocytes in the cortex region. The total magnification and scale bar of the photomicrograph are as stated in their respective picture.

2.4.2 Histological Analysis or XCR1 and hLtn in Reactive Lymph Nodes

In the cervical lymph nodes (**Figure 2.6**), diffuse XCR1 expression was seen in lymphocytes. B and T lymphocytes has been previously reported to express XCR1 and hLtn (Huang *et al.*, 2001). Strong expression of hLtn was seen in germinal centres where mature B lymphocytes proliferate and differentiate, suggestive of hLtn involvement in B lymphocyte proliferation. Additionally, stronger XCR1 and hLtn staining was seen found in the cortex and paracortex peripheral region. Endothelial cells lining the vascular and lymphatic channels as well as the subcapsular sinus (SS) in the lymph nodes also expressed both XCR1 and hLtn. These may be important in trafficking lymphocytes and tumour into the lymph node.

(A) H&E (200×)

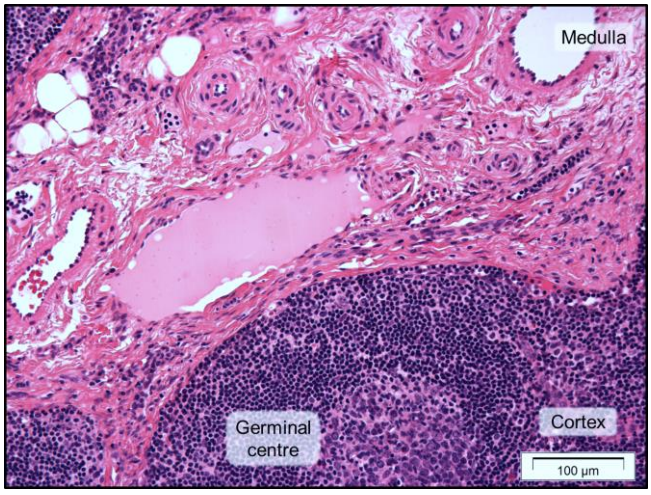

(B) XCR1 (200×)

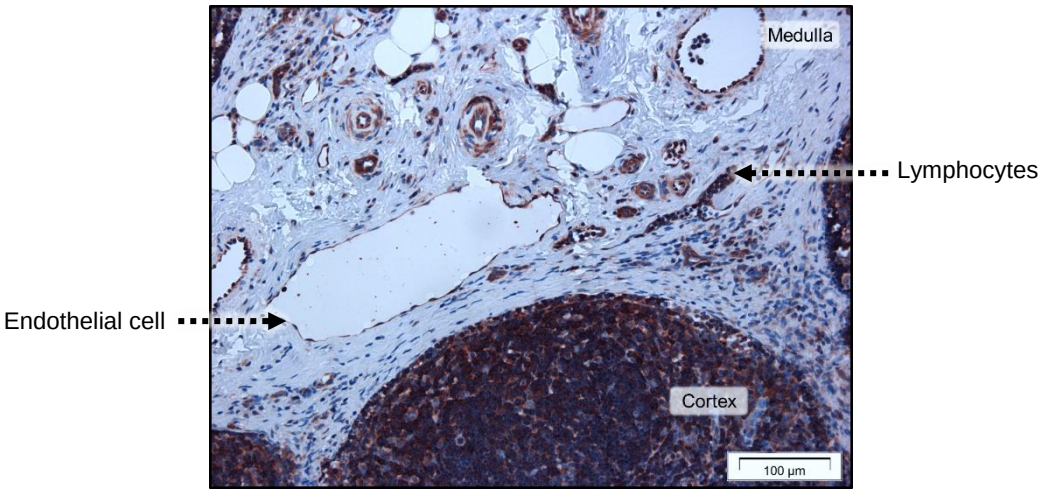

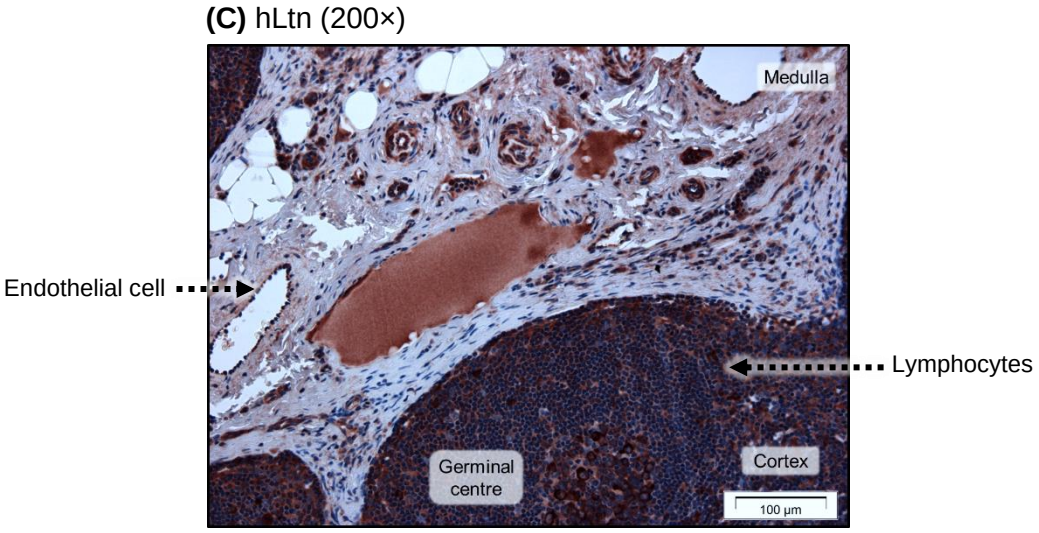

Figure 2.6: XCR1 and hLtn staining in cervical lymph nodes (representative photomicrograph). **(A)** H&E, **(B)** XCR1, and **(C)** hLtn staining at 200× magnification. Staining for both was seen in lymphocytes in the peripheral cortex region and medulla. Endothelial cells also stained positive for both XCR1 and hLtn, as well as fibroblasts.

2.4.3 Quantitative Comparative Analysis of XCR1 and hLtn Expression in Primary and Metastatic Tumour.

To understand whether OSCC progression correlates with the expression of XCR1 receptor and hLtn, the expression in patient tissue was quantified using HistoQuest software. Staining was evaluated in terms of positivity and the intensity in the tumour and the stroma.

High expression of XCR1 was present in OSCC with 90.68% ± 4.246 and 94.18% ± 3.308 in primary and metastatic tumours respectively. There was no significant difference in staining between primary and metastatic tumour. However, regarding expression intensity, the metastatic tissue with 59.73% ± 7.889 was significantly higher (p=0.019) compared to the primary tumour with 34.27% ± 3.655 (**Figure 2.7 (a)**). In the stroma, the metastatic tumours had significantly higher XCR1 expression (p=0.0175) with a mean of 74.51% ± 16.51 than primary tumours (mean: 24.85% ± 2.076) (**Figure 2.7 (b)**). No significant difference in expression intensity was detected between metastatic deposit stroma (mean: 37.22% ± 9.205) and primary OSCC stroma (mean: 24.93% ± 2.074).

Unlike the hLtn distribution in the tumour tissue, there were no significance difference in staining between metastatic (mean: 95.57% ± 0.916) and the primary OSCC (mean: 72.19% ± 15.06) (**Figure 2.8 (a)**). The expression intensity in metastatic tumour (mean: 53.95% ± 8.756) was slightly lower than primary tumour (mean: 58.32% ± 3.219) with no significant difference. Moderate positive expression of hLtn in the stromal cells of both primary (mean: 48.35% ± 13.39) and metastatic OSCC (mean: 71.67% ± 9.771) was observed (**Figure 2.8 (b)**). A similar pattern was identified for the expression intensity. Both the amount of positive expression and the intensity of staining for hLtn between primary and metastatic tumour was not significantly different.

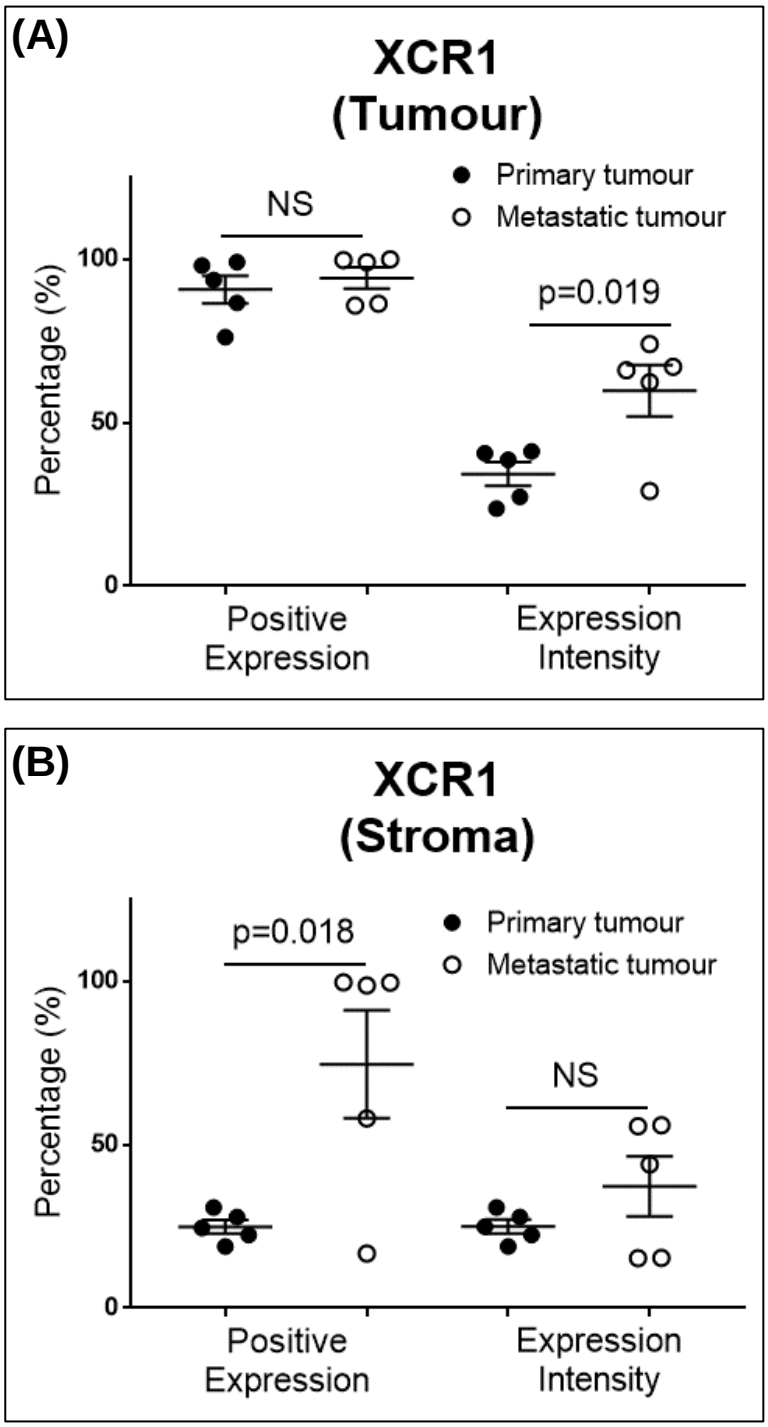

Figure 2.7: Histological quantification of XCR1 positive and intensity expression between primary and metastatic in oral **(A)** tumour and **(B)** stroma (n=5). The settings can be referred in Appendix 6.

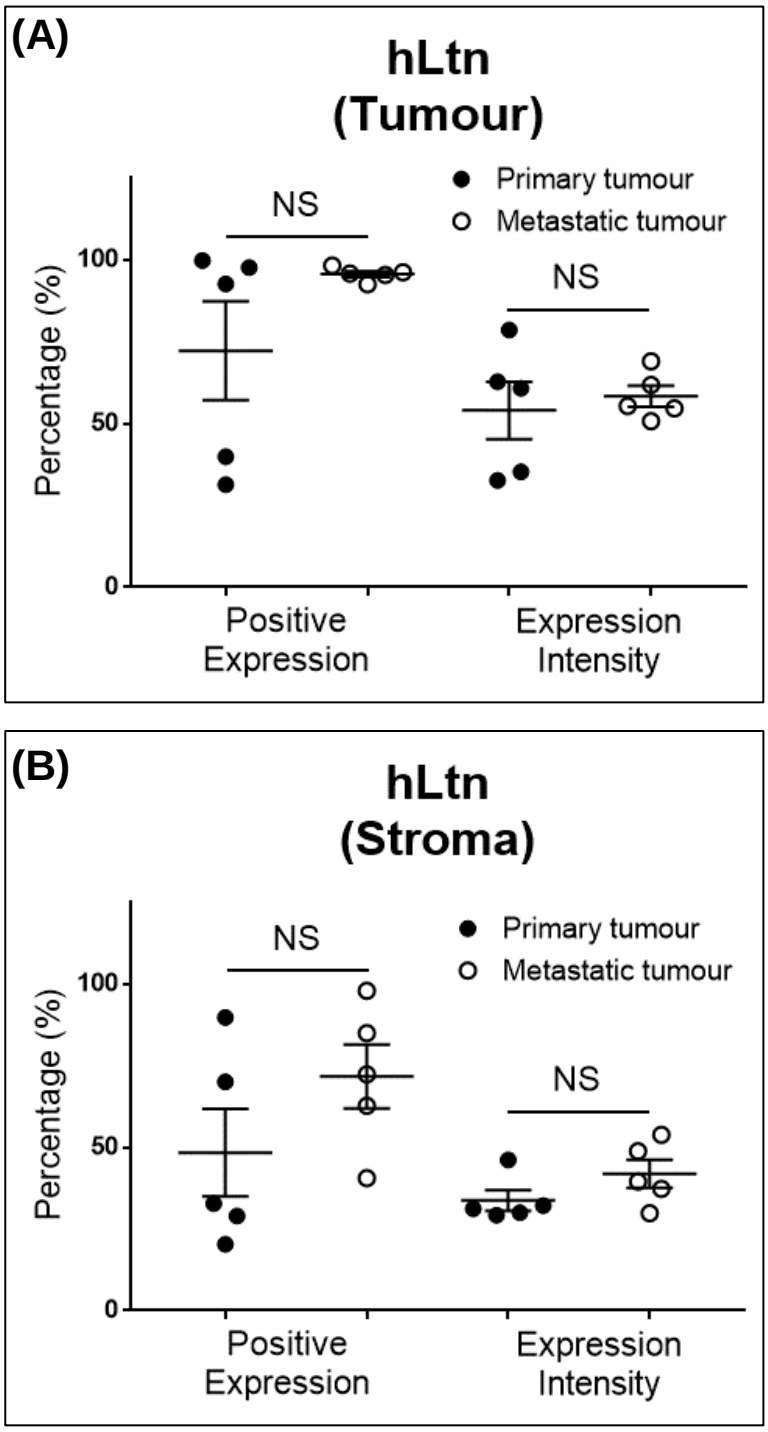

Figure 2.8: Histological quantification of hLtn positive and intensity of expression between primary and metastatic in oral **(A)** tumour and **(B)** stroma (n=5). The settings can be referred in Appendix 6.

2.5 DISCUSSION

The results show XCR1 and hLtn are present in oral tissue, in normal reactive lymph nodes as well as primary and metastatic oral squamous cell carcinoma (OSCC). This is in agreement with the novel findings of Khurram *et al.* (2010) showing XCR1 expression in oral tissues. From the results of this investigation and the previous study, XCR1 expression can be seen primarily in the basal (Khurram *et al.*, 2010). This raises the possibility that XCR1 could be a stem cell or basal layer marker in oral epithelia. This is quite interesting as the basal layer of oral epithelium is highly populated with adult/progenitor stem cells (Costea *et al.*, 2006), and the expression profile of XCR1 appears similar to that of CD44, a stem cell marker seen in normal human oral mucosa (Papagerakis *et al.*, 2014). Another argument is that the epithelial lining in the mouth undergoes constant renewal to allow resistance to wear and tear in response to mastication, requiring constant tissue renewal. Another argument is that XCR1 might serve as positional marker allowing the cells to distinguish their position in the tissue.

The examination of the OSCC tissue suggests that XCR1 and hLtn are expressed at the primary as well as metastatic stage. Chemokine receptors are known to be upregulated in cancer and it is thought this facilitates the growth and dissemination of the tumour. Previous studies have shown XCR1 expression in OSCC (Khurram *et al.*, 2010). This is not the case for other epithelial tissue. In breast cancer, XCR1 expression can only be seen in oestrogen receptor positive breast carcinoma and no expression is detected in normal primary breast epithelial tissue (Yang *et al.*, 2017). In a similar way, normal ovarian tissue and ovarian epithelial cell lines derived from normal cells do not express XCR1, although it is found in both primary and metastatic ovarian cancers and cell lines (Kim *et al.*, 2012). In lung, primary lung carcinoma shows a weak or absent expression which is upregulated in lung cancer bone metastasis (T. Wang *et al.*, 2015). Most papers show qualitative and subjective assessment of the expression while neglecting the quantitative analysis or vice versa. Our results show that metastatic OSCC has higher XCR1 expression with nearly 80% positive expression by the tumour. A transcriptomic analysis has revealed that low expression of XCR1 correlates with cancer progression and poor prognosis in hepatocellular carcinoma (Yanru *et al.*, 2018) which is contradictory to our result. The paper also mentioned XCR1 associates with migration and invasion but not proliferation of liver cancer cells. This is probably the tissue bias of chemokine receptor, where it behaves differently in different type of tissue/cell. Histological quantification performed showed that XCR1 receptor expression was high (more than 80% of the observed tumour population) in both primary tumour and lymph node metastatic OSCC compared to normal tissue. Furthermore, our assessment was

performed on OSCC tissue samples investigating the XCR1 receptor protein expression rather than the transcriptomes.

hLtn was found to be expressed in mammary gland yet no further description was available in breast cancer (Yang *et al.*, 2017). hLtn mRNA was confirmed to be expressed in primary lung cancer and associated with bone metastasis in clinical samples (T. Wang *et al.*, 2015). In ovarian carcinoma, hLtn was shown in both epithelial ovarian carcinoma ascites and cell lines (Kim *et al.*, 2012).

Connective tissue components such as endothelial cells also stained strongly for XCR1. This is important as OSCC cells can influence endothelial cells to form blood or lymphatic vessels resulting in angiogenesis and facilitating tumour growth and metastasis. This supports the idea that the hLtn and XCR1 interaction can contribute to angiogenesis in oral cancer, i.e. tumour or stromal can act on endothelial cells expressing XCR1 (Keeley, Mehrad and Strieter, 2011).

Other chemokines have been shown to be important during cell development in zebrafish (Bussmann and Raz, 2015), directing cells to appropriate destination in the body. The XCR1/hLtn axis can recruit intraepithelial lymphocytes (IEL) to fight the infections and invasion as first line of defence as seen in intestinal immune homeostasis (Ohta *et al.*, 2016). IEL has been shown to express XCR1 and hLtn (Khurram *et al.*, 2010), and can be a potential source of hLtn in the OSCC mucosa. This may further facilitate tumour cell migration and invasion. Our results also show lymphocytes expressing XCR1 in the superficial connective tissue near the basal oral epithelium with strong hLtn expression.

The reactive lymph nodes stained positive for both hLtn and XCR1 suggesting XCR1/hLtn axis is integral in the organ. Lymph nodes contain T lymphocytes, natural killer cells, neutrophils and B lymphocytes and have been shown to express the XCR1 receptor and its ligand (Kelner and Zlotnik, 1995; Kennedy *et al.*, 2000; Huang *et al.*, 2001). Interestingly, expression can be seen in germinal centres, suggesting that XCR1 and hLtn are involved in mature B cell proliferation and differentiation. There is strong evidence that the hLtn-XCR1 axis can activate MAPK signalling in cells to promote cellular division in cancer (Khurram *et al.*, 2010; Yang *et al.*, 2017). XCR1-hLtn interactions may contribute to B cell differentiation, but there is a lack of published evidence. Dendritic cells (DC) are involved in programming lymphocytes through antigen-presentation. Some evidence suggests that the XCR1-hLtn axis facilitates maintenance of immature dendritic cells by T lymphocytes (Park and Bryers, 2013; Ohta

et al., 2016). Follicular dendritic cells are involved in antigen processing with B cells (El Shikh *et al.*, 2010), which is why the germinal centre stain positive for XCR1 .

Previous studies have shown that human dendritic cells harvested from bone marrow do not express XCR1 receptor (Huang *et al.*, 2001). Although some also reported that CD11c+CD141+ DC subsets originating from the same group do express XCR1 (Bachem *et al.*, 2010). This shows that only a certain subset of DC expresses XCR1, but these studies were performed using cells harvested from circulating plasmacytoid DC and not those that are resident in lymph nodes. Another study in mice showed that XCR1 is expressed in a DC subset (Yamazaki *et al.*, 2013) and the cross-presentation antigen contributes to recruitment of memory T cells in infection (Alexandre *et al.*, 2016) and facilitates T cell survival (Ohta *et al.*, 2016). In addition, the peripheral and stromal expression of XCR1 and hLtn may provide a platform for hLtn to attract XCR1+ carcinoma and contribute to growth, spread and intranodal extension into lymph nodes. In conclusion, the results provide information to support a possible route of lymph node metastasis through the XCR1-hLtn axis.

The stromal expression seen in our results suggests that endothelial cells in normal, OSCC and lymph node tissue are positive for XCR1 and hLtn. Endothelial cells have been shown to express chemokine receptors that mediate endothelium organo-specificity, however not much is known about XCR1 and hLtn endothelial cell expression in other organs (Hillyer and Male, 2005; Crola Da Silva *et al.*, 2009). This is expected as chemokine-chemokine receptor interactions contribute to extravasation of lymphocytes into blood vessels, allowing them to patrol the circulatory system and move towards the site of injury or infection (Middleton *et al.*, 2002). Dendritic cells also can move across lymphatic endothelium with using a similar mechanism (Vaahtomeri *et al.*, 2017). Fibroblasts also expressed XCR1 with more prominent staining seen in the OSCC stroma. XCR1 expression by human gingival fibroblasts has also been reported in one study (Khurram *et al.*, 2010) but a different study reported lack of expression (Buskermolen, Roffel and Gibbs, 2017). A possible explanation is probably due to fibroblast heterogeneity and differential expression between person to person (Sriram, Bigliardi and Bigliardi-Qi, 2015).

The presence of hLtn was also seen in the extracellular matrix of oral tissue and lymph node stroma. The extracellular matrix is abundant with glycosaminoglycans (Yue, 2014), which allows the hLtn dimer to bind (Fox, Tyler, *et al.*, 2015) providing a gradient concentration in the stroma. The expression of XCR1 receptor and hLtn in OSCC and lymph node tissue can be summarized in **Figure 2.9**. The results suggest that hLtn and

XCR1 has the potential to influence oral cancer progression by moderating cancer cell survival and spread.

2.6 SUMMARY

This chapter shown that XCR1 receptor and its ligand expression are present in all investigated cases in both primary carcinoma and its metastatic counterpart. Metastatic stromal cells express higher total expression indicating its function further in the disease. Furthermore, XCR1 could be useful as an oral cancer biomarker. Additional data of XCR1 and hLtn expression in OSCC tissue are required to provide a statistically significant clinicopathological correlation.

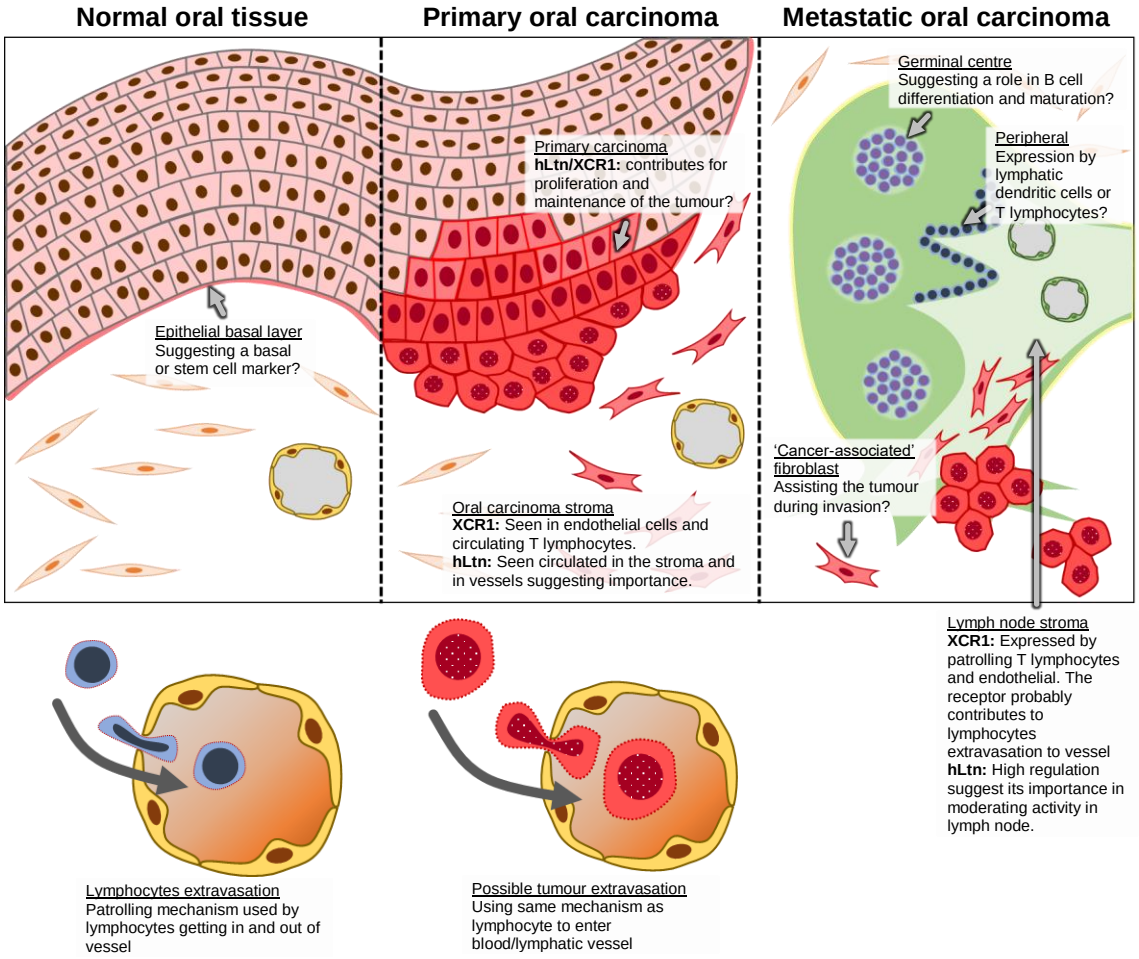

Figure 2.9: Summary map of XCR1 and hLtn expression based on IHC staining.

CHAPTER 3

REGULATION OF XCR1 AND XCL1 EXPRESSION IN ORAL CANCER CELL LINES BY hLtn & CONDITIONED MEDIA FROM ORAL FIBROBLASTS

CHAPTER 3: REGULATION OF XCR1 AND XCL1 EXPRESSION IN ORAL CANCER CELL LINES BY hLtn & CONDITIONED MEDIA FROM ORAL FIBROBLASTS

3.1 INTRODUCTION

Chemokine receptors are very sensitive to external stimuli which leads to receptor desensitization through internalisation and recycling of the receptor (Ferguson, 2001). This is highly dependent on external stimuli such as receptor activation upon ligand engagement (Kroeze *et al.*, 2012), hypoxia (Schioppa *et al.*, 2003), reactive oxygen species (Saccani *et al.*, 2000), or change in pH and ionic strength (Dairaghi *et al.*, 1997).

Previous studies have shown that most chemokines can act in an autocrine manner (Kroeze *et al.*, 2012). Expression of both hLtn and XCR1 by OCCL suggests that hLtn may have the potential to act on XCR1 expressing cells in an autocrine manner. The previous chapter gives us an insight into the expression of XCR1 receptor and its ligand by oral carcinoma tissue. Therefore, this chapter aimed to investigate whether exposure of oral cancer cells to wild type hLtn influences the expression of XCR1 receptor at the mRNA level and protein expression on the cell surface.

Additionally, this chapter will investigate the cross-talk between oral fibroblast and cancer cell lines. It is well known that cancer progression is highly influenced by the tumour microenvironment. This chapter investigates whether soluble factors expressed by oral fibroblasts can affect the expression of XCR1 receptor and hLtn by oral cancer cell lines (OCCLs). This was performed by exposing OCCLs to conditioned media from primary oral fibroblasts. Several types of oral fibroblasts were selected such as normal oral fibroblast (NOF), myofibroblasts (‘activated’ NOF), senescent NOF and cancer-associated fibroblasts (CAF).

3.2 METHODS

3.2.1 Materials

List of detailed information of the materials (reagents, kits, equipment, software and miscellaneous) used in the chapter can be found in **Appendix 1-5**.

3.2.2 Basic Cell Culture

All oral cancer cell lines were acquired from the Department of Oral and Maxillofacial Pathology in the School of Clinical Dentistry, the University of Sheffield (**Table 3.1**). The human primary normal oral fibroblasts (NOF) were isolated as previously described by Hearnden *et al.* (2009) (Sheffield Research Ethics Committee Ref. 09/H1308/66) (**Table 3.2**). Human primary oral cancer-associated fibroblasts (CAF) were isolated from fresh tissue from patients with OSCC undergoing resections within Charles Clifford Dental Hospital (Sheffield Research Ethics Committee Ref. 13/NS/0120, STH17021; CAF002 and CAF004) were kindly provided by Amy Harding and Dr. Helen Colley (Kabir *et al.*, 2016). All experiments were performed under sterile conditions in a Class II biohazard laminar flow cabinet. Good cell culture practice (GCCP) guidelines were exercised during the whole process.

3.2.2.1 Passaging the Cells

Cells were grown in T75 cell culture flasks with filter caps (Greiner Bio-One Ltd, UK) until ~80% confluent. Media was aspirated, and the cells washed with phosphate buffered saline (PBS) (Sigma-Aldrich, Dorset, UK) without Mg^{2+} or Ca^{2+}. After two washes, PBS was removed. 2-3 mL of Trypsin-EDTA solution (Sigma-Aldrich) was added for 3-5 minutes at 37^{o}C in an incubator. Cells were dislodged using gentle agitation and 3 mL of media added to the flask to neutralise the trypsin. This was transferred to a Falcon tube and centrifuged at 1000×g for 5 minutes. The supernatant was decanted, and the cell pellet re-suspended in fresh medium followed by addition to a new T75 flask.

Table 3.1: Table description of oral cancer cell lines and respective culture media.

Cell line	Description
H357	**Description:** Human oral squamous cell carcinoma from a 74-year-old male patient. **Tissue origin:** Tongue. (ECACC 06292004)
	Culture media: Keratinocytes growth media (KGM) (see **Appendix 8**)
SCC4	**Description:** Human squamous cell carcinoma from a 55-year-old male patient. Adherent cell line with epithelial-like morphology. **Tissue origin:** Tongue. (ATCC® CRL-1624)
	Culture media: Dulbecco's Modified Eagle's Medium (DMEM) (low glucose) and Ham's Nutrient Mixture F12 combination (ratio 1:1) containing 10% FCS, 2 mM L-glutamine and 1% (v/v) Penicillin/Streptomycin.
FADU	**Description:** Human squamous cell carcinoma derived from 56-year-old male patient. Adherent cell line with epithelial morphology. **Tissue origin:** Pharynx. (ATCC® HTB-43™)
	Culture media: Eagle's Minimum Essential Medium (EMEM) containing 10% FCS, 2 mM L-glutamine and 1% (v/v) Penicillin/Streptomycin.
TR146	**Description:** Human oral squamous cell carcinoma derived from a 67-year-old female neck node. **Tissue origin:** Buccal. (ECACC 10032305)
	Culture media: HAMS-F12 containing 10% FCS, 2mM L-glutamine and 1% (v/v) Penicillin/Streptomycin
BICR16	**Description:** Adherent cell line derived from a recurrent OSCC of a Caucasian male. **Tissue origin**: Tongue. (ECACC 06031001)
	Culture media: DMEM (low glucose) containing 10% FCS, 2 mM L-glutamine and 1% (v/v) Penicillin/Streptomycin.
BICR22	**Description:** Adherent cell line of a lymph node metastasis OSCC of a Caucasian male. **Tissue origin:** Tongue. (ECACC 04072106)
	Culture media: DMEM (low glucose) containing 10% FCS, 2 mM L-glutamine and 1% (v/v) Penicillin/Streptomycin.
All the information on the item catalogue number is available in **Appendix 1**	

Table 3.2: Table description of human primary fibroblasts and their respective culture media.

Cell line	Description
NOF	**Description:** Human primary normal oral fibroblast extracted from the buccal of health volunteers attending the Charles Clifford hospital. **Tissue origin:** Buccal
	Culture media: Dulbecco's Modified Eagle's Medium (DMEM) (low glucose) containing 10% FCS, 2 mM L-glutamine and 1% (v/v) Penicillin/Streptomycin.
CAF	**Description:** Human primary oral cancer-associated fibroblasts isolated from fresh tissue from patients with OSCC undergoing resections in Charles Clifford hospital. **Tissue origin:** *CAF002* obtained from floor of the mouth and *CAF 004* from lateral tongue.
	Culture media: Dulbecco's Modified Eagle's Medium (DMEM) (low glucose) containing 10% FCS, 2 mM L-glutamine and 1% (v/v) Penicillin/Streptomycin.
All the information on the item catalogue number is available in **Appendix 1**	

3.2.2.2 Cell Storage in Liquid Nitrogen

Cells were counted, and a 1×10^6 cells/mL suspension prepared using 10% (v/v) dimethyl sulfoxide (DMSO) (Sigma-Aldrich) in growth medium. Then, 1 mL of the cell suspension was pipetted into a cryovial and sealed tightly. The cryovial was stored in a freezing container (Nalgene®, Sigma-Aldrich) containing propan-2-ol. The container was stored at -80^{o}C for 24 hours before transferring the cryovial into a liquid nitrogen container.

3.2.2.3 Thawing Cells from Liquid Nitrogen Storage

A cryovial containing the desired cell line was removed from the liquid nitrogen container using appropriate safety protection and thawed in a 37^{o}C water bath. The contents were transferred to a Falcon tube and 2 mL of respective growth media was added. The cell suspension was centrifuged (RT, 1000×g) for 5 minutes to remove DMSO from the solution. The pellet was re-suspended in 1 mL respective growth media and transferred to a T75 flask. 10 mL media was added afterwards and incubated in 5% CO_2 at 37^{o}C. The growth medium was replaced every 2-3 days.

3.2.2.4 Quantification of cell number and concentration

The number of cells present in a suspension was quantified using a haemocytometer with Trypan blue exclusion. The cells were collected as described in **Section 3.2.2.1** and resuspended in 2-5 mL growth medium. 5 µL of cell suspension was mixed with an equal amount of Trypan blue solution 0.4% (Sigma-Aldrich, UK) was transferred haemocytometer with a glass cover slip. Living cells do not take-up the dye, while the dead cells are stained blue. The total number of viable cells was estimated as below:

$$\frac{\text{Number of viable cells}}{\text{mL}} = \frac{\text{n} \times \text{dilution factor} \times 10^4}{4}$$

n = total number of cell in four squares

3.2.3 Flow Cytometry Analysis for XCR1 Surface Receptor Expression

Principle: Flow cytometry is a powerful tool to analyse the surface protein expression. This can be performed by either using a directly conjugated antibody or unconjugated antibody, where the latter requires addition of appropriately labelled-secondary antibody for detection. Propidium iodide (PI), a fluorescent DNA intercalating agent can assist in the evaluation cell viability. PI is unable to cross a healthy cell membrane allowing it to distinguish live and dead cells in flow cytometry analysis. Dead cells tend to bind non-specifically to many reagents leading to a false positive result.

Procedure: Cells were washed and fully detached using cell-dissociation buffer (Cat#: 13151014; Thermo Fisher Scientific, Paisley, UK). Detached cells were then re-suspended in serum free medium at a density of 1×10^5 cells per tube. Tubes were centrifuged at 500×g for 5 minutes at room temperature and the supernatant was carefully removed. 500 µL of flow buffer (PBS + 10% FCS) was added to each tube. 10 µg/mL of anti-XCR1 human antibody (extracellular domain) IHC-plus™ LS-A158 (human anti-rabbit) (LifeSpan Bioscience Inc., WA, USA) was added for 60 minutes on ice. Unbound antibody was removed using three washes in flow buffer. Cells were re-suspended in 500 µL of flow buffer followed by addition of 8 µg/mL goat anti-rabbit IgG (H+L) secondary antibody, Alexa Fluor® 488 conjugate (Life Technologies Ltd, Paisley, UK). All steps were performed on ice with minimal exposure to light. Cells were incubated with the secondary antibody 30 minutes followed by three further washes. Cells were re-suspended in 500 µL flow buffer and kept on ice before flow cytometry cell analysis using BD FACSCalibur (BD Bioscience) with BD CellQuest™ Pro software (BD Bioscience, Oxford, UK). Prior to the run, all samples were treated with propidium iodide (1 µg/mL) for cell viability evaluation. The run was stopped when the 10,000 cells threshold was reached. The data analysis was performed using FlowJo (LLC, USA). For the assessment of the effect of hLtn on the XCR1 receptor expression, the OCCLs were treated with hLtn (Peprotech) (concentration: 100 ng/mL) in low-serum medium (containing 1% FCS) (LSM) for 24 hours at 37°C. The vehicle control flask was incubated with LSM only.

3.2.4 mRNA Expression Analysis

qPCR is a powerful tool to quantify mRNA expression of target genes in cells. It requires RNA extraction from the cells followed by RNA translation into complementary DNA (cDNA). This is because the primer probe for real-time PCR requires DNA for amplification. The primer probe with a fluorescence label binds to complementary sequence on the DNA strands. When it is amplified, a fluorescence signal is induced and quantified. Two different systems are usually employed: SYBR green and TaqMan probe. While SYBR green is cheap and easy to use, TaqMan is more specific and sensitive (Soltany-Rezaee-Rad *et al.*, 2015). In this study, real-time PCR was performed using TaqMan probes for XCR1 and hLtn while for α-SMA, SYBR Green technique was employed.

3.2.4.1 Total RNA Extraction and Purification from Cultured Cells

The extraction and purification of RNA from cultured cells was carried out using an ISOLATE II RNA Mini Kit (Cat#: BIO-52072; Bioline Reagents Limited, London, UK) in accordance with the manufacturer's instructions. The samples were homogenised by adding 350 µL of lysis buffer RLY (containing 250 µL lysis buffer RLY and 3.5 µL β-mercaptoethanol) per sample and vortexed vigorously. The lysate was filtered by loading into a 2 mL collection tube through an ISOLATE II filter (violet) and centrifuged (1 min at 11,000×g). The filter was discarded, and RNA binding conditions were adjusted by adding 350 µL 70% ethanol to the homogenised lysate followed by mixing using a pipette. The ISOLATE II RNA mini column (blue) was placed in a 2-mL collection tube for RNA binding. The cell lysate was loaded onto the column and centrifuged (30 s at 11,000×g). A new collection tube was then used and 350 µL of membrane desalting buffer (MEM) was used to desalt the silica membrane. Centrifugation was performed to dry the membrane (1 min at 11,000×g). DNase I was prepared by adding 10 µL DNase I to 90 µL reaction buffer for DNase I (RDN). 95 µL of the mixture was applied directly to the centre of the silica membrane which was incubated at room temperature for 15 minutes. Three washing steps were carried out: the first wash using 200 µL wash buffer RW1, the second wash and third washes using 600 µL wash buffer RW2. Each washing step required centrifugation (30 s at 11,000×g for the first and second and 2 minutes at 11,000×g for the third wash). After the third wash, the column was placed into a nuclease-free 1.5 mL collection tube (supplied with the kit) to collect the RNA. Elution was performed by adding 60 µL of RNase free H_2O directly to the centre of silica membrane, incubating for 1 minute and then centrifuging at 11,000×g) for a minute. The

concentration of eluted RNA was estimated using a NanoDrop 1000 Spectrophotometer (Thermo Scientific, DE, USA). For storage, RNA was kept at -80°C.

3.2.4.2 Measurement of RNA concentration and purity

High purity of the extracted RNA is essential, and the observed A260/280 ratio must be ~2.0. The RNA concentration required for cDNA reverse transcription was calculated using the equation below.

$$\text{Total volume of RNA required (per 10mL)} = \frac{100\ \text{ng/mL}}{\text{Total concentration of RNA (ng)}}$$

3.2.4.3 High Capacity cDNA Reverse Transcription

Reverse transcription is required as the qRT-PCR probe can only be used on DNA. Therefore, transcription of RNA samples is essential and was carried out using High Capacity cDNA Reverse Transcription Kit (Cat#: 4368814; Life Technologies Ltd, Paisley, UK). The master mix solution (reagents supplied in kit) was prepared (see **Table 3.3**). The components were thawed and placed on ice.

Table 3.3: High Capacity cDNA RT master mix (all supplied in the kit).

Components	Volume/Reaction (µL)	
	with Multiscribe™	without Multiscribe™
10× RT Buffer	2.0	2.0
25× dNTP Mix (100 mM)	0.8	0.8
10× RT Random Primers	2.0	2.0
Multiscribe™ Reverse Transcriptase	1.0	-
RNase Inhibitor	1.0	1.0
Nuclease-free H_2O	3.2	4.2
TOTAL per reaction	10.0	10.0

10 µL of RT master mix was pipetted into individual PCR tubes along with 10 µL of the RNA sample. 500 ng of RNA was used per sample reaction. Samples were briefly centrifuged to spin down the contents and eliminate any air bubbles. The tubes were then placed in DNA Engine Dyad® Peltier Thermal Cycler (Bio-Rad Laboratories Ltd., Hertfordshire, UK) to run on a set programme (see **Table 3.4**). For the negative control, nuclease-free H_2O was used. Each RNA sample is prepared with and without Multiscribe to determine the extent of RNA contamination and the effectiveness of real-time PCR. cDNA was stored at -20°C prior to further use.

Table 3.4: Thermal cycler programme for cDNA RT reaction.

	Step 1	Step 2	Step 3	Step 4
Temperature (°C)	25	37	85	4
Time (min)	10	120	5	∞

3.2.4.4 Quantitative Real-time PCR (qRT-PCR) using Taqman probe

cDNA quantification for XCR1 and hLtn (XCL1) mRNA was performed using TaqMan probes (information available in **Table 3.5**). The XCR1 specific primers were ordered from Life Technologies. To analyse the data, primers to β-2-microglobulin (B2M) was used as an endogenous control. A control tube with nuclease-free water was included to ensure the integrity of the sample run.

The master mix solution (including the probes) (see **Table 3.5**) was prepared and mixed gently. 9.5 µL of this solution was pipetted into respective wells of a 96 well PCR semi-skirted plate (STARLAB (UK) Ltd, Milton Keynes, UK). 0.5 µL of cDNA samples were added to respective wells and nuclease-free water used in negative control wells. The plate was sealed using advanced polyolefin StarSeal film (STARLAB (UK) Ltd, Milton Keynes, UK). All components were thawed on ice prior to preparation.

Table 3.5: TaqMan master mix.

Component		Volume (µL)
TaqMan Gene Expression Master Mix (Cat#:4369016; Life Technologies, Paisley, UK)		5.0
B2M probe (TaqMan Gene Expression Assays) (Cat#:4331182; Life Technologies, Paisley, UK) Amplicon length: 64	**Reference gene**	0.5
XCR1 probe (TaqMan Gene Expression Assays) (Cat#:4331182; Life Technologies, Paisley, UK) Amplicon length: 61	**Target gene**	0.5
XCL1 probe (TaqMan Gene Expression Assays) (Cat#:4331182; Life Technologies, Paisley, UK) Amplicon length: 108		
Nuclease-free water (Cat#:AM9914G; Life Technologies, Paisley, UK)		3.5
TOTAL per each sample		**9.5**

The plate was centrifuged (1000×g, 2mins, RT) before being loaded into the 7900HT Fast Real-Time PCR System (Life Technologies Ltd, Paisley, UK). The desired setting on SDS v2.4 (Life Technologies Ltd, Paisley, UK) was chosen before the run and RQ Manager 1.2.1 software (Life Technologies Ltd, Paisley, UK) was used as an analysis and quantification tool.

3.2.4.5 Quantitative Real-time PCR (qRT-PCR) using SYBR Green.

The quantification of the α-SMA cDNA was performed using a SYBR Green technique. The primers with specified sequence was purchased from Sigma-Aldrich (**Table 3.6**). The endogenous control of U6 snRNA was used.

Table 3.6: List of primers for mRNA expression analysis using SYBR Green technique.

Name	Sequence	Supplier
U6 snRNA (Reference gene)	**Fwd** 5′-CTCGCTTCGGCAGCACA-3′ **Rev** 5′-AACGTTCACGAATTTGCGT-3′	Sigma-Aldrich, UK
α-SMA (Target gene)	**Fwd** 5′-GAAGAAGAGGACAGCACTG-3′ **Rev** 5′-TCCCATTCCCACCATCAC-3′	
The melting curve of the primers are available in **Appendix 9**.		

The master mix solution was prepared and mixed gently (**Table 3.7**). The solution was then pipetted into respective wells of a 96 well PCR semi-skirted plate (STARLAB (UK) Ltd, Milton Keynes, UK) and 0.5 µL of cDNA samples were added into respective wells. Nuclease-free water used in negative control wells. The plate was sealed using advanced polyolefin StarSeal film (STARLAB (UK) Ltd, Milton Keynes, UK). All components were thawed on ice prior to preparation. The reference and target gene samples were prepared separately.

Table 3.7: SYBR™ Green Master Mix

Component	Volume (µL)
SYBR™ Green PCR Master Mix (Cat#:4309155; Thermo-Fisher Scientific, Paisley, UK)	5.0
Forward primer (concentration: 20 µg/mL)	0.5
Reverse primer (concentration: 20 µg/mL)	0.5
Nuclease-free water (Cat#:AM9914G; Life Technologies, Paisley, UK)	3.5
TOTAL per each sample	**9.5**

3.2.4.6 qRT-PCR Analysis

The quantitation of the qRT-PCR data was performed using the ΔΔCt method (Livak and Schmittgen, 2001; Schmittgen and Livak, 2008). The relative expression levels were calculated and compared between the untreated samples (treatment control) and treated samples. These samples were compared to respective reference gene of the samples (housekeeping gene) to normalize the variation in individual sample quality and quantity. The normalized values (ΔCt value) were then used to calculate the ΔΔCt values using the equation below.

Calculation for the ΔCt values of the treated and untreated samples

$$\Delta \mathbf{Ct}_{\mathbf{treated}} = \Delta\text{Ct target}_{\text{treated}} - \Delta\text{Ct reference}_{\text{treated}}$$

$$\Delta \mathbf{Ct}_{\mathbf{untreated}} = \Delta\text{Ct target}_{\text{untreated}} - \Delta\text{Ct reference}_{\text{untreated}}$$

ΔΔCt value for the treated samples

$$\Delta\Delta \mathbf{Ct\ sample}_{\mathbf{treated}} = \Delta\text{Ct sample}_{\text{treated}} - \Delta\text{Ct sample}_{\text{untreated}}$$

$$\textbf{Relative Quantification (RQ)} = 2^{-\Delta\Delta Ct}$$

$$\textbf{Fold difference} = \log 2\ (RQ) = -\Delta\Delta CT$$

3.2.5 Exposure of Oral Cancer Cell Lines (OCCLs) to Oral Fibroblast Conditioned Media

Procedure: Normal oral fibroblast (NOF) and cancer-associated fibroblast (CAF) cells were derived as described in **Section 3.2.2**. The NOF cells were also differentiated into myofibroblasts and senescence fibroblasts (**Section 3.2.6** and **3.2.7** respectively). The cells were left in SFM for another 24 hours to obtain the 'conditioned media'. Conditioned media was recovered, filter-sterilised (0.22 µm) to remove cell debris and either used immediately for experimentation or stored at -20°C until required. Concurrently, the OCCLs were seeded and incubated with SFM for 24 h prior treatment with conditioned media obtained from the oral fibroblasts. Additionally, for senescent NOFs, the cells were induced with genotoxic stimuli and cultured for 14 days before collecting conditioned media (details available in **Section 3.2.7**). For vehicle control, the oral cancer cells were treated only with SFM. The summary of the experiment can be found in **Figure 3.1** and **Figure 3.3**.

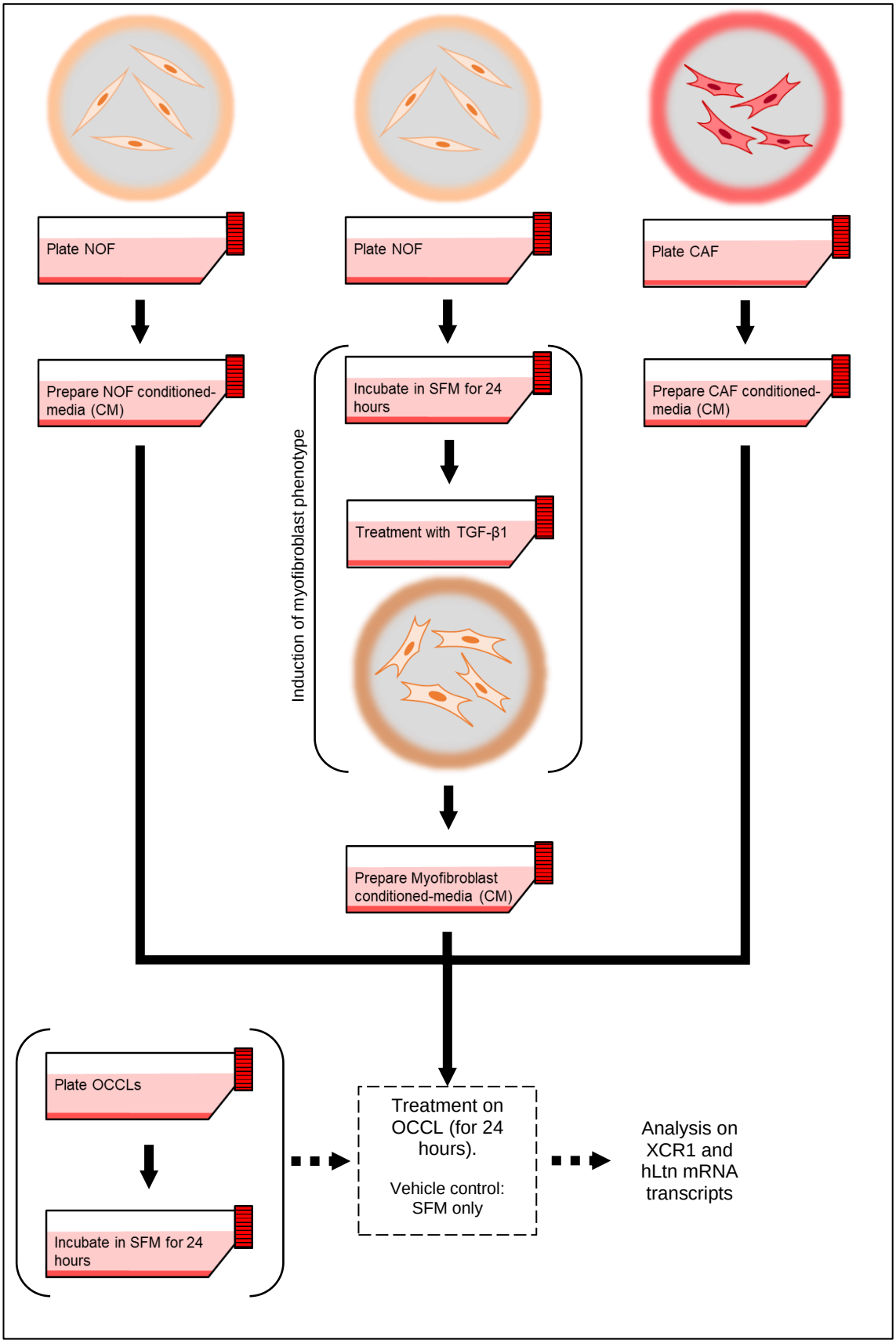

Figure 3.1: Experimental design for the treatment of OCCLs with conditioned medium from NOF, myofibroblast and CAF on OCCLs.

3.2.6 Transforming Growth Factor-beta 1 (TGF-β1) Treatment of Normal Oral Fibroblast

Procedure: The cells were seeded at an appropriate cell density and left to attach for overnight. Before treatment with 5 ng/mL of TGF-β1 (R&D system, Abingdon, UK) for 24 hours, the cells were cultured in serum-free media (SFM; containing DMEM supplemented with 2mM L-glutamine.

3.2.6.1 Immunocytochemistry

Procedure: Coverslips were sterilised with 70% ethanol for at least 10 minutes followed by washing twice with PBS and leaving to dry. 5×10^4 cells were seeded onto each coverslip and left to attach overnight in an incubator at 37°C. Medium was aspirated, and cells were washed with PBS three times. Cells were fixed using 100% methanol at room temperature for 20 minutes before the cells were permeabilized with 4 mM sodium dexoxycholate in dH_2O for another 10 minutes. Cell were then incubated with blocking buffer (2.5% (w/v) BSA in PBS) for 30 min before antibody treatment to reduced non-specific binding. Incubation with an α-SMA FITC-conjugated primary antibody (1:100 in blocking buffer) (Cat#: ab8211, Abcam, Cambridge, UK) was performed for an hour at 37ºC in the dark. Coverslips were then washed with PBS three times before addition of a drop of VectaShield antifade mounting medium with DAPI (Cat#: H-1200; Vector Laboratories, Peterborough, UK). Coverslips were then carefully transferred onto glass slides before viewing the staining using a fluorescence microscope. Nail polish can be used to immobilize and seal the coverslip. The slides were kept covered in aluminium foil at 4°C for storage and analysed as soon as possible to reduce the chance of photo-bleaching.

3.2.7 Senescence-induced Normal Oral Fibroblast with Genotoxic Stimuli

Principle: Senescent cells behave differently to normal cells. It is a state where the cells do not grow but are still able to perform functions such as synthesis and secretion of proteins. NOF cells were treated with hydrogen peroxide (H_2O_2) to induce oxidative stress allowing pre-mature senescent within a short period of time (Chen, Ozanne and Hales, 2007).

Procedure: NOFs were to approximately 70% confluence before treatment with 500 µM H_2O_2 (Cat#: 10687022; Fisher Chemical, Loughborough) in serum-free media for 2 hours. Immediately after incubation, the H_2O_2 was removed and the cells were left in growth media for 14 days to allow cells to senesce. Media was changed every 2-3 days. To determine if the induction of senescence was successful, senescence-associated β-galactosidase staining assay was performed (refer **Section 3.2.7.1**).

3.2.7.1 Senescence-Associated β-galactosidase Staining Assay

Principle: This assay is to determine cellular senescence by using β-galactosidase as a biomarker (Debacq-Chainiaux *et al.*, 2009). Senescence is characterized by arrest growth and inability to undergo DNA synthesis, a characteristic shared with quiescent cells. Although the enzyme overexpression and accumulation are specific to senescent cells, it is not required during the process to senescence. The X-gal reacts with the β-galactosidase enzyme that accumulates in senescent cells and reacts to form a blue precipitate indicating positive cell senescence (**Figure 3.2**).

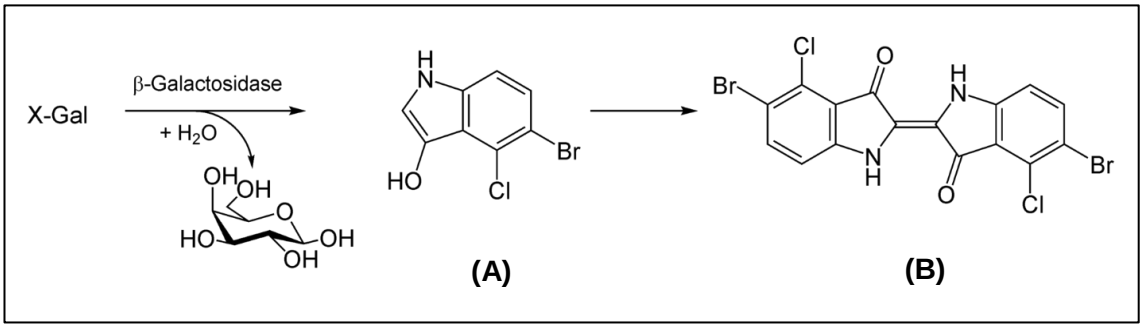

Figure 3.2: Principle of the β-galactosidase assay. X-gal reacts with β-galactosidase yielding galactose and **(A)** 5-bromo-4-chloro-3hydroxyindole. Later this spontaneously dimerizes and oxidized into **(B)** 5,5' dibromo-4,4'-dichloro-indigo, an intense insoluble blue precipitate.

Procedure: The assay was performed using a senescence detection kit (Cat#: ab65351 Abcam). 1×10^4 cells were seeded per well of reaction for 24 h. Cells were washed with PBS twice before adding 500 µL of fixative solution for 20 minutes. A total of 500 µL of staining solution was added to each well overnight in an incubator at 37ºC 5% CO_2. The plate was covered in aluminium foil to exclude light. The composition of the staining solution is as below:

- 25 µL of 20 mg/mL X-gal (20 mg/mL 20 mg lyophilized X-gal was dissolved in 1 mL DMSO),
- 470 µL of 1× staining solution, and
- 5 µL of staining supplement.

For analysis, a light bright-field microscope with attached camera was used to estimate the percentage of blue stained cells per microscopic field.

3.2.8 Statistical Analysis

All the experimental data are presented as at least three independent experiments performed in triplicate unless stated otherwise with mean ± SEM. Student's t-test was used to analyse the statistical significance of XCR1 mRNA and protein expression, and hLtn (XCL1) mRNA expression of the treatment sample compared to the experimental control using Graph Pad Prism 7 (La Jolla, CA, USA). All the mRNA data analysis in this chapter were compared to a normalised vehicle control (in fold change). A p-value <0.05 was considered as statistically significant and denoted with * symbol.

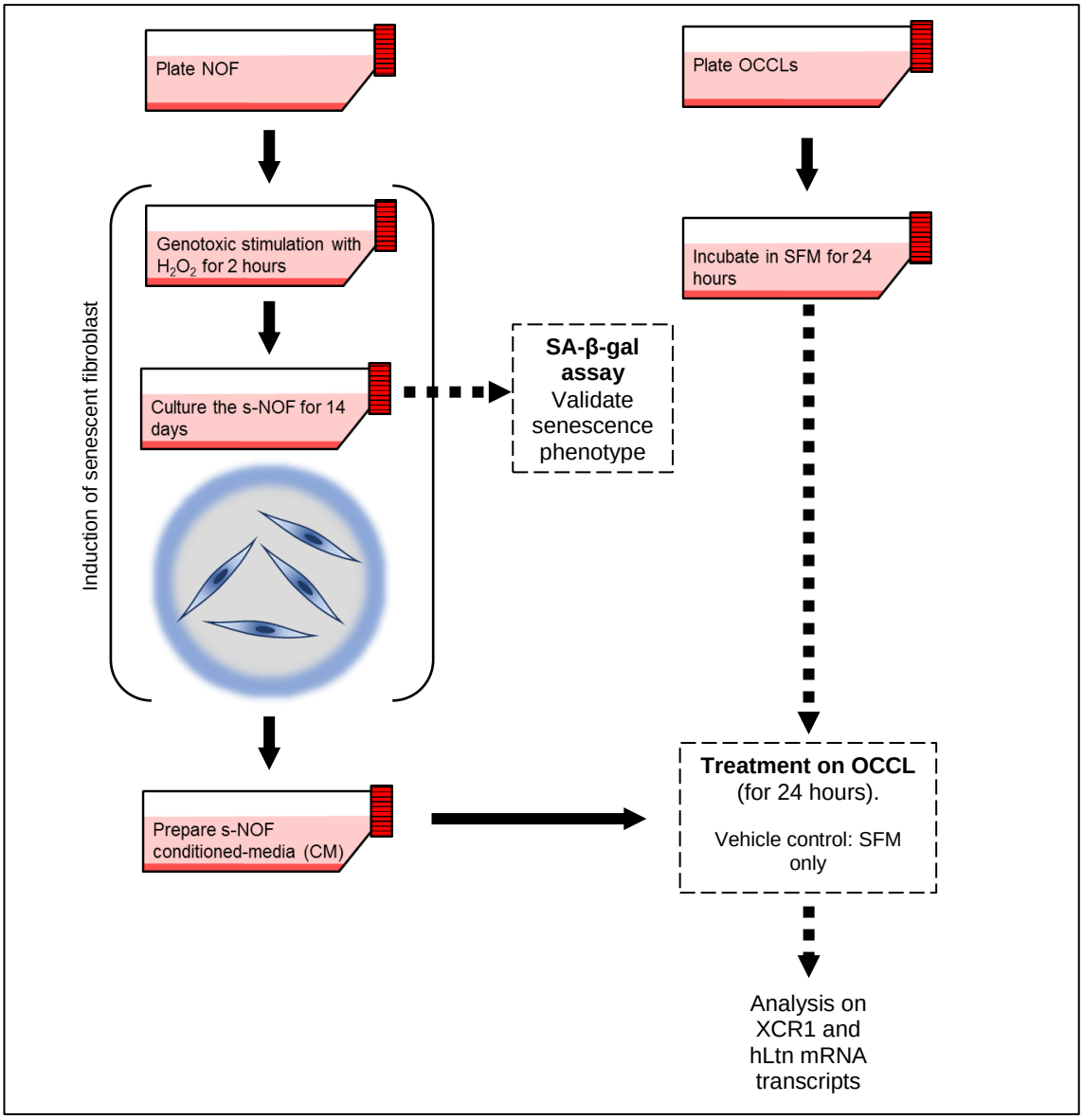

Figure 3.3: Experimental design for treatment of OCCLs with CM from senescent-NOFs.

3.3 RESULTS

3.3.1 Effect of hLtn on XCR1 Surface Expression in OCCL

3.3.1.1 XCR1 Surface Receptor Expression in OCCL

An initial experiment was performed to quantify the surface expression of the XCR1 receptor in different oral cancer cell lines (refer **Table 3.1**). All the selected cancer cell lines expressed the receptor to varying degrees (**Figure 3.4**) The highest expression was seen in SCC4 cell line with more than 88% ± 2.256 of the cell population expressing XCR1 and the lowest was by H357 cell line with 29% ± 2.829. SCC4 cells showed a wider forward-scatter cell population suggesting that the cell size is larger than all other cell lines, possibly providing a larger surface area for XCR1 receptor on its surface. TR146, FADU and BICR22 cell lines all showed moderate expression (mean 32% ± 0.6658, 36% ± 0.2999 and 42% ± 3.732 respectively). BICR16 cell line, a recurrent carcinoma has quite a high expression of XCR1 receptor with 68% ± 0.2848 expression. Further information on the flow cytometry analysis such the dot plot for the size scatter-gram, dot-plot channel for cell viability and target protein are available in **Appendix 10**.

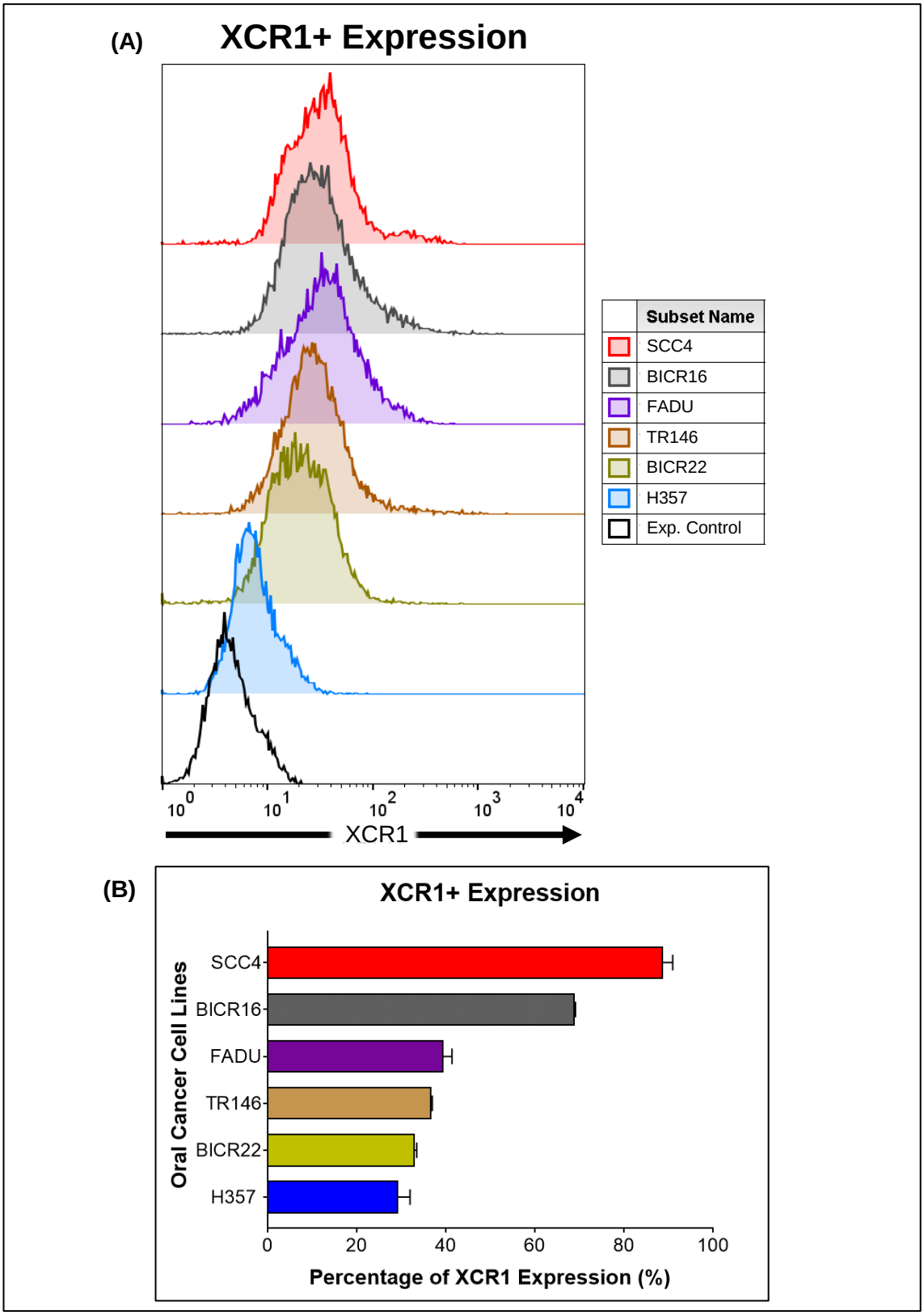

Figure 3.4: Oral cancer cell lines surface expression of XCR1 receptor. **(A)** Histogram diagram of XCR1 receptor expression for each cell lines, where shift to the right signifies greater expression of XCR1 in the cell population. **(B)** Bar chart summarising the percentage expression. Three independent experiments were performed with triplicates. Data is expresses in mean ± SEM.

3.3.1.2 Regulation of XCR1 Receptor Expression in OCCL through hLtn Stimulation

This part of the study was to observe whether hLtn can act in an autocrine manner and influence expression of its receptor. Several oral cancer cell lines were used to compare the receptor expression (refer **Table 3.1**). The oral cancer cell lines: H357, SCC4, FADU, TR146, BICR16 and BICR22 were derived from OSCC.

Positive expression of XCR1 on normal oral keratinocytes and OCCLs has been reported previously (Khurram *et al.*, 2010). XCR1 cell surface expression was observed in all the tested cell lines in the current study (**refer Figure 3.4**). For the surface protein expression (**Figure 3.5**), only the oral squamous cell carcinoma-derived cell lines (H357, SCC4 and FADU) showed significant changes in their surface XCR1 expression after exposure to hLtn (100 ng/mL) for 24 hours. FADU showed an increase (~16%) and SCC4 showed a decrease (p=0.0145) of the XCR1 surface receptor expression (refer to **Table 3.8** for the mean and p-value). H357 surface XCR1 expression was reduced by 8% while FADU showed an increase ~16% in the surface receptor expression after the treatment.

BICR22, TR146 (both lymph node metastatic-derived cell lines), and BICR16 (a recurrent carcinoma-derived) showed a trend for decreased in receptor expression but this reduction was not significant.

Exposure to 100 ng/mL hLtn resulted in a significant upregulation in the XCR1 mRNA expression in SCC4 cells (mean 1.287 ± 0.05785, p=0.0077) but not in other cell lines (**Figure 3.6**).

Table 3.8: Result of XCR1 expression after treatment with hLtn for 24 hours.

Cell line	XCR1 Expression (%)			p-value
	Untreated	Treated	Differences	
SCC4	88.67 ± 2.256	72.83 ± 3.099	-8.14 ± 2.839	0.0145*
H357	36.66 ± 0.299	29.02 ± 3.323	-15.83 ± 3.833	0.0456*
FADU	39.13 ± 2.829	55.37 ± 4.720	+16.23 ± 5.503	0.0420*
TR146	42.00 ± 3.732	36.37 ± 0.203	-5.633 ± 3.738	0.2063
BICR16	68.83 ± 0.285	62.37 ± 3.340	-6.467 ± 3.352	0.1259
BICR22	32.80 ± 0.666	20.63 ± 6.274	-12.17 ± 6.309	0.1260

* indicates p<0.05

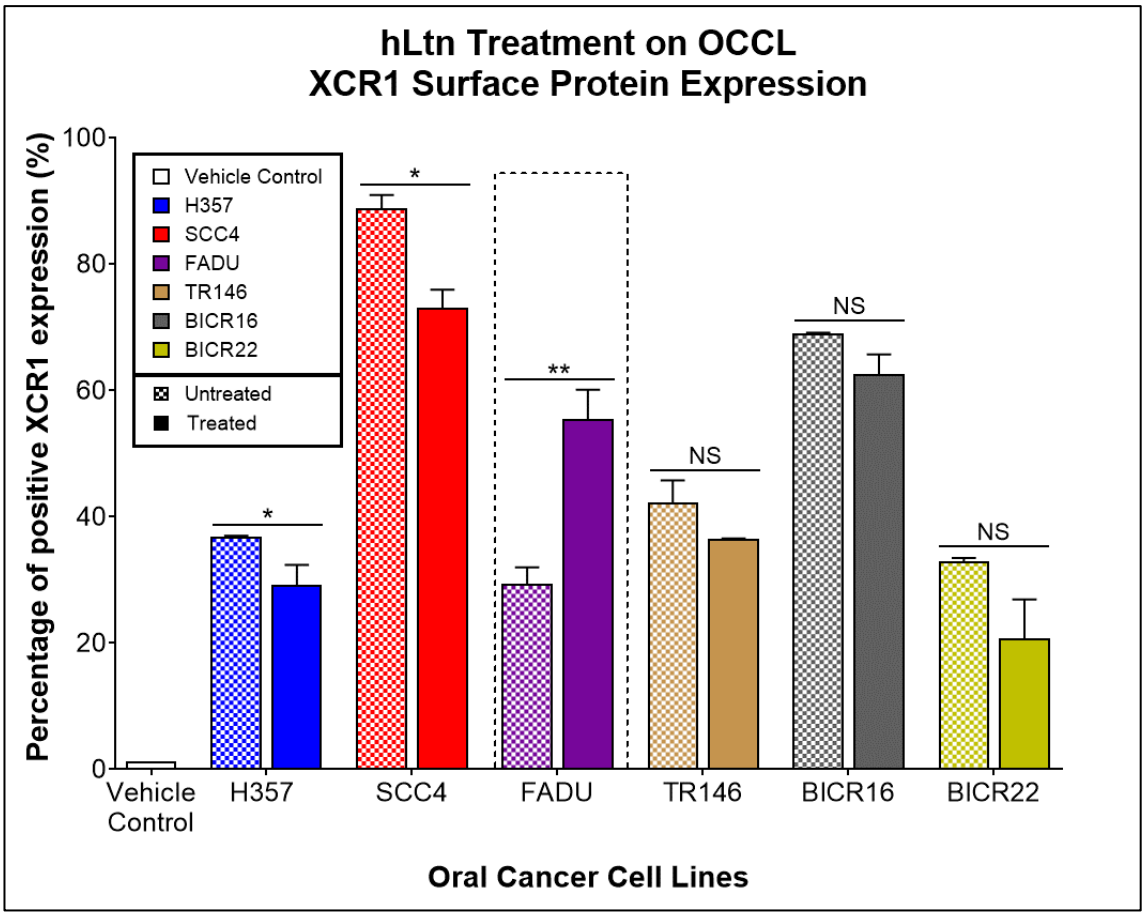

Figure 3.5: Percentage of XCR1 expression by the oral cancer cell lines (OCCLs). The bars with white-box pattern represent the respective OCCLs (colour coded) without treatment and the fully coloured bars represents the OCCLs exposed to hLtn (Peprotech) treatment (100 ng/mL). FADU cells showed an upregulation of the surface protein receptor (in dashed box) compared to other OCCLs. Three independent experiments were performed with triplicates with error bar in SEM. (* p-value<0.05, ** p-value<0.01, and NS is not significant).

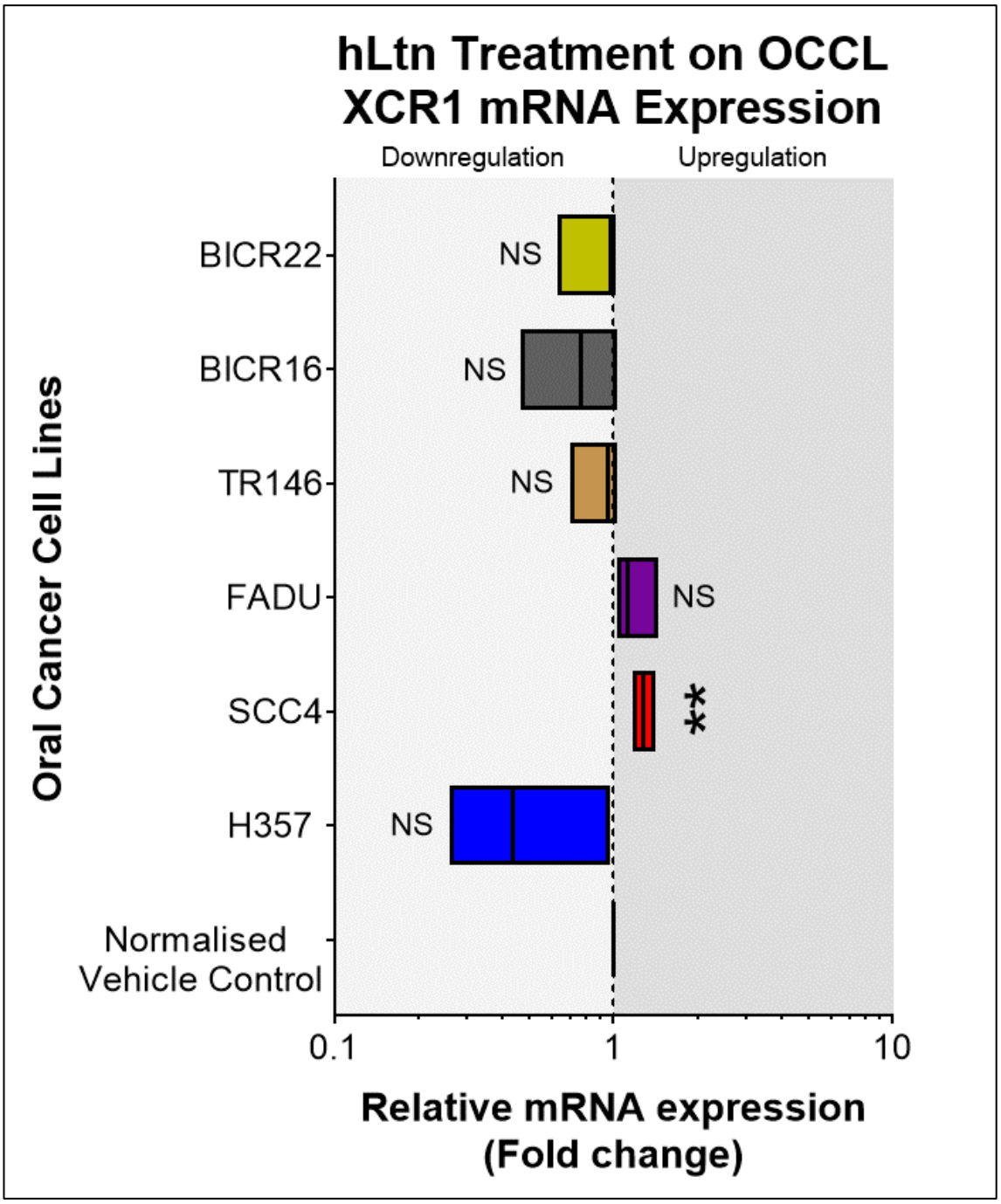

Figure 3.6: XCR1 mRNA expression. The OCCLs were treated with hLtn (100 ng/mL) (Peprotech) for 24 hours. The relative expression was compared to the endogenous control of β-2-myoglobulin (B2M) and expressed as fold change (normalised to control). The graph represents minimum and maximum (with median line). (** p-value<0.01, and NS is not significant).

3.3.2 Effect of Normal Oral Fibroblast, Myofibroblast, and Cancer-associated Fibroblast Conditioned Medium on the Expression of XCR1 and hLtn mRNA by OCCLs.

Oral fibroblasts comprise most of the mesenchymal cells in the oral stroma. Therefore, to study their interaction with the oral cancer cells, we investigated several types of oral fibroblasts that can exist in an OSCC stroma; including normal oral fibroblast (NOF), myofibroblasts and cancer-associated fibroblasts (CAF). Indirect co-culture was used to study the effect of secreted factors in the media (conditioned media) by NOF, myofibroblast and CAF on oral cancer cell lines (OCCLs) and the level of expression of XCR1 receptor and XCL1 (hLtn) determined.

3.3.2.1 Phenotype Assessment of α-SMA expression for Oral Fibroblast Cells.

The α-SMA protein expression was compared between the normal oral fibroblast (NOF804 was used in this experiment) and its myofibroblast counterpart (or 'activated' NOF). TGF-β1 exposure resulted in an increase in α-SMA protein in NOF (**Figure 3.7**) after 24 hours and the expression lasted for a further 24 hours in serum-free media (**Figure 3.8**). No noticeable expression was seen in NOF without the treatment. Cancer-associated fibroblast (CAF), expressed the α-SMA protein without exposure to TGF-β1 (**Figure 3.9**). Preliminary exposure of TGF-β1 to CAF showed no impact on the α-SMA fibres expression. Phenotypically, our result showed that cancer-associated fibroblasts are similar to the oral myofibroblast.

For the α-SMA mRNA expression (**Figure 3.10**), the results were similar to protein expression. The relative expression was compared to the endogenous housekeeping U6 small nuclear RNA (U6 snRNA). Normal oral fibroblasts (NOF804) exposed to TGF-β1 for 24 hours, and cancer-associated fibroblasts (CAF002 and CAF004) had a similar high relative expression of α-SMA mRNA ($p=0.0152$, $p=0.0091$ and $p=0.005$ respectively). α-SMA mRNA expression was detected even in unstimulated cancer-associated fibroblasts.

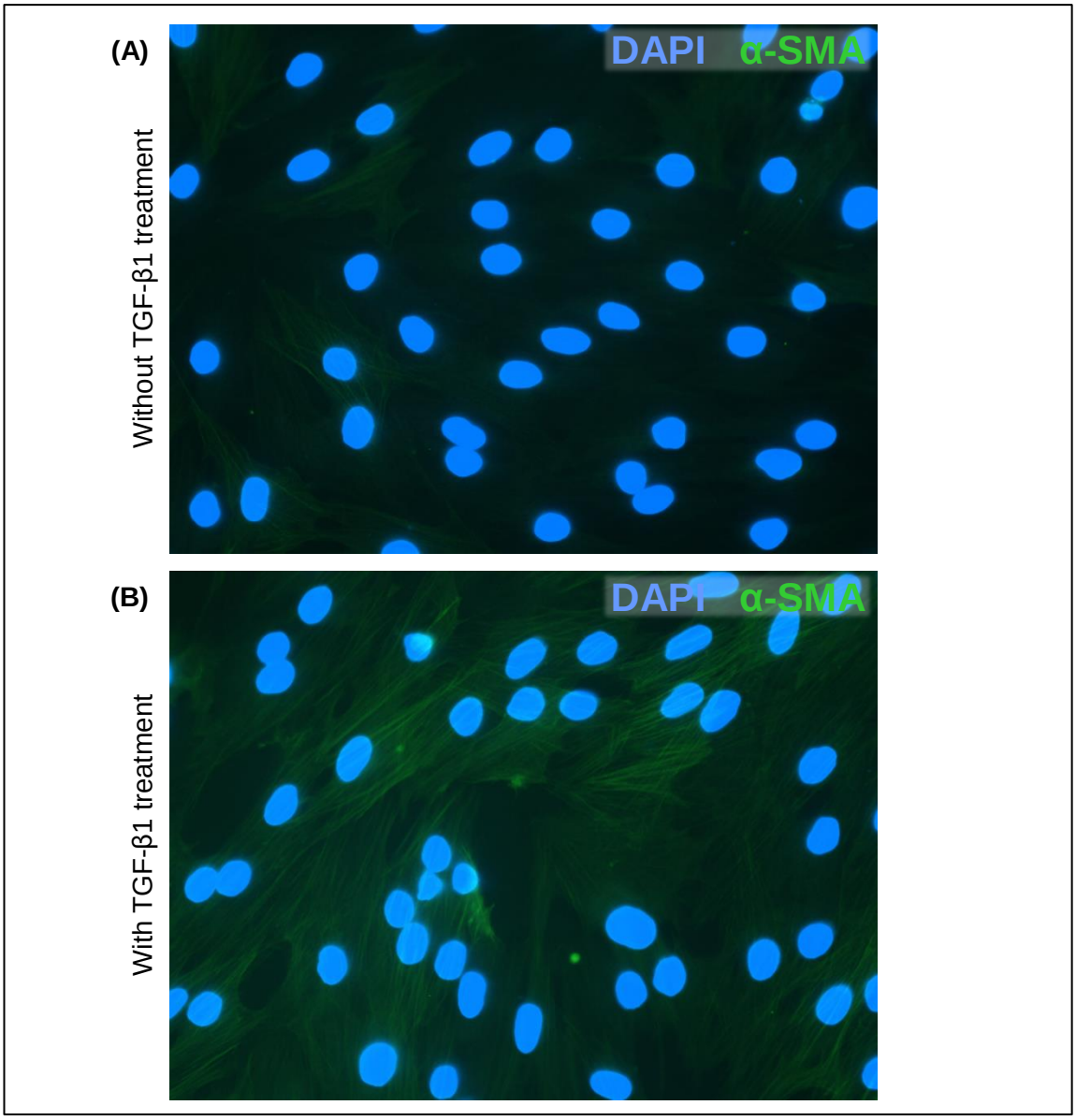

Figure 3.7: Representative photomicrograph of α-SMA expression seen by immunofluorescence in normal oral fibroblast (NOF804). The treatment consists of **(A)** without and **(B)** with 5ng/mL of TGF-β1 treatment after 24 hours. The cell nucleus is stained in **blue (DAPI)** and the α-SMA fibres in **green (FITC)**. (Magnification: 400×).

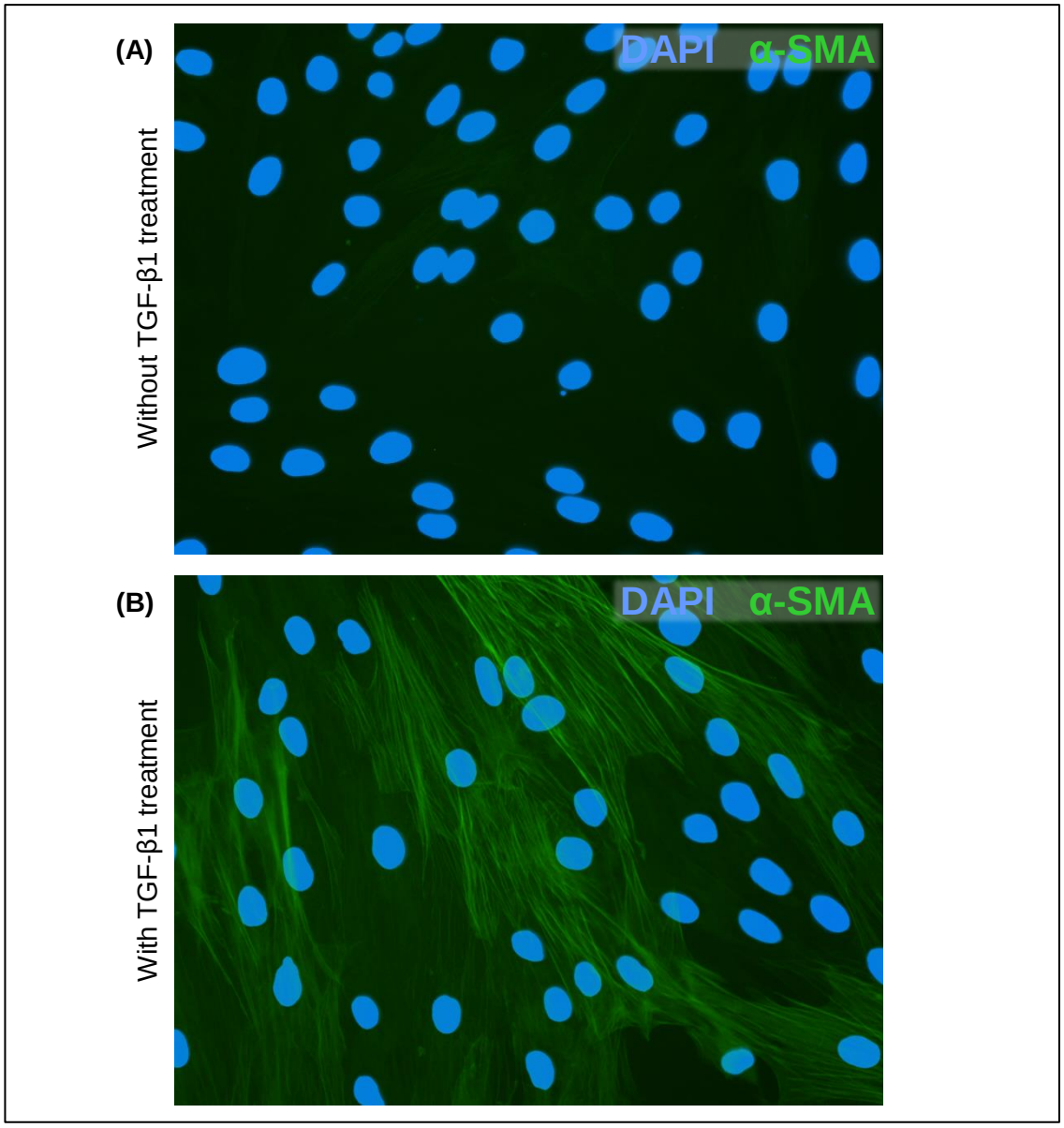

Figure 3.8: Representative photomicrograph of α-SMA immunofluorescence expression in stimulated normal oral fibroblast (NOF804). The treatment consists of **(A)** without and **(B)** with 5 ng/mL of TGF-β1 treatment for 24 hours and further left in SFM for another 24 hours (total of 48 hours). The cell nucleus is stained in **blue (DAPI)** and the α-SMA fibres in **green (FITC)**. (Magnification: 400×).

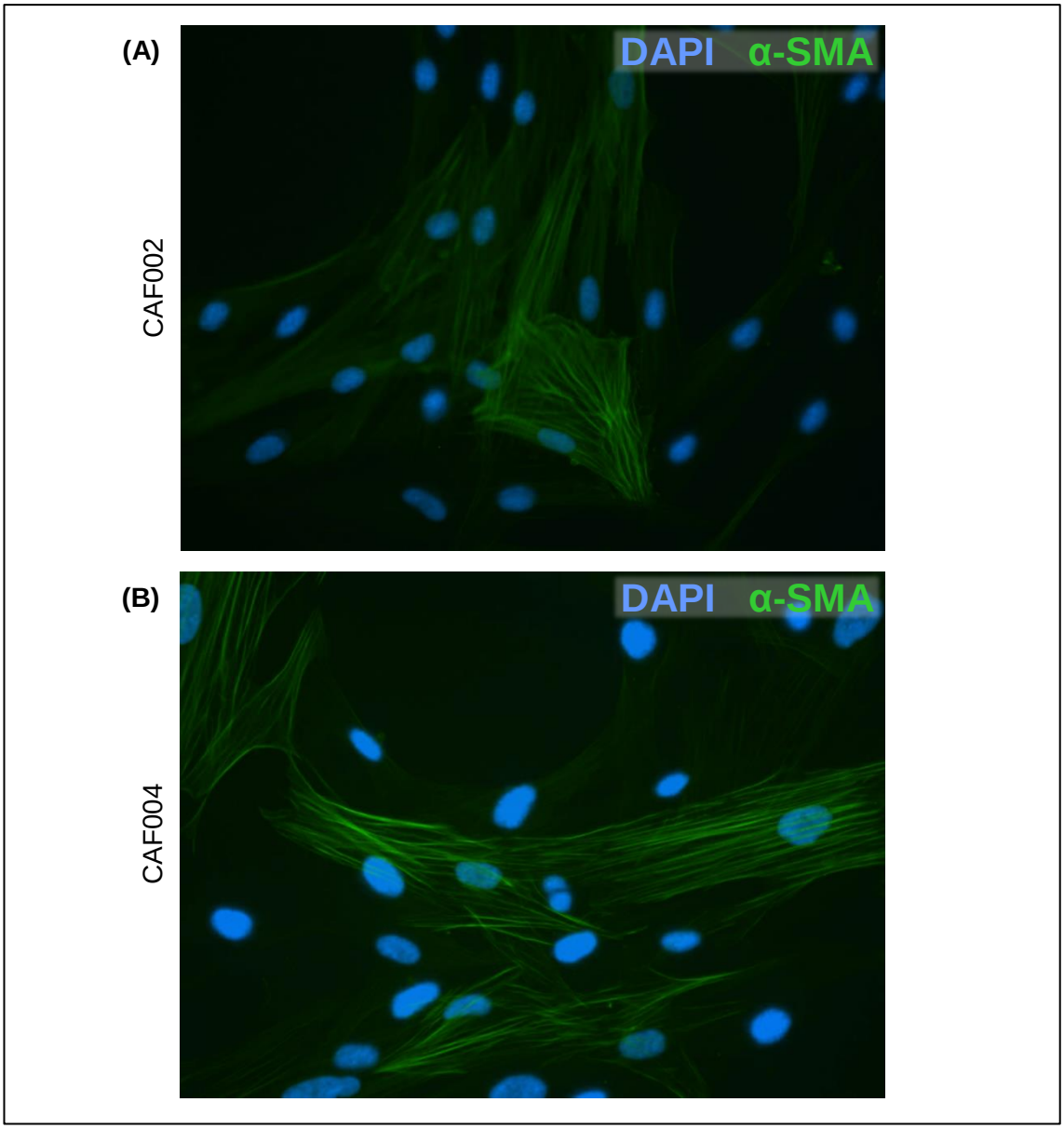

Figure 3.9: Representative photomicrograph of α-SMA immunofluorescence of cancer-associated oral fibroblast (CAF). Two populations of CAF were stained (refer **Table 3.2** for the tissue origin): **(A)** CAF002 (from floor of the mouth) and **(B)** CAF004 (from lateral tongue). The cell nucleus is stained in **blue (DAPI)** and the α-SMA fibres in **green (FITC)**. (Magnification: 400×).

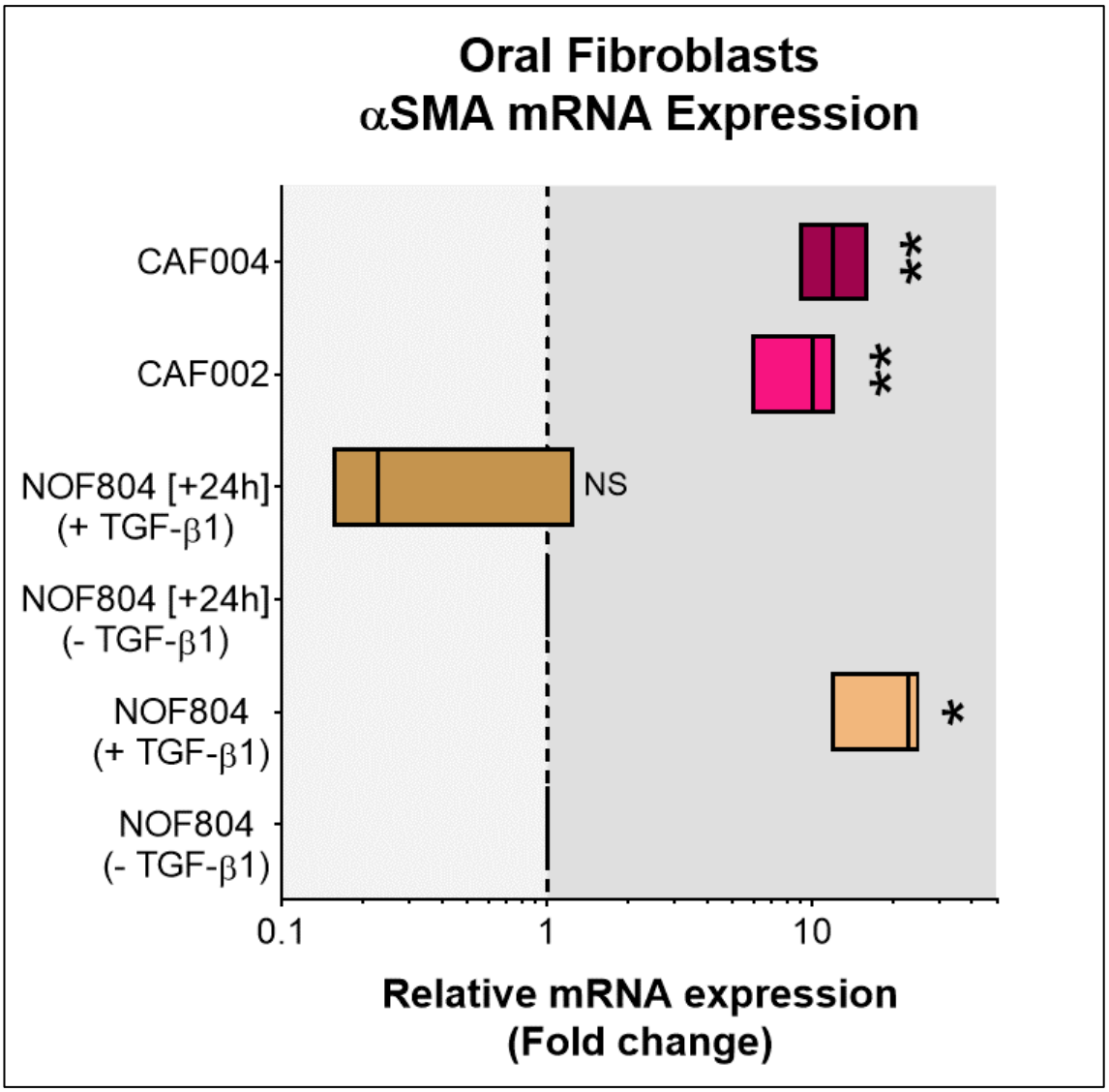

Figure 3.10: α-SMA mRNA expression in oral fibroblasts. Normal oral fibroblasts (NOF) were exposed to TGF-β1 (5 ng/mL) (Abcam) for 24 hours to promote transformation into myofibroblasts. Similarly, additional 24 hours of treatment in SFM was performed to compare the expression. Cancer-associated fibroblasts were not treated and αSMA expression compared to NOF in fold change (normalise to control). Endogenous control to U6 snRNA was used. The graph represents with minimum to maximum (with median line). (* p-value<0.05, ** p-value<0.01, and NS is not significant).

3.3.2.2 Effect of Conditioned Media from Normal Oral Fibroblast, Myofibroblast, and Cancer-associated Fibroblast on OCCL XCR1 and hLtn mRNA Expression.

In continuation from the phenotype assessment of the oral fibroblast derivatives, an experiment was performed to investigate the effect of conditioned media (CM) derived from the fibroblasts on selected oral cancer cell lines, SCC4 and H357 cells by using an indirect co-culture method. After the exposure to the CM for 24 hours, both the mRNA expression of XCR1 and hLtn were investigated.

The XCR1 mRNA expression by SCC4 cells was upregulated after the treatment with CM derived from normal oral fibroblast (NOF), and the cancer-associated fibroblasts (CAF002 and CAF004) (**Figure 3.11 (A)**). The highest XCR1 mRNA fold increase was from exposure to CM derived from NOF (mean 2.57 ± 0.284), followed by CAF002 (mean 2.213 ± 0.2113) and CAF004 (mean 1.453 ± 0.1473) which was significant when compared to normalised vehicle control (treated with SFM only) (p=0.0052, p=0.0046, and p=0.0371 respectively). Interestingly, CM from myofibroblasts showed a significant downregulation of XCR1 mRNA expression in SCC4 (mean 0.4426 ± 0.1354, p=0.0146).

In the case of XCL1 mRNA expression by SCC4 cells, a similar trend was seen (**Figure 3.11 (B)**). However, only exposure to the CM from myofibroblasts (mean 0.3372 ± 0.1264, p=0.0146) and CAF004 (mean 1.633 ± 0.1768, p=0.0232) showed a significant change. The result was similar to that in XCR1 where CM from myofibroblast upregulate and CAF004 downregulated the XCL1 mRNA expression.

For H357 cells, we observed that the XCR1 mRNA expression had a similar trend to SCC4 cells (**Figure 3.12 (A)**). CM from NOF caused significant upregulation of XCR1 mRNA in H357 cells (mean 2.68 ± 0.5961, p=0.0479). In contrast to CM from myofibroblasts, the mRNA expression was significantly downregulated (mean 0.4844 ± 0.0334, p=0.0001). Both CM from CAF002 and CAF004 showed no significant changes in the mRNA expression.

Expression of XCL1 mRNA in H357 cells (**Figure 3.12 (B)**) was significantly downregulated after exposure to CM from myofibroblasts (mean 0.3608 ± 0.1252, p=0.0069). Both CAF002 and CAF004 conditioned media displayed a significant upregulation in the XCR1 mRNA expression in H357 cells (mean 2.306 ± 0.3538, p=0.021 and mean 1.629 ± 0.167, p=0.0197 respectively).

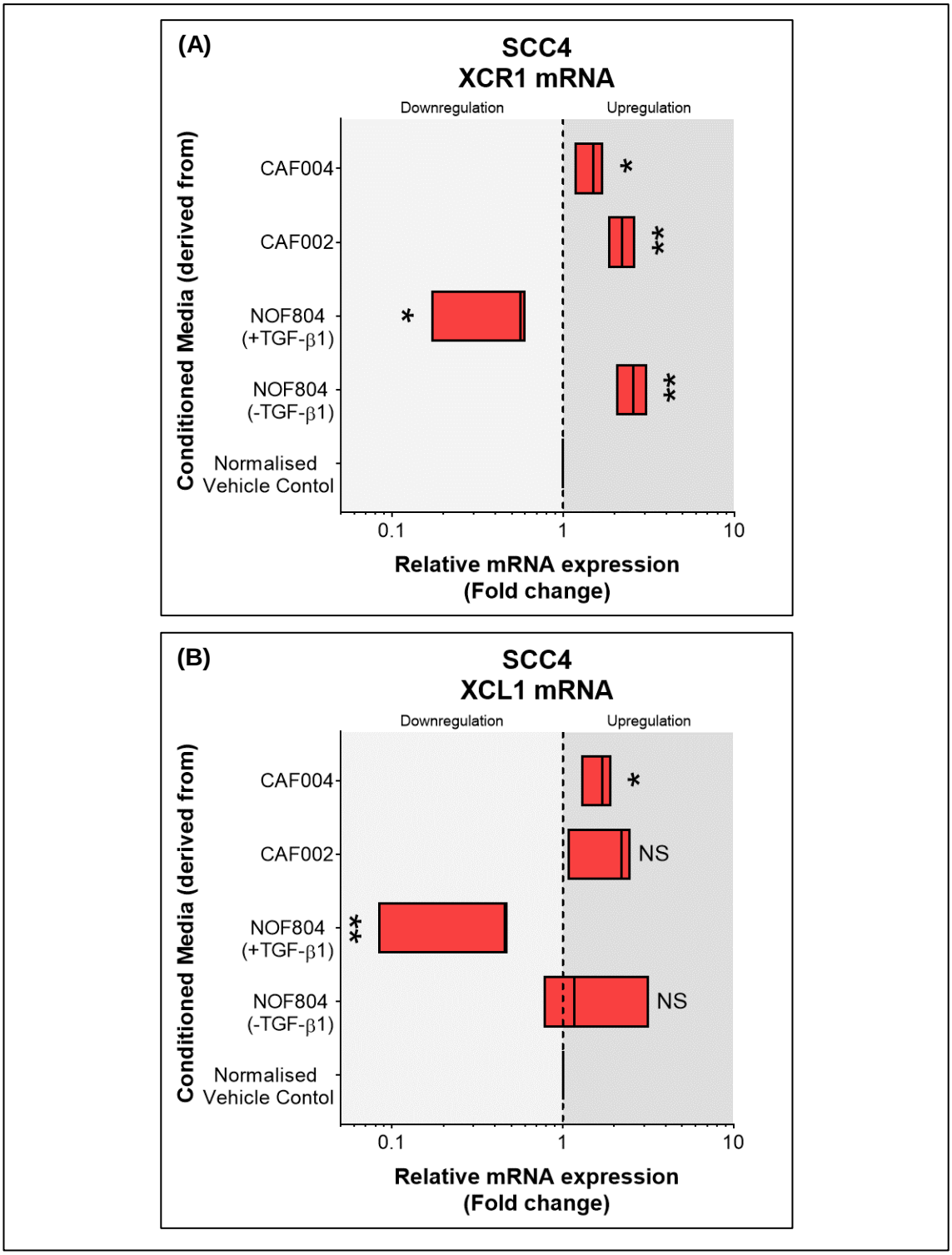

Figure 3.11: mRNA expression of SCC4 cells after exposure to conditioned media from normal oral and cancer-associated fibroblasts (NOF and CAF respectively). The relative quantification of **(A)** XCR1 and **(B)** XCL1 mRNA expression was compared to the normalised control (in fold change). Endogenous control to B2M was used. The graph represents with minimum to maximum (with median line). (* p-value<0.05, ** p-value<0.01, and NS is not significant).

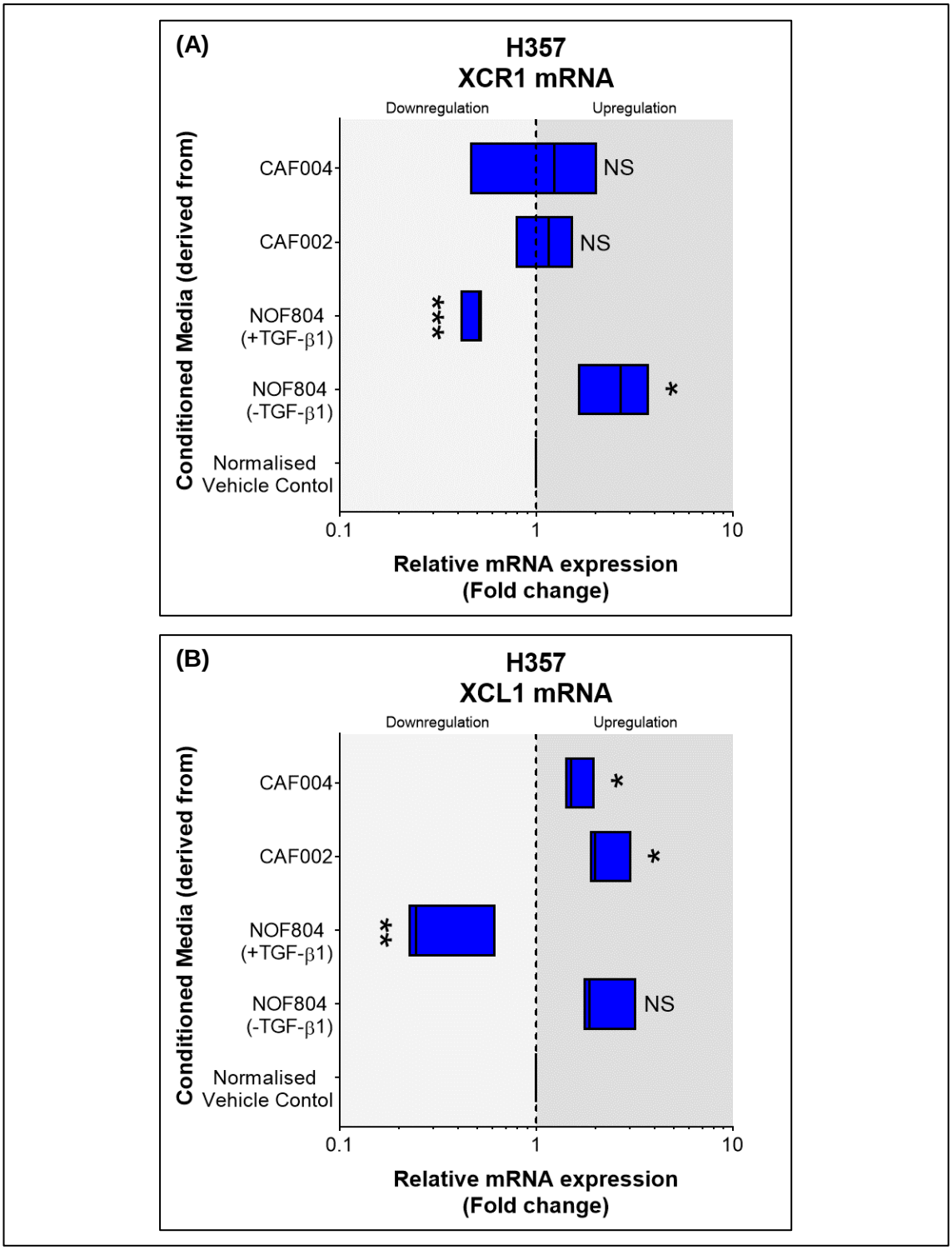

Figure 3.12: mRNA expression of H357 cells after exposure to conditioned media from normal oral and cancer-associated fibroblasts (NOF and CAF respectively). The relative quantification of **(A)** XCR1 and **(B)** XCL1 mRNA expression was compared to the normalised control (in fold change). Endogenous control to B2M was used. The graph represents with minimum to maximum (with median line). (* p-value<0.05, ** p-value<0.01, *** p-value<0.001, and NS is not significant).

3.3.3 Effect of Senescence-induced Fibroblast Conditioned Medium on OCCLs XCR1 and hLtn mRNA Expression.

In Chapter 2, results show that the XCR1 expression in OSCC was upregulated compared to its normal counterpart. The epidemiological data on oral cancer shows a significantly increased risk of disease in patients over 45 with further increased rate with ageing (Ram *et al.*, 2011). Cellular senescence is highly associated with age, contributing to higher risk of developing further disease (van Deursen, 2014; Childs *et al.*, 2015). Senescent fibroblast have been shown to have the potential to promote tumorigenesis (Krtolica *et al.*, 2001). Therefore, in this sub-chapter we investigated the potential of cross-talk between senescence fibroblasts and oral cancer cells in relation to chemokine receptor XCR1 and its ligand hLtn.

3.3.3.1 Phenotype Assessment of the Senescence-induced Oral Fibroblast Cells.

X-gal staining was used to compare senescence in normal oral fibroblast cultures (**Figure 3.13**). A small percentage of senescent cells was detected in NOF (mean 11.6% ± 1.435) following hydrogen peroxide for 2 hours and 14 days in growth media, more than 80% of the NOFs were senescent compared to NOF ($p<0.0001$).

3.3.3.2 Effect of Conditioned Media from Senescence-induced Normal Oral Fibroblast on OCCLs XCR1 and hLtn mRNA Expression.

Following the assessment of the senescence phenotype assessment, the conditioned media from s-NOF was collected and used to study its effect on XCR1 and hLtn mRNA expression in SCC4 and H357 cells by using an indirect co-culture method. After the exposure to the CM for 24 hours, mRNA expression of XCR1 and hLtn was examined.

The SCC4 cells showed a significant downregulation in both XCR1 (mean 0.3214 ± 0.07342, $p=0.0008$) and hLtn (mean 0.0076 ± 0.0015, $p<0.0001$) mRNA expression when compared to the normalised vehicle control (**Figure 3.14**). No significant changes in H357 cells in either mRNA expression level was observed.

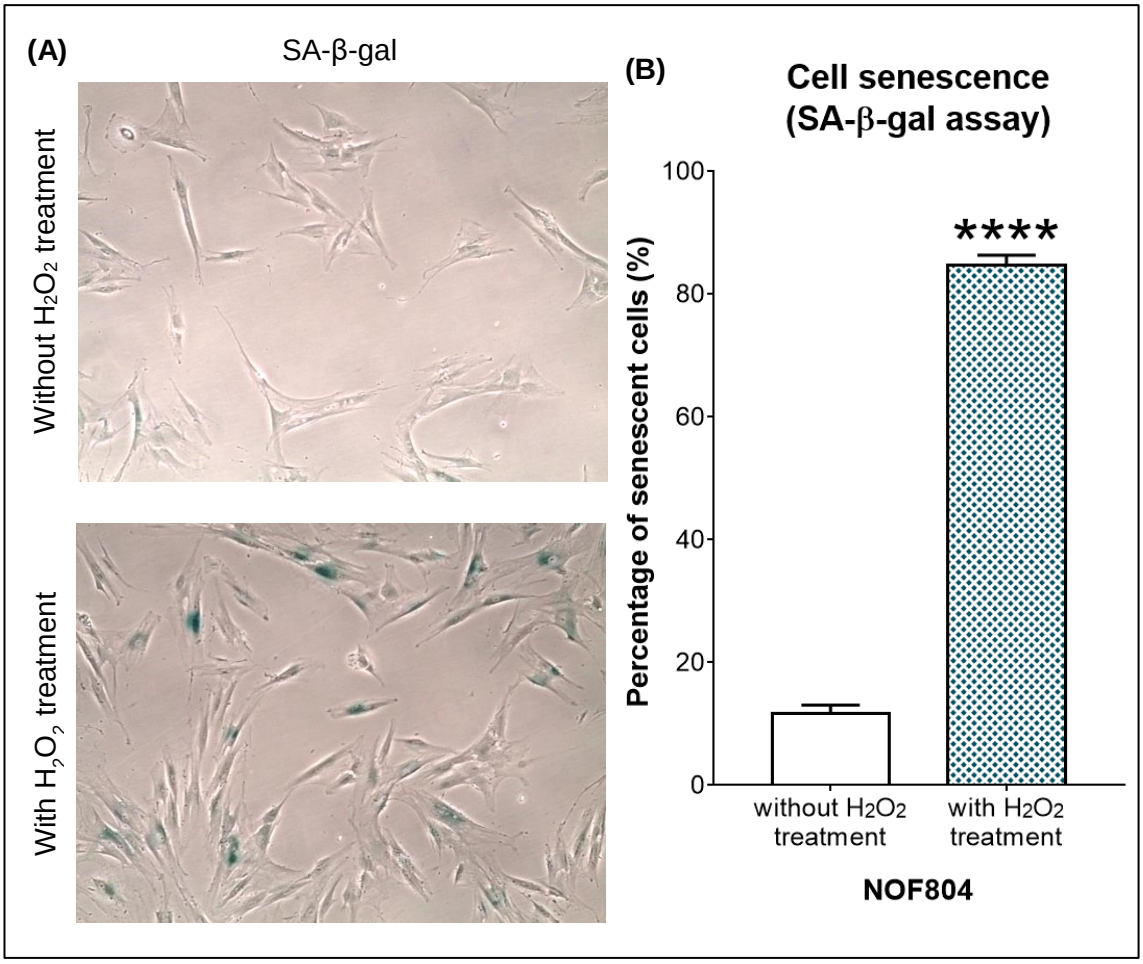

Figure 3.13: Senescence-associated β-galactosidase (SA-β-gal) assay of senescence normal oral fibroblast (s-NOF804). **(A)** Representative image of the cells with and without hydrogen peroxide treatment for 2 hours after 14 days. **(B)** The percentage of senescent cells with and without treatment with 500 µM H_2O_2 (an average of five different optical views) with SEM. (**** p-value<0.0001). (Total magnification: 400×).

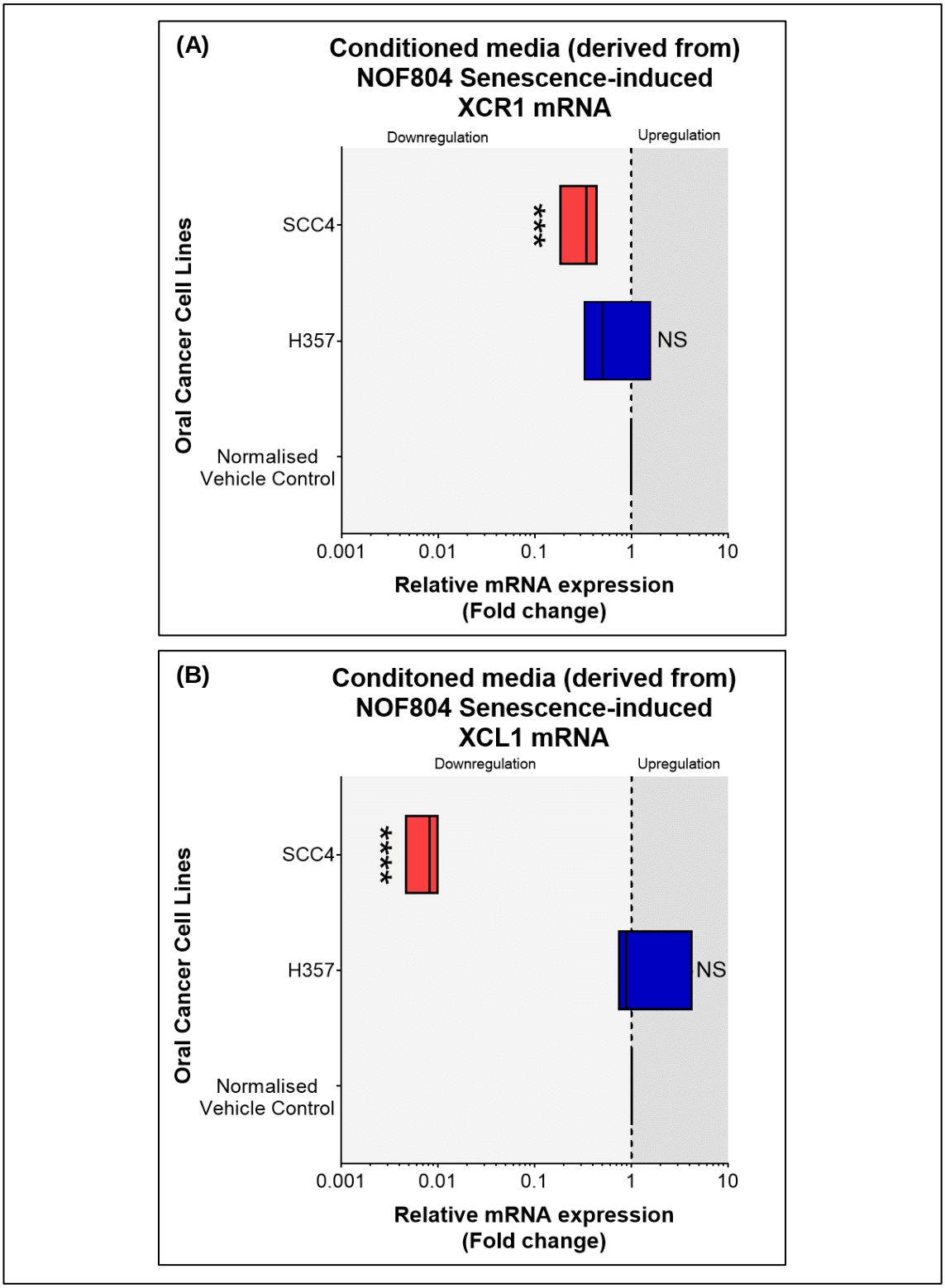

Figure 3.14: mRNA expression of SCC4 (in **red**) and H357 (in **blue**) cells after exposure to the conditioned media from senescence-induced normal oral fibroblast (s-NOF804). The relative quantification of **(A)** XCR1 and **(B)** XCL1 mRNA expression was compared to normalised control (in fold change). Endogenous control to B2M was used. The graph is represented with min to max bar (with median line). (*** p-value<0.001, **** p-value<0.0001, and NS is not significant).

3.4 DISCUSSION

3.4.1 Regulation of XCR1 Surface Expression in OCCL through hLtn Stimulation.

XCR1 receptor expression has been shown in oral normal and carcinoma tissue, as well as several oral cancer cell lines (OCCL) (Khurram *et al.*, 2010). The evidence in Chapter 2 and results in this chapter support the previous findings (refer **Section 3.31**). XCR1 was expressed by all selected OCCL with varying degrees of expression. SCC4 cells showed the highest percentage of XCR1 expression (~80%) and the lowest was H357 cells (~35%) similar to the findings of by Khurram *et al.* (2010). Both OCCLs was derived from tongue OSCC. Recurrent OSCC-derived BICR16 cells population had ~70% expression of XCR1. Both TR146 and BICR22 are derived from neck lymph node OSCC metastasis, which originate from buccal and tongue mucosa respectively and show moderate expression of XCR1 receptor (~40% and ~30% respectively). A transcriptomic analysis has revealed that low expression of XCR1 correlates with cancer progression and poor prognosis in hepatocellular carcinoma (Yanru *et al.*, 2018) which is contradictory to our result. This is probably chemokine receptor tissue bias, where the receptor behaves differently in different type of cell. Histological quantification performed in Chapter 2 showed that XCR1 receptor expression was high (more than 80% of the observed tumour population) in both primary tumour and lymph node metastatic OSCC compared to normal tissue. Furthermore, our assessment was performed on OSCC tissue samples investigating the XCR1 receptor protein expression rather than the transcriptomes. Variations in expression are probably due to the OCCLs originating from different patients with different risk factors, sites and associated factors. Tumour heterogeneity within a cell line population can also effect the expression of chemokine receptors as seen in breast cancer cell line (Norton, Popel and Pandey, 2015). Furthermore, this heterogeneity can also arise from the stem cell-like cancer cells population within the cancer cell lines (Kondo, 2007). This could also influence the expression of XCR1 in OCCLs.

Our findings suggest that the activation of XCR1 receptor by its ligand hLtn can regulate the XCR1 mRNA transcript and receptor surface expression. Only H357 and SCC4 cell lines, derived from tongue OSCC were found to significantly downregulate the surface receptor protein. Both TR146 and BICR22, lymph node metastatic cell lines, as well as recurrent cell line, BICR16 showed a decrease in XCR1 expression but the result was not significant. FADU was the only cell line which showed an upregulation of XCR1. A possible explanation for this is that this cell line is derived from pharynx compared to others which are derived from tongue and buccal mucosa (oral cavity). Both oral cavity

and pharynx have different development (German and Palmer, 2006), presentation and prognosis with distinct pattern of cancer growth and spread (Tshering Vogel, Zbaeren and Thoeny, 2010).

Receptor downregulation may be due to the surface receptor desensitization and internalisation after activation. The β-arrestin signalling pathway is involved in desensitization of chemokine receptors such as CCR2 and CCR7, that leads to receptor internalisation and recycling (Bennett, Fox and Signoret, 2011). Two different types of internalisation of a chemokine receptor exist: an agonist-independent (Class A); and agonist-dependent (Class B) chemokine receptor desensitization. To date, the only chemokine receptor known to belong to Class B are the agonist-treated CXCR4, CCR2 and CCR5 (Bennett, Fox and Signoret, 2011). Moreover, CCR2 and CCR5 receptors can also undergo internalisation through clathrin or caveolin-mediated endocytosis, although this is cell-type dependent (Bennett, Fox and Signoret, 2011). The agonist itself can influence the fate of the activated receptor such in CCR5 receptor, it follows the recycling route, however this may be agonist specific due to promiscuity of chemokine-chemokine receptor binding.

Interestingly, β-arrestin interactions with the intracellular domains of different chemokine receptors appears to have different functional effects. Interaction with specific residues (Ser or Thr) of the C-terminus tail initiate receptor internalization and desensitization, essential requirement for β-arrestin-mediated signalling event (Borroni *et al.*, 2010; Smith and Rajagopal, 2016). Certain chemokine receptor requires additional binding to the third intracellular loops to induce the process. This was also observed in the G-protein coupled opioid receptor (Cen *et al.*, 2001). Nevertheless, even without β-arrestin mediation, the receptor can still be internalized but not recycled (Vines *et al.*, 2003). XCR1 contains C-terminal Ser/Thr residues, providing a possibility of receptor internalisation through β-arrestin. This give an indication that XCR1 receptor internalisation could belong to Class B. Chemokine receptors including XCR1 have complex mechanism of regulation which are not well understood. Further investigation is required to confirm this signalling pathway.

3.4.2 Effect Indirect Co-culture of Oral Fibroblast Conditioned Medium on OCCL XCR1 and hLtn mRNA Expression.

Oral fibroblasts the most dominant constituent of the cell population in OSCC stroma and play a vital role in tumour growth, invasion and metastasis. Several types of oral fibroblast were chosen: normal oral fibroblasts (NOF), myofibroblasts and cancer-associated fibroblasts (CAF). Our results correlate with previous findings on the 'activated' phenotype of myofibroblast and CAF (Kalluri, 2016).

Two CAFs were used to compare effect of their conditioned media. Cell population is distinct in each human giving a unique expression profile. Additionally, unlike immortalized epithelial cell line, fibroblast subpopulation is heterogeneous (Sriram, Bigliardi and Bigliardi-Qi, 2015). In oral fibroblasts, even different area in the mouth; e.g. gingival fibroblast and periodontal ligament fibroblast has different fibroblasts population with distinct functions and expression profile (German and Palmer, 2006). CAF have been shown to express different markers between normal fibroblasts and CAFs in nemosis (a novel way of fibroblast activation (Vaheri *et al.*, 2009)) further adding to fibroblast heterogeneity.

Cancer progression is a dynamic process involving changes in cancer cells, stroma and also changes in extracellular matrix topology which contributes to increased matrix stiffness and chemokine secretion by CAF (Kharaishvili *et al.*, 2014). In ovarian cancer, CAF has been shown to secrete numerous chemokines (CCL5, and CXCL1,11 and 12), cytokines and soluble factors to facilitate its progression (Thuwajit *et al.*, 2017).

The results showed that the mRNA transcripts of both XCR1 and hLtn (XCL1) had a similar trend in both SCC4 and H357 cells when exposed to conditioned media (CM) from the fibroblasts. CAF-CM upregulated XCR1 and hLtn (XCL1) transcripts in SCC4. In contrast, myofibroblast-CM showed a downregulation in both transcripts compared to NOF. This was unexpected as our initial assumption was that the myofibroblast-CM would be similar to that of CAF due to their phenotype similarity. Both myofibroblast and CAF express similar markers and soluble factors such as vimentin, α-SMA, VCAM1, ICAM1, cytokines and matrix metalloproteinase (MMP) (Kalluri, 2016), although enhanced in the latter.

Previously, conditioned media harvested from endometrial carcinoma CAF has been shown to contain chemokines that promote the proliferation and migration of endometrial carcinoma cell lines. Additionally, human CAFs promoted the growth and tumorigenesis compared to normal fibroblast through CXCL12/CXCR4 axis in a xenograft model (Teng *et al.*, 2016). The chemokine-chemokine receptor interaction

increases PI3K/Akt and MAPK/Erk through paracrine signalling, and MMP-2 and MMP-9 in an autocrine manner. CAF-CM has also been shown to induce proliferation and angiogenesis in ovarian cancer cells in vitro through TGF-β1, VEGF and PCNA (mRNA only) (Xu *et al.*, 2013), and regulating invasion, migration, proliferation, and apoptosis in hepatocellular carcinoma (Ding *et al.*, 2015). Oral CAFs were found to secrete cytokines and regulate heat-induced apoptosis in OCCL through the CXCL9/CXCR3 axis (Bian *et al.*, 2012). This suggests that the oral CAFs may be able to influence oral cancer cell behaviour in a paracrine-dependent manner through the hLtn/XCR1 axis.

Another part of our experiment was to investigate the effect of CM from senescence-induced normal oral fibroblast (s-NOF). CM from s-NOF significantly influenced the regulation of mRNA expression for both XCR1 and hLtn (XCL1) in SCC4 cells. Our findings show that the senescence-associated secretory phenotype (SASP) from senescent fibroblast greatly reduces transcript expression when compared to normalised vehicle control. This showed that senescent cells can control the expression of XCR1 and hLtn through paracrine signalling.

Our initial hypothesis was based on the correlation between cancer incidence and increasing age, and the increased presence of senescent cells (Campisi, 2013). Conversely, senescent-aged fibroblasts induce proliferation of prostate epithelial cells through secretion of CCL5 (Eyman *et al.*, 2009). There is a possibility that the senescent-aged fibroblasts produce different soluble factors than those that are stress-induced fibroblast either by genotoxic stimuli (i.e.: H_2O_2 or cisplatin) or replicative senescence. Ectopic expression of CXCR2 has been shown to cause premature senescence via a p53-dependent mechanism where the cells undergo oncogene-induced cellular senescence (OIS) and secrete multiple CXCR2-binding chemokines regulated by the NF-κB and C/EBPβ transcription factors (Acosta *et al.*, 2008; Guo *et al.*, 2013). SASP has been seen to have the potential to promote and supress tumour progression (Lecot *et al.*, 2016). SASP involves the secretion of numerous growth factors, inflammatory cytokines and proteases, rendering a favourable microenvironment for tumour growth (Velarde, Demaria and Campisi, 2013). Therefore, our result suggests that SASP may suppress tumour progression by influencing XCR1/hLtn signalling.

3.5 SUMMARY

Results in this chapter demonstrate that XCR1 function is affected by autocrine signalling through its ligand. Paracrine signalling by the soluble factors secreted by cancer-associated fibroblasts can highly influence the production of XCR1 and hLtn by promoting their mRNA transcript in oral cancer cells. This shows the importance of the tumour microenvironment in supporting the progression of OSCC through XCR1 receptor and hLtn. Further investigation of the identity of the other soluble factors present in the conditioned medium can be examined through specific chemokine ELISA or by use of mass spectrometry to profile the protein components.

CHAPTER 4(a)

DESIGNING THE RECOMBINANT PROTEIN hLtn

CHAPTER 4(a): DESIGNING THE RECOMBINANT PROTEIN hLtn VARIANTS

4.1 INTRODUCTION

In the modern biotechnology era, pure, soluble and functional proteins are in increasing demand. Natural protein sources do not always meet the requirements for quantity, price and ease of isolation; thus recombinant technology is the method of choice to fulfil this demand (Rosano and Ceccarelli, 2014). Recombinant cell factories are constantly employed to produce the proteins. *Escherichia coli* (*E. coli*) is a commonly used as the host due to its low cost, rapid and high-density growth, and the vast availability of compatible molecular tools facilitating protein expression by its low cost (Chen, 2012). Alas, expression of recombinant proteins with *E. coli* often encountered with insoluble and/or non-functional proteins despite of all its advantages. Overcoming these obstacles require new approaches such as the use of strategies focusing on either controlled expression of target protein in an unmodified form or by fusion protein modifications using solubility tags (Sørensen and Mortensen, 2005).

This chapter will discuss the design for production of hLtn and its mutant variants (the wild type, CC3 variant and W55D variant) that will be used in further experiments. The first part of this chapter will explain the design of the recombinant hLtn DNA sequence and its considerations. The next part mainly involves the methodology behind protein production and purification. Several optimisations are required for protein expression and purification. SDS-PAGE and Western blotting was used for protein confirmation. For recombinant hLtn activity and efficacy, the harvested protein was compared with commercial recombinant human lymphotactin (XCL1) (Cat#:300-20; Peprotech, London, UK). XCR1-expressing cells were used to measure the functional activity of the recombinant hLtn using calcium signalling assay.

4.2 METHODS

4.2.1 Protein Sequence Analysis

The protein sequences used in this chapter were obtained from the NCBI website (https://www.ncbi.nlm.nih.gov/protein). The tertiary structure and detailed information of the protein was acquired from the RCSB Protein Data Bank (PDB). The structure of the recombinant fusion protein was generated using the RaptorX tool and then investigated and presented using Pymol. Additionally, the protein sequence was analysed using Expasy ProtParam for a theoretical molecular weight of the protein and distribution of amino acid residues of the protein. List of the tools used are listed in **Table 4.1**.

Table 4.1: List of software tools and its function with link.

Software tool	Function	Link
Protein Data Bank (PDB)	To obtain 3D information of previously crystalized protein structure	http://www.rcsb.org/pdb/home/home.do
Pymol	3D protein structure investigation and imaging	https://www.pymol.org/
Expasy ProtParam	Compute theoretical information (various physical and chemical parameters) of given protein stored in the protein database or user's protein sequences	http://web.expasy.org/protparam/
RaptorX	Create prediction of protein structure tertiary structure based on existing protein crystal structure data	http://raptorx.uchicago.edu/StructurePrediction/predict/

4.3 STUDY DESIGN

4.3.1 Recombinant Fusion Protein Design

The recombinant DNA sequence of XCL1 or hLtn was constructed based on the wild type hLtn sequence obtained from the NCBI website (NP_002986) (**Figure 4.1**). Alternatively, the detailed information regarding the protein can be obtained from UniProt KB website (P47992). Several considerations are required to produce and purify the recombinant hLtn.

Expression organism. The production machine used was *E. coli* because this bacterial system is well established, inexpensive, requires less time and produces a higher yield compared to mammalian, yeast (Baeshen *et al.*, 2014) and insect cells (Gecchele *et al.*, 2015). Most human proteins undergone post-translational modification (PTM) such as glycosylation and this also the case for hLtn. Glycosylation is a unique mechanism in mammalian cells which tags produced proteins for them to be recognized by specific mammalian cells. Many proteins such as antibodies are not functional unless glycosylated. hLtn is unique because even though it is glycosylated, the protein is still active when unglycosylated although this form has lower activity (Dong *et al.*, 2005).

Fusion protein design. Small recombinant proteins are difficult to produce as they are susceptible to degradation by *E. coli*. Moreover, small proteins are difficult to detect using gel electrophoresis. Polyhistidine-tag is usually incorporated into the sequence to facilitate purification. This is not feasible for hLtn as the N-terminal is important for receptor recognition and activation (Rajagopalan and Rajarathnam, 2006). While, truncation of N-terminal has been shown to improve the agonistic properties of chemokine (Lee *et al.*, 2002), adding polyhistidine will abolish the ligand activity. A fusion partner is often incorporated to increase protein stability followed by linker region containing a cleavage site before target protein. This is summarized in **Figure 4.2** below. Each fusion protein domain will be explained in detail below.

Target gene/protein. The design has five important components with hLtn sequence being the main. hLtn contains 114 amino acids including a signal peptide (**Figure 4.1**) whereas mature hLtn only contains 93 amino acids. Only the mature sequence is planned to be incorporated in the sequence design in the current study due to the inability of *E. coli* to cleave the signal peptide. Note that throughout this chapter, hLtn is referred to human XCL1 (UniProtKB-P47992) and not its paralog human XCL2 (UniProtKB-Q9UBD3).

```
        10         20         30         40         50
MRLLILALLG ICSLTAYIVE GVGSEVSDKR TCVSLTTQRL PVSRIKTYTI
        60         70         80         90        100
TEGSLRAVIF ITKRGLKVCA DPQATWVRDV VRSMDRKSNT RNNMIQTKPT
       110
GTQQSTNTAV TLTG
```

Figure 4.1: Human lymphotactin sequence. Total of 114 amino acids including signal peptide (1-21 AA) highlighted in grey and mature protein sequence in yellow (22-114 AA) (UniProtKB-P47992).

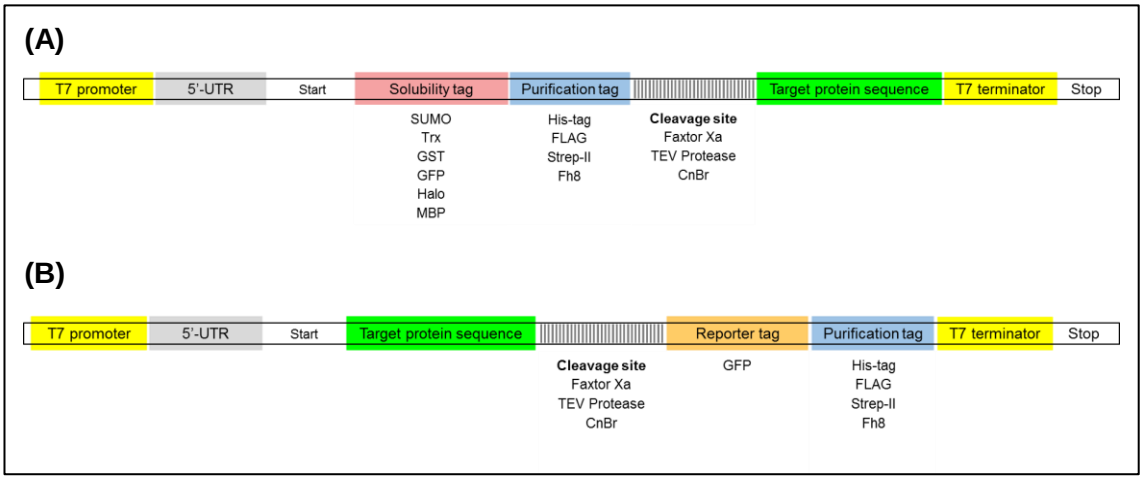

Figure 4.2: Basic expression vector configuration for high throughput expression in E. coli for **(A)** cytoplasmic protein and **(B)** membrane protein. The difference in the configuration is the location of the purification tag, either N- or C-terminal. T7 promoter is used to control the recombinant protein expression in *E. coli*. Tandem affinity tags are essential for high-throughput assay where protein expression initiation, protein solubility and soluble detection involves large tag, while purification requires smaller tag. UTR: Untranslated region.

Affinity tag. Several affinity tags are commonly used to facilitate recombinant protein purification. The most commonly affinity tag is a polyhistidine-tag, ranging from 2 – 10 histidine residues. A cleavable polyhistidine-tag allows production of a large quantity (approximately 10 – 100 mg) of highly pure protein (Kimple, Brill and Pasker, 2013). Commercial expression vectors are designed with at least an affinity tag and sometimes specific to a certain plasmid such as glutathione S-transferase (GST)-tag to pGEX vector and maltose binding protein (MBP)-tag to pMAL and pIVEX vectors (Kimple, Brill and Pasker, 2013). The pET24a plasmid with a strong T7 promoter was chosen as an

expression vector because it is ideal for expressing soluble, nontoxic recombinant proteins in *E. coli* with high levels of expression. The plasmid contains two different affinity tags: T7 tag, which also a reporter tag and a C-terminal His-tag (**Figure 4.3**). Both tags are in the multiple cloning site (MCS) region and can be manipulated accordingly using appropriate endonucleases. Cytoplasmic expression is preferred for the proposed recombinant protein (refer **Figure 4.2**), therefore the polyhistidine sequence will be purposely added at the N-terminus of the fusion protein. The usual strategy is to prefer a N-terminal polyhistidine-tag; and if the recombinant protein does not express or is insoluble, a C-terminal polyhistidine-tag will be considered.

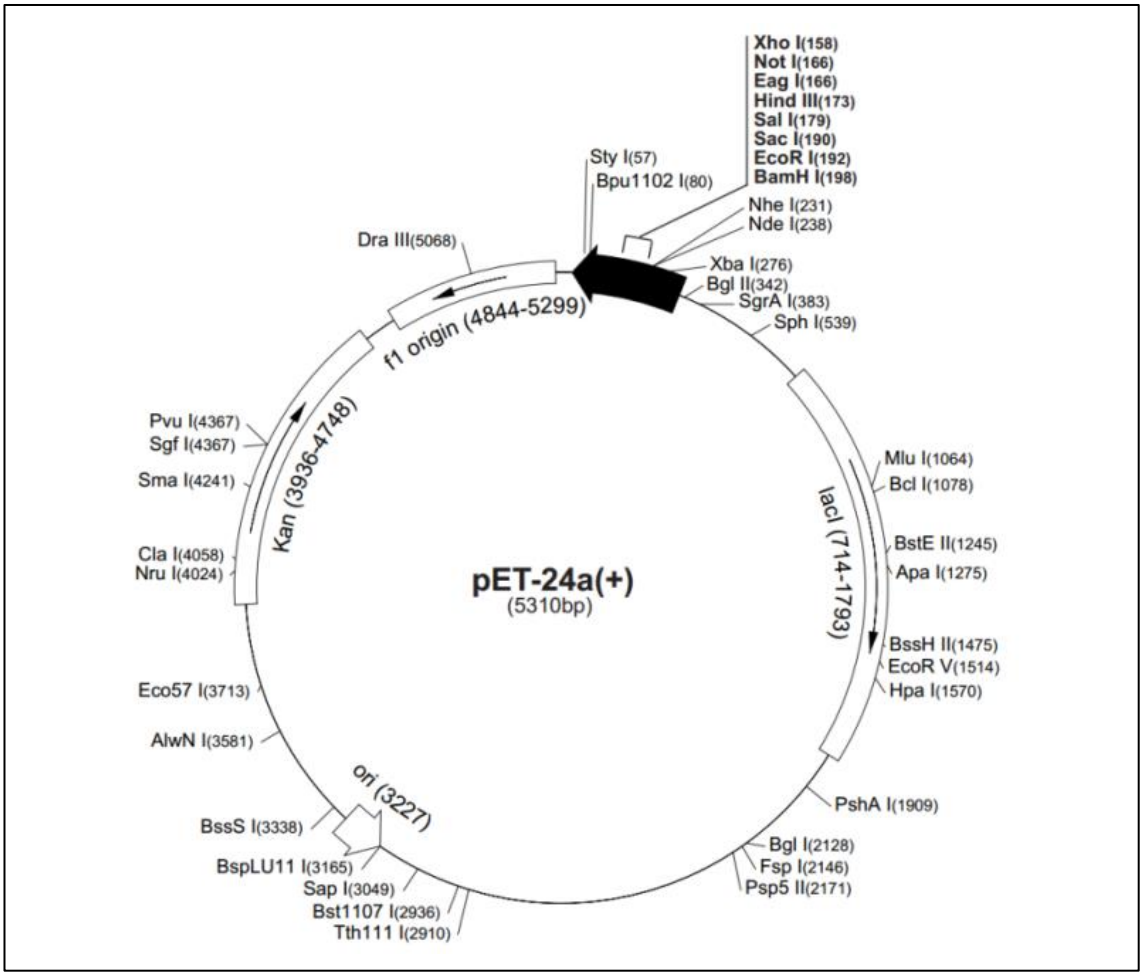

Figure 4.3: pET24a expression plasmid for protein expression from Novagen. The pET-24a vector contains the N-terminal T7 promoter and kanamycin resistance selection marker.

Fusion partners. An alternative method to increase the stability and solubility of the recombinant protein is by adding a fusion partner. There are a number of solubility-enhancing fusion proteins including glutathione-S-transferase (GST), maltose binding protein (MBP), disulphide oxidoreductase (DsbA), nutilization substance A (NusA), small ubiquitin-related modifier (SUMO), thioredoxin (TrxA), and hyper-acidic protein tags (Lebendiker and Danieli, 2014). For our experiments, the solubility enhancer considered was the lipoyl domain from *B. stearothermophilus*, an acidic fusion partner. Lipoyl domains can be found in various species but 1LAC, a lipoyl domain from *Bacillus stearothermophilus* (Dardel *et al.*, 1993) containing 85 amino acids was selected. The lipoyl domain provides an electrostatic protection which reduces protein aggregation, thus providing an adequate time to allow correct protein folding. Another advantage of the lipoyl domain is it is extremely soluble and often prevents formation of inclusion bodies of the recombinant protein as well as resistant to protease activity.

Linker protein. To increase the flexibility of the protein during purification and cleavage, a linker region was added connecting the His-Lipoyl domain to the hLtn sequence. The linker region also further increases the solubility of the protein. It acts as a "neck" which gives mobility to the tag proteins allowing them to attach more easily to the purification column. The length of the linker used is 19 amino acids as this has been previously shown to increase the solubility and protein folding and unfolding (Robinson and Sauer, 1998).

Cleavage proteases. The majority of the recombinant hLtn design (see **Figure 4.2 (A)**) for the protein sequence design) and production procedure was adopted from Peterson *et al.* (2004) with some modifications to fit our purification scheme. Peterson's method made some modifications to the hLtn sequence; (1) conversion of Methionine (Met) to Alanine (Ala): M63A and M72A, and (2) insertion of the tripeptide G-M-V at the beginning of the mature sequence. The G-M dipeptide is required for CNBr treatment which removes the protein tag during purification and the conversion of Met tot Ala is to remove the possibility of unintentional cleavage of the hLtn. The initial cleavage protease of choice was Factor Xa which recognize IEGR↓ protein sequence. Alternatively, TEV protease was used for another construct which recognizes the amino acid sequence ENLYFQ↓G. Both were added to facilitate removal of the tag region from the mature hLtn.

Restriction sites. For protein expression, the pET24a plasmid was used (refer **Figure 4.3**). In order to ligate the recombinant sequence into the plasmid, several strategic restriction sites were included to allow transfer of the target DNA sequence into

other plasmids. A NdeI restriction site was positioned at the beginning of the sequence, BamHI positioned inside the linker region and EcoRI at the end. The restriction sites are essential to cut the recombinant DNA ends and ligate them into the expressing vector. The DNA sequence is then optimized by GenScript (**Appendix 11**). A stop codon TAA increases the efficiency of translational termination suggested by the vector manufacturing company and another terminal codon TAG was also included.

By considering above specifications, two fusion protein designs were considered: fusion protein hLtn (IEGR) and hLtn (TEV) (**Figure 4.4**). The 3D structure of the fusion proteins was generated using online tool RaptorX (Chicago, USA) (**Figure 4.5**). Additionally, the differences between the hLtn variants, wild type, CC3 and W55D mutants can be found in **Figure 4.6**.

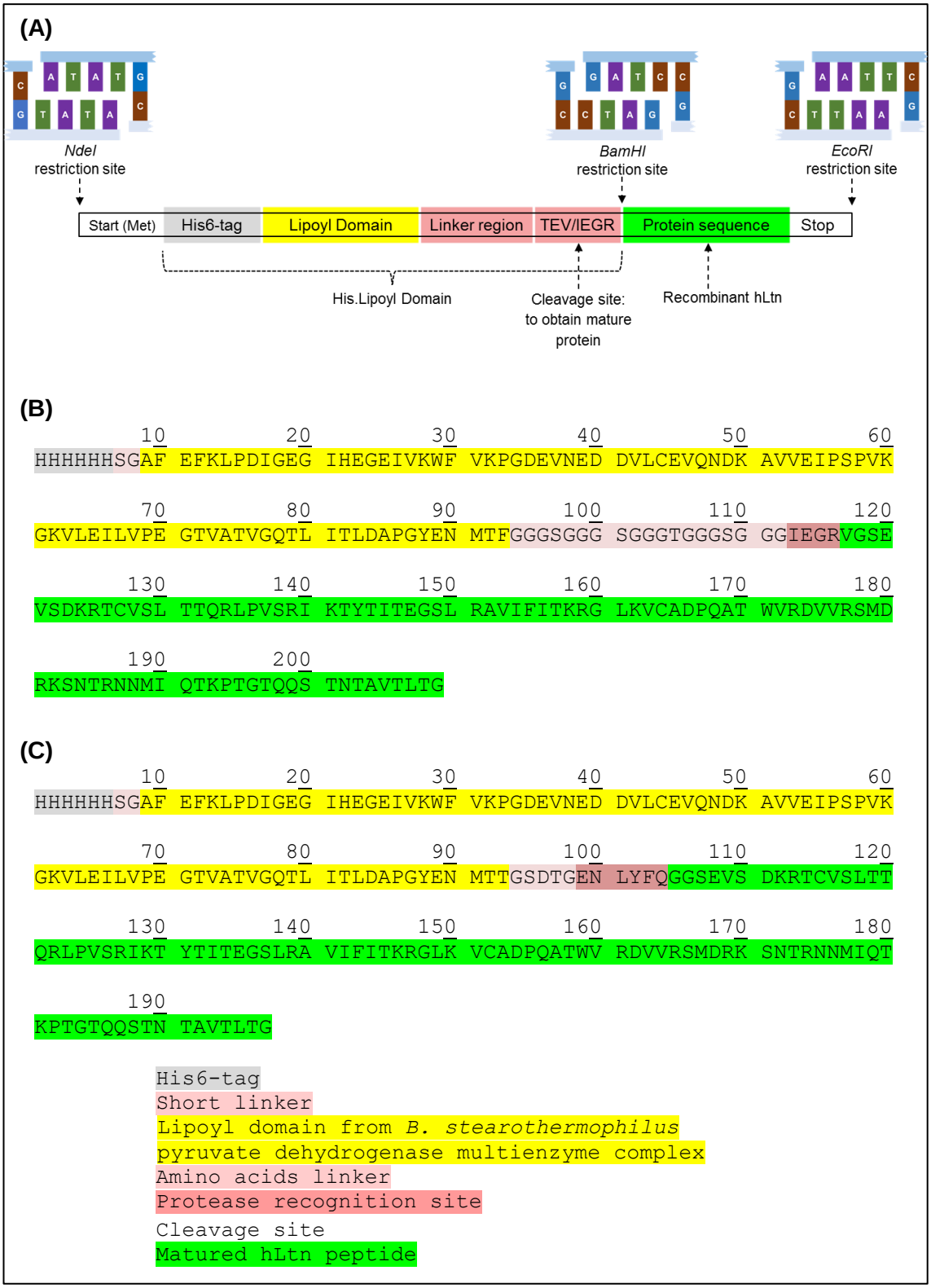

Figure 4.4: Recombinant fusion protein hLtn design. **(A)** Base design template of the fusion protein with specific locations of endonuclease restriction site. Protein sequence of the recombinant fusion protein with **(B)** Factor Xa and **(C)** TEV protease cleavage sites.

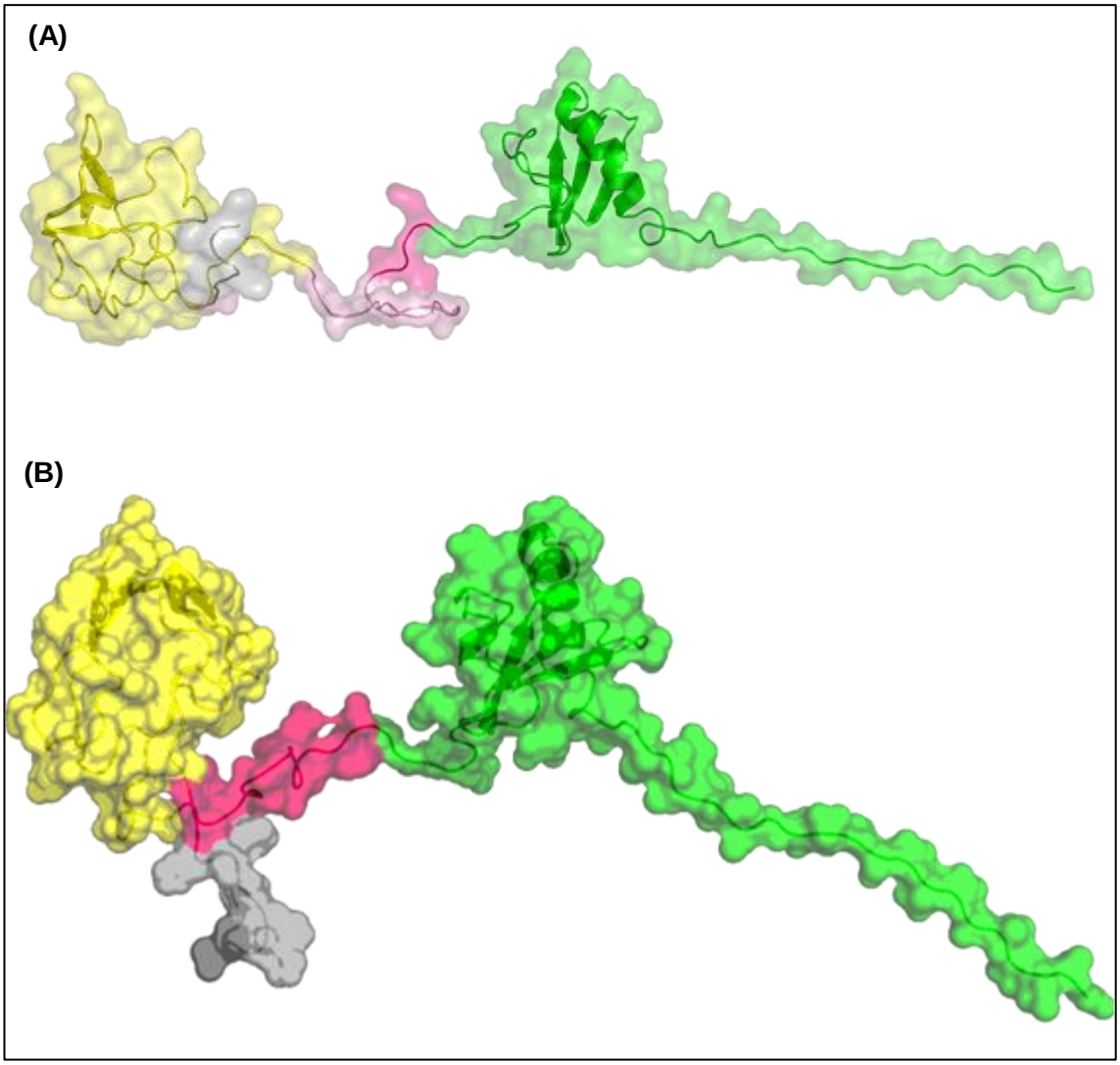

Figure 4.5: Fusion protein sequence prediction generated using RaptorX online tool (Chicago, USA). The 3D protein structure was created using Pymol (Schrödinger, LLC, USA). The 3D structure of the fusion protein with **(A)** Factor Xa and **(B)** TEV cleavage site. Each section has specific functions to facilitate hLtn production and purification. The fusion protein contains N-terminal polyhistidine-tag followed by a lipoyl domain, linker region, protease cleavage site and mature hLtn.

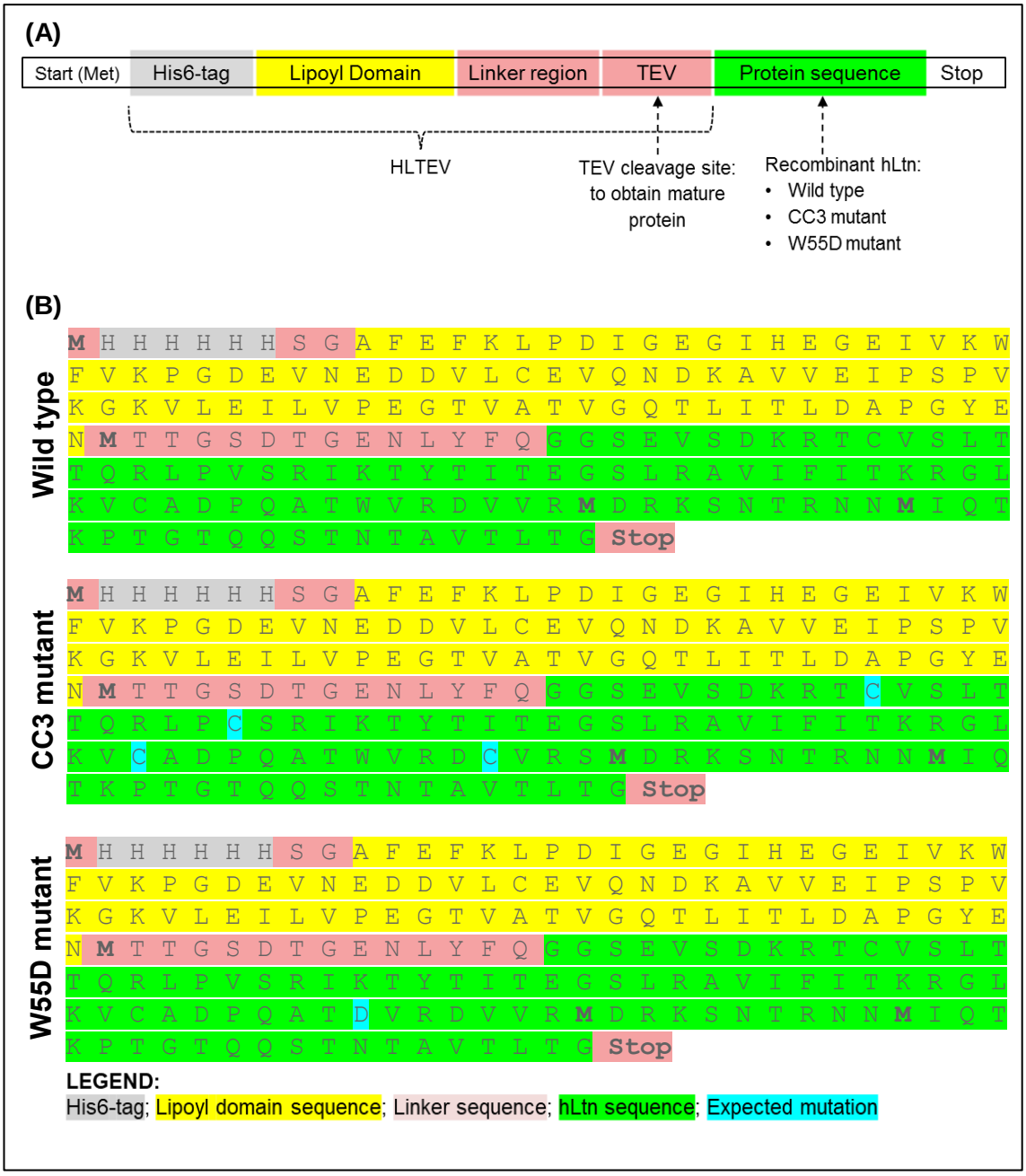

Figure 4.6: The recombinant hLtn variant constructs. **(A)** Base design for the recombinant fusion protein. **(B)** The recombinant protein sequence for wild type, CC3 and W55D mutants.

4.3.2 Recombinant Fusion Protein Expression and Purification

Two steps are involved in producing the protein: Upstream and downstream processing. The upstream processing mostly involves preparation of the expression plasmid and downstream processing involves the protein purification.

***Bacterial host strains*.** To initiate protein expression, the first consideration is to select the appropriate expression system that is suitable to express the recombinant fusion protein. As explained earlier, the *E. coli* system is the most practical and has been used previously to express hLtn (Volkman, Liu and Peterson, 2009), although several modification were considered for the fusion protein containing hLtn. Two different *E. coli* strains were considered for the expression which were BL21 (DE3) and C41 (DE3). C41 (DE3) strain is derived from BL21 (DE3) with several modification to accommodate expression of toxic proteins (Dumon-Seignovert, Cariot and Vuillard, 2004). As we have no information of the fusion protein behaviour in *E. coli*, this optimization was considered.

Protein purification method. There are several types of purification, but a suitable purification method must be considered to ensure optimal recombinant protein purification. Immobilized metal affinity chromatography (IMAC) was considered to be the most appropriate method. Metal ions that are usually used for IMAC are copper, nickel, zinc, and cobalt. Each metal has a different affinity and specificity towards the polyhistidine tag (**Figure 4.7**). Nickel is the best choice with moderate-high affinity and moderate specificity to polyhistidine. Additionally, the purification format was also considered. Batch purification was opted for as it enables longer incubation time (up to 24 hours) and can be performed at low temperature (4°C) when compared to spin column and cartridge methods.

Buffer content. Common buffer recipes for protein purification are either a Tris-base or sodium phosphate buffer. The buffer recipe was a modification from Volkman (2006) and Tuinstra (2008). Sodium phosphate buffer with pH 7.5 was preferable to mimic physiological condition. Expasy ProtParam analysis shown that the theoretical isoelectric pH (pI) for the fusion protein (**Table 4.2**) and the mature hLtn variants (**Table 4.3**) are ~6 and ~10 respectively. As a rule of thumb, the buffer pH should be ~2 pH units above or below the pI. This is to facilitate the protein purification allowing it to be charged in the buffer solution. The buffer pH must be precisely controlled as this is required to keep the protein charged, thus allowing electrostatic repulsion to prevent the protein from aggregating. Also, it is important to keep in mind that a basic pH is essential to avoid the His protein from being protonated which would reduce its binding to the metal ions.

Furthermore, addition of glycerol can help reduce protein aggregation (Lebendiker and Danieli, 2014). IMAC purification can sometimes introduce binding besides the target protein. Addition of 10 mM imidazole can further reduce contamination by unwanted His-rich proteins produced by *E. coli*.

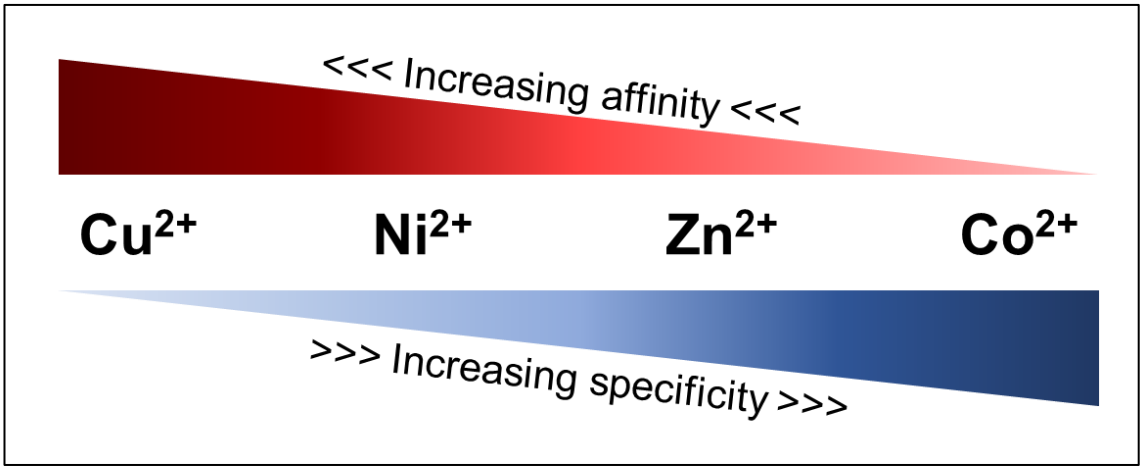

Figure 4.7: Polyhistidine-tag affinity and specificity towards different metals ions. Metal ion with higher specificity to polyhistidine has a lower affinity and vice versa. The metal ions that are usually used in IMAC purification are copper (Cu^{2+}), nickel (Ni^{2+}), zinc (Zn^{2+}) and cobalt (Co^{2+}).

By using all the information, the flow of protein production is summarized in **Figure 4.8**.

Table 4.2: Expasy ProtParam analysis for recombinant HL.IEGR-hLtn and HL.TEV-hLtn.

	HL.IEGR-hLtn	**HL.TEV-hLtn**
Number of amino acids	209 amino acids	198 amino acids
Molecular weight	22163.92 Da (~22 kDa)	21671.42 Da (~22 kDa)
Theoretical pI	6.41	5.98
Total number of negatively charged residues (Asp + Glu)	24	25
Total number of positively charged residues (Arg + Lys)	22	21
Extinction coefficient (M^{-1} cm^{-1} at 280 nm measured in water) Abs 0.1% (=1 g/L)	assuming all pairs of Cys resides form cystines	
	14105	15595
	0.636	0.720
	assuming all Cys residues are reduced	
	13980	15470
	0.631	0.714
Estimated half-life	3.5 hours (mammalian reticulocytes, *in vitro*) 10 min (yeast, *in vivo*) >10 hours (*E. coli*, *in vivo*)	
Instability index (II)	28.34	19.27
	This classifies the protein as stable	
Aliphatic index	77.27	80.10

Table 4.3: Expasy ProtParam analysis for recombinant hLtn variants.

	Wild type	CC3 mutant	W55D mutant
Number of amino acids	93 amino acids		
Molecular weight	10229.70 Da (~10 kDa)	10237.71 Da	10158.58 Da
Theoretical pI	10.63	10.16	10.36
Total number of negatively charged residues (Asp + Glu)	6		7
Total number of positively charged residues (Arg + Lys)	15		
Extinction coefficient (M^{-1} cm^{-1} at 280 nm measured in water) Abs 0.1% (=1 g/L)	assuming all pairs of Cys resides form cystines		
	7115 0.696	7240 0.707	1615 0.159
	assuming all Cys residues are reduced		
	6990 0.683	6990 0.683	1490 0.147
Estimated half-life	30 hours (mammalian reticulocytes, in vitro) >20 hours (yeast, in vivo) >10 hours (*E. coli*, in vivo)		
Instability index (II)	25.51	21.82	28.04
	This classifies the protein as stable		
Aliphatic index	74.30	68.06	74.30

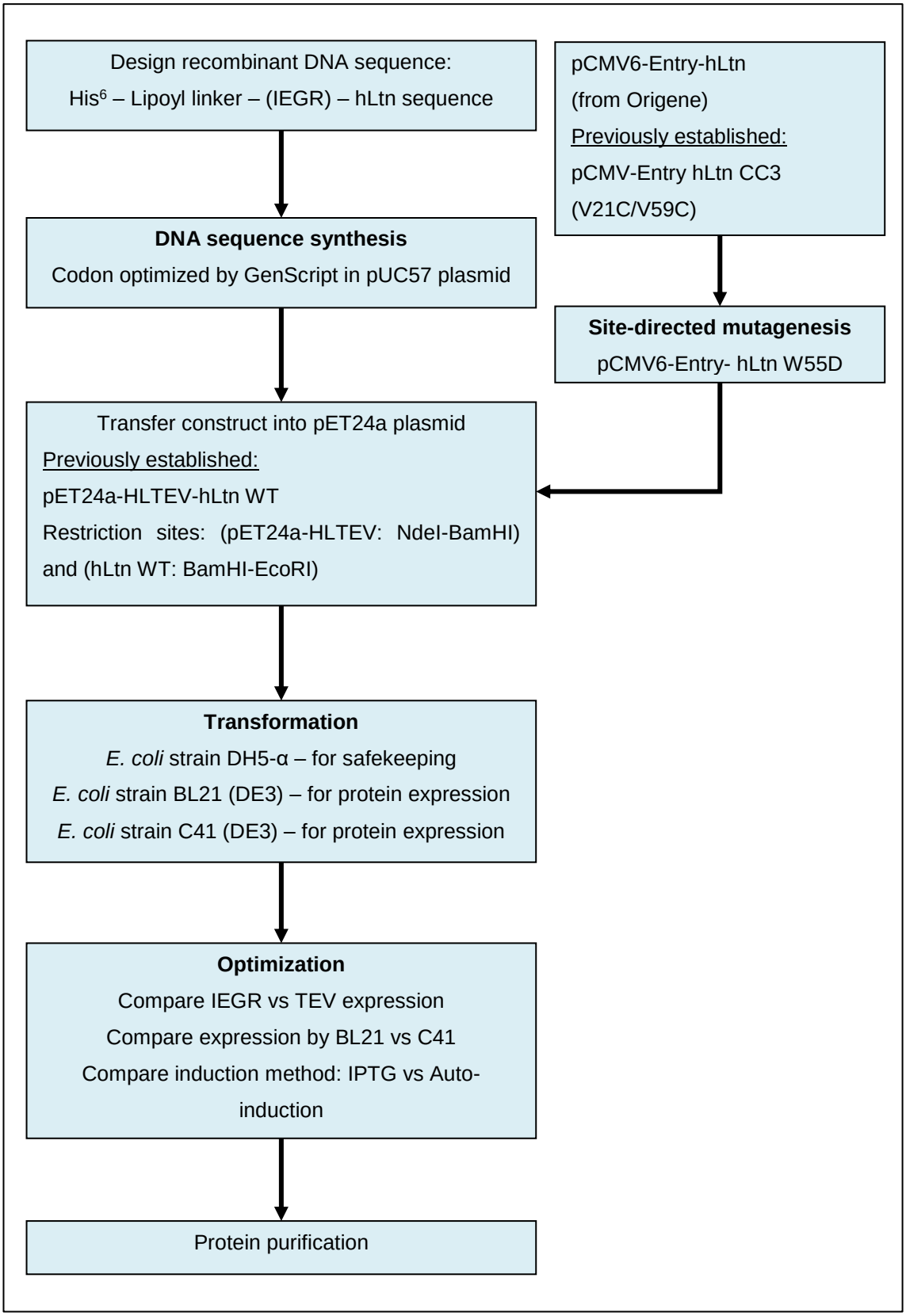

Figure 4.8: Upstream processing for hLtn protein production

CHAPTER 4(b)

PRODUCTION OF THE RECOMBINANT hLtn VARIANTS

CHAPTER 4(b): PRODUCTION OF THE RECOMBINANT hLtn VARIANTS

4.1 INTRODUCTION

The *E. coli* system has been a ubiquitous system to express recombinant protein, even for those of eukaryotic origin. However, there are some challenges in expressing the protein in its original form as nearly half of all proteins of human origin are glycosylated. Glycosylation has an important functional and structural influence in many key biological processes (Krištić and Lauc, 2017). hLtn has an unusual feature of O-linked glycan attached to a C-terminal structure in a portion of the purified protein from mammalian culture. While there are some proteins that are not functional without glycosylation, hLtn has been shown to activate its receptor with lower activity (Dong *et al.*, 2005).

Production and purification of hLtn using the *E. coli* system has been established previously (Volkman, Liu and Peterson, 2009). Various techniques have been applied to produce hLtn variants available in the literature, notably by Volkman's group where changes in certain amino acids to accommodate the purification and structural analysis. Most of the protein produced this way forms protein aggregates which result in insoluble protein. In this chapter, further possibility was explored to produce a soluble protein.

Protein insolubility is the common challenge in protein production and purification. It is time consuming due to introduction of additional purification steps as well as decreasing the protein yield (Rosano and Ceccarelli, 2014). This problem is partially due to 1) expression in a different system such as expressing a mammalian protein in bacterial system; 2) improper protein folding due to macromolecular crowding, where exposed hydrophobic core allowing protein tendency to form dimer and 3) incorrect disulphide linkage due to protein-protein interaction.

The aim of this chapter is to implement an alternative method to produce and purify the chemokine protein. Additionally, by introducing a lipoyl domain to the fusion protein (as discussed in **Chapter 4a**), we attempted to reduce the formation of protein aggregation.

4.2 EXPERIMENTAL

4.2.1 Materials

List of detailed information of the materials (reagents, kits, equipment, software and miscellaneous) used in the chapter can be found in **Appendix 1-5**.

.

Table 4.1: Primer designs used for the cloning and sequence check of hLtn into pET24a vectors.

Name	Sequence	
T7 promoter T7 terminator	**Fwd** **Rev**	5′-TAATACGACTCACTATAGGG-3′ 5′-GCTAGTTATTGCTCAGCGG-3′
Lipoyl check	**Fwd** **Rev**	5′-AAACATGACGTTTGGCGGTGG-3′ 5′-CATTCTGAACTTCGCACAGC-3′
hLtn check	**Fwd** **Rev**	5′-CATATGCATCATCATCATCATCACTCGGGTG-3′ 5′-GAATTCATTAACCCGTCAGCGTCACTGC-3′

4.2.2 *E. coli* Culture and Growth Media Preparation

Three different *E. coli* strains were used: DH5-α, BL21 (DE3) and C41 (DE3). The *E. coli* culture was provided by Dr. Tuck Seng Wong (ChELSI Institute and Advanced Biomanufacturing Centre, Department of Chemical and Biological Engineering, The University of Sheffield). Tryptone-yeast extract (TYE) culture media was prepared with 16 g tryptone, 10 g yeast extract, 5 g sodium chloride in 1 L and sterilized by autoclaving. TYE agar plates were prepared with 10 g tryptone, 5g yeast extract, 4 g sodium chloride, 15 g agar, and sterilize by autoclave. Appropriate antibiotics were added into the agar before plating (100 µM ampicillin or 50 µM kanamycin).

4.2.3 Molecular Cloning

4.2.3.1 Site-directed Mutagenesis of W55D

The pCMV6 Entry-XCL1 (NM_002995) human chemokine construct (Cat#: SC309015; Cambridge Bioscience Ltd., Cambridge, UK) was purchased from OriGene. The mutagenic primer (**Table 4.2**) was designed using the OneClick programme (link: http://tucksengwong.staff.shef.ac.uk/OneClick/). The PCR mixture can be found in **Table 4.3** and the programme in **Table 4.4**.

Table 4.2: Primers used for the mutagenesis.

W55D (OneClick)	**Fwd**	5′-CAAGCCACAGACGTGAGAGACGTGGTCAGGAGCATGGACAGGAAAT-3′
	Rev	5′-GTCTCTCACGTCTGTGGCTTGTGGATCAGCACAGACTTTTAGGCCA-3′

Table 4.3: PCR mixture.

Component	**Stock conc'**	**Volume per Reaction (µL)**	
		TubeF (Forward Primer)	**TubeR (Reverse Primer)**
Distilled Water	-	41.5	41.5
Cloned Pfu reaction buffer	10×	5	5
dNTPs	10 mM each	1	1
DNA template	100 ng/µL	0.5	0.5
Primer 1	20 µM (20 pmol/µL)	1	0
Primer 2	20 µM (20 pmol/µL)	0	1
Pfu Turbo DNA Polymerase	2.5 U/µL	1	1
Total		**50**	**50**

Table 4.4: Two-stage PCR programme.

Step	**Temperature (°C)**	**Time**
1	95	2 minutes
2	95	30 seconds
3	55	30 seconds
4	72	5 minutes 18 seconds
5	-	Go to Step 2, repeat 9 times
6	-	Pause, mix TubeF and TubeR, redistribute equally, and continue
7	95	30 seconds
8	55	30 seconds
9	72	5 minutes 18 seconds

10	-	Go to Step 7, repeat 19 times
11	72	10 minutes
12	8	Hold

4.2.3.2 Restrictive Digestion

The reaction mixture for restrictive digestion was as **Table 4.5** below. The reaction mixture was incubated in PCR machine at 37°C. PCR product was purified using QIAquick PCR purification kit (Cat#: 28106; QIAGEN, Manchester, UK) or QIAquick gel extraction kit (Cat#: 28706; QIAGEN, Manchester, UK).

Table 4.5: Reaction mix for restrictive digestion.

Component	Stock conc'	Volume (µL)	Final conc'
Water		88 – x	
Buffer 4	10×	10	1×
PCR plasmid product/Plasmid	Measure using Nanodrop	x	
Restriction enzyme 1: *BamH*I (NEB)	20 U/µL	1	20 U/100 µL
Restriction enzyme 2: *EcoR*I (NEB)	20 U/µL	1	20 U/100 µL
Total		**100**	

4.2.3.3 Ligation of hLtn Variants Gene Sequence into pET-24a

The ligation was achieved using a PCR machine. The reaction mixture used was prepared as in **Table 4.6** below. The reaction mixture was incubated in PCR machine at 16°C. After the reaction, 5 µL was transformed into *E. coli* strain DH5-α.

Table 4.6: Ligation reaction mixture.

Component	Stock conc'	Volume (µL)	Final conc'
Water		16 – x – y	
Buffer	10×	2	1×
Digested plasmid	Measure using Nanodrop	x	50 ng
Digested insert	Measure using Nanodrop	y	3× the amount of plasmid used (3 insert molecules: 1 plasmid molecule)
T4 DNA ligase (NEB)	400 cohesive end unit/µL	2	40 U/µL
Total		**20**	

4.2.3.4 Polymerase Chain Reaction (PCR)

The reaction mixture used was prepared as in **Table 4.7** below. The reaction mixture was incubated in PCR machine using programme described below (**Table 4.8**). The PCR products were purified using QIAquick PCR purification kit or QIAquick gel extraction kit. The template DNA was separated from the PCR product using DNA gel electrophoresis followed by gel extraction. For PCR purification, 1-2µL *Dpn*I was added into the PCR mixture and was incubated for overnight at 37°C to remove methylated or hemi-methylated template DNA prior to the purification step.

Table 4.7: PCR reaction mixture.

Component	Stock conc'	Volume (µL)	Final conc'
Water		36	
HF Buffer	5×	10	1×
dNTP mix	10 mM each	1	0.2 mM each
Forward primer	20 µM (20 p.mol/µL)	1	0.4 µM
Reverse primer	20 µM (20 p.mol/µL)	1	0.4 µM
Template DNA	Measure using Nanodrop	0.5	
Phusion DNA polymerase (NEB)	2 U/µL	0.5	1 U/50 µL
Total		**50**	

Table 4.8: PCR programme.

Step	Temperature (°C)	Time
1	98	30 seconds
2	98	10 seconds
3	72	30 seconds
4	72	60 seconds
5	-	Go to Step 3, repeat 29 times
6	72	2 minutes
7	8	Hold

4.2.3.5 Gel Extraction (Nucleospin Gel and PCR Clean Up)

The DNA gel extraction was executed using QIAquick Gel Extraction Kit (QIAGEN, Manchester). The desired DNA band was excised with the help of a transilluminator for the band location visualisation. The gel piece was then transferred into a 15 mL centrifuge tube and the weight of the gel was recorded to determine the volume of buffer required. For each 100-mg agarose gel, 200 µL Buffer NTI was required. The tube was then incubated in 50°C water bath with gentle shaking. When the gel was fully dissolved, the tube was briefly vortexed. The dissolved gel was pipetted up to 700 µL onto a spin column and centrifuged at 5000 rpm at RT for 1 minute. The flow through was discarded and the protocol continued until all solutions was applied to the column. The column was washed with 700 µL Buffer NT3 and the column was left to stand before centrifugation. The centrifuge was set at 5000 rpm at RT for 1 minutes. The flow-through was again discarded and the column washed with Buffer NT3 for the second time. Maximum speed centrifugation at RT for additional 2 minutes was used to remove residual ethanol. The column was then placed in a fresh 1.5 mL centrifuge tube before incubating at 70°C for 5 minutes using a thermoblock. Consequently, Buffer NE was also incubated on the thermoblock. The DNA was eluted with 35 µL Buffer NE and left to stand at RT for 2 minutes. Maximum speed centrifugation for 1 minute was used to obtain the DNA. DNA quantification was performed using NanoDrop (Thermo Fisher Scientific, Paisley, UK)

4.2.3.6 Gene Sequencing Analysis

Eurofin Sequencing (Eurofin Genomics UK, Wolverhampton, UK) service was used to identify the sequence quality of the plasmid. The sequence was then analysed using FinchTV (PerkinElmer, UK) or ApE plasmid software (by Wayne Davis, University of Utah, USA). Protein sequence translation was performed using Expasy Translate Tool (https://web.expasy.org/translate/).

4.2.4 Bacterial Transformation using $CaCl_2$ Heat-Shock Method

Principle: Calcium chloride ($CaCl_2$) transformation is a laboratory tool to incorporate plasmid DNA into prokaryotic cells. The positively charged calcium ions (Ca^{2+}) bind to the negatively charge outer core of the lipopolysaccharide (LPS) of the bacterial cell wall as well as encasing the negatively charged plasmid DNA. This promotes molecular

binding of the two components. Heat shock is applied to ferry the plasmid DNA into the bacterial cell through pores in the cell membrane which forms when cells are chilled (on ice) and heated at 42°C for a short time.

Procedure: An overnight culture of *E. coli* was grown in 5 mL 2×TYE media at 37°C, 250 rpm. 50 µL of the overnight culture was then inoculated in 5 mL 2×TYE media and grown at 37°C with shaking at 250 rpm. The optical density (OD) was monitored at 600 nm. When OD_{600} reached ~0.5-0.6, 1-mL aliquot per transformant was transferred to a sterile 1.5 mL microcentrifuge tube. Following centrifugation at 2800 rpm, RT, for 2 minutes, the supernatant was removed by pipetting, followed by gentle re-suspension of the cells in 500 µL sterile pre-chilled 50 mM $CaCl_2$, re-centrifugation and removal of the supernatant before incubating the cells in $CaCl_2$ on ice for 30. For transforming intact plasmid, 10 minutes of incubation is acceptable. Cells were heat shocked at 42^{o}C for 1 minutes and further incubated in ice for additional 2 minutes. 800 µL of pre-warmed 2×TYE media (37°C) was added and cells left to grow at 37°C, 250 rpm for 60 minutes. Subsequently, TYE agar plates were pre-warmed (with antibiotics) at 37^{o}C. The cells were centrifuged at 2800 rpm, RT, for 2 minutes and most of the media removed. The remaining 200-300 µL media was used to re-suspend the cells gently before plating them on pre-warmed agar plates. The plates were incubated overnight at 37°C to allow the transformed colony to grow.

4.2.5 Isolation of plasmid DNA using QIAprep Spin Miniprep Kit

The plasmid DNA was isolated from E. coli DH5-α using QIAprep Spin Miniprep Kit (Qiagen, Manchester, UK). 3 mL of overnight culture (with plasmid of interest) was harvested by centrifugation (5000 rpm, RT, 2 minutes). The excess media was removed by inverting and tapping the tube carefully on paper towel. Cell pellet was re-suspension was performed by vortexing in 250 mL Buffer P1. Cells lysis was achieved by adding 250 µL Buffer P2. The lysis was performed by gently inverting the tube, not exceeding 5 minutes. Once lysed, 350 µL Buffer N3 was added immediately followed by centrifugation (maximum speed, RT, 10 minutes). The supernatant was transferred to a Qiagen column and centrifuged at 5000 rpm at RT for 2 minutes. The flow-through was discarded prior to adding 750 µL Buffer PE to the column. The flow-through was discarded following centrifugation at 5000 rpm at RT for 2 minutes before a final centrifuge at maximum speed at RT for additional 2 minutes to remove residual ethanol. The column was placed in a fresh 1.5 mL centrifuge tube to collect the eluted DNA using 35 µL of Buffer EB. The

tube was left stand for 2 minutes for good DNA recovery before centrifuged at maximum speed at RT for 2 minutes. The DNA concentration was measured using a NanoDrop 1000 Spectrophotometer (Thermo Scientific, DE, USA).

4.2.6 DNA Purification (QIAquick PCR Purification Kit)

The DNA purification was performed using QIAquick PCR purification kit. A ratio of 5 parts buffer PB to 1-part DNA sample was mixed and vortexed briefly in a 1.5-mL centrifuge tube. The entire mixture was then transferred into a Qiagen column and centrifuged at 5000 rom at RT for 2 minutes. The flow-through was discarded and the column was washed with 750 µL Buffer PE. Column was centrifuged and the flow-through was discarded. An additional 2 minutes of centrifugation at maximum speed was used to remove residual ethanol. The column was then placed in a fresh 1.5-mL centrifuge tube to elute the DNA using 35 µL Buffer EB. The elution was collected by centrifugation at maximum speed for 2 minutes. DNA concentration was measured using NanoDrop.

4.2.7 DNA Gel Electrophoresis

Procedure: 0.7% (w/v) agarose gel was prepared in 1×TBE buffer (by dissolving 0.35g of agarose in 50 mL buffer). The percentage of gel used is dependent on the size of the DNA fragment to be analysed. Low percentage gels (0.7-0.8%) are used for high Mw DNA fragments and high percentage gel (1-1.5%) for low Mw DNA fragment. To ensure the agarose was fully dissolved, heating was performed using microwave. 2 µL of ethidium bromide solution was added and the gel was casted using gel caster, gel tray and gel comb when only the agarose gel temperature cooled to room temperature. The gel allowed to cool down and solidify, before loading 6 µL of 1 kb DNA ladder (Cat#: N3232L; New England Biolabs, Hitchin, UK) and appropriate volume of DNA samples. The electrophoresis was run at constant voltage of 100 V for 60 minutes. The gel image was captured using a gel documentation system.

4.2.8 Protein Overexpression using the *E. coli* system

4.2.8.1 TEV Protease

Cell- based protein expression was carried out using *E. coli* strain BL21 (DE3). Cells were transformed with the pRSET vector containing TEV A Protease constructs (engineered for higher expression) using the $CaCl_2$ heat-shock method, and plate inoculation was carried out on 2×TYE agar supplemented with 100 µM ampicillin. Protein expression was initiated in 2×TYE media with 100 µM ampicillin using isopropyl β-D-thiogalactopyranosidase (IPTG) at final concentration of 1 mM when the growth reached ~ 0.6 OD. Cells were incubated at 25°C with shaking at 250 rpm for 24 hours to allow expression to occur. Cells were harvested post-expression and centrifuged at 8000 rpm for 15 minutes at 4°C. Cell pellets were either analysed for protein expression or stored at -20°C.

4.2.8.2 hLtn variants

Protein overexpression was carried out using both *E. coli* strain BL21 (DE3) and C41 (DE3) to identify most suitable strain. Cells were transformed with a pET24a vector containing respective hLtn variants constructs (wild type, CC3 and W55D mutants) using the $CaCl_2$ heat-shock method. Plate inoculation was carried out on 2×TYE agar supplemented with 50 µM kanamycin. Protein expression was initiated in TYE auto-induction media (Studier, 2014) with 50 µM kanamycin. Expression was performed at 25°C in an incubator shaker at 250 rpm for 24 hours. Cells were harvested post-expression and centrifuged at 8000 rpm for 15 minutes at 4°C. Cell pellets were either analysed for protein expression or stored at -20°C.

4.2.9 Analysis of Protein Expression

4.2.9.1 SDS-PAGE Analysis

Procedure: A 15% acrylamide-SDS gel was prepared for the analysis throughout the experiments due to the low molecular weight of the protein expressed. There were two parts of the gel preparation: the resolving gel (lower part) and the stacking gel (upper part). The composition of each layer was as described in **Figure 4.1** below. Following the addition of the polymerisation initiators, the gel was allowed to solidify, before loading 5 µL of PageRuler^{TM} unstained broad range protein ladder (Cat#: 26630; Thermo Fisher Scientific) and appropriate volume of protein sample. The electrophoresis was run at constant voltage of 200 V for 40 minutes. Protein gel was stained with Commassie Brilliant Blue staining dye and counterstained with de-staining solution. The gel image was captured using gel documentation system.

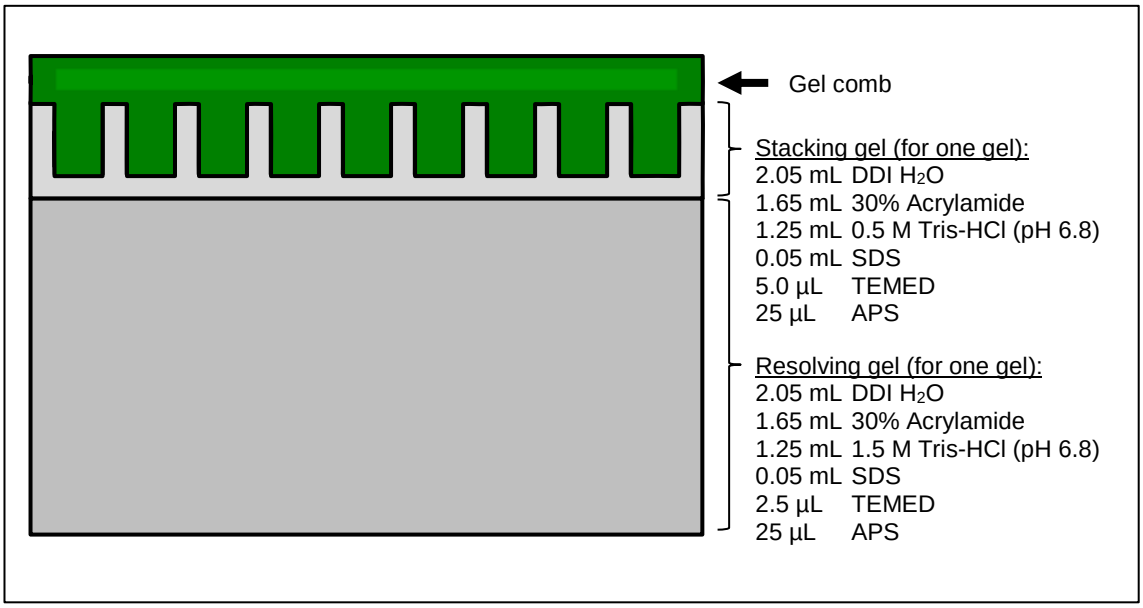

Figure 4.1: Protein electrophoresis and the composition of a 15% SDS-polyacrylamide gel.

4.2.9.2 Western Blot

Procedure: Prior running a western blot, protein gel electrophoresis as described previously was performed (refer **Section 4.2.9.1**). For wet transfer, a piece of Immobilon P Transfer Membrane (Millipore) pre-treated with 100% methanol for 45 seconds followed by rinsing in distilled water. The Watman papers, sponges and the transfer membrane were thoroughly soaked in 1× transfer buffer containing 10% (v/v) methanol (prepared from 10× transfer buffer containing 12 mM Tris base, 96 mM glycine in 1 L). The whole unit stack was prepared and placed in a X-cell II Blot Module (Cat#: EI9051; ThermoFisher Scientific, Paisley, UK). The blot module was inserted into the running chamber and locked. The blot module and running chamber were submerged in 1× transfer buffer and run at 30 V for 60 minutes. The membrane was carefully transferred in 1× TBS (prepared from 10× TBS containing 500 mM Tris base and 1.5 M NaCl adjusted to pH 7.6 in 1 L) for 10 minutes twice. Membrane was then incubated in 1× blocking buffer from the Penta.His HRP Conjugate Kit (QIAGEN, Manchester, UK) for 1 hour. 1× TBST (containing 20 mM Tris base, 500 mM NaCl, 0.05% (v/v) Tween-20 and 0.2% (v/v) Triton x-100 adjusted to pH 7.5 in 1 L) was used to wash the membrane for 10 minutes twice followed by another wash with 1×TBS for another 10 mins. Incubation of membrane with the Anti-His antibody solution from the Penta.His HRP Conjugate Kit (dilution 1:1000 in 1× blocking buffer) was performed for 1 hour. After antibody incubation, the membrane was washed in 1× TBST for 10 minutes twice followed by TBS for another 10 minutes.

4.2.10 Protein Purification of Recombinant Protein

Principle: Nickel resin purification is an immobilised metal affinity chromatography (IMAC) method that is widely utilised in purifying recombinant proteins with polyhistidine tags (Block *et al.*, 2009). There are other metals that can be used to charge the column such as zinc, cobalt and copper but generally, nickel resin offers the highest yield. The binding is achieved through electrostatic attraction to the nickel beads or resin, although non-specific binding can occur which can be reduced by addition of sodium chloride to the buffer. The polyhistidine binds tightly with micromolar affinity to the metal and can be removed by addition of a high concentration of imidazole, which competes with the polyhistidine tag for binding to the column.

4.2.10.1 Polyhistidine Tag-Nickel Purification using Fast Protein Liquid Chromatography (FPLC)

Procedure: Histidine tagged proteins purification was carried out using HisTrap HP 5mL column (GE Healthcare Life Sciences) on an ÄKTA Pure FPLC system (GE Healthcare Life Sciences). Cell sonication was performed to lyse the cell (settings: total time of 10 minutes (10 seconds on, 20 seconds off) with 70% sonicating amplitude). Binding buffer was composed of 50 mM Tris-HCl pH 8.0, 300 mM NaCl, 10 mM imidazole, 10% (v/v) glycerol and 0.1% (v/v) 2-mercaptoethanol. Lysis buffer was composed of binding buffer with 2 tablets of Pierce™ protease inhibitors mini tablets (Thermo Fisher Scientific), 10 µg/mL DNase, 10 µg/mL RNase and 10 µg/mL lysozyme. The elution buffer was composed of 50 mM Tris-HCl pH 8.0, 300 mM NaCl, 250 mM imidazole, 10% (v/v) glycerol and 0.1% (v/v) 2-mercaptoethanol (added before use). Purified protein sample fractions were collected, aliquoted and analysed, or stored at -80°C in 10% glycerol solution for long-term storage.

4.2.10.2 Polyhistidine Tag-Nickel Purification using Batch Resin

Procedure: Soluble protein fractions were transferred into 50 mL Falcon tube with the 1 mL nickel resin, equal to 1 column volume (CV). Binding buffer was composed of 50 mM sodium phosphate (NaH_2PO_4) buffer, 300 mM NaCl and 10 mM imidazole (pH 7.5). Lysis buffer was composed of binding buffer with 2 tablets of Pierce™ protease inhibitors mini tablets (Thermo Fisher Scientific), 10 µg/mL DNase (Brand), 10 µg/mL RNase (Brand) and 10 µg/mL lysozyme (Brand). The wash buffer pH 7.5 was composed of 50 mM

sodium phosphate (NaH_2PO_4) buffer, 300 mM NaCl and 20 mM imidazole. The elution buffer was composed of 50 mM sodium phosphate (NaH_2PO_4) buffer, 300 mM NaCl and 250 mM imidazole (pH 7.5). The mixture was then left overnight at 4°C on a rolling platform to allow even mixing. The solution was transferred into a filter column and allowed to flow through the column by gravity to remove any unbound protein. Samples were collected for analysis at each step. The resin was then washed with 5 CV wash buffer at least three times before eluting the protein. The resin was then treated with elution buffer and left for at least a minute before retrieving the sample. The eluted protein fractions were analysed to identify which fraction contained the desired protein. The flow of the nickel purification can be found in **Figure 4.2**.

Buffer	
Binding	50 mM NaH_2PO_4 + 300 mM NaCl + 10 mM imidazole (pH 7.5)
Lysis	50 mM NaH_2PO_4 + 300 mM NaCl + 10 mM imidazole (pH 7.5) + protease inhibitors + 10 µg/mL DNase + 10 µg/mL RNase + 10 µg/mL lysozyme
Wash	50 mM NaH_2PO_4 + 300 mM NaCl + 20 mM imidazole (pH 7.5)
Elution	50 mM NaH_2PO_4 + 300 mM NaCl + 250 mM imidazole (pH 7.5)

4.2.10.3 Desalting: Removal of Imidazole Salt from the Protein Solution

Principle: Size exclusion chromatography is a technique to separate biomolecules according to differences in their molecular weight. A dextran gel matrix is usually used for gel filtration, where molecules larger than the largest pores are excluded from the matrix and are eluted first. Sephadex G-25 has a fractionation range of 1000 – 5000 Da.

Procedure: The desalting process was performed using Sephadex G-25 in a PD-10 desalting column (GE Healthcare Life Science, Buckinghamshire, UK). Both the column equilibration and elution buffer were composed of 50 mM phosphate buffer (NaH_2PO_4), 300 mM NaCl and 10 mM imidazole (pH 7.5). The column was equilibrated by allowing the solution to enter the packed bed completely. The flow-through was discarded and approximately 25 mL equilibration buffer was used in total. Samples were applied in 2.5 mL, samples less than his volume were brought up to 2.5 mL before application to the column. The sample was allowed to enter the packed bed completely before discarding the flow-through. For sample elution, 3.5 mL of buffer was used, and the eluate was collected. The process was repeated until all the sample was completely treated. The recovery protein range is 70 -90% of the initial concentration.

Buffer	
Wash & Elution	50 mM NaH_2PO_4 + 300 mM NaCl + 10 mM imidazole (pH 7.5)

4.2.10.4 Fusion Protein Cleavage using TEV Protease A

The fusion protein was separated into two domains by introducing TEV protease to the first-step of the purification. The protein was treated with protease overnight at 4°C on a rolling platform to allow even mixing (concentration ratio 1 OD_{280} TEV to 100 OD_{280} protein).

4.2.10.5 Second-step Polyhistidine Purification using Batch Resin

Procedure: Protein soluble fractions were transferred into 50 mL Falcon tubes with the 1 mL nickel resin, equal to 1 column volume (CV). The mixture was then left overnight at 4°C on a rolling platform to allow even mixing. The solution was transferred into a filter column and allowed to flow through the column by gravity to remove any unbound protein. Samples were collected for analysis at each step. The resin was then washed with 5 CV binding buffer at least three times before eluting the protein. The resin was treated with elution buffer and left for at least a minute before retrieving the sample. The eluted protein fractions were analysed to identify which fraction contains the desired protein

Buffer	
Binding	50 mM NaH_2PO_4 + 300 mM NaCl + 10 mM imidazole (pH 7.5)
Wash	50 mM NaH_2PO_4 + 300 mM NaCl + 20 mM imidazole (pH 7.5)
Elution	50 mM NaH_2PO_4 + 300 mM NaCl + 250 mM imidazole (pH 7.5)

First –step Purification (Negative Nickel resin)

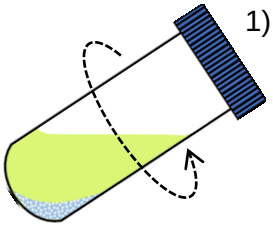

1) Incubation with Ni-NTA resin at 4°C with constant rolling overnight.

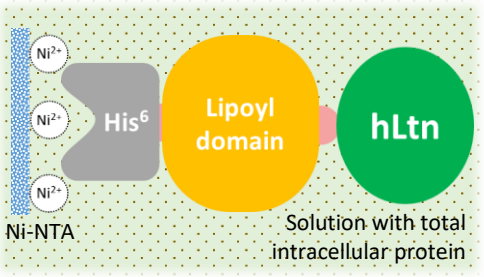

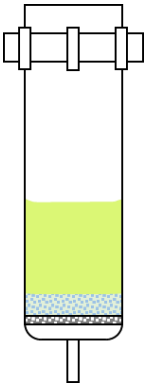

2) Transfer the soluble fraction + nickel resin onto a filter column and allow the flow-through by gravity. Sample of the *flow-through* was collected for analysis.

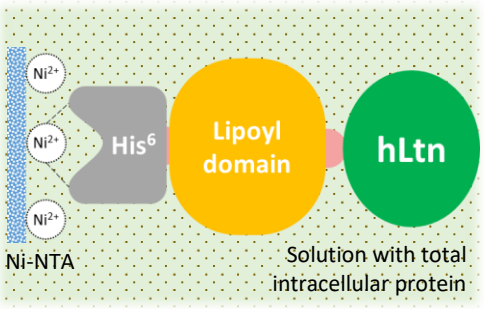

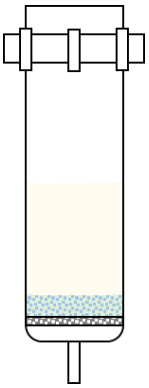

3) Wash the resin using 5 CV wash buffer allow the buffer to flow by gravity. Sample of the *wash buffer* was collected for analysis.

Wash buffer (pH 7.5):
50 mM NaH_2PO_4
300 mM NaCl
20 mM imidazole

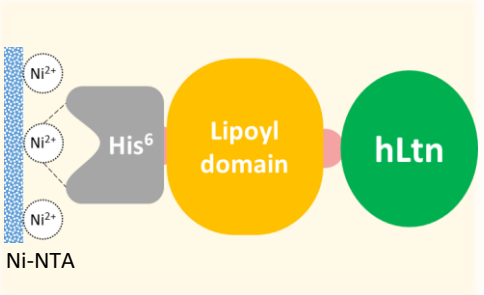

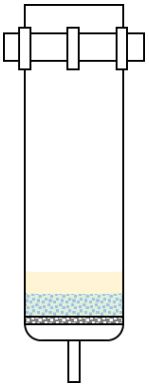

4) Protein bound to the resin was removed using 2CV elution buffer. The resin was left in the buffer for at least 2 minutes to increase protein removal yield in the first eluate. Sample of the *eluate* was collected for analysis.

Elute buffer (pH 7.5):
50 mM NaH_2PO_4
300 mM NaCl
250 mM imidazole

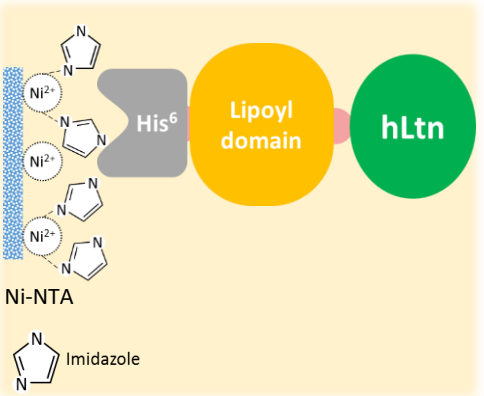

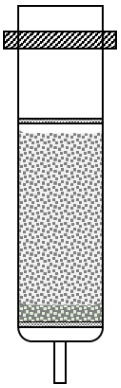

5) Removal of the imidazole salt by running the eluate from first-step of the purification in a size exclusion column with Sephadex G-25.

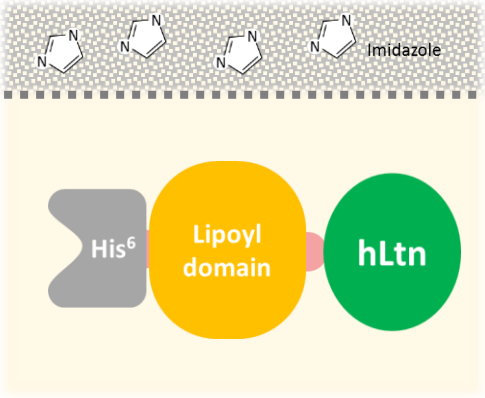

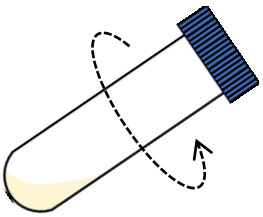

6) Cleavage of fusion protein to release mature hLtn peptide from the lipoyl domain.

First-step eluate + TEV protease (Desalted)

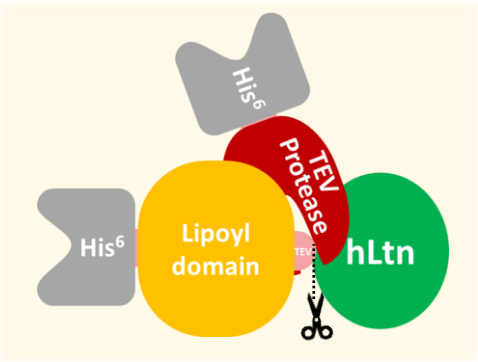

Second –step Purification (Negative Nickel resin)

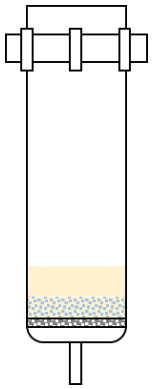

7) Capture of His.Lipoyl domain and His-TEV protease on a nickel resin

Flow-through (Purified hLtn variants)

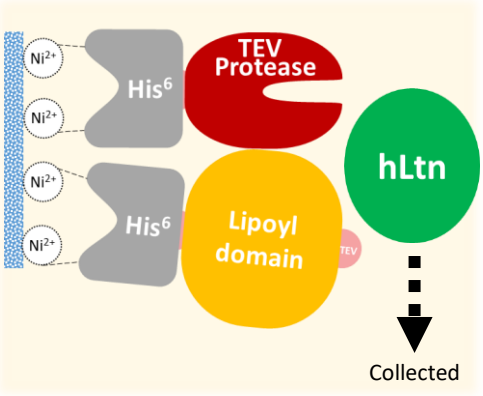

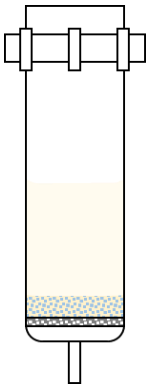

8) Wash the resin using 5 CV wash buffer allow the buffer to flow by gravity. Sample of the *wash buffer* was collected for analysis.

<u>Wash buffer (pH 7.5)</u>:
50 mM NaH_2PO_4
300 mM NaCl
20 mM imidazole

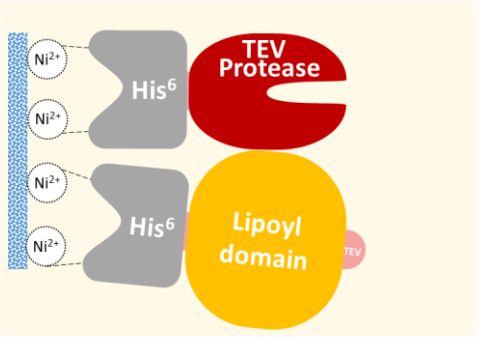

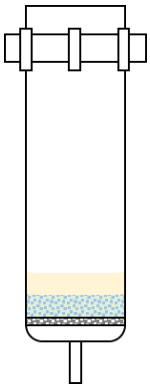

9) Protein bound to the resin was removed using 2CV elution buffer. The resin was left in the buffer for at least 2 minutes to increase protein removal yield in the first eluate. Sample of the *eluate* was collected for analysis. Additional washing using buffer with high imidazole concentration (500 mM) to strip any residual bounded protein

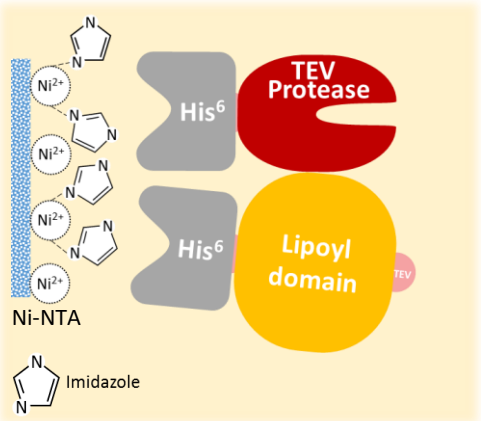

<u>High imidazole buffer (pH 7.5)</u>:
50 mM NaH_2PO_4
300 mM NaCl
500 mM imidazole

10) Wash the resin for storage

Wash buffer → distilled H_2O 2× → 20% (v/v) Ethanol 2×; and storage in 20% (v/v) ethanol.

Figure 4.2: Flow diagram of the two-step IMAC batch purification with nickel resin protocol used for hLtn variants purification.

4.2.11 Protein Analysis

4.2.11.1 Protein Concentration Determination using UV-Spectrometer

The concentration of the protein was measured by using a UV spectrometer at a wavelength 280 nm. The concentration was then corrected using the Beer-Lambert's law equation. This was performed by considering the extinction co-efficient of each protein species obtained from Expasy ProtParam analysis (refer **Chapter 4(a)**).

$$A = \epsilon \times b \times c$$

Where; **A** is the absorbance, **ϵ** is the wavelength-dependent molar absorptivity co-efficient (M^{-1} cm^{-1}), **b** is the path length and c is the analyte concentration

4.2.11.2 Calcium Flux Assay

Principle: This method uses Indo-1 AM ester (**Figure 4.3**), a ratiometric fluorescent dye that is loaded into cells and can be detected by UV laser excitation to measure intracellular calcium levels. The emission wavelength depends on whether the dye binds to calcium (~420 nm) or is free (~510 nm). Intracellular calcium concentration changes can be determined by the ratio of the two wavelengths value (Dustin, 2000).

Whilst, Indo-1 is not cell permeable, the addition of the potassium salt penta acetoxymethyl (AM) to the dye allows it to cross the cell membrane as well as increasing the solubility. Once inside the cell, an intracellular esterase will cleave the AM, leaving Indo-1 free to chelate to intracellular calcium.

Procedure: To investigate the effect of the hLtn variants functional activity, highly XCR1-positive OCCL (SCC4 cells) were used. 1×10^5 cells/mL were prepared in a centrifuge tube. Cells were re-suspended in 1 mL cell loading media (CLM) consist of Dulbecco's PBS with $MgCl_2$ and $CaCl_2$ (Cat#: D8552; Sigma-Aldrich, Dorset) with 0.5% (w/v) BSA. Indo-1 AM (Cat#: 21030, AAT BioQuest (by Stratech), Suffolk). 4 µg/mL of Indo-1 AM (4 µM) was added to the cell suspension and incubated at 37ºC for 30 in the dark. Gentle mixing of the solution was performed every 10 minutes. After incubation, the cells were centrifuged at 400×g for 5 minutes and re-suspended in CLM. The cells were left for 15 minutes before starting the calcium flux analysis. The analysis was performed by using a BD™ LSRII flow cytometer (BD Bioscience, Oxford, UK). A detailed flow cytometer settings optimisation and preparation can be found in **Appendix 12**. The cells were kept

at 37ºC before the run to allow maximal calcium flux activity. The programme was executed at 200 events/s for 30 s before introducing the treatments. Ionomycin (1 mg/mL) was used as positive control and all the hLtn variants (100 mg/mL) were tested. The data was then analysed using FlowJo software (LLC, Oregon, US). This method was adapted from protocol used successfully by the Feinstein Research Institute and others in UCL Institute of Health, London (Round, 2007).

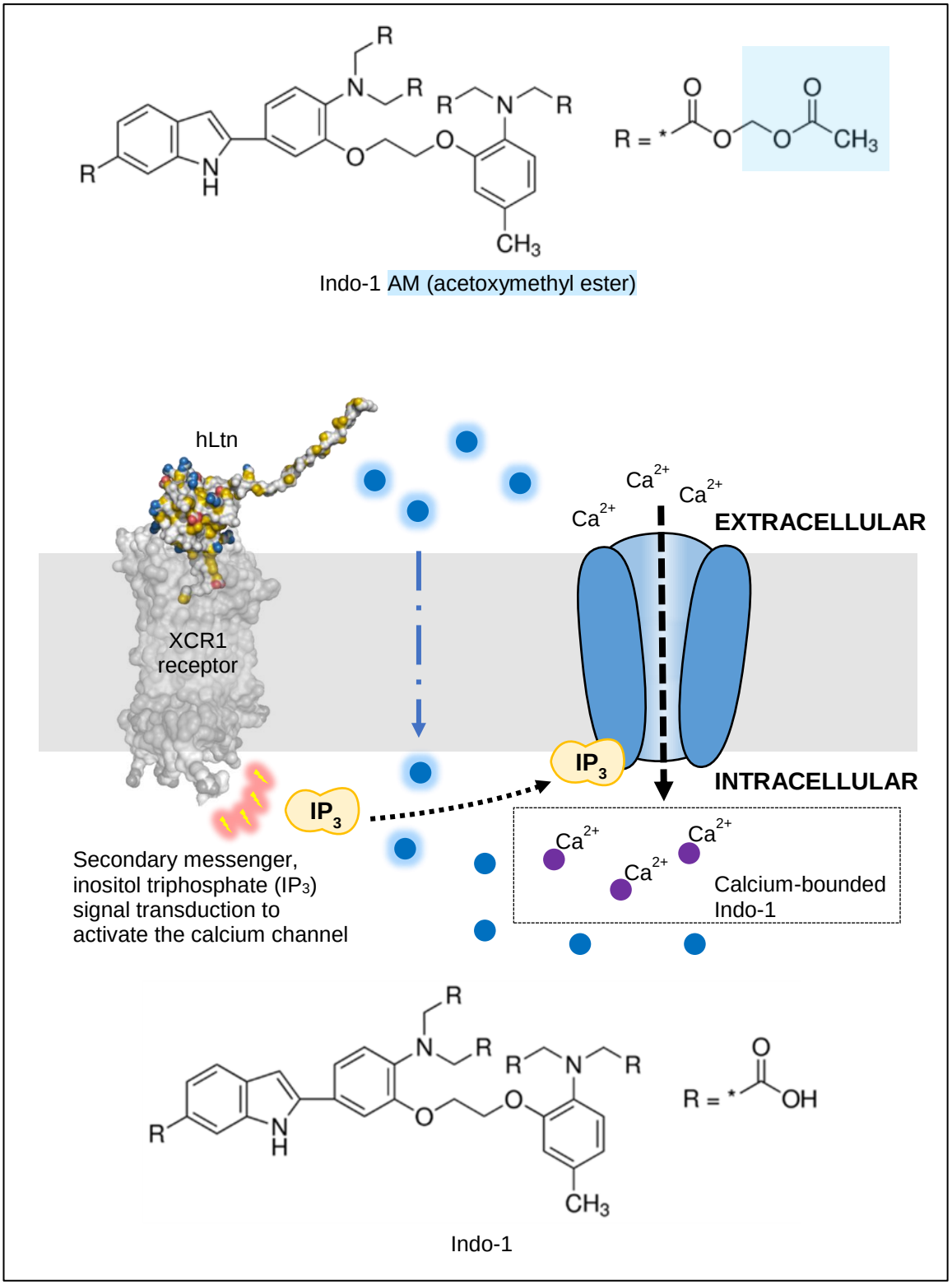

Figure 4.3: Mechanism of ion channel gate activation by second messengers from inside the cell through the interaction of chemokine-chemokine receptor. The chemical structure of Indo-1 AM before entering the cell (top) and Indo1 inside the cell after removal of the penta-acetoxymethyl by intracellular esterase is also shown.

4.3 RESULTS

4.3.1 Molecular Cloning of hLtn Expressing Vector

4.3.1.1 Preparation of hLtn W55D from pCMV6 Entry-XCL1 (WT) by Site-directed Mutagenesis

The mutagenesis was performed on the pCMV6-Entry-hLtn plasmid from Origene, XCL1 (Myc-DDK-tagged)-Human chemokine (C motif) ligand 1 (Cat#: RC218177; Origene EU, Herford, Germany). The primers used for the mutagenesis were generated using OneClick Mutagenesis online tool and was performed as described in the methods section (see **Section 4.2.3.1**) to generate the mutagenic primers and experimental conditions. The expected total size of the PCR product was 5292 kb (pCMV6-Entry: 4947 kb + hLtn: 345 kb) and **Figure 4.4** indicates that the whole plasmid amplification was successful (marked with an arrow) as evidenced by the thick band (Warburton *et al.*, 2015). The DNA sequence for the protein variant identity was confirmed (**Appendix 13**). The pCMV6-Entry-hLtn CC3 mutant plasmid had already been established previously.

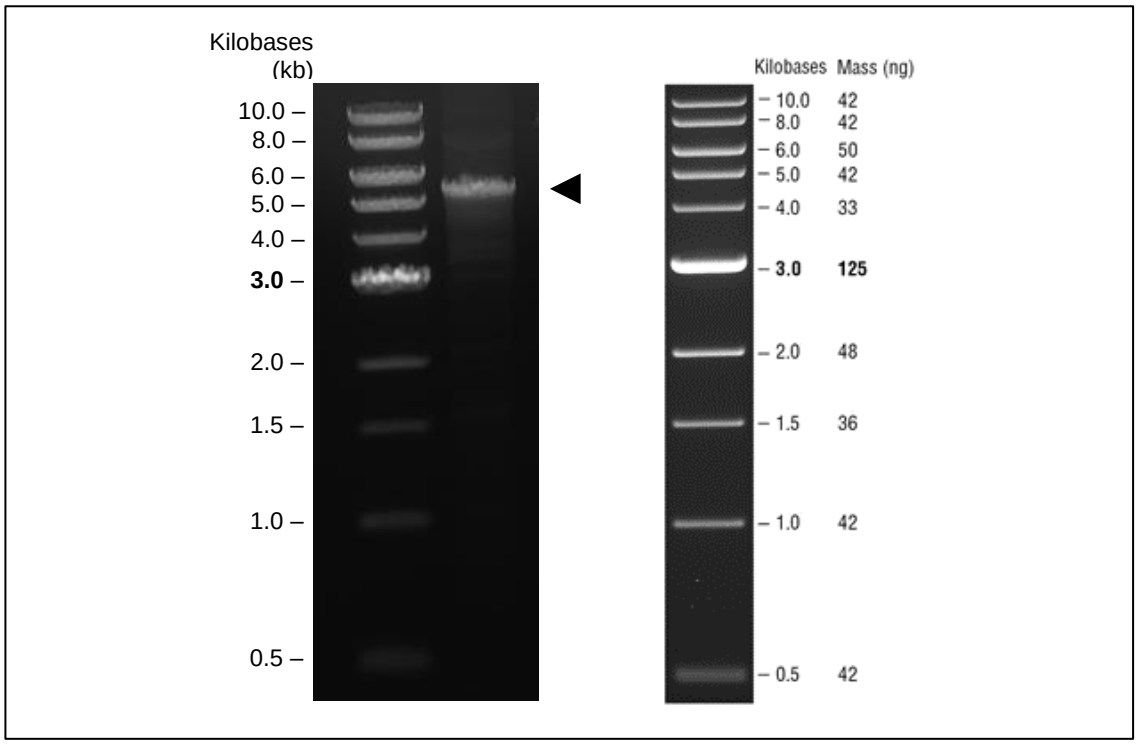

Figure 4.4: PCR analysis of the site-directed mutagenesis from pCMV6-Entry-hLtn WT to W55D sequence. The product was monitored by DNA gel electrophoresis (1% (w/v) agarose gel). *M*: 1 kb DNA ladder (NEB). *Lane 1*: PCR product. The theoretical size of the plasmid DNA is 5292 kb (shown at arrow ◄).

4.3.1.2 Preparation of Plasmid pET24a-HLTEV-hLtn Variants for Protein Expression

The plasmid backbone was obtained from pET24a-HLTEV-p53.QMFL. Excision of the p53.QMFL sequence was performed using the restriction enzymes BamHI and EcoRI. The digested product was then separated using DNA gel electrophoresis to retrieve the desired plasmid backbone (**Figure 4.5**). Initially, the plasmid backbone was planned to be retrieved using the established pET24a-HLTEV-hLtn WT. However, due to the small size of the hLtn WT DNA sequence, it was difficult to discern if the digestion was successful (result not shown). Similarly, due to the small size (300 bp) of the target gene sequence (the CC3 and W55D mutants), the DNA sequence extraction was difficult to achieve. Alternatively, the gene sequence of CC3 and W55D mutants from the pCMV6 cassettes (as described in previous **Chapter 4(a)**) were amplified using PCR (**Figure 4.6**). The CC3 and W55D PCR products were treated with BamHI and EcoRI restriction enzymes before ligation using T4 DNA ligase with the previously digested pET24a-HLTEV plasmid with the same endonucleases (to obtain DNA sticky ends). The ligated product was then transformed into *E. coli* strain DH5-α and the success of the ligation was monitored by growth of colonies on the kanamycin plate (**Figure 4.7**).

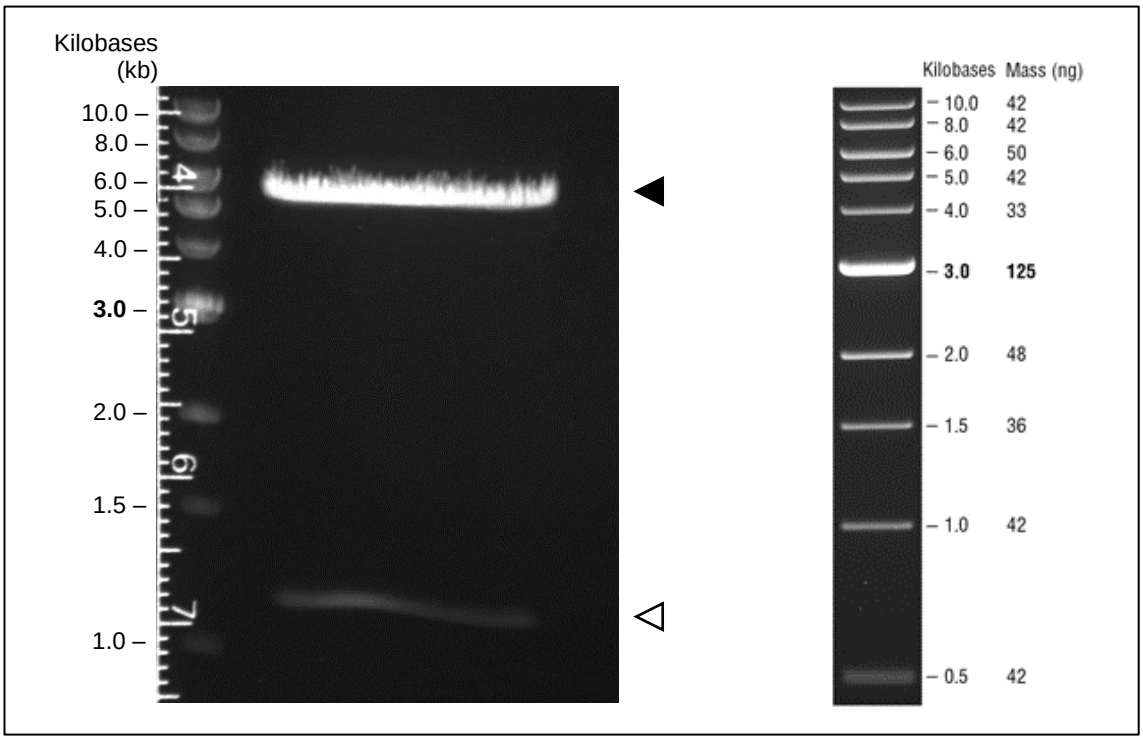

Figure 4.5: DNA digestion of pET24a-HLTEV-p53 QFML at restriction site BamHI – EcoRI. The product was monitored by DNA gel electrophoresis (1% (w/v) agarose gel). The digested product consisted of pET24a-HLTEV (high molecular weight – arrow ◄) and p53 QFML (low molecular weight – arrow ◁) with sticky ends. The DNA size was determined 1 kb DNA ladder (NEB).

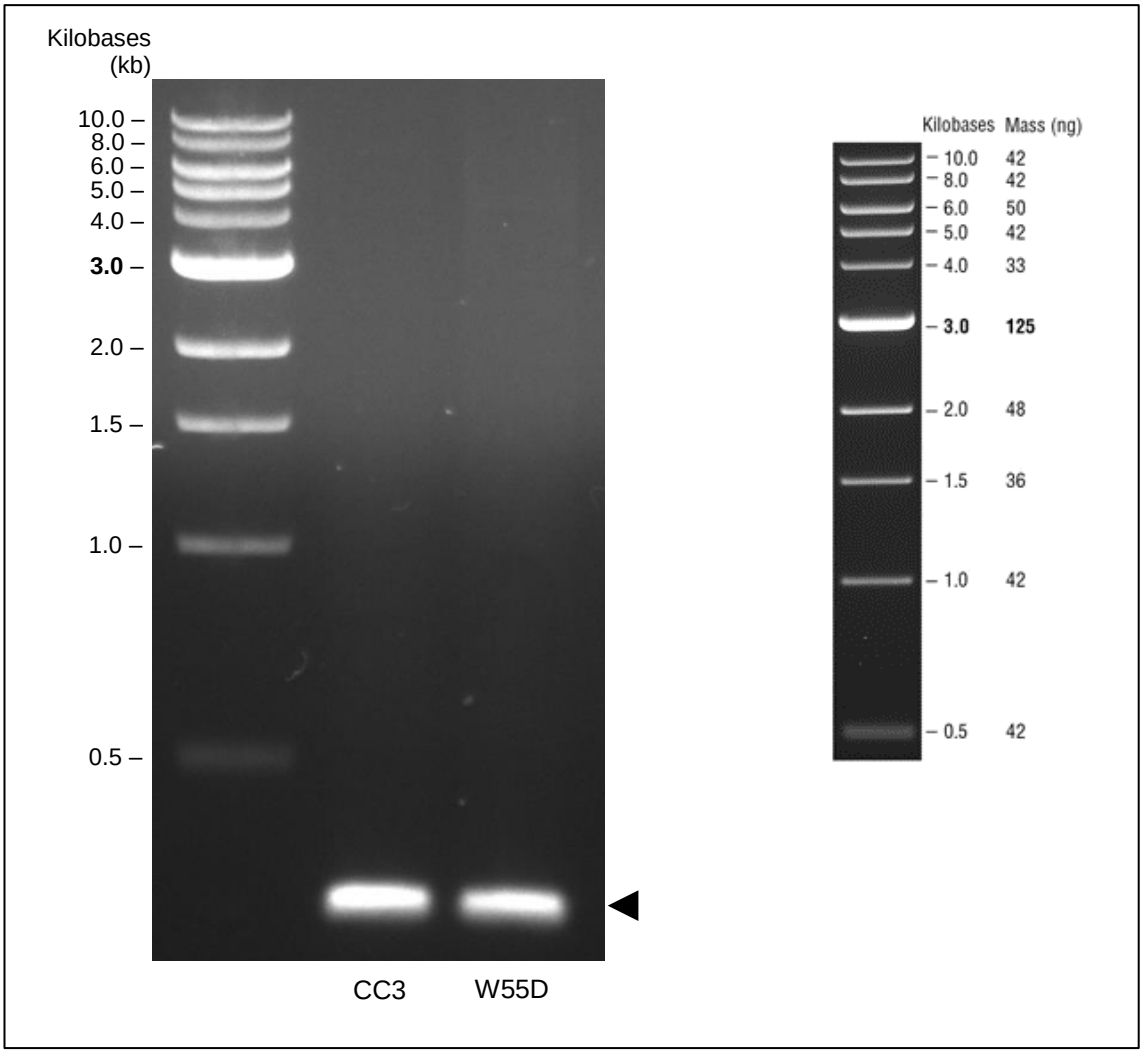

Figure 4.6: PCR amplification of CC3 and W55D variants peptide gene sequence from their respective pCMV6 cassette. The product was monitored by DNA gel electrophoresis (1% (w/v) agarose gel). The expected PCR product is around 300 base pairs (shown at arrow ◄). The DNA size was determined 1 kb DNA ladder (NEB).

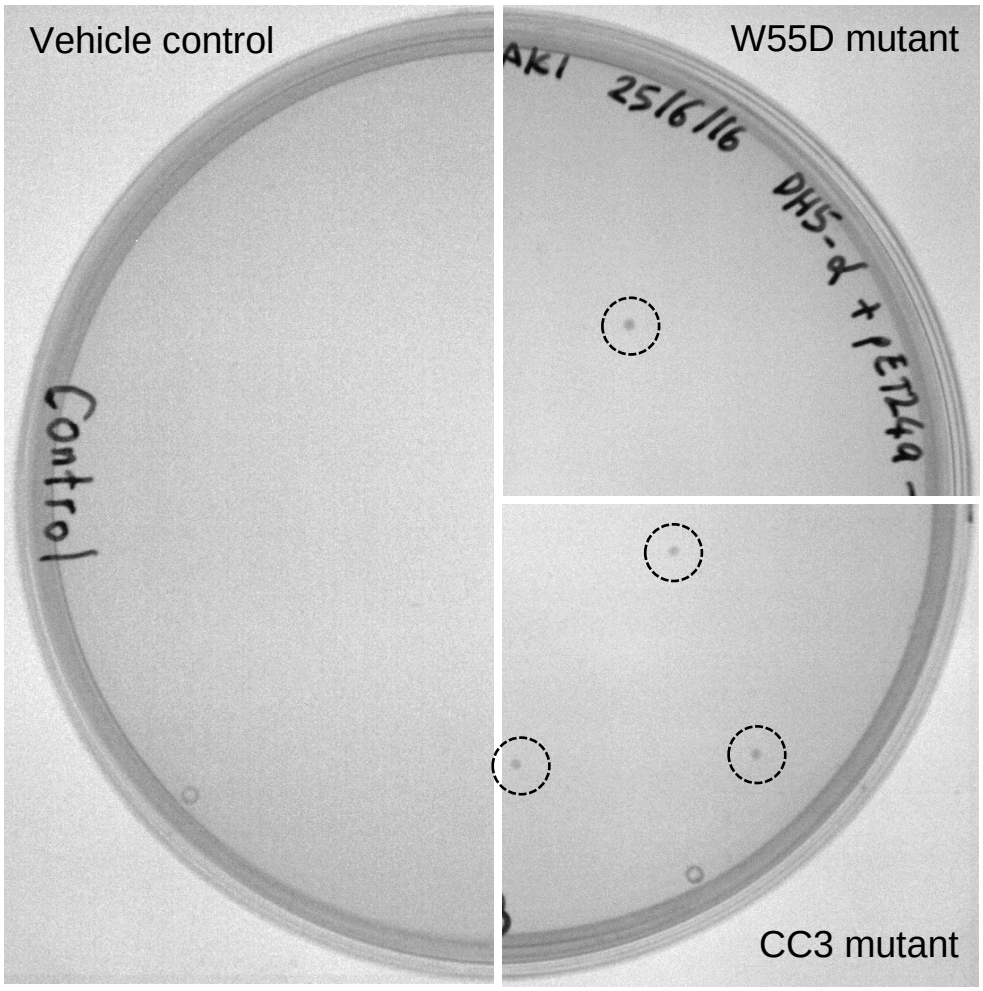

Figure 4.7: hLtn mutant variants plasmid ligation. The inoculated *E. coli* strain DH5-α colonies transformed with ligated product of pET24a-HLTEV with respective hLtn variants (CC3 and W55D mutants) on 2×TYE agar plate with kanamycin. The excision was performed at BamHI and EcoRI cleavage site of the gene construct. The control plate contained cut pET24a-HLTEV plasmid to observe the ligation background.

4.3.2 Comparative Study of pET24a-(IEGR) and pET24a-(TEV) hLtn Constructs

In this sub-chapter, two different plasmid constructs were studied to verify the best suited construct for the hLtn variants expression. The construct used was the plasmid containing hLtn wild type (as explained in **Chapter 4(a)**). Additionally, different modes of expression induction for either isopropyl-β-D-thiogalactopyranosidase (IPTG) or auto-induction were also considered. Initial protein expression was performed in *E. coli* strain BL21 (DE3)

Protein gel electrophoresis was used to monitor the expressed protein. Result showed auto-induction is the preferred method for the fusion protein (**Figure 4.8**). There was no protein expression detected with IPTG induction. Protein expression with plasmid construct pET24a-(TEV) was higher than pET24a-(IEGR). The fusion protein size was estimated be around 26 kDa as examined using the protein gel. The fusion protein *in silico* analysis (refer **Chapter 4 (a)**) calculated that the theoretical molecular weight was ~22 kDa. Therefore, western blot analysis for His-tag was performed to confirm the result obtained using protein gel. The result revealed that the protein size was around ~26 kDa when running on a protein gel (**Figure 4.9**). TEV construct expression was higher than the IEGR construct when examined for their total protein and soluble fraction. Due to lack of protein expression by pET24a-(IEGR) plasmid, the protein expression was proceed using the pET24a-(TEV) plasmid.

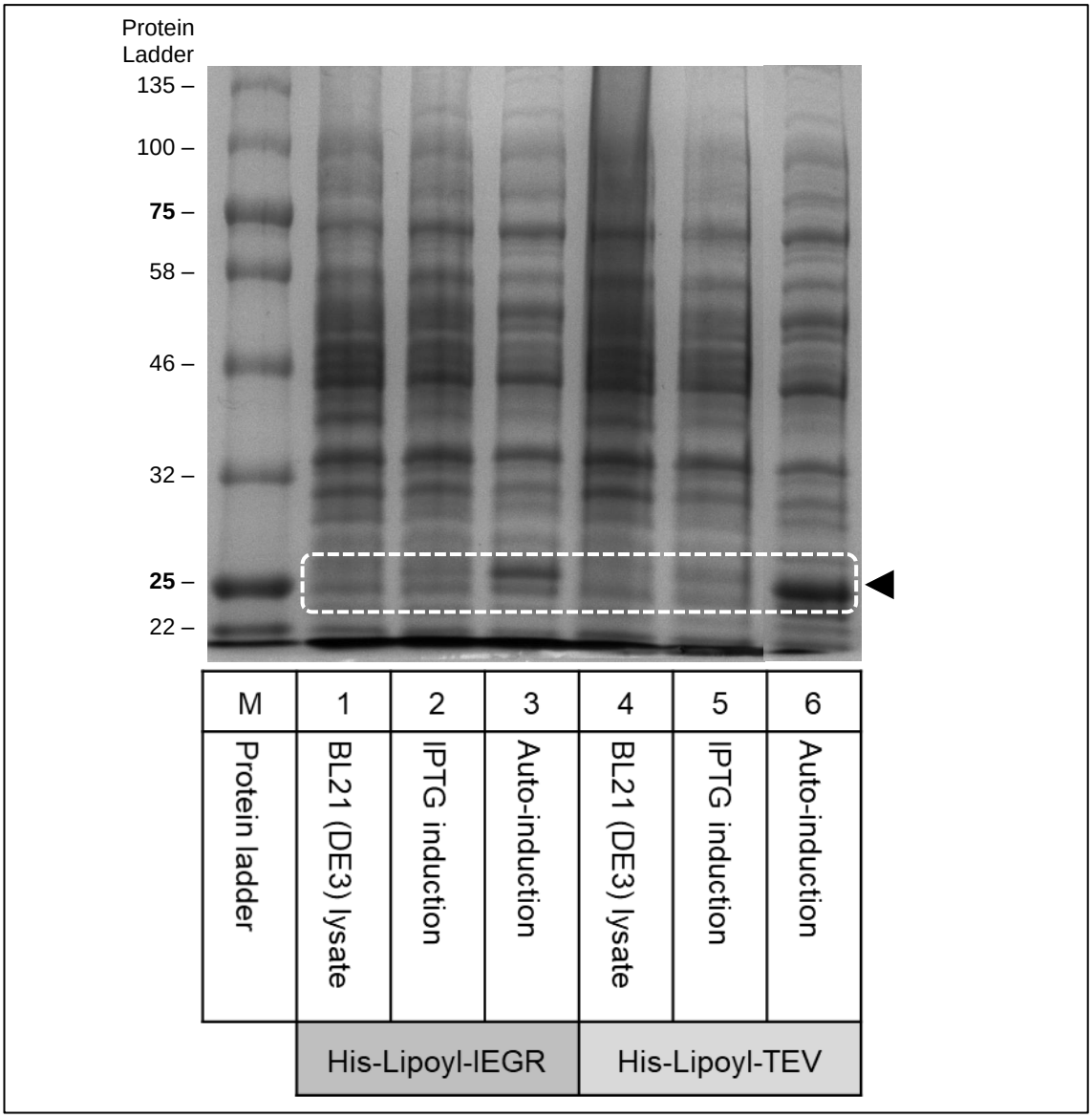

Figure 4.8: Comparison between fusion proteins constructs and different induction schemes. pET24a-(IEGR) and pET24a-(TEV) hLtn constructs were expressed using *E. coli* strain BL21 (DE3) monitored by Coomassie blue dye-stained SDS-PAGE (10% polyacrylamide gel). *M*: molecular weight standard (kDa). On the *left* (His.Lipoyl-IEGR construct): *Lane 1*: Total intracellular protein before induction. *Lane 2*: Total intracellular protein after IPTG induction. *Lane 3*: Total intracellular protein after auto-induction. On the *right* (His.Lipoyl-TEV construct): *Lane 4*: Total intracellular protein before induction. *Lane 5*: Total intracellular protein after IPTG induction. *Lane 6*: Total intracellular protein after auto-induction. The arrow ◄ is the expected fusion protein size (~26 kDa).

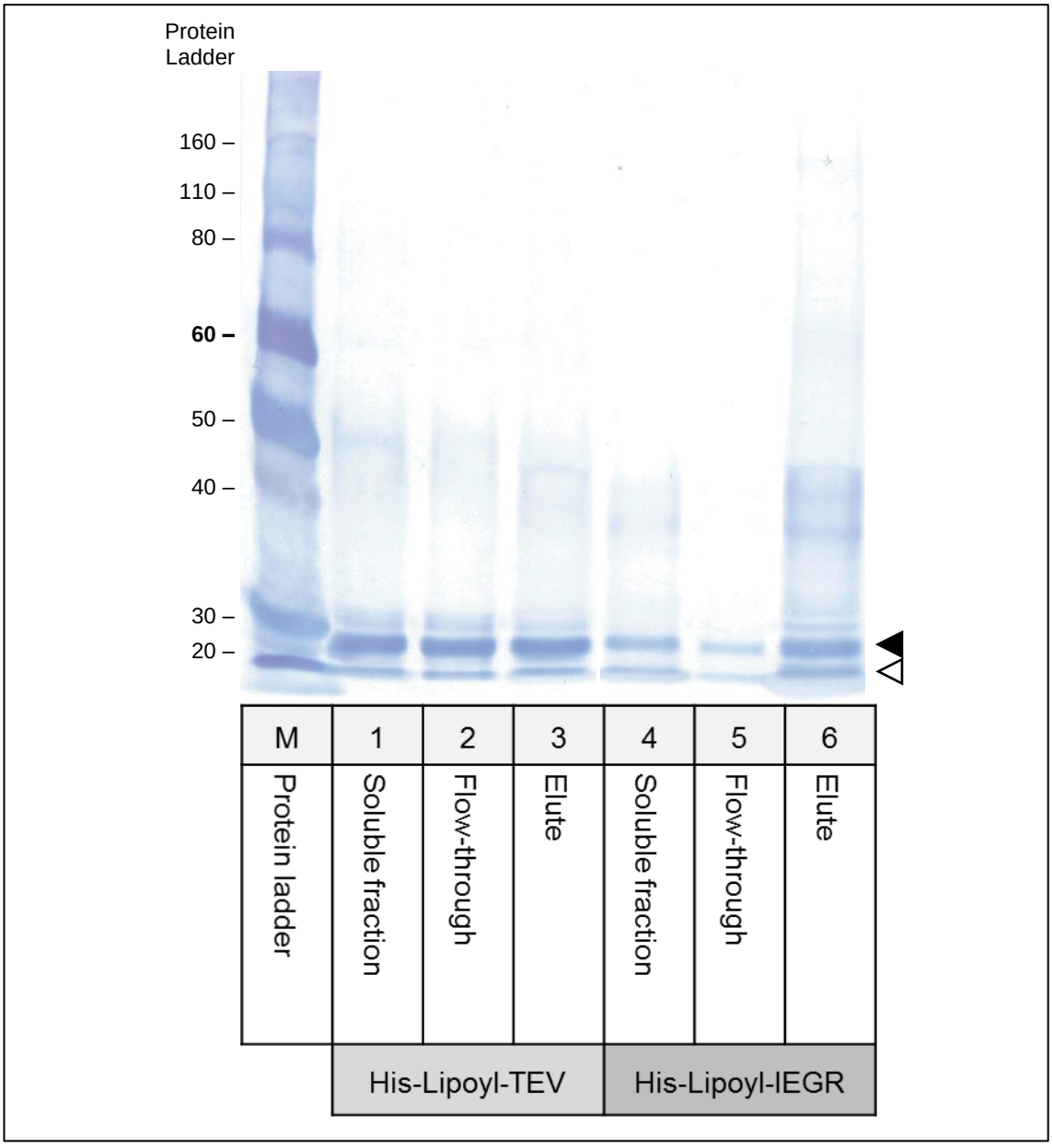

Figure 4.9: Western blot analysis between fusion proteins constructs. The pET24a-(IEGR) and pET24a-(TEV) hLtn constructs was expressed using *E. coli* strain BL21 (DE3) from SDS-PAGE (10% polyacrylamide gel). *M*: Novex® Sharp Pre-Stained Protein Standard (kDa) (Thermo Fisher Scientific). On the *left* (His.Lipoyl-TEV construct): *Lane 1*: Soluble cell extract. *Lane 2*: Flow-through. *Lane 3*: Insoluble cell extract. On the *right* (His.Lipoyl-IEGR construct): *Lane 4*: Soluble cell extract. *Lane 5*: Flow-through. *Lane 6*: Insoluble cell extract. The arrow ◄ is the expected fusion protein (~26 kDa). Truncated fusion protein was also noticeable at arrow ◁.

4.3.3 Comparative Study of pET24a-(TEV) hLtn Constructs using Different *E. coli* Strains and Induction Schemes

E. coli C41 (DE3) and BL21 (DE3) were used to study the suitable strain to express the recombinant fusion protein. The success of the transformation into each strain was monitored by growth of the colonies on the kanamycin plate (**Figure 4.10**). The transformation rate was higher in BL1 (DE3) compared to C41 (DE3). Additionally, different induction schemes for the protein expression was also considered. The result of total intracellular protein analysis showed that there was no protein expressed through IPTG induction for both strains (**Figure 4.11**). Additionally, expression can be seen by both *E. coli* strains through TYE and TB auto-induction. There was a slight difference in the protein profile expression between C41 (DE3) and BL21 (DE3). BL21 (DE3) has much more 'cleaner' expression and no differences were observed between both auto-induction media for the total protein expressed.

To further ascertain the preferable conditions for the fusion protein expression, soluble and insoluble protein from the cell extracts between strains and media were examined. Good protein expression was observed by BL21 (DE3) in both auto-induction media but expression was observed to be higher in TYE auto-induction (**Figure 4.12**). Furthermore, the protein expressed by BL21 (DE3) had an increased soluble fraction compared to the insoluble fraction. In the case of C41 (DE3), there was little amount of protein expressed and most of the protein was truncated in both induction media. Some truncation of the protein was also observed in the BL21 (DE3) lane but this was not as severe.

(A) BL21 (DE3)

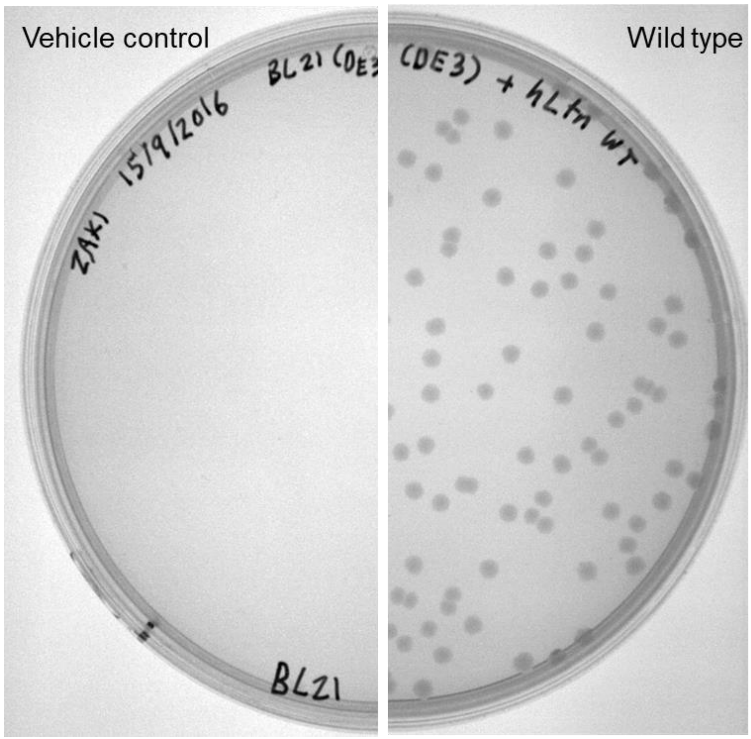

(B) C41 (DE3)

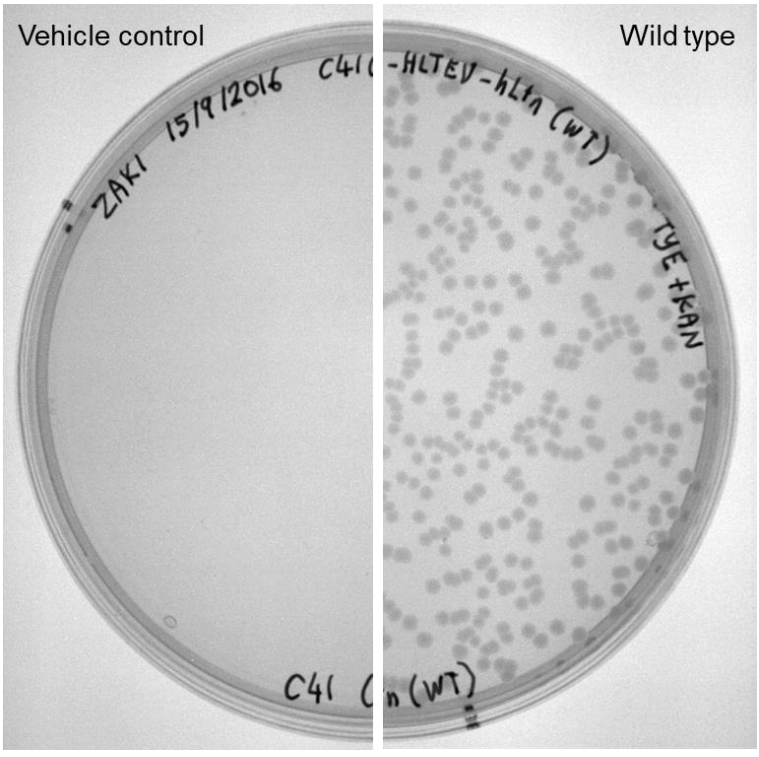

Figure 4.10: The inoculated of *E. coli* strain **(A)** BL21 (DE3) and **(B)** C41 (DE3) colonies transformed with pET24a-HLTEV hLtn variants wild type on 2×TYE agar plate with kanamycin.

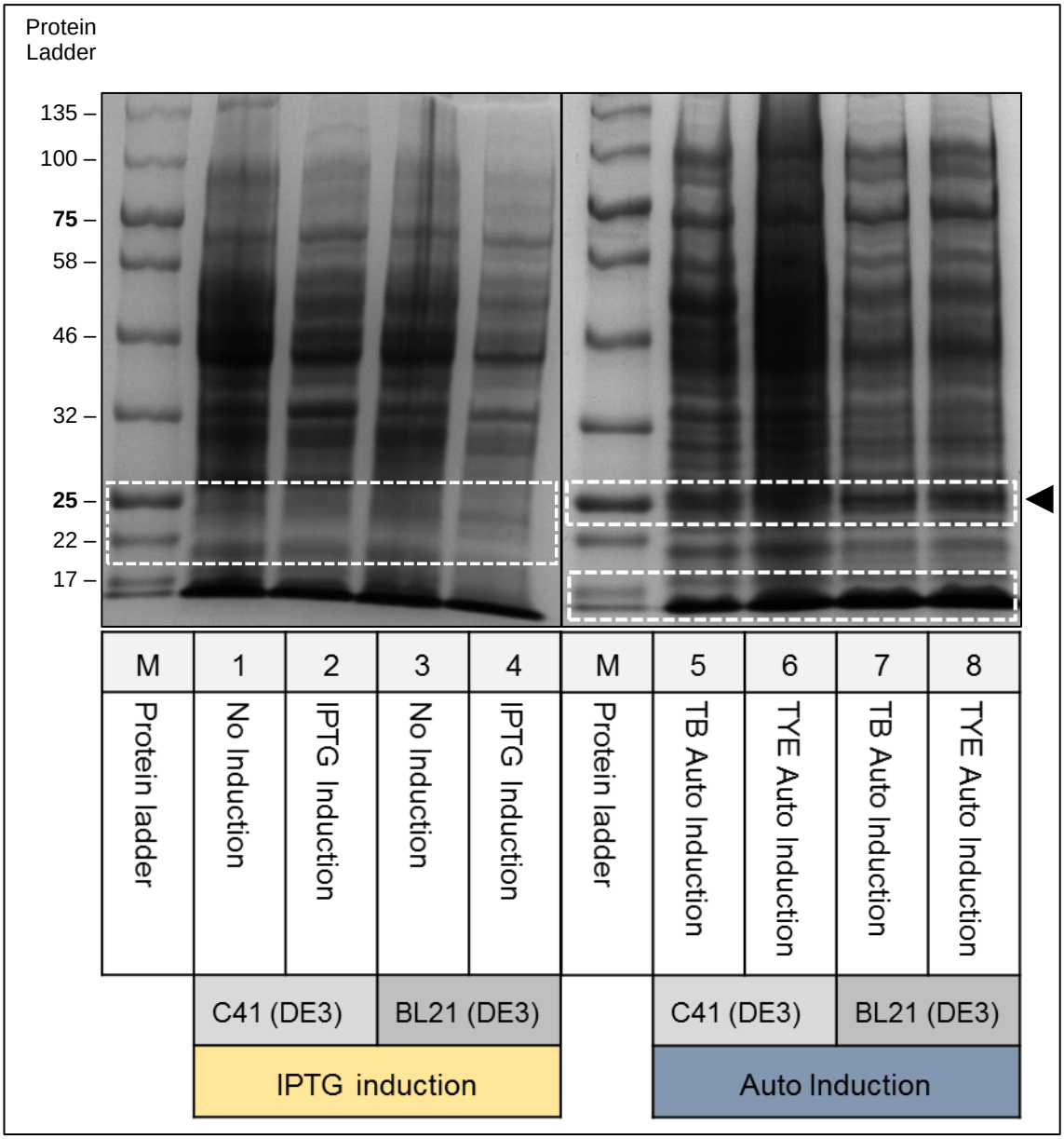

Figure 4.11: Comparison between fusion protein expression in different *E. coli* strains and induction schemes. pET24a-(IEGR) and pET24a-(TEV) hLtn constructs were expressed using *E. coli* strain BL21 (DE3) monitored by Coomassie blue dye-stained SDS-PAGE (10% polyacrylamide gel). *M*: molecular weight standard (kDa). *Lane 1*: Total intracellular protein before induction. *Lane 1&3*: Total intracellular protein without induction in TYE media. *Lane 2&4*: Total intracellular protein after IPTG induction in TYE media. *Lane 5&7*: Total intracellular protein after TB auto-induction. *Lane 6&8*: Total intracellular protein after TYE auto-induction. The arrow ◄ is the expected fusion protein size (~26 kDa).

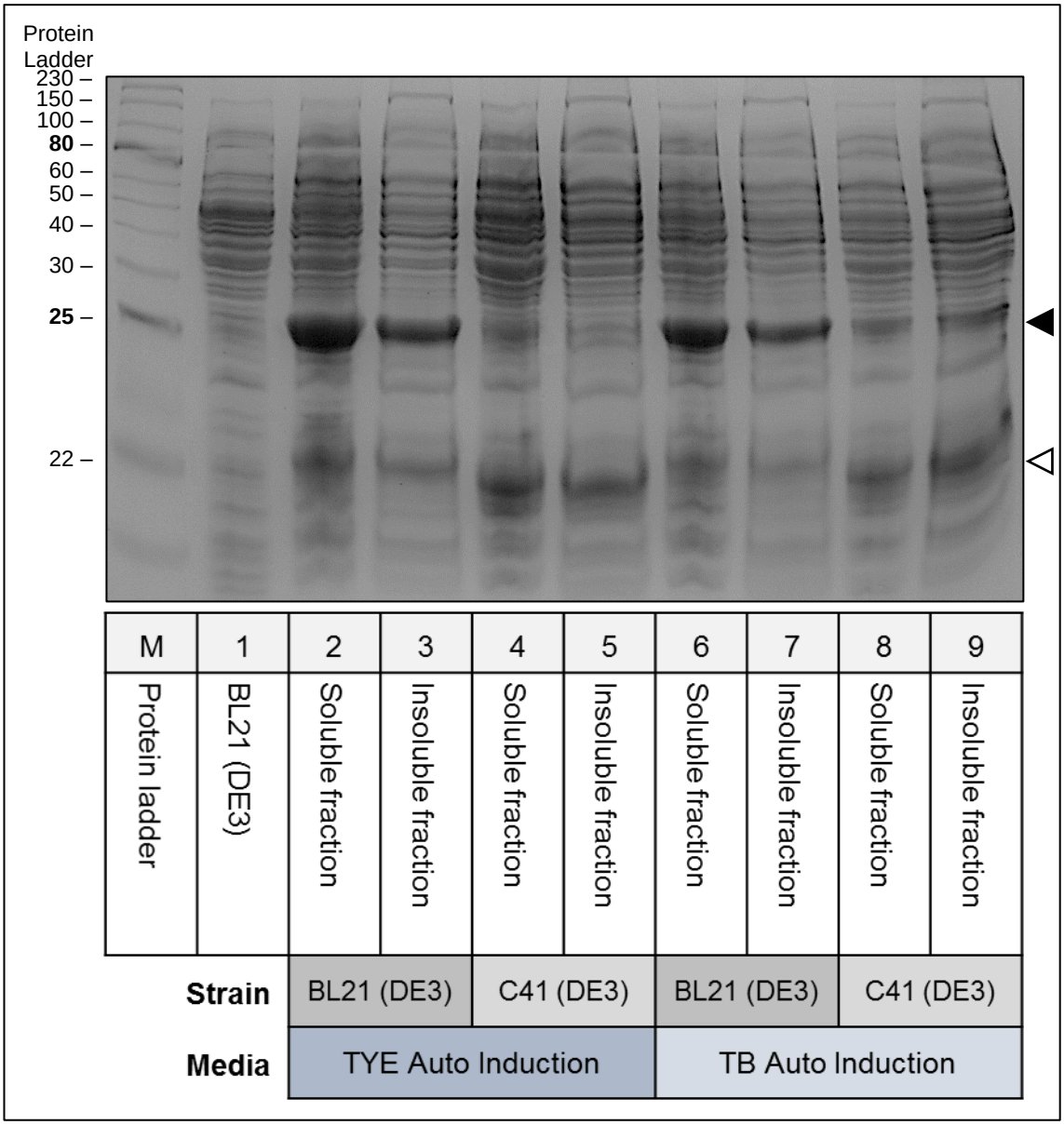

Figure 4.12: Comparison between the soluble and insoluble fusion protein expression in different *E. coli* strain and auto-induction media. pET24a-(TEV) hLtn constructs was expressed using *E. coli* strain BL21 (DE3) and C41 (DE3) monitored by Coomassie blue dye-stained SDS-PAGE (15% polyacrylamide gel). *M*: molecular weight standard (kDa). *Lane 1*: Total intracellular protein without induction. *Lane 2-5*: Soluble and insoluble cell extract from BL21 (DE3) and C41 (DE3) expression using tryptone-yeast extract (TYE) auto induction media. *Lane 6-9*: Soluble and insoluble cell extract from BL21 (DE3) and C41 (DE3) expression using terrific broth (TB) auto induction media. The arrow ◄ is the fusion protein size (~26 kDa). Protein truncation at arrow ◁ was also observed.

4.3.4 TEV Protease Protein Purification

TEV protease is an enzyme widely used to remove an affinity tag from recombinant proteins by site-specific endoproteolysis (Tropea, Cherry and Waugh, 2009) through recognition of the ENFLYQ↓X sequence. The TEV protease construct used in this experiment contained a polyhistidine tag to accommodate affinity purification followed by a lipoyl domain to increase protein quantity and solubility in a pRSET vector to obtain a high-copy number of expression (Ramos *et al.*, 2004). Two of the constructs were tested and both were engineered to have a high yield. The TEV protease containing the lipoyl domain has a total molecular weight of ~36 kDa. The colony size of BL21 (DE3) with the TEV A Protease construct is smaller compared to TEV S Protease (**Figure 4.13**). For the protease purification, the result showed a good profile for TEV A protease (**Figure 4.14**) while not for TEV S Protease (**Figure 4.15**).

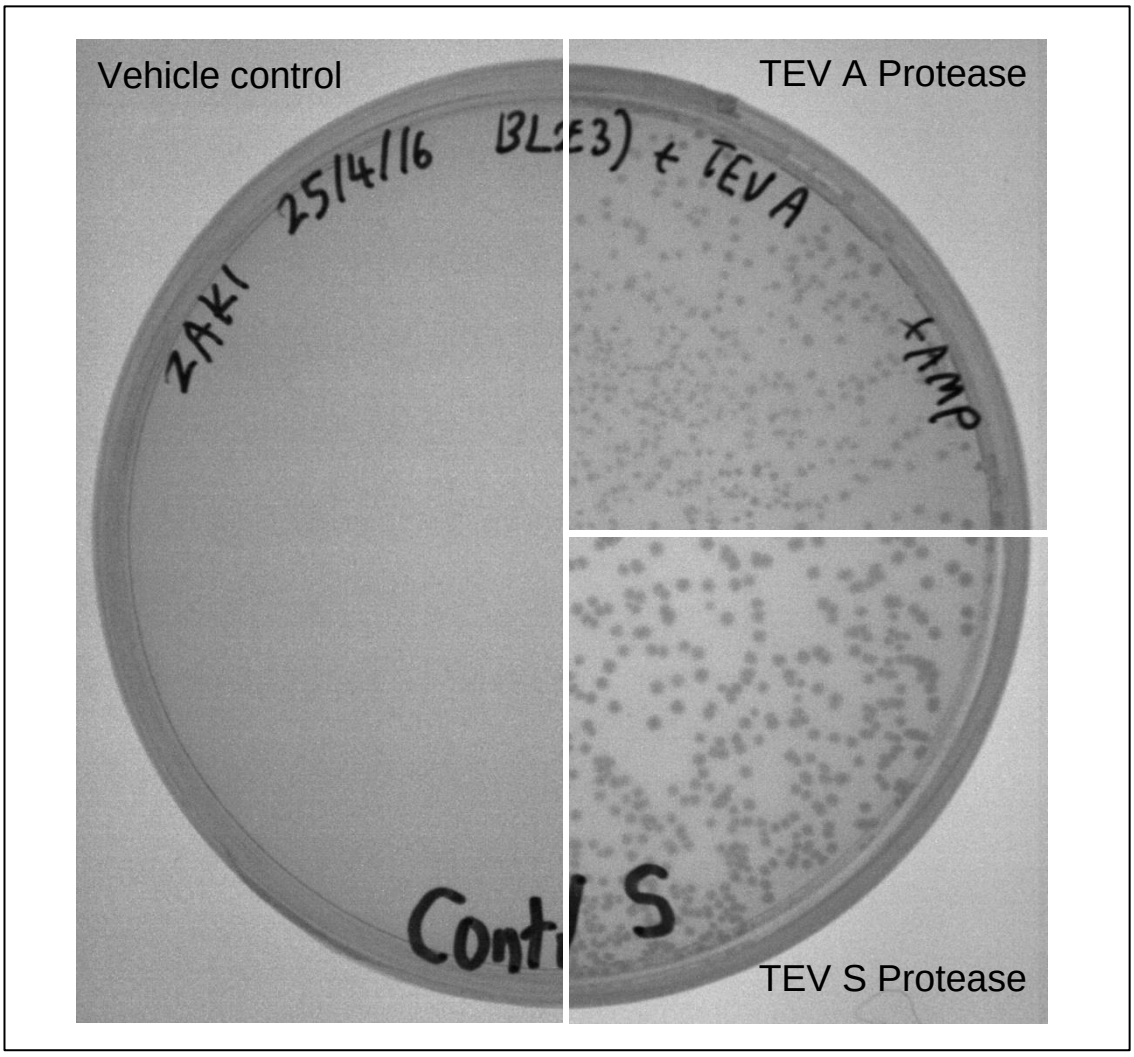

Figure 4.13: Inoculated of *E. coli* strain BL21 (DE3) colonies transformed with pRSET-His.Lipoyl TEV proteases on 2×TYE agar plate with ampicillin.

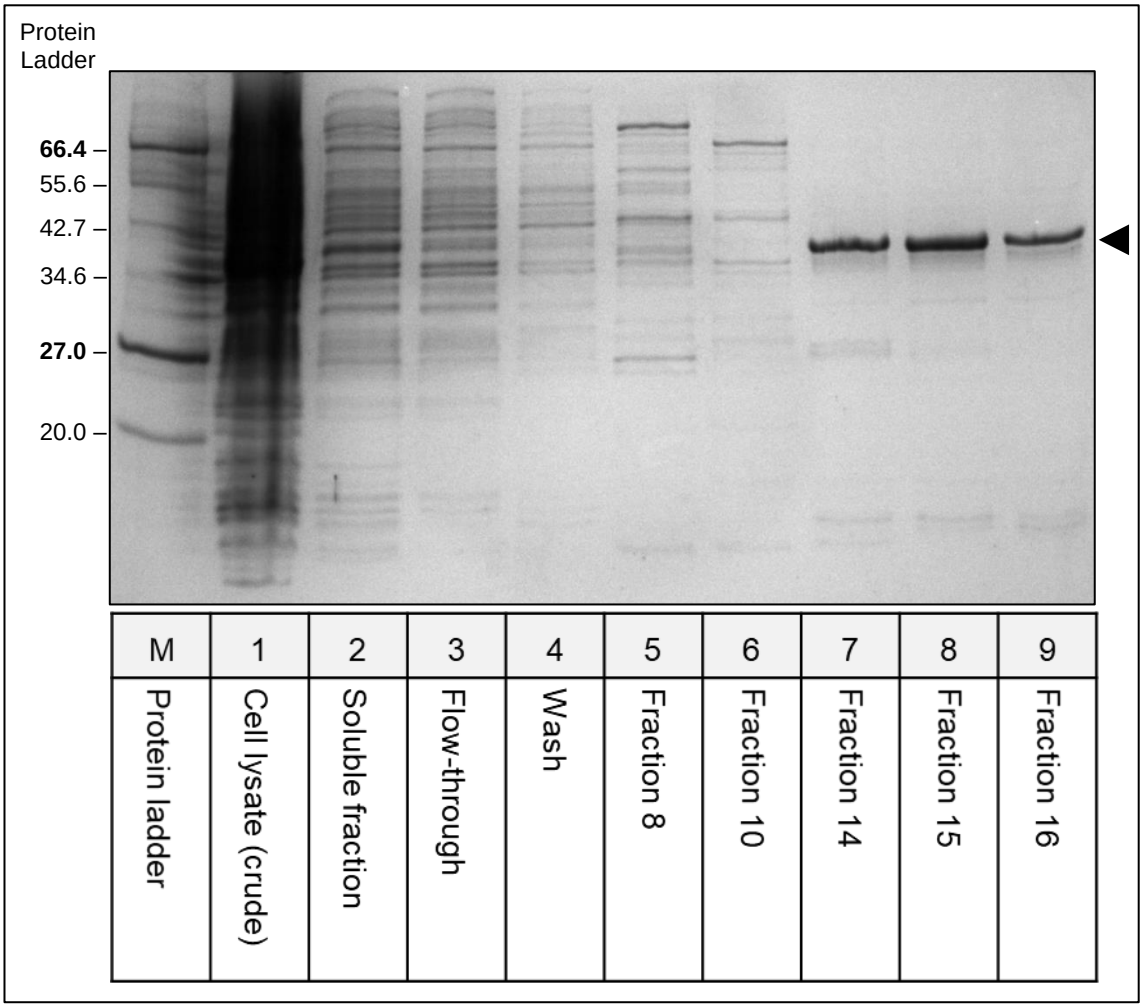

Figure 4.14: Purification of TEV A protease using the FPLC ÄKTA Pure system. The product was monitored by Coomassie blue dye-stained SDS-PAGE (10% polyacrylamide gel). *M*: molecular weight standard (kDa). *Lane 1*: Total intracellular protein after induction. *Lane 2*: Soluble cell extract. *Lane 3*: Flow-through. *Lane 4*: Washing residual. *Lane 5*: Elute fraction 8. *Lane 6*: Elute fraction 10. *Lane 7*: Elute fraction 14. *Lane 8*: Elute fraction 15. *Lane 9*: Elute fraction 16. The arrow ◄ is the expected MW of the His.Lipoyl TEV Protease (~36 kDa).

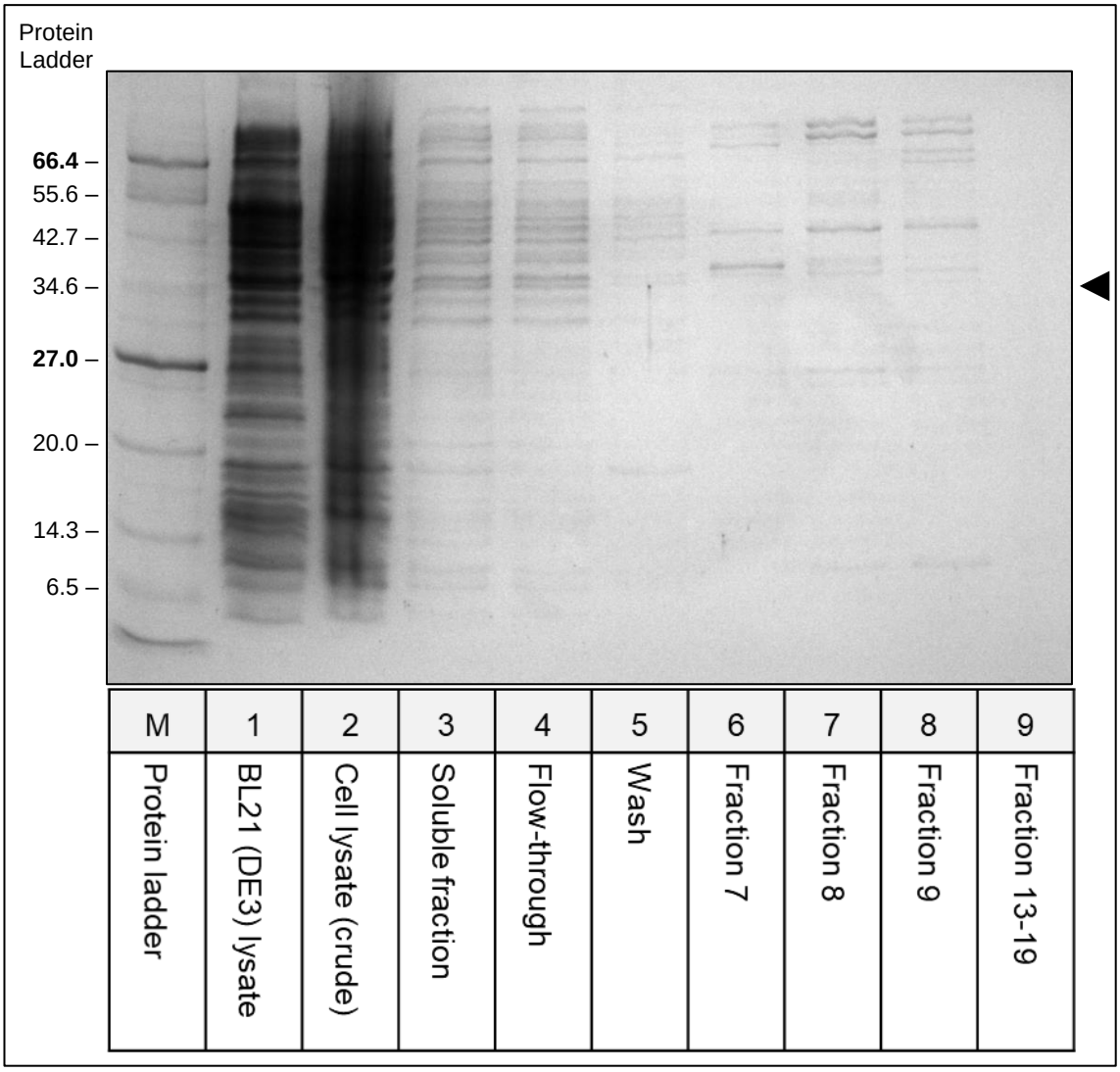

Figure 4.15: Purification of TEV S protease using the FPLC ÄKTA Pure system. The product was monitored by Coomassie blue dye-stained SDS-PAGE (10% polyacrylamide gel). *M*: molecular weight standards (kDa). *Lane 1*: Total intracellular protein before induction. *Lane 2*: Total intracellular protein after induction. *Lane 3*: Soluble cell extract. *Lane 4*: Flow-through. *Lane 5*: Washing residual. *Lane 6*: Elute fraction 7. *Lane 7*: Elute fraction 8. *Lane 8*: Elute fraction 9. *Lane 9*: Elute fraction 13-19. The arrow ◄ is the expected protein band of the TEV Protease.

4.3.5 Protein Purification of hLtn Variants

4.3.5.1 Wild type Recombinant hLtn

Initial expression of the fusion protein was performed on the wild type construct. The expected size of the fusion protein is ~26 kDa (as discussed in **Chapter 4(a)**). Results showed that the protein expressed is highly soluble (**Figure 4.16**) by comparing the soluble (refer *Lane 3*) and insoluble fraction (refer *Lane 4*). This indicates that the fusion protein construct with the lipoyl domain has improved the protein solubility. Treatment with the nickel resin highly purifies the fusion protein, although there are still some impurities observed and a noticeable truncated form of the protein.

The next step was to obtain the mature hLtn peptide by digestion the TEV protease cleavage site of the fusion protein. Before the digestion and re-introducing the fusion protein to the nickel resin, the protein was treated beforehand in a size exclusion chromatography column to remove excess imidazole salt. The presence of the salt can interfere with binding of polyhistidine tag to the nickel affinity resin. The result shows that the recovery of the mature hLtn peptide very low as most of it remains bound to the nickel beads (**Figure 4.17 (a)**). Moreover, the cleaved protein size for the His-Lipoyl domain and mature hLtn protein was at ~15 kDa and ~13 kDa respectively, with a total size higher than the undigested fusion protein (only ~26 kDa). The observed recombinant hLtn had a higher molecular weight (~13 kDa) than the theoretical (~10 kDa). Therefore, we ran the commercially available hLtn on the gel to clarify the result. The recombinant hLtn gel migration was slightly slower than expected which was comparable to the commercial hLtn (refer **Figure 4.17 (b)**). The recombinant hLtn produced had a slightly higher molecular weight compared to the commercial as it contains two extra amino acids on the N-terminal. The lipoyl domain corresponds to the correct theoretical molecular weight at ~16 kDa. Interestingly, the mature recombinant hLtn peptide gel migration shows a higher molecular weight <10 kDa (**Figure 4.12 (a)** *Lane 3*) compared to the expected theoretical molecular weight generated using Expasy ProtParam analysis (refer **Chapter 4 (a)**).

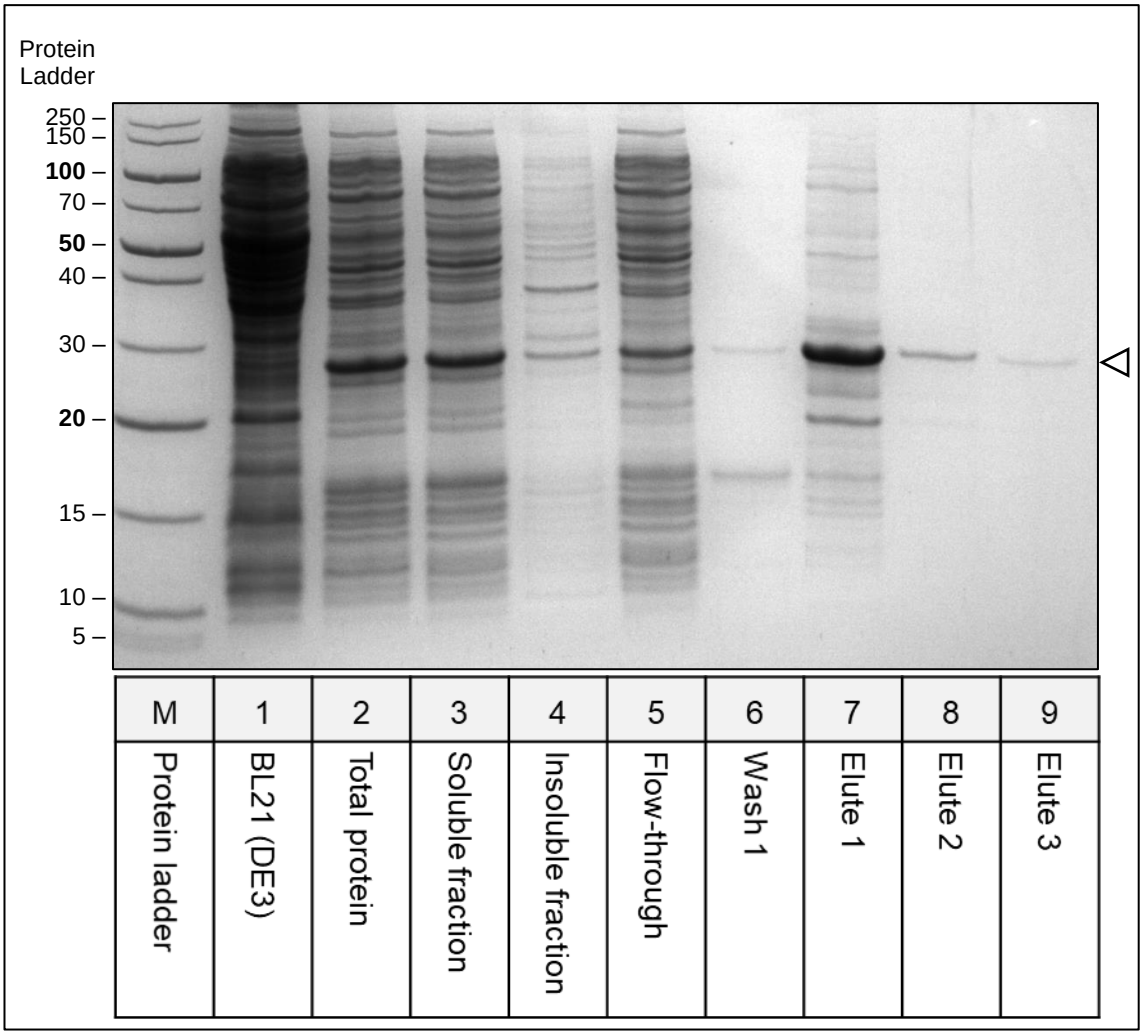

Figure 4.16: First-step of Ni-NTA purification of recombinant HLTEV-hLtn WT. The product was monitored by Coomassie blue dye-stained SDS-PAGE (15% polyacrylamide gel). *M*: molecular weight standards (kDa). *Lane 1*: Total intracellular protein without induction. *Lane 2*: Total intracellular protein after induction. *Lane 3*: Soluble cell extract. *Lane 4*: Insoluble cell extract. *Lane 5*: Flow-through. *Lane 6*: Washing residual. *Lane 7*: First elution. *Lane 8*: Second elution. *Lane 9*: Third elution. The arrow ◁ is the fusion protein (theorectical MW ~26 kDa)

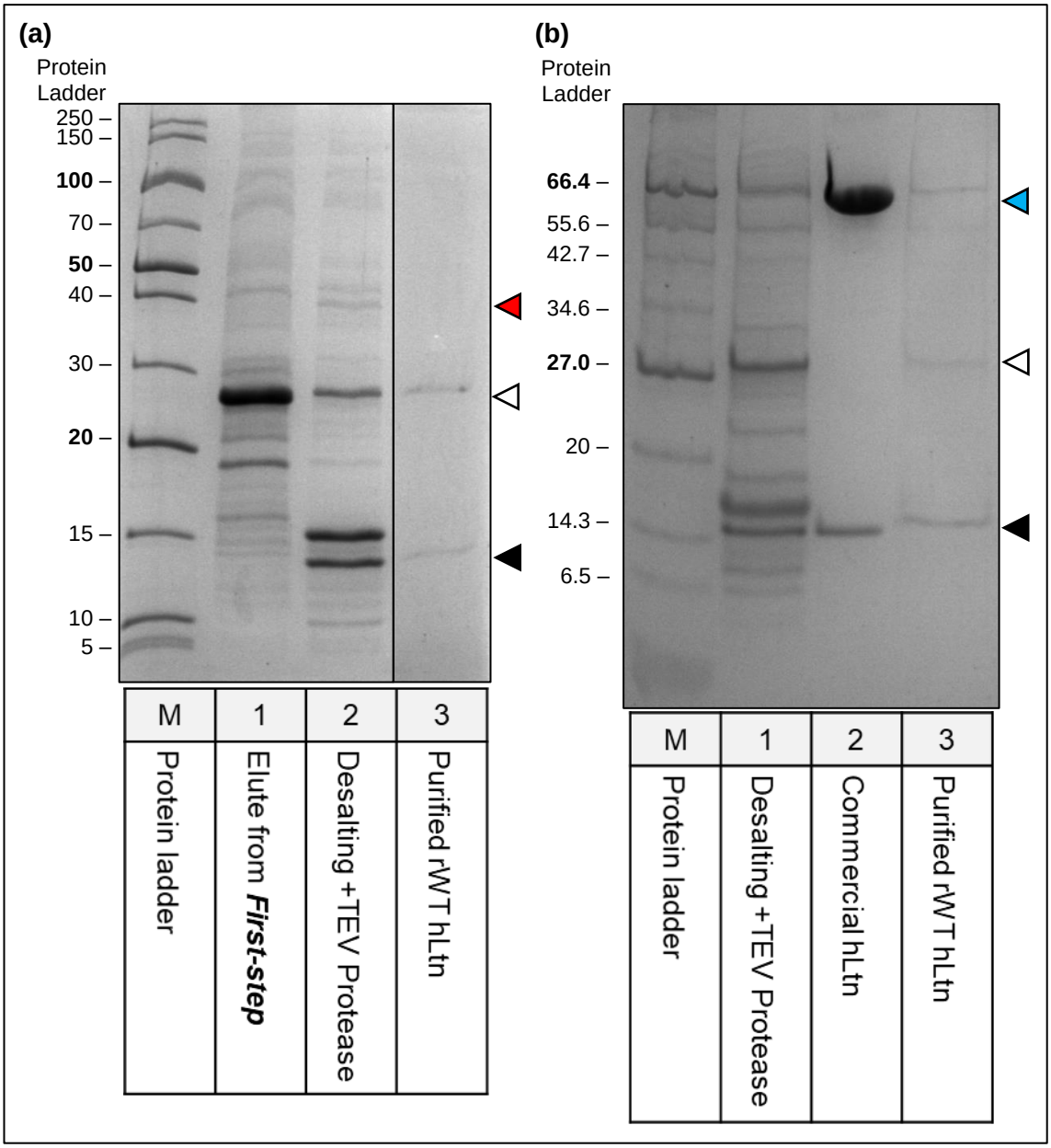

Figure 4.17: Second-step of Ni-NTA purification of recombinant HLTEV-hLtn WT. The product was monitored by Coomassie blue dye-stained SDS-PAGE (15% polyacrylamide gel). On the left **(a)**: *M*: molecular weight standards (kDa). *Lane 1*: Elution from first-step purification. *Lane 2*: Digestion of desalted fusion protein with His.Lipoyl-TEV protease. *Lane 3*: Purified recombinant hLtn. On the right **(b)**: *M*: molecular weight standards (kDa). *Lane 1*: Digestion of desalted first elution fusion protein with His.Lipoyl-TEV protease. *Lane 2*: Commercial hLtn (Peprotech®) diluted in 1% (w/v) BSA (arrow ◁). *Lane 3*: Purified recombinant wild type hLtn. The arrow ◀ is the His.Lipoyl-TEV Protease (theoretical MW ~36 kDa); ◁ is the fusion protein (theoretical MW ~26 kDa) and ◀ is the recombinant hLtn (theoretical MW ~10 kDa).

4.3.5.2 Recombinant CC3 and W55D Mutants of hLtn

Purification of the hLtn mutant variants was carried on once the purification profile has been established with the recombinant wild type hLtn. Similar profile in the mutant protein purification was observed compared to the wild type, as there are no differences in the hLtn variants sequence only replacement of strategic amino acids. Both CC3 (**Figure 4.18**) and W55D (**Figure 4.20**) mutant fusion protein expressed at ~26 kDa. Noticeably, the W55D mutant fusion protein has more truncation of the fusion protein (cleaved of the fusion protein before treatment with protease) compared to CC3.

The second-step in the purification of the mutants revealed that while the digestion of the TEV linker site was successful, there was some residual fusion protein which was not cleaved by the protease. The purified recombinant CC3 (**Figure 4.19** *Lane 4*) and W55D (**Figure 4.21** *Lane 4*) mutants contained less impurities than in the wild type. Unfortunately, more than half of the protein was lost due to non-specific binding to the nickel resin was observed (refer **Figure 4.19 and 4.21** *Lane 6*).

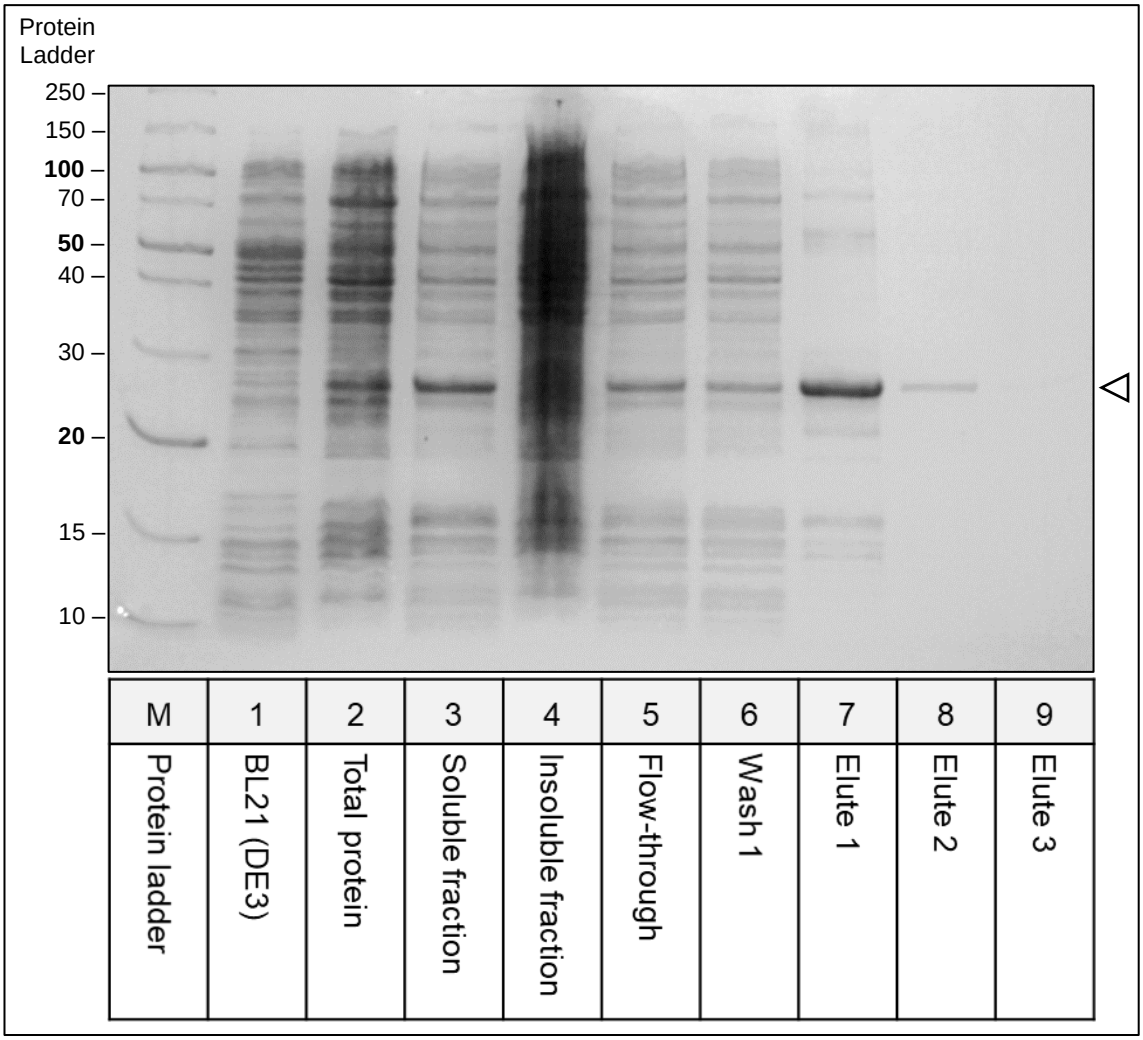

Figure 4.18: First-step of Ni-NTA purification of recombinant HLTEV-hLtn CC3 (rCC3) mutant. The product was monitored by Coomassie blue dye-stained SDS-PAGE (15% polyacrylamide gel). *M*: molecular weight standards (kDa). *Lane 1*: Total intracellular protein without induction. *Lane 2*: Total intracellular protein after induction. *Lane 3*: Soluble cell extract. *Lane 4*: Insoluble of cell extract. *Lane 5*: Flow-through. *Lane 6*: Washing residual. *Lane 7*: First elution. *Lane 8*: Second elution. *Lane 9*: Third elution. The arrow ◄ is the His.Lipoyl.TEV-hLtn CC3 (theoretical MW 26 kDa).

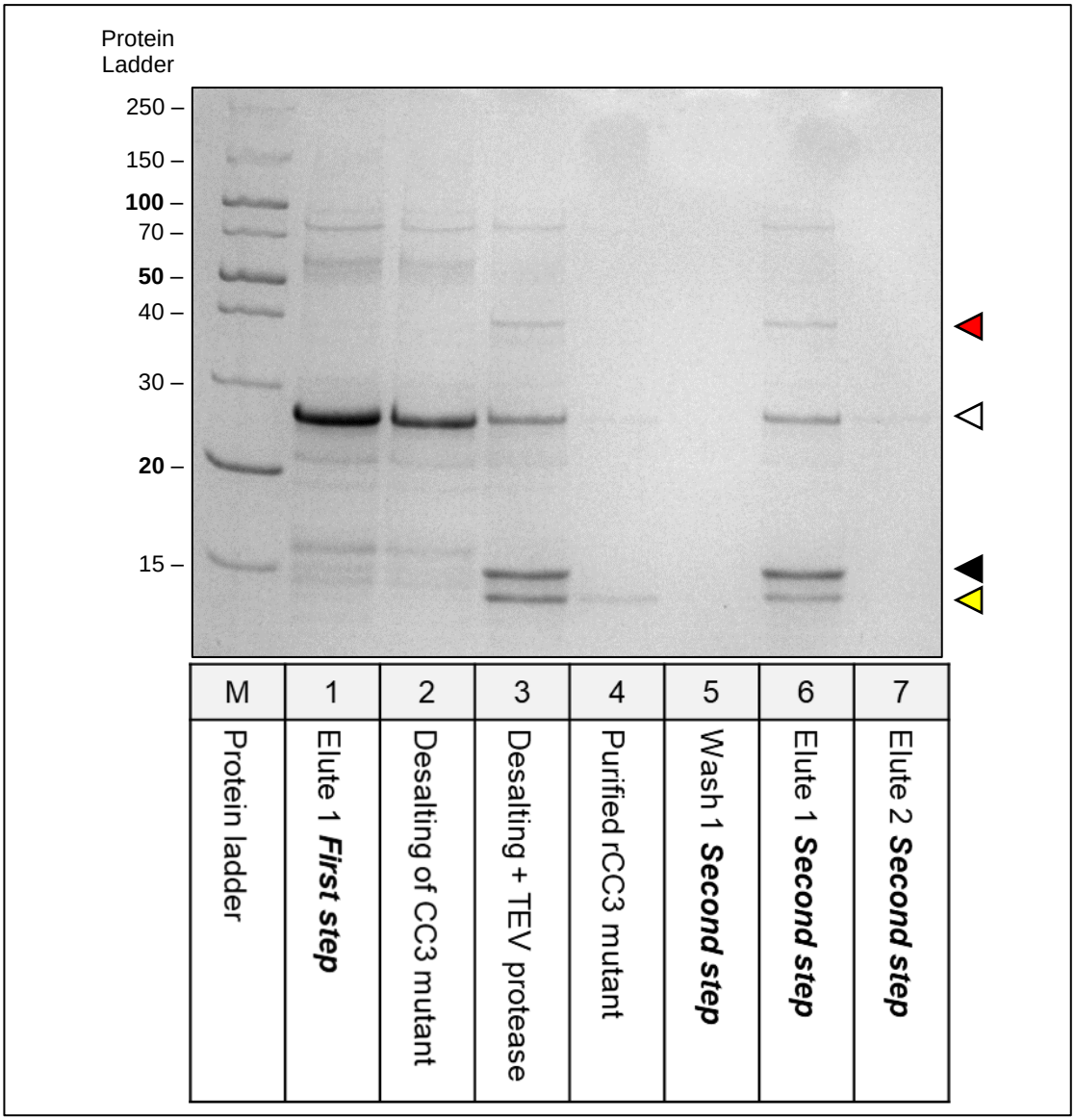

Figure 4.19: Second-step of Ni-NTA purification of recombinant HLTEV-hLtn CC3 (rCC3) mutant. The product was monitored by Coomassie blue dye-stained SDS-PAGE (15% polyacrylamide gel). *M*: molecular weight standards (kDa). *Lane 1*: Elution from first-step purification. *Lane 2*: Desalted first-step elution. *Lane 3*: Digestion of desalted first elution fusion protein with His.Lipoyl-TEV protease. *Lane 4*: Purified recombinant CC3 mutant hLtn. *Lane 5*: Washing residual. *Lane 6*: First elution. *Lane 7*: Second elution. The arrow ◀ is the His.Lipoyl-TEV Protease (~36 kDa); ◁ is the CC3 (theoretical MW ~26 kDa); ◀ is the lipoyl domain of the fusion protein (~16 kDa); and ◁ is the rCC3 hLtn (~10 kDa).

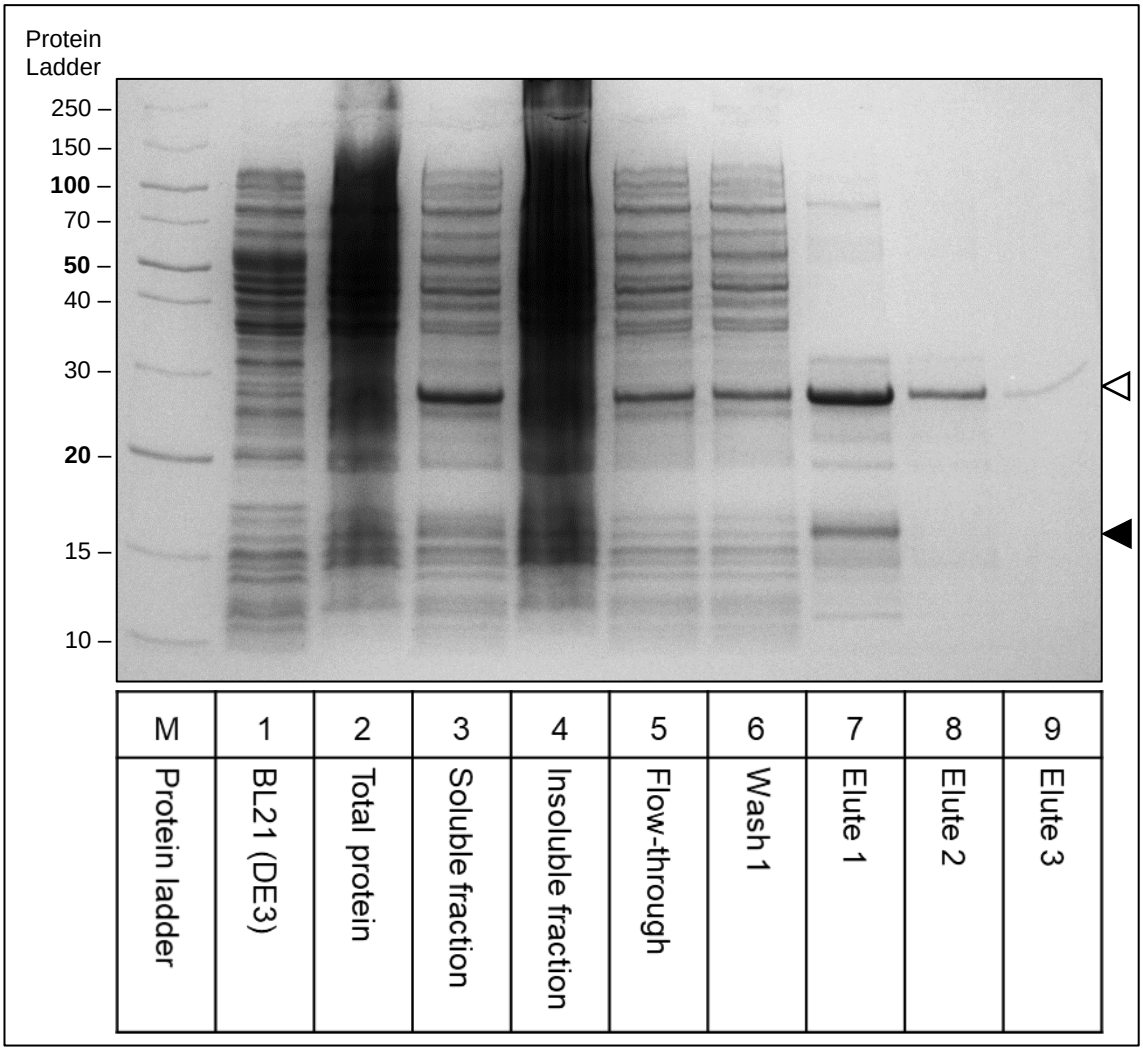

Figure 4.20: First-step Ni-NTA purification of recombinant HLTEV-hLtn W55D (rW55D) mutant. The product was monitored by Coomassie blue dye-stained SDS-PAGE (15% polyacrylamide gel). *M*: molecular weight standards (kDa). *Lane 1*: Total intracellular protein without induction. *Lane 2*: Total intracellular protein after induction. *Lane 3*: Soluble cell extract. *Lane 4*: Insoluble body of cell extract. *Lane 5*: Flow-through. *Lane 6*: Washing residual. *Lane 7*: First elution. *Lane 8*: Second elution. *Lane 9*: Third elution. The arrow ◁ is the His.Lipoyl.TEV-hLtn W55D (theoretical MW 26 kDa) and arrow ◀ is the truncated protein.

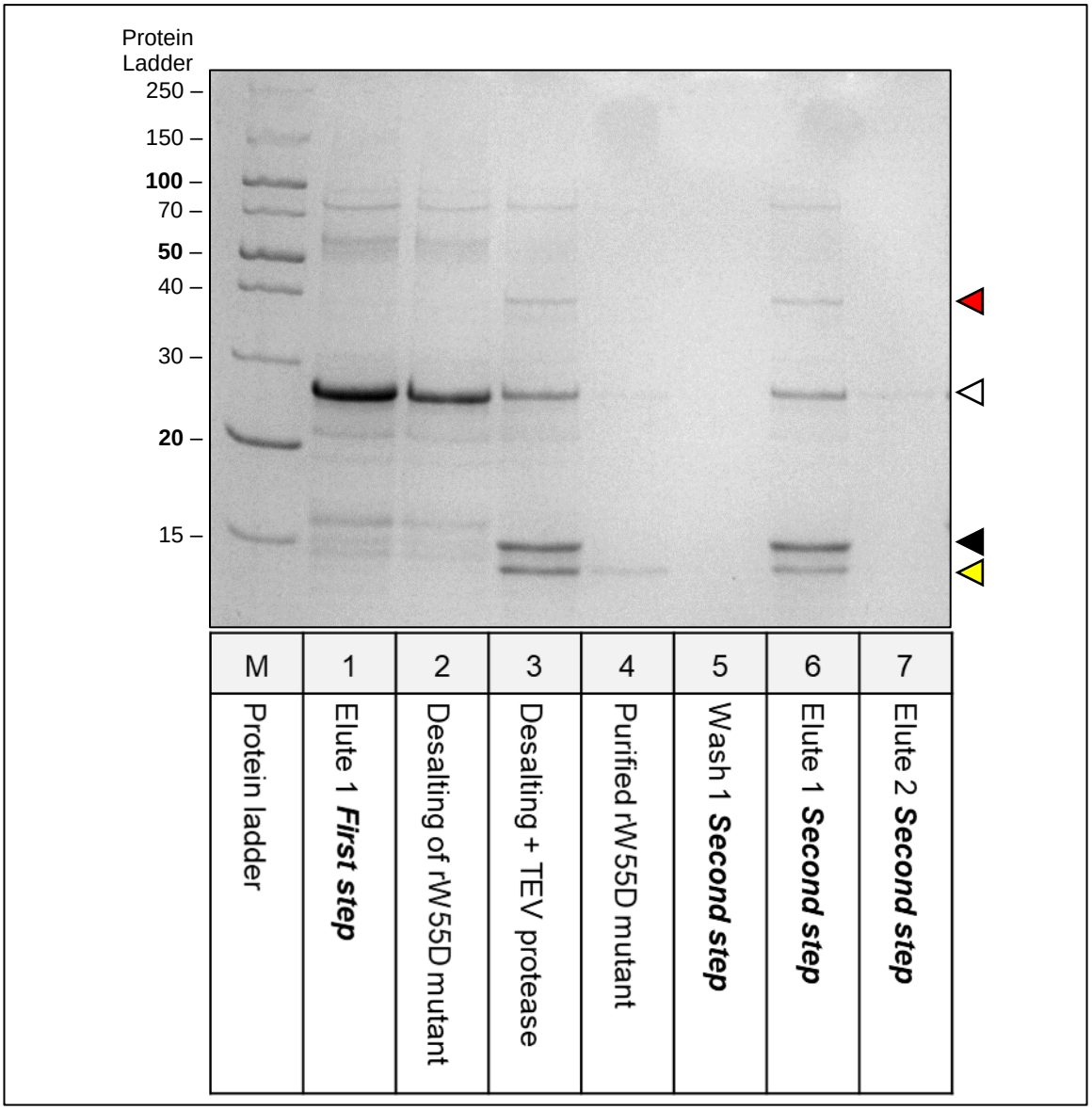

Figure 4.21: Second-step Ni-NTA purification of recombinant HLTEV-hLtn W55D (rW55D) mutant. The product was monitored by Coomassie blue dye-stained SDS-PAGE (15% polyacrylamide gel). *M*: molecular weight standards (kDa). *Lane 1*: Elution from first-step purification. *Lane 2*: Desalted first-step elution. *Lane 3*: Digestion of desalted first elution fusion protein with His.Lipoyl-TEV protease. *Lane 4*: Purified recombinant CC3 mutant hLtn. *Lane 5*: Washing residual. *Lane 6*: First elution. *Lane 7*: Second elution. The arrow ◀ is the His.Lipoyl-TEV Protease (~36 kDa); ◁ is the rW55D (theoretical MW ~26 kDa); ◀ is the lipoyl domain of the fusion protein (~16 kDa); and ◁ is the rW55D hLtn (~10 kDa).

4.3.5.3 Concentration of Recombinant Protein Produced

The concentration of recombinant hLtn variants produced were measured and concentration assumption correction was re-calculated based on the extinction co-efficient provided in **Chapter 4(a)** (refer **Table 4.3**).

Table 4.9: Recombinant hLtn variants protein concentration.

hLtn variants	Optical Density			[Protein] (mg/mL)
	A260	A280	A340	
Wild type	0.615	0.578	0.387	0.843
CC3 mutant	0.271	0.246	0.105	0.360
W55D mutant	0.133	0.115	0.055	0.782

4.3.6 Analysis of the Functional Activity of Recombinant hLtn Variants using Calcium Flux Assay

The functional activity of recombinant protein is important to investigate whether the produced protein behave and function similarly to its native protein. Calcium flux assay was performed to determine the protein activity due to chemokine ability to activate calcium flux signalling in cells through their receptor. Previous publications had shown behaviour of hLtn variants in calcium signalling [hLtn WT, CC3 and W55D mutant (Tuinstra *et al.*, 2007, 2008)]. The results (**Figure 4.22**) show that the recombinant hLtn variants produced were functional. Both canonical fold hLtn, hLtn WT and CC3 displayed the ability to promote calcium flux whilst this was not the case for W55D.

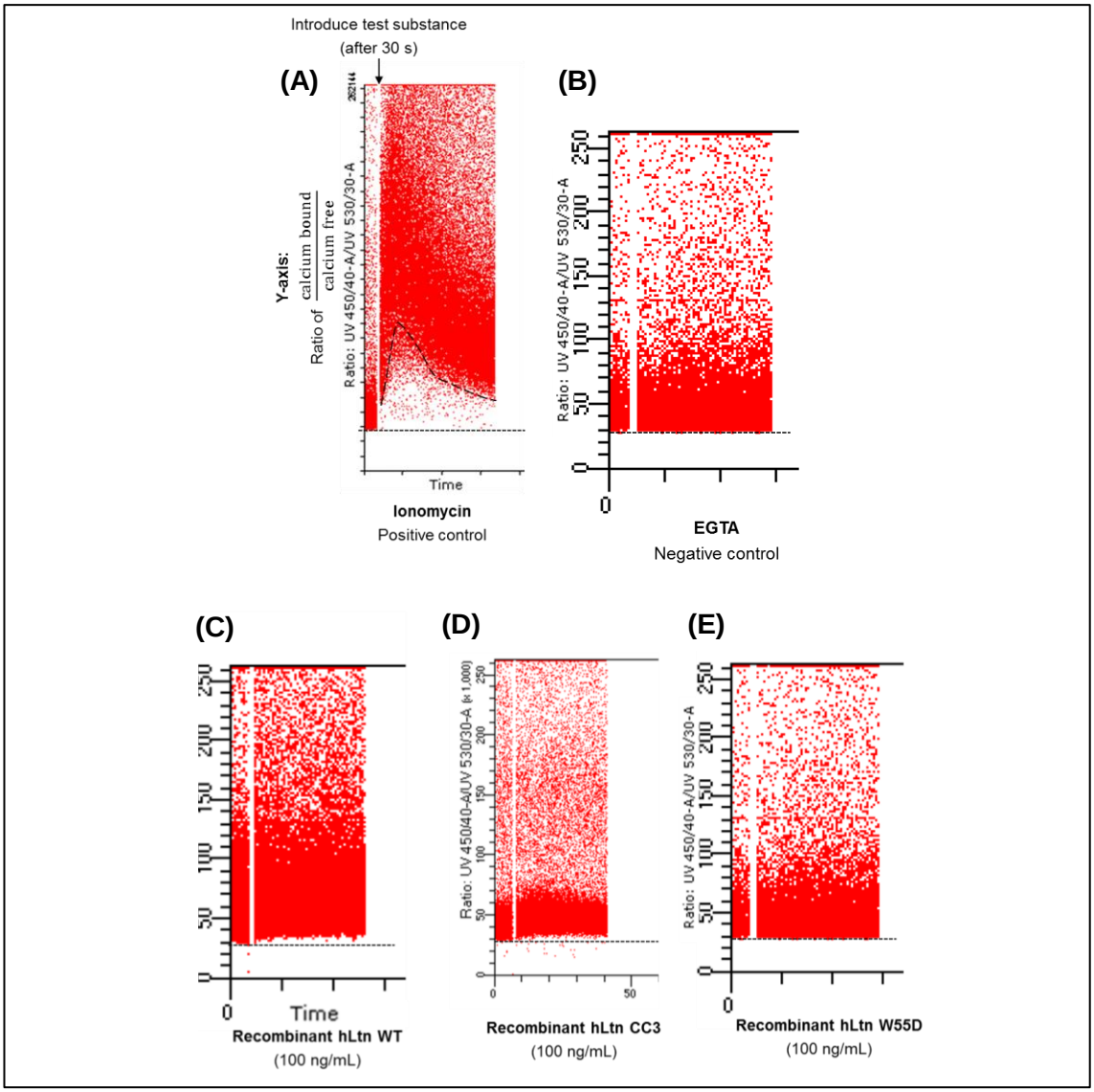

Figure 4.22: Calcium flux assay of SCC4 cells using Indo-1 dye. **(A)** Ionomycin and **(B)** EGTA was used as positive and negative controls respectively. The cells were treated with 100 mg/mL hLtn **(C)** WT, **(D)** CC3 and **(E)** W55D. The dotted line (- - - -) is the base line of the unbound Indo-1 SCC4 cells before stimulation.

4.4 DISCUSSION

There are number of challenges in producing and purifying large number of protein in high-throughput manner (Jia and Jeon, 2016). Small proteins are especially difficult such as the protein being easily degraded by the expressing organism, usually in *E. coli* or problems with purification. Chemokines are categorised as small proteins due to its molecular weight being around 10 – 12 kDa. To facilitate purification, tag vectors or fusion protein partners can assist in the expression. Continuation of the work from **Chapter 4(a)**, this sub-chapter was to produce and purify the designed protein using all the information obtained from the *in-silico* analysis.

4.4.1 Molecular Cloning of Plasmid pET24a-His.Lipoyl-TEV hLtn Variants

Two different constructs were produced to study hLtn protein expression in *E. coli*. The pET24a-(IEGR) construct was designed and generated using GenScript services. The sequence was codon-optimised to accommodate expression in *E. coli*. Meanwhile, pET24a-(TEV) was constructed from pCMV6-Entry hLtn where the hLtn/XCL1 DNA sequence is from human. Distinct differences between the two constructs were the use of different linkers and the cleavage site.

The OneClick tool was used to generate the mutagenesis primers and the experimental conditions (Warburton *et al.*, 2015). The whole-plasmid amplification was successful, and the PCR product corresponded to the expected size of the DNA and desired amino acid mutation. Expression in *E. coli* requires a different vector, therefore the hLtn variant DNA sequences were required to be transferred into pET24a-HLTEV plasmid cassette.

4.4.2 Comparative Study of pET24a-(IEGR) and pET24a-(TEV) hLtn Expressing Plasmid Constructs

There are different ways to induce the plasmid promoter. The operon ‘substrate’ is highly dependent on the nature of the promoter. IPTG is a synthetic molecule that mimics allolactose, a structural analogue which triggers the transcription of lac operon to induce recombinant protein expression. In contrast auto-induction recipe uses lactose in the media (Studier, 2014) which drives the protein expression after depletion of glucose.

The protein was not expressed as highly with IPTG induction as for auto-induction. One of the possible explanations for this is that IPTG can provide stress to the *E. coli* system as due to its synthetic nature and is unable to be metabolised by the cell. It was found that IPTG exacerbates haloalkene substrate induced toxicity that can causes a metabolic burden to *E. coli* as well as stimulating expression of exogenous genes (Dvorak *et al.*, 2015). Lactose is a natural inducer of lac operon and can effectively reduce the negative influence on the metabolic pathways, making it a better inducer than IPTG for heterologous protein expression in BL21 (DE3) (Dvorak *et al.*, 2015). Moreover, the induction is highly dependent on the binding and dissociation rates of IPTG and lactose to the lac repressor (Daber *et al.*, 2007). However, some issues of induction with IPTG can be rectified by adjusting the concentration.

The fusion protein migration in SDS-PAGE runs slower than expected and therefore appears to have a higher molecular weight compared to theoretical analysis generated by the Expasy ProtParam tool (refer **Chapter 4(a) Table 4.2**). This is not unusual as aberrations in protein migration in SDS-PAGE can be due to the process, where the separation is by charge rather than mass. Additional protein domains or abundance of particular amino acids can affect the process. Moreover high content of basic or acidic amino acids (Guan *et al.*, 2015), and partial reduction of the protein thus retaining its disulphide bonds (Okamoto *et al.*, 2014) can also contribute to why the molecular weight results in protein migration 3-4 kDa above the expected size. Further examination using western blot for the His-tag confirmed the SDS-PAGE protein size at 26 kDa.

The codon-optimised IEGR construct showed lower expression than the TEV construct, in contrast to expectations. Usually codon-optimisation allows a higher expression of recombinant protein as codon frequency is different in each organism. Furthermore, this juxtaposition may due to the addition of a fusion partner at the N-terminus which often results in high level expression of the fusion protein (Steinmetz and Auldridge, 2017) which facilitates the expression of TEV construct. Further contributions to the disparity may come from the content of the amino acids in the linker region. In conclusion, pET24a-(TEV) construct was selected in further experimentation.

4.4.3 Comparative Study of pET24a-(TEV) hLtn Expression in Different *E. coli* Strains and Induction Scheme

Two *E. coli* strains BL21 (DE3) and C41 (DE3) were used to study their ability to express the novel fusion protein. C41 (DE3) is a mutant strain of BL21 (DE3) that can overcome the toxicity associated when overexpressing recombinant proteins (Dumon-Seignovert, Cariot and Vuillard, 2004). Induction with IPTG resulted in similar problems as previously explained for both strains, although TB and TYE auto-induction has positive total protein expression. While there is little difference in the expression, C41 (DE3) was shown to express slightly more protein compared to BL21 (DE3). This is probably due to the differences between the two strains, where C41 (DE3) has a higher transformation success rate and expression of heterologous protein compared to its parental strain, BL21 (DE3) (Dumon-Seignovert, Cariot and Vuillard, 2004). Also, TB media is a highly enriched compared to TYE media with increased concentration of peptone, yeast extract and glycerol as carbon source.

Additional investigations of the protein expression between the strains and auto-induction recipe were performed by comparing their soluble and insoluble protein fractions. Interestingly, C41 (DE3) had a poor expression in this analysis making BL21 (DE3) the suitable vehicle for the fusion protein expression. The content of soluble protein was higher compared to the insoluble, which was expected due to the incorporation of the lipoyl domain in the fusion protein. Truncation of protein was observed, highly in C41 (DE3). As C41 (DE3) is a mutated strain of BL21 (DE3), it behaves differently and is not compatible with the fusion protein. Presence of endogenous proteases is a possible cause of the truncation as their function is to remove abnormal and misfolded proteins (Gottesman, 1996) although BL21 (DE3) has a knockout of OmpT and Lon proteases. This can be remedied by introducing a sufficient concentration of exogenous protease inhibitor.

4.4.4 Protein Purification of Functionally Active hLtn Variants

After rigorous examination of the expressing conditions, the hLtn variants were expressed and purified. SDS-PAGE analysis was performed to observe the recombinant protein purification profile. A similar protein size was observed between the fusion protein of hLtn WT, CC3 and W55D fusion proteins.

The first-step of purification was performed to isolate protein using the affinity tag. Non-specific proteins were detected to bind to the resin and eluted along with the fusion protein. BL21 (DE3) has shown to produce small number of native proteins that has a high affinity to nickel ions even in presence of a high concentration of imidazole (Bartlow *et al.*, 2011; Robichon *et al.*, 2011), allowing some amount of unwanted proteins bind to the nickel resin.

A size exclusion chromatography step was sandwiched between the first and second purification steps for removal of imidazole salt before re-introducing the fusion protein to a nickel resin. Imidazole can interfere with the binding resulting in poor protein purity. A second IMAC purification was used to capture the residual 'nickel-loving' protein, including both the His-Lipoyl TEV protease and the His-Lipoyl domain of the fusion protein after digestion. The intention was to release the mature hLtn protein in to the solution. Unfortunately, when executing the 'negative nickel' attachment, a high amount of the purified hLtn variants still bound to the nickel resin even though the polyhistidine tag was removed. Some possible explanations for this behaviour are: 1) the abundance of free electron pair amino acids (His, Cys, Met, Arg, Lys), and 2) the buffer conditions such as pH, salt content, addition of reducing agent or stabilising elements. There is some report shown that high content of glutamine (Gln), aspartic acid (Asp) and can contribute to non-specific binding to the nickel resin. The enrichment of electron pair amino acids potentially sufficient to interact with sequestered Ni^{2+} ion. Untagged protein has natural affinity to for Ni-NTA and is dependent on the proximity of histidine including the previously described amino acid residues on its surface. The amino acids will deprotonate in pH higher than 7 and readily bind to metals. Nevertheless, this still does not explain low recovery of the purified hLtn. Besides, the overall positively charged residues of the hLtn protein, increasing the likelihood that the protein feebly adsorbs to Ni^{2+} resin, reducing its capability to be released into the solution.

The observed pattern of the protein migration in the SDS=PAGE for hLtn WT, CC3 and W55D mutant after TEV cleavage were interesting. The mature hLtn protein ran slightly higher on the gel suggesting its molecular weight was larger than the

theoretical value. This aberrant mobility may be contributed by the overall charge of the protein. hLtn protein contains high number of positively charge amino acids and has the possibility to be saturated with SDS (Dolnik and Gurske, 2011). SDS-PAGE protein migration is highly dependent on charge, therefore this 'gel-shifting' phenomenon is to be expected. Similar behaviour was observed by using the commercially available hLtn (refer **Figure 4.17**), where documented the molecular weight is documented at 10 kDa when measured by mass spectrometry.

Calcium flux assay was performed to test the functional activity of the purified recombinant hLtn. The results obtained were contrast to those of Tuinstra *et al.* (2007), where they showed that any modification at the hLtn N-terminal did not stimulate the calcium flux. Our commercially bought XCL1 from Peprotech did activate the calcium signalling (contains 2-93 AA of native XCL1 $V^{2}GSE$) and our in-house recombinant hLtn variants has additional glycine 'leftover' due to an artefact of TEV protease cleavage ($G^{-1}VGSE$). The difference in calcium signalling is probably due to the use of XCR1+ oral cancer cell line expressing native chemokine receptor whilst other studies have used stably expressing XCR1 human embryonic kidney (HEK) cells. Also, the calcium flux assay method in the literature was different where spectrofluometer was used to detect Fluo-2 fluorescence. Alternatively, high-throughput flow cytometer quantification using Indo-1 dye were used in this experiment. Comparatively, Indo-1 is more sensitive than Fluo-2 in detecting intracellular calcium flux (Bailey and Macardle, 2006). In conclusion, the recombinant hLtn WT, CC3 and W55D can be produced using the method described in this chapter.

4.5 SUMMARY

This chapter demonstrates that the production and purification methods used are applicable for small sized proteins (≤ 10 kDa) such as chemokines. The incorporation of the lipoyl domain, a hyper acidic fusion tag at the N-terminus of the fusion protein further facilitated the solubility of the protein domain in *E. coli*. This technique can be generally applied to improve production of chemokines although additional optimisation should further refine the process on case-by-case basis. The produced chemokine was functionally active as observed by its ability to induce calcium flux activity. All the recombinant hLtn variants in this chapter will be used in Chapter 5 to study their influence on the behaviour of oral cancer cells.

CHAPTER 5

THE EFFECT OF RECOMBINANT hLtn ON THE BEHAVIOUR OF ORAL CANCER CELL LINES

CHAPTER 5: THE EFFECT OF RECOMBINANT hLtn ON THE BEHAVIOUR OF ORAL CANCER CELL LINES

5.1 INTRODUCTION

Previous chapters covered the design, development and production of recombinant hLtn variants and expression of XCR1 in oral cancer cell lines (OCCLs). hLtn has been shown to mediate cell proliferation, adhesion, migration and invasion in cancer cells but the studies have been limited to the wild type variant. hLtn is a metamorphic protein that can interconvert between two different protein conformations, one that activates the chemokine receptor (hLtn10) while the other does not (hLtn40). To date, there have been no studies investigating the effect of the hLtn variants on epithelial cells. Therefore, this chapter explores the effect of these variants on oral cancer cell lines (OCCL).

Several functional assays were used to investigate the behaviour of oral cancer cell lines (OCCL) after treatment with the hLtn variants. Characteristics such as proliferation, adhesion to extracellular matrix (ECM) components, and migration towards the variants was studied.

Proliferation is a key cell characteristic with an upregulation in case of cancer. It has been shown previously that hLtn mediates cell proliferation in OCCL through its receptor XCR1 (Khurram *et al.*, 2010). However, it is not known whether this interaction is associated with the canonical chemokine fold only.

For the adhesion study, several ECM components abundant in oral connective tissue were selected including collagen I and fibronectin. Collagen I is the most abundant main structural component in the ECM and expressed in all connective tissues (Shoulders and Raines, 2009; Ricard-Blum, 2011). Fibronectin is an ECM glycoprotein that is involved in cell growth, differentiation, adhesion and migration (Pankov and Yamada, 2002; Singh, Carraher and Schwarzbauer, 2010). Fibronectin is secreted by various cells, primarily as a soluble protein dimer, which is then assembled into an insoluble matrix, providing a structural support and signal for cells through integrin binding. Similarly, fibronectin binds to other ECM structures such as collagen, fibrin and heparin sulphate proteoglycans. Collagen IV is a basement membrane component in primarily found in the basal lamina epithelial and endothelial cells to separate tissue compartments (Lu, Weaver and Werb, 2012). Interaction with collagen IV is key in cancer progression as invasion through the basement membrane (predominantly comprising of

collagen IV) is the first step in OSCC invasion. These ECM components are important in cancer invasion providing anchorage to cancer cells and facilitating spread.

While it has been previously reported that hLtn is a chemokine with a canonical fold able to activate the receptor and mediate calcium flux signalling, the exact contribution of different hLtn conformations in cancer is still unknown. Different cell types behave differently towards a certain stimulus and in cancer cell, this is often aberrant. Therefore, this chapter further investigate the role of hLtn variants on oral cancer cell behaviour.

5.2 MATERIALS AND METHODS

5.2.1 Materials

List of detailed information of the materials (reagents, kits, equipment, software and miscellaneous) used in the chapter can be found in **Appendix 1-5**.

5.2.2 Basic cell culture

Methods performed in this chapter can be referred in Chapter 3 **Section 3.22.**

5.2.3 Proliferation assay

Principle: The proliferation assay was conducted utilising a tetrazolium compound, ([3-(4,5-dimethylthiazol-2-yl)-5-(3-carboxymethoxyphenyl)-2-(4-sulfophenyl)-2H-tetrazolium, inner salt; MTS]) to determine the number of living cells. The dye reaction is dependent on the availability of NAD(P)H flux because of cellular metabolic activity and indirect method to quantify cell number.

Procedure: Cells were prepared and seeded at a density of 2×10^3 cells per 100 µL in 96-well plates. Overnight incubation at 37°C was performed allowing the cells to adhere to the plate. Several wells were pre-treated with anti-human XCR1 antibody for an hour to block the receptor activity. Treatment with hLtn variants (wild type, CC3 and W55D mutants) was performed at a concentration 100 ng/mL (or ~10 nM) in serum-free media (SFM). For positive and negative controls, full-serum media and SFM were used respectively. In addition, mitomycin C (concentration 1 µg/mL) was used to arrest cell proliferation, serving as baseline for the cell proliferation. The plate was incubated at 37°C in 5% CO_2 incubator. After 48 h and 72 h, 20 µL of MTS was added into each well and further incubated for another hour before absorbance measurements were taken. Absorbance was quantified using an Infinite® M200 Pro Series (Tecan UK Ltd) at 492 nm accompanied by Magellan™ Data Analysis Software (Tecan UK Ltd).

5.2.4 Adhesion Assay

96-well tissue culture plates were coated with collagen type I, solution from rat tail (Sigma-Aldrich), collagen IV from human cell culture (Sigma-Aldrich) or plasma fibronectin (Sigma-Aldrich) (concentration: 0.1 – 10 µg/mL) for an hour in an incubator at 37˚C. Control wells were not coated but left in phosphate buffed saline (PBS) (Sigma-Aldrich). Non-specific binding sites were blocked using serum free medium (SFM) with 1% (w/v) BSA for one hour at 37°C. Cells were prepared by detaching the cells using 0.05% (v/v) Trypsin-EDTA solution (Sigma Aldrich) in PBS. For cell treatment, cells were incubated with 100 ng/mL (~10 nM) of recombinant human lymphotactin (XCL1) (Peprotech, London, UK) for 24 hours at 37°C with serum-free medium in a T75 flask. Using centrifugation (1000×g, 5 min, 28ºC), cell pellets were collected, re-suspended and counted. 4×10^4 cells in 100 µL were seeded in each well (number of cells was determined after optimisation assays). Cells were left to adhere for another 1 hour in the incubator. Unattached cells were removed by washing twice using serum free medium. 100 µL of fresh medium was added to each well followed by addition of 20 µL of CellTiter 96® Aqueous One Solution Cell Proliferation Reagent in the dark (Promega, Southampton, UK). The reagent contains a tetrazolium compound, 3-(4, 5-dimethylthiazol-2-yl)-5-(3-carboxymethoxyphenyl)-2-(4-sulfophenyl)-2H-tetrazolium, inner salt (MTS) which is metabolically cleaved by viable cells. After 1 hour, absorbance was recorded at 492 nm using an Infinite® M200 Pro Series (Tecan UK Ltd) accompanied by Magellan™ Data Analysis Software (Tecan UK Ltd). All assays were performed in triplicate and a standard curve for each assay used to determine the cell numbers. Data analysis was performed, and graphs prepared using GraphPad Prism (GraphPad Software, CA, USA). Statistical analysis using paired Student's t-test and one-way ANOVA were also analysed using GraphPad Prism). A p-value < 0.05 was considered significant.

$$\text{total number of adhered cells} = \frac{\text{absorbance value (OD at 492 nm)} - c}{m}$$

$$\%\ \text{of cell adhesion} = \frac{\text{total number of adhered cells}}{\text{40,000 cells (initial seed count)}}$$

Where; c is the intercept value at y-axis, and m is the value of gradient (refer **Appendix 14**)

5.2.5 Migration assay

Procedure: Chemotaxis/migration assay was performed using Corning® Transwell® polycarbonate membrane cell culture inserts with 8.0 µm pores (Cat#: CLS3422-48EA; Sigma-Aldrich, UK). The under-side of the membrane was coated with 10 µg/mL of fibronectin for an hour in incubator at 37°C and blocked by 1% (w/v) BSA for another one hour. 1×10^5 cells in 100 µL were seeded on the top chamber and 500 µL of chemokine solution to the bottom well (as **Figure 5.1**). Four hours of incubation at 37°C incubator allowed the migration to occur. After this incubation, the residual cells and media on the top chamber was removed and membrane was fixed in formalin at least for 20 min. 0.5% (w/v) crystal violet (in 10% ethanol) was used to stain the cells for 5 to 10 minutes for quantification. Cells on the top chamber were removed with a cotton bud and the inserts washed with distilled water to remove residual crystal violet stain. The formalin-fixed membrane was cut and mounted on a microscope slide for analysis. The migrated cells were counted in five random field of views at magnification 100× using FIJI software.

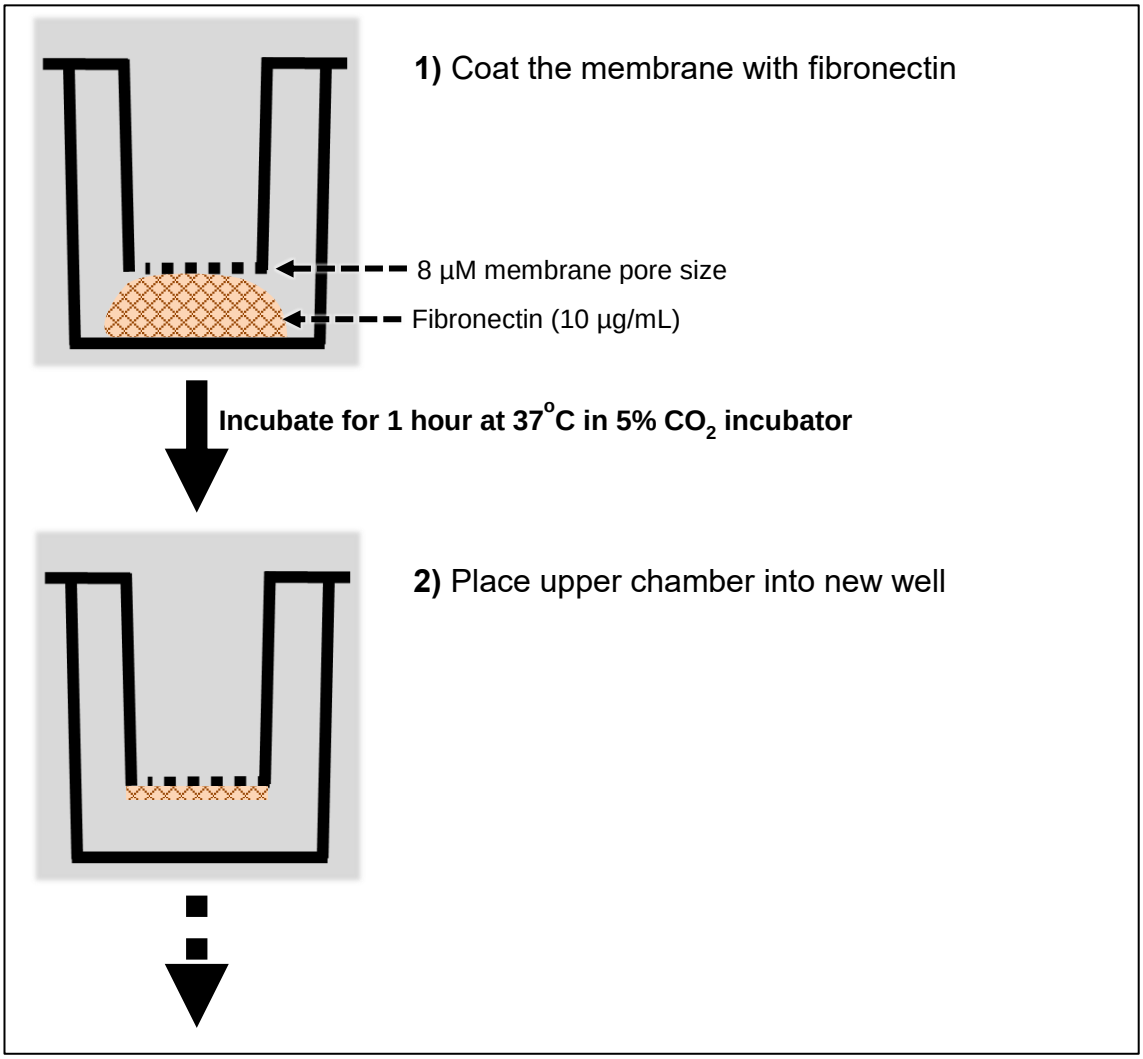

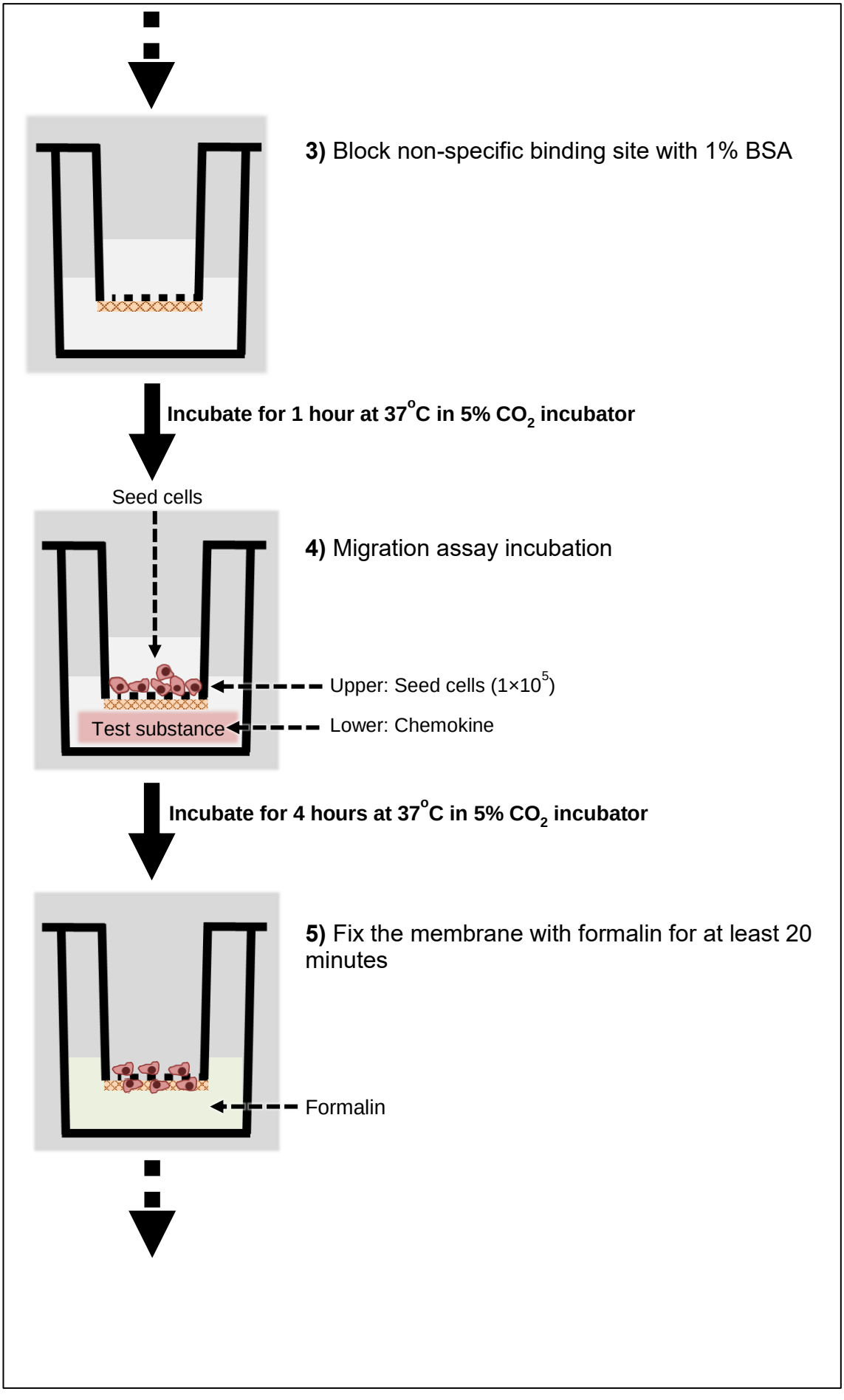
3) Block non-specific binding site with 1% BSA
Incubate for 1 hour at 37°C in 5% CO2 incubator
Seed cells
4) Migration assay incubation
Upper: Seed cells (1×10^5)
Test substance
Lower: Chemokine
Incubate for 4 hours at 37°C in 5% CO2 incubator
5) Fix the membrane with formalin for at least 20 minutes
Formalin

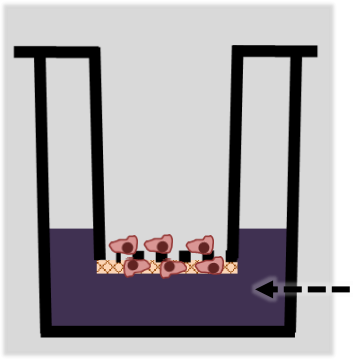

6) Stain the cells with 0.5% (w/v) of crystal violet (diluted in 20% (v/v) EtOH) for 5-10 minutes.

Crystal violet

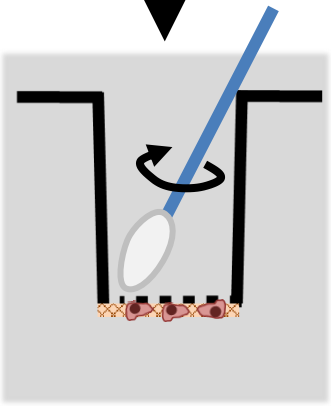

7) Remove excess cells from the upper chamber. Clean the membrane gently using cotton bud.

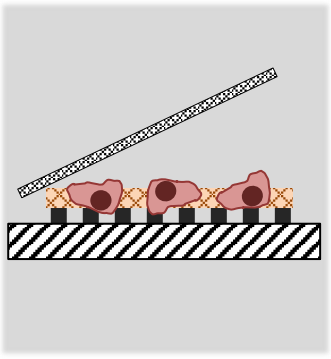

8) Cut the membrane and mount on microscope slide.

9) Migrated cells were analysed using light microscope and the picture was taken for number of cell migrated per 100× view.

Figure 5.1: Overview of migration assay steps using Transwell Boyden chamber.

5.2.6 Statistical Analysis

All experiments were performed in triplicate with at least three independent repeats. The mean average and standard deviation for each sample were calculated, and the significance value was calculated using paired Student's t-test and ANOVA. A p-value less than 0.05 was considered significant.

5.3 RESULTS

5.3.1 Proliferation of OCCL on hLtn variants

Exposure to media with 10% (v/v) FCS significantly increased the proliferation of H357 and SCC4 cells after 48h (p=0.0003 and p=0.0022 respectively) (see **Figure 5.2 A-B**). OCCLs also showed proliferation in SFM alone compared to cells treated with mitomycin C. The proliferation further increased when exposed to hLtn variants. For H357 cells, WT, rCC3, and rW55D significantly increased proliferation (p=0.016, p=0.0015, and p=0.0101 respectively). There was no significant difference between the different hLtn variants treatments. Exposure to all hLtn variants also significantly increased the proliferation of SCC4 cells after 48 hours for WT (p=0.0258), rWT (p=0.0326), rCC3 (p=0.0088), and rW55D (p=0.0301). Analysis of variance (ANOVA) was performed and the proliferation for both H357 and SCC4 was significant compared to control (p<0.0001 and p=0.0024 respectively). No significant increase of observed after 72 hours for H357 cells but the SCC4 cells retained the same proliferation profile as after 48 hours.

The data demonstrates that SCC4 cells (with higher XCR1 expression) were more proliferative and in response for longer duration to hLtn variants compared to H357 (**Figure 5.3**). This suggests that cell proliferation mediated through hLtn/XCR1 is correlated to XCR1 expression.

Table 5.1: Rate of proliferation of H357 and SCC4 cells.

Cell line	Treatment duration	Proliferation rate (normalised to initial seeding)		
		Mitomycin C	Negative control	Positive control
H357	48 h	0.85 ± 0.0633	2.95 ± 0.3249	7.47 ± 0.5210
	72 h	0.30 ± 0.1525	5.33 ± 1.1450	9.66 ± 1.5080
SCC4	48 h	1.13 ± 0.2024	1.72 ± 0.2083	4.89 ± 0.5830
	72 h	0.34 ± 0.0186	2.17 ± 0.4337	5.50 ± 0.1406

Mitomycin C was used to arrest the cell proliferation, the negative control well only contained serum-free media, while the positive control was treated with 10% (v/v) FCS.

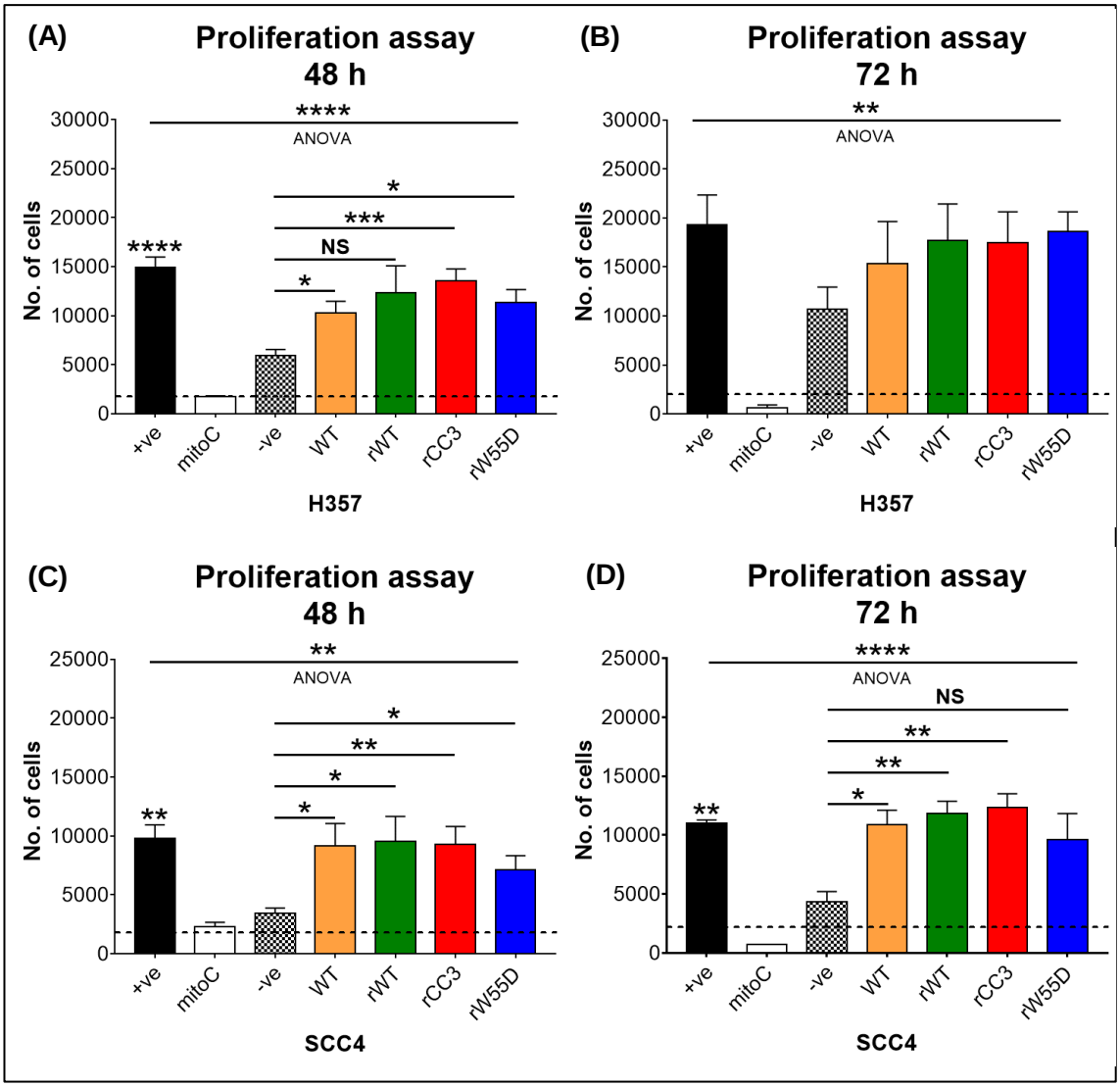

Figure 5.2: Proliferation of H357 and SCC4 cells after treatment with hLtn variants for **(A & C)** 48h and **(B & D)** 72h. Positive controls were grown in medium with 10% (v/v) FCS and negative control in SFM only. Mitomycin C (mitoC) was used to stop cell growth. All the treatments were prepared in SFM with respective hLtn variants where WT is commercial wild type from Peprotech, rWT is recombinant wild type, rCC3 is recombinant CC3 mutant, and rW55D is recombinant W55D mutant. The dashed line (- - -) indicates the initial seeding baseline. The number of cells were calculated using equation from the linear regression graph (see **Appendix 14**). Data are from three independent repeats (n=3), mean ± SEM. (* p-value<0.05, ** p-value<0.01, *** p-value<0.001, **** p-value<0.0001, NS indicates not significant).

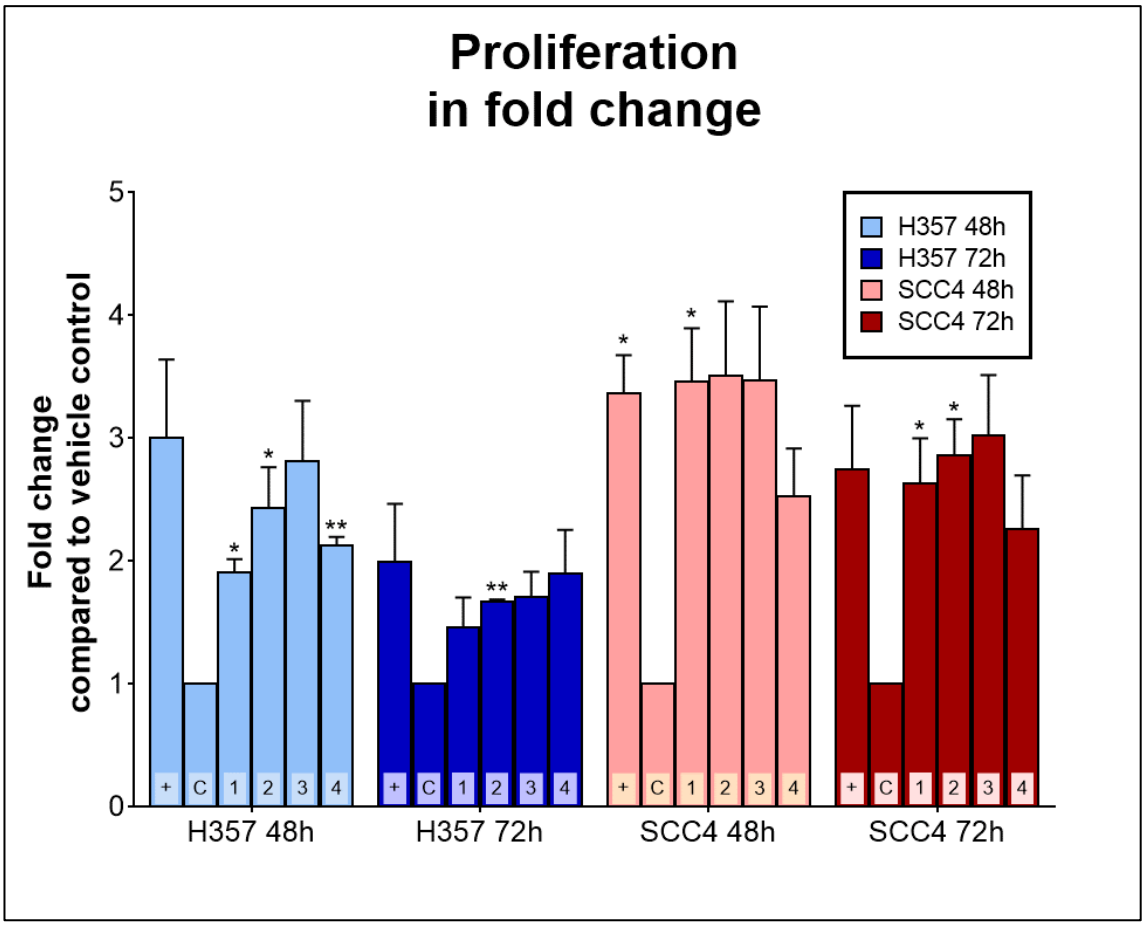

Figure 5.3: The proliferation fold change compared to control (SFM) for H357 and SCC4 after exposure to hLtn variants for 48 h and 72 h. The annotation used above is as follows: the positive control (**+**) (10% (v/v FCS)), the vehicle control (**C**) (SFM only), and the hLtn variants are arranged as follows - position **1**: commercial hLtn (WT), position **2**: recombinant WT (rWT), position **3**: recombinant CC3 mutant (rCC3), and position **4**: recombinant W55D (rW55D). Data are from three independent repeats (n=3), mean ± SEM. (* p-value<0.05, ** p-value<0.01).

5.3.2 Adhesion of OCCL after exposure to hLtn variants

The results (see **Figure 5.4 A-B**) shows increased adhesion of oral cancer cells to Collagen I with the highest adhesion at 10 µg/mL concentration. SCC4 cells showed higher adhesion than H357 at 10 µg/mL ($p<0.0001$ and $p=0.0008$ respectively) compared to control. Compared between the two OCCL, more SCC4 cells attached to Collagen I than H357 cells. SCC4 cells showed significant adhesion to Collagen I at most concentrations (**Figure 5.4 B**) while H357 cells only showed significantly higher attachment at higher concentrations, 3 µg/mL ($p=0.0022$) and 10 µg/mL ($p=0.0008$) (**Figure 5.4 A**). ANOVA for H357 and SCC4 adhesion to the different concentration of Collagen I was statistically significant ($p=0.0022$ and $p<0.0001$ respectively).

For Collagen IV, OCCL adhesion was relatively low at lower concentration (see **Figure 5.4 C-D**). The highest percentage of cell adhesion was approximately 15% for both cell lines on 10 µg/mL of Collagen IV. The adhesion at concentration 10 µg/mL was significant to control for SCC4 ($p=0.0005$) and H357 ($p=0.0016$). ANOVA to different concentrations of Collagen IV for H357 was significant ($p<0.0001$) but not for SCC4. This was considerably different to Collagen I where the same concentration showed 50% or more cell adhesion. Thus, OCCLs showed more attachment to Collagen I (significant difference from controls at most concentrations) than Collagen IV (significant difference to control only at high concentrations).

Low adherence to fibronectin was observed for H357 compared to SCC4. The highest adhesion for both was at 10 µg/mL concentration with 11.96% for H357 cells ($p=0.0008$) and 45.69% for SCC4 cells ($p=0.0014$) (**Figure 5.4 E-F**). Both cell lines show increased adhesion with increasing concentration of fibronectin. ANOVA for both H357 and SCC4 adhesion to fibronectin was significant with $p<0.0001$ and $p=0.0055$ respectively.

The results show that OCCL adhesion to ECM proteins follows a similar general trend where adherence to collagen I > fibronectin > collagen IV, although in H357 (with lower XCR1 expression), the adhesion to fibronectin and collagen IV were somewhat similar. SCC4 cells had more than twice the adherence compared to H357 for both collagen I and fibronectin. Similar adherence to collagen IV was observed in both cell lines.

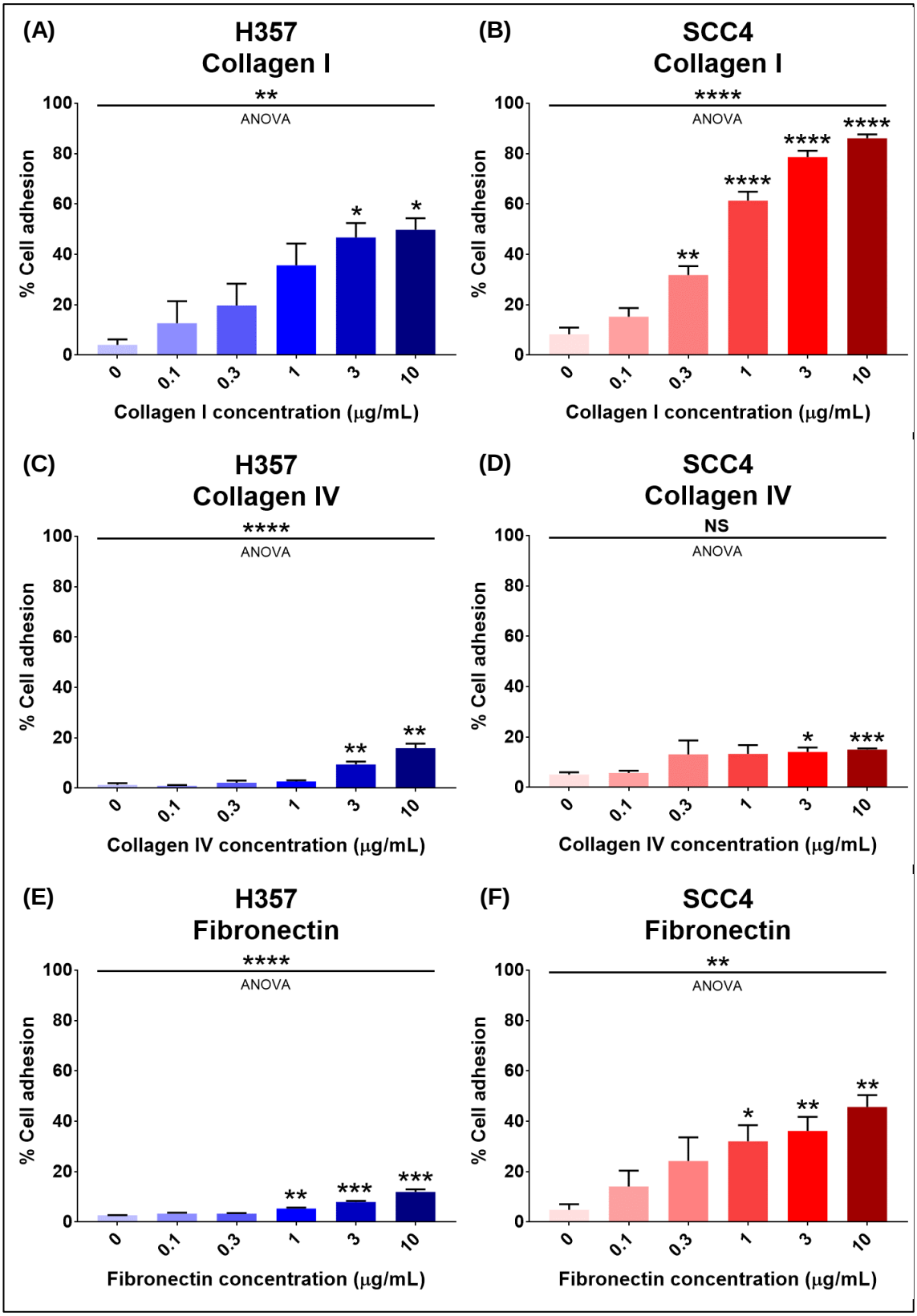

Figure 5.4: Adhesion of OCCL to collagen I **(A-B)**, collagen IV **(C-D)**, and fibronectin **(E-F)**. The concentration range used was 0-10 µg/mL. Data are from three independent repeats (n=3), mean ± S.E.M. Statistical analysis with Student's t-test and ANOVA analysis were performed. (* p-value<0.05, ** p-value<0.01, *** p-value<0.001, **** p-value<0.0001).

To study the effect of hLtn on OCCL adhesion, cells were incubated for 24 hours with the commercial hLtn wild type (WT). There was an approximately 10% for H357 cell line (p=0.0159) (see **Figure 5.5**) and ~20% increase in adhesion for SCC4 cell line (p=0.0174) (**Figure 5.6**) at 10 µg/mL concentration of collagen I after treatment. However, the increase in adhesion to collagen IV was relatively low compare to collagen I (see **Figure 5.5 B**). For H357 cells, the increased adhesion was ~5% (p=0.0149) as well as for SCC4 cells (p=0.0183) at concentration 10 µg/mL

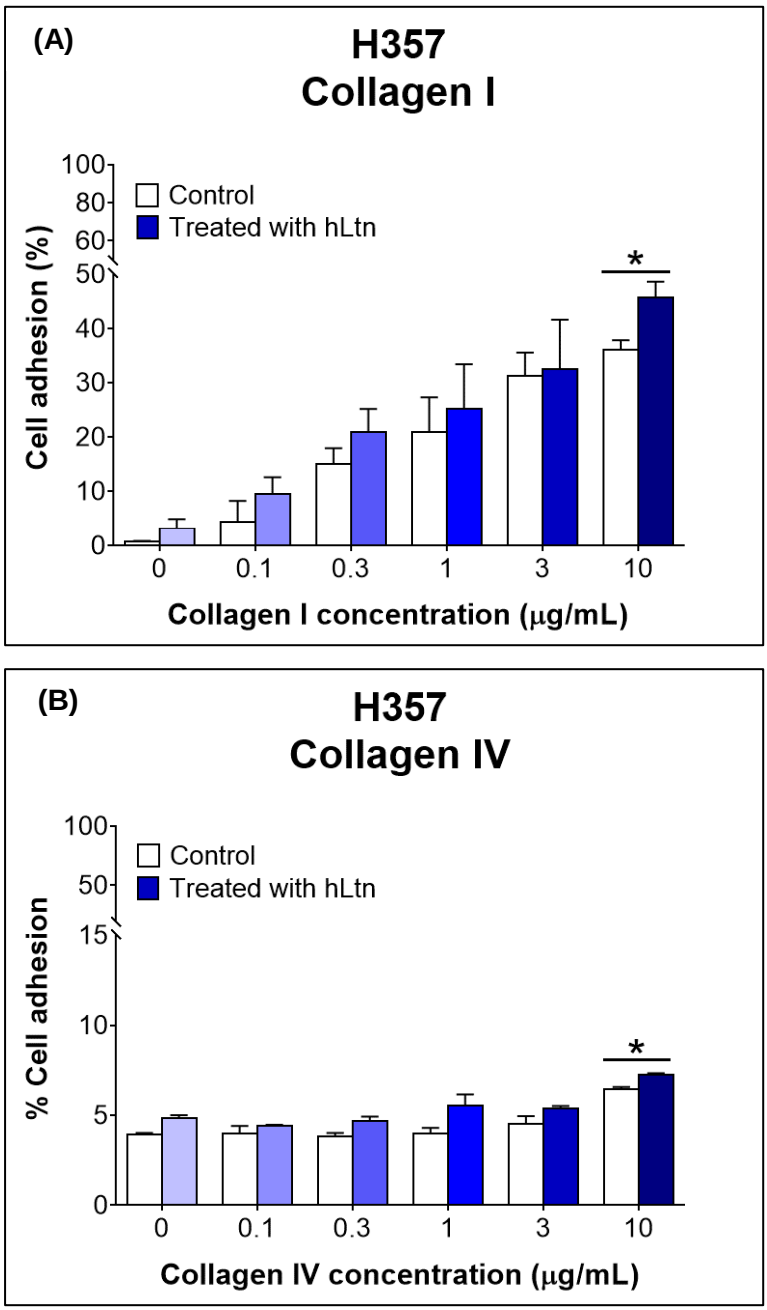

Figure 5.5: Adhesion of H357 cells after 24-hours hLtn stimulation (100 ng/mL) to **(A)** Collagen I and **(B)** Collagen IV (concentration range: 0-10 µg/mL). All assays were performed for three independent repeats (n=3) with error bar represents SEM. (* p-value<0.05).

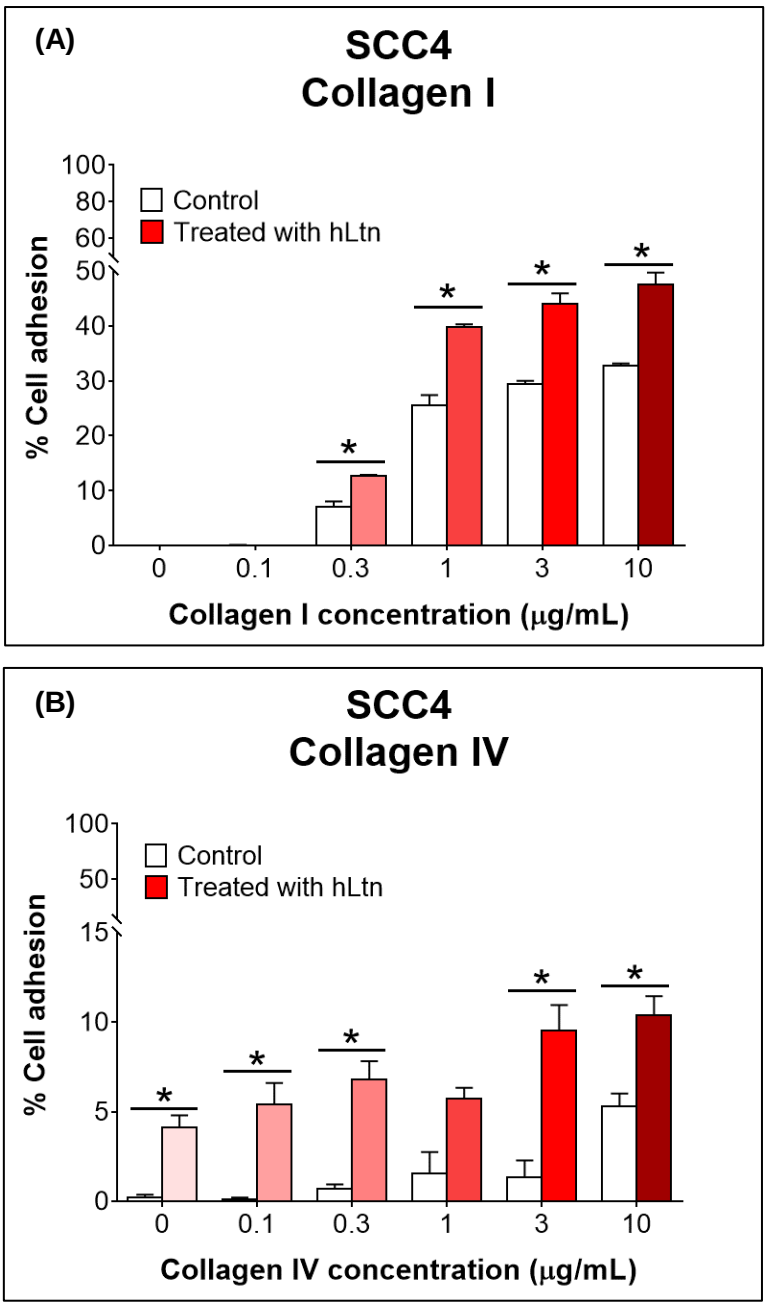

Figure 5.6: Adhesion of SCC4 cells after 24-hours hLtn stimulation (100 ng/mL) to **(A)** Collagen I and **(B)** Collagen IV (concentration range: 0-10 µg/mL). All assays were performed for three independent repeats (n=3) with error bar represents SEM. (* p-value<0.05, ** p-value<0.01).

5.3.3 Migration of OCCL towards hLtn variants

SCC4 cells were used for the chemotaxis/migration assays, as nearly 80% of the cell population are XCR1-positive (as described in **Chapter 3**). Also, the number of cells migrating towards the positive control was the highest ($p<0.01$) compared to control (**Figure 5.7**). All the canonical chemokine fold hLtn variants, including commercial hLtn wild type (WT), and recombinant hLtn wild type (rWT) and CC3 mutant (rCC3) caused a significant increase in migration compared to control ($p=0.0404$, $p=0.0181$ and $p=0.004$ respectively). The highest migration was observed towards rCC3, followed by rWT and Comm. rCC3 induces higher migration compared to the WT and rWT ($p=0.0015$ and $p=0.0101$ respectively). Interestingly, we found that the rWT causes significantly more migration than the commercially available WT ($p=0.0357$). No significance difference in migration towards the recombinant W55D mutant (rW55D) was seen. However, some migration was seen towards rW55D and the level was higher than to WT, although this was inconsistent.

Additionally, the recombinant hLtn variants were also compared to cells that were treated with XCR1 antibody prior to migration to ensure specificity of migration. All the cells with antibody treatment showed minimal migration comparable to the negative control.

.

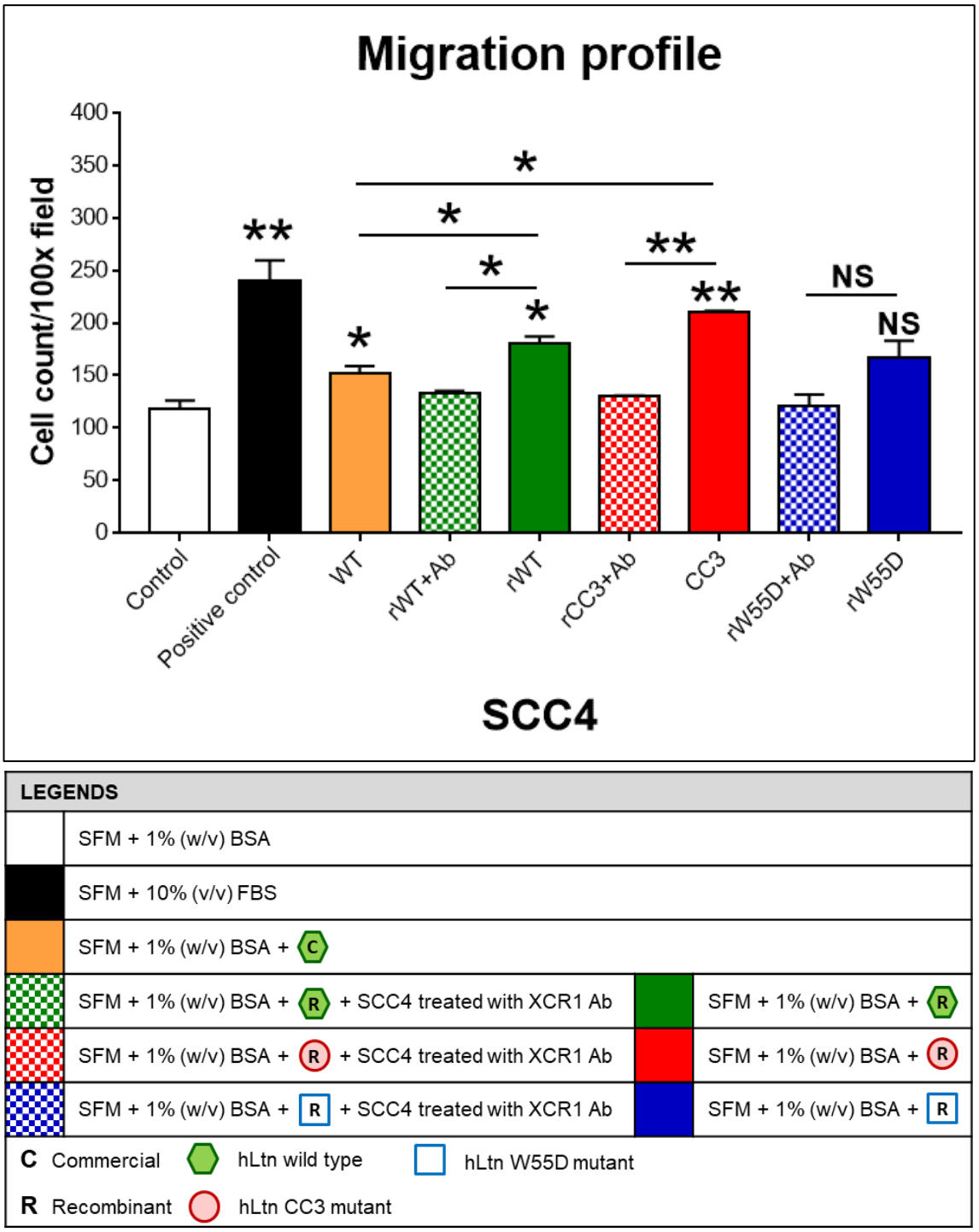

Figure 5.7: Migration of SCC4 cells towards hLtn variants. The assay was carried out using Transwell® Boyden chambers. The legend describes the experimental condition for each well. Treatment with XCR1 antibody 30 mins prior to exposure to hLtn variants was performed to ensure the chemokine migration was XCR1-specific. Annotation: WT is the commercially available hLtn (Peprotech); rWT is the recombinant hLtn wild type; rCC3 is the recombinant hLtn CC3 mutant; rW55D is the recombinant hLtn W55D mutant; and Ab indicates treatment with XCR1 antibody. Data are representative of three independent experiments (n=3) with SEM. (* p-value<0.05, ** p-value<0.01, and NS is not significant).

5.4 DISCUSSION

The aim of this part of the study was to investigate the functional effect of hLtn variants on the behaviour of OCCLs. Previously, hLtn has been shown to induce proliferation, migration and invasion in oral cancer as well as in other types of cancer. Due to unique nature of hLtn, it exists in two distinct conformations in physiological conditions, a canonical chemokine fold and a dimer. To date, there is no information about the role of these conformations in disease processes. Therefore, these different conformations were studied including a locked structure (CC3 and W55D mutants) to understand their contribution to cancer pathology.

5.4.1 Proliferation profile of OCCL after exposure to hLtn variants

Proliferation is integral for tissue biology to maintain a balance between cell loss and cell division. This process is tightly regulated in normal cells. However, cancer cells proliferation is dysregulated leading to uncontrolled growth or failure of the cells to undergo apoptosis.

Chemokines have been shown to induce cell proliferation by acting through their receptors on immune cells (Badr *et al.*, 2012; Dirice *et al.*, 2014), mesangial cells (Wörnle *et al.*, 2004) and cancers (Balkwill, 2004a, 2012). In periodontal disease and oral cancer, chemokine-chemokine receptor interaction has been shown to promote cell growth (Sahingur and Yeudall, 2015; Panda, Padhiary and Routray, 2016) through CXCR1 (ligand CXCL8 or IL-8), CXCR2 (ligand or CXCL1 or GROα) (Khurram *et al.*, 2014), and XCR1 (ligand XCL1 or hLtn). Although XCR1, has been shown to play a role in cell proliferation, the role of each hLtn conformation in this process is not known.

As expected, the commercial and recombinant wild type hLtn (rWT) increased proliferation of both H357 and SCC4 cells after 48 h. The fold increase in proliferation of SCC4 cells compared to controls was higher than H357. This is probably due to the abundance of XCR1-expressing cells in SCC4 compared to H357, allowing more receptor activation and downstream signalling (Khurram *et al.*, 2010). The recombinant hLtn was designed with a different amino acids in the N-terminal compared to the nature and chemokine N-terminus which have been shown to be important in receptor activation by recognizing the grooves of the chemokine surface (Szpakowska *et al.*, 2012). This has been shown in CCR2 where the N-terminal region interact with minor sub-pockets of the receptor to trigger distinct interactions (Huma *et al.*, 2017). The modified N-

terminus of the recombinant hLtn may bind with a higher affinity to the conserved sulfotyrosine-binding pocket by stabilizing the interaction.

The recombinant CC3 mutant induced higher proliferation in both H357 and SCC4 compared to the wild type. This is because its structure is locked in the active chemokine fold, while the wild type exists in two different conformations in physiological conditions (active chemokine fold and dimer). Both the wild type and CC3 mutant have the canonical chemokine fold, but the W55D mutant was designed to exist in the dimer conformational state. The result show that the mutant also induces proliferation in both OCCLs but to a lesser extent. The mutant usually exists in dimer, where it binds strongly to heparin (Tuinstra *et al.*, 2008), blocking HIV viral infection (Fox, Tyler, *et al.*, 2015; Guzzo *et al.*, 2015), and has potent antimicrobial properties (Nevins *et al.*, 2016) but its role in inducing proliferation has not been reported so far. There are also no published reports of the W55D mutant activating the XCR1 receptor. Previous reports, show that the CXCL2 dimer has an agonistic properties and is a potent activator of CXCR2 receptor (Ravindran *et al.*, 2013). Small-molecule agonist can also activate the receptor by binding to allosteric sites such as in CCR3 (Wise *et al.*, 2007; Jensen and Rosenkilde, 2009) and CXCR3 (Scholten *et al.*, 2012), suggesting that the signalling activation does not require the whole chemokine to trigger the process but only important amino acids residues.

Proliferation after exposure to the hLtn variants (excluding rW55D) was similar to treatment with 10% (v/v) serum in SCC4 cells. Proteomic profiling of serum compared to plasma has previously shown that amongst the growth factors, 11 chemokines level was elevated including lymphotactin (Ayache *et al.*, 2006). This explains the similar fold increase to the hLtn variants. The fold difference to serum was not profound in H357 cells. The result indicates that hLtn/XCR1 highly influences the cell growth in SCC4 cells and partially in H357 cells. SCC4 cells express more XCR1 than H357 cells resulting in greater influence in cell proliferation through the hLtn/XCR1 axis.

The proliferation of OCCLs relative to control was higher at 48 hours than 72 hours. Previously, stimulation of OCCL proliferation through the hLtn/XCR1 axis has been shown after 72 hours (Khurram *et al.*, 2010) but not after 48 hours. This discrepancy may be partially due to the protein half-life and stability, as small proteins such as cytokines and chemokines have a short half-life (Panicker *et al.*, 2007; Zhou *et al.*, 2010). The estimated half-life for hLtn *in vitro* is 30 hours as determined using Expasy ProtParam (ExPASy Bioinformatics Resource Portal, Swiss Institute of Bioinformatics).

5.4.2 Adhesion profile of OCCL to extracellular matrix (ECM) components

The interaction between cancer cells and the ECM components are fundamental for each stage of cancer progression. This ranges from involvement in local invasion of cancer cells to facilitating intravasation/extravasation of primary tumour through basement membrane of vessels. Additionally, adherence of cancer cell to ECM components is essential in tumour progression and metastatic spread (Todd *et al.*, 2016).

SCC4 cells showed higher adhesion to collagen I and fibronectin compared to H357 cells. The data is comparable to the findings of Khurram et al. (2010) who showed similar results for both collagen I and fibronectin but did not study adhesion to collagen IV. Interestingly the trends for adhesion to collagen I and IV for both H357 and SCC4 cells were different. This is probably due to the different structural arrangement and components that make up the collagen, thus presenting a different surface for cell adhesion. Fibronectin provides glycoprotein anchor between the cell and collagen primarily type 1, giving an intermediate adherence towards it. Collagen I structure is fibrillar (Lu, Weaver and Werb, 2012) while collagen IV structure resembles an interconnected network (Kalluri, 2003) explaining the differences in cell attachment. It also suggests that the OCCL used probably have different expression or activation of integrins responsible in collagen IV associated attachment. Concurrently, SCC4 cells has highest adherence collagen I, followed by fibronectin and collagen IV suggesting different distribution of integrins that responsible for attachment. In H357 cells, attachment to Collagen I was the highest, whereas adherence for both collagen IV and fibronectin was similar suggesting the distribution level of the responsible integrins are the same. Several integrins are related closely to basal membrane such as α2β1, α3β1 and α6β4 (Janes and Watt, 2006). Some evidence suggests that focal loss of α2, α3, α6 and β4 subunits is observed when normal oral epithelium undergoes malignant transformation (Jones *et al.*, 1993). In addition, α6 and β4 integrin subunit loss is related to loss of basal membrane protein (Downer, Watt and Speight, 1993; Jones, Watt and Speight, 1997). β1 subunit is important in basal membrane as it is expressed higher than basal stem cells (Liang et al., 2014). Furthermore, β1 subunit heterodimerises with α2 for receptor to Collagen IV, and with α3 to laminin (Alonso and Fuchs, 2003). Additionally, in cancer, integrin-related signalling can promote the production of MMP that facilitate cancer migration and invasion (Koistinen and Heino, 2013).

Integrins are heterodimers of two protein subunits: an α subunit and a β subunit. They mediate interactions either between cells or to ECM proteins by activating MAPK/ERK (mitogen-activated protein kinases/extracellular signal-regulated kinases)

pathway within the cell. Integrins bind to a number of extracellular ligands, with the highest number binding to fibronectin (12 integrins), followed by laminin (6 integrins), and collagens (4 integrins) (Plow *et al.*, 2000). Integrin subunit αv expression has identified in OSCC (Jones, Watt and Speight, 1997) has been shown to be involved in invasion as its overexpression allows rapid phosphorylation of focal adhesion kinase (FAK) (Hayashido *et al.*, 2014). Furthermore, introduction of the α9 subunit results in an increase in OSCC cell adhesion to collagen I (Roy *et al.*, 2011). Others report that high expression of integrin α2β1 and α3β1 facilitates metastasis in OSCC (Soares *et al.*, 2015). Modulation of integrin activity or expression is a possible explanation for the increased adherence of OCCL to ECM after exposure to hLtn (**Figure 5.8**).

Previous reports have shown that H357 cells express α2, α3, α5, α6, β1 and β4 integrins (Thomas *et al.*, 2001). Additionally, increased expression of α9 integrin mediates adhesion and migration towards tenascin-C but not proliferation (Roy *et al.*, 2011). Reports have also shown expression of α9 integrin subunit in oral epithelium, specifically in suprabasal and prickle layer and upregulation in their cancer counterpart. Furthermore, hLtn had shown to enhance α9 integrin-dependent cell migration *in vivo* and *in vitro* in autoimmune disease (Matsumoto *et al.*, 2017).

Inside-out signalling of integrin is regulated by talin and kindlin in the cytoplasmic domain of the cell (Calderwood, Campbell and Critchley, 2013) with assistance of G-protein activation (Das *et al.*, 2014). Integrin signalling requires recruitment of both monomeric small G-proteins and heterotrimeric G-proteins, where the G-protein subunit $G\alpha_{13}$ binds to the β subunit (Shen, Delaney and Du, 2012) such as in integrin αIIbβ3 (Gong *et al.*, 2010). Chemokine receptors are G-protein coupled and their activation is tightly associated to integrin upregulation in cancer such as in CXCR4 and α4β1 integrin (Sosa-Costa *et al.*, 2016).

Previous reports have shown a correlation between increased adhesion and XCR1 receptor expression on the cell surface (Khurram *et al.*, 2010). The result here also shows that SCC4 has higher adhesion to Collagen I. Adhesion to Collagen I is mediated through the interaction of α1β1 and α2β1 integrin (Jokinen *et al.*, 2004).

Khurram et al. (2010) also showed an increase in OCCL adhesion to Collagen I after 2 hours of hLtn treatment. This effect can still be seen after 24 hours (see **Figure 5.5 and 5.6**) suggesting that the mechanism through which hLtn mediates cell adhesion is quickly initiated and manifests itself for a long period. It is possible that this increase in adhesion is related to an increase in integrin expression, or increased activity avidity

of already expressed integrins. However, further work is required to establish the relationship between XCR1 and integrin expression/avidity. As OSCC is derived from oral epithelial cells, most of the integrins: α6β4, α6β1, α2β1 and α3β1 are expressed in cancer but at different levels (Desgrosellier and Cheresh, 2010). Integrins such as αvβ6 have been shown to be upregulated in OSCC but loss of certain integrins has also been reported. However, the precise set of integrins involved in oral cancer progression remains unknown. In ovarian cancer, β1 integrin is overexpressed which increases the metastasis of ovarian carcinoma cells (Shen *et al.*, 2012). Further work is required to establish the expression of these integrins on H357 and SCC4 cells and their interaction with hLtn and XCR1.

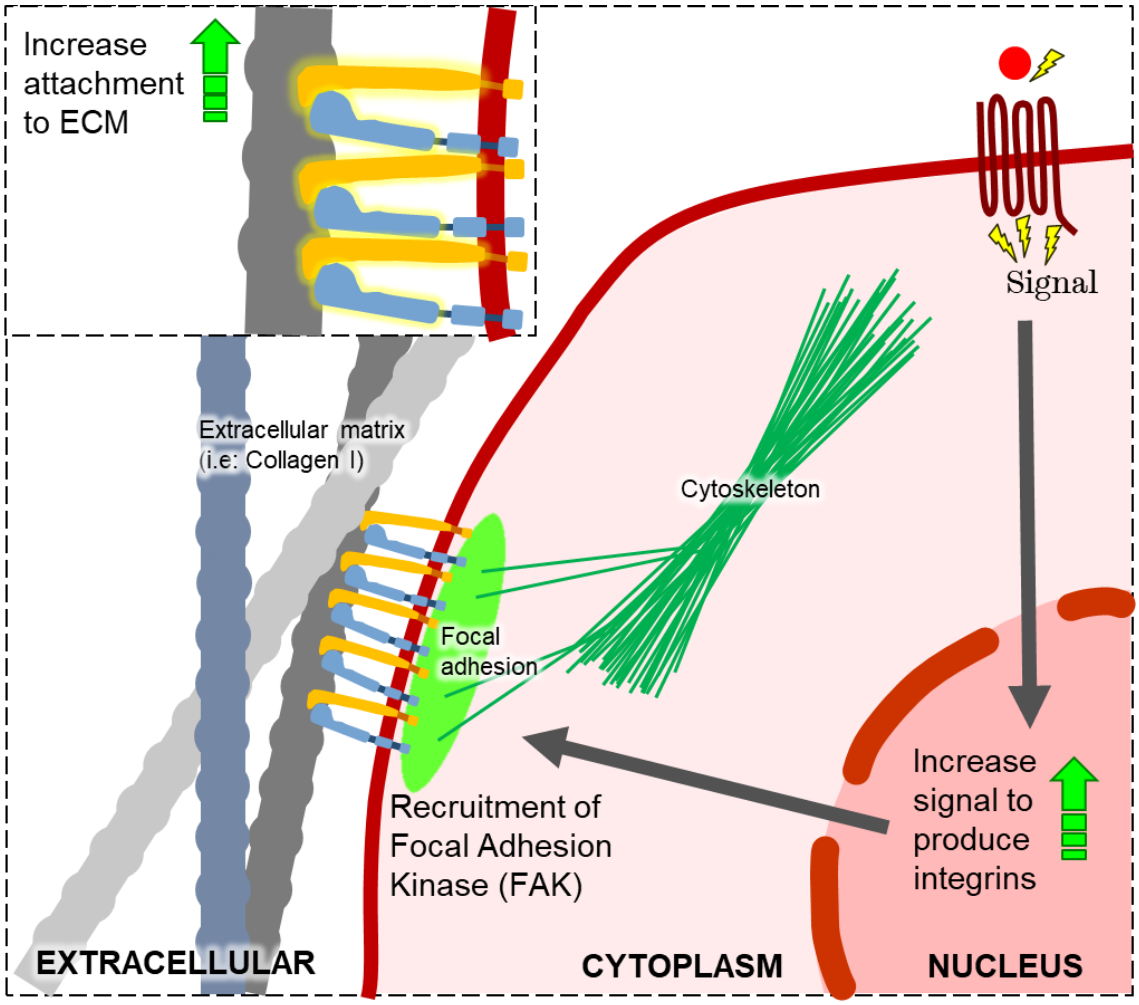

Figure 5.8: Diagram for possible interaction for hLtn/XCR1 mediated integrins attachment to ECM. The signalling cascade activates G-protein followed by downstream signalling through possible MAPK/ERK pathway. This signal amplifies the gene expression to recruit integrin attachment.

5.4.3 Migration profile of OCCL after exposure to recombinant hLtn variants

Migration assays were performed to understand the extent to which the hLtn conformational state contributes to OSCC chemotaxis. Recombinant hLtn has been previously shown to promote migration of XCR1+ oral cancer cells (Khurram *et al.*, 2010). SCC4 cell line was chosen for the assay as it highly expresses XCR1 (~80% positive expression). The results suggest that migration is significantly enhanced by hLtn variants with canonical chemokine fold.

Recombinant hLtn wild type facilitated greater migration compared to the commercial hLtn. As explained earlier in the discussion (**Section 5.4.1**), the additional amino acids at the N-terminal may increase the triggered binding interaction (Huma *et al.*, 2017) resulting in higher downstream signalling that could influence cell migration. Furthermore, the recombinant CC3 mutant stimulated higher migration than other hLtn variants due to its locked fold, allowing it to remain in the canonical chemokine fold (Tuinstra *et al.*, 2007). This differs from hLtn WT that interconverts between two conformations and has a slightly lower migration index.

By blocking the XCR1 receptor, the migration of SCC4 cells was significantly reduced and comparable to the controls, indicating the specificity of the migration. While there are numerous reports of hLtn inducing migration in cancer cells, none have studied the contribution of the variants in the process.

5.5 SUMMARY

To summarize, the results for the first time show that the OCCLs respond to hLtn variants. The recombinant variants with the canonical fold promote greater chemotaxis compared to the commercial hLtn showing that the recombinant chemokines are functional. The initial hypothesis was that the dimer can act as a natural inhibitor. A preliminary study showed that the dimer form can either attach or blocking the receptor in some sort of manner (refer **Appendix 15**). The only known antagonist for XCR1 receptor is vCCL2 (or vMIP-II), a viral chemokine produced by herpes-virus. Original assumption was that the dimer has no agonistic properties due to its non-canonical chemokine fold. This finding showed that it influences the oral cancer cells proliferation while not inducing chemotaxis. This adds to the complexity and dynamic of chemokine-chemokine receptor interaction. Probing more on this idea can potentially be used for drug development.

CHAPTER 6

GENERAL DISCUSSION, CONCLUSION & FUTURE PERSPECTIVES

CHAPTER 6: GENERAL DISCUSSION & FUTURE PERSPECTIVES

6.1 Thesis Overview

Our results show the expression of XCR1 in normal epithelium, and oral squamous cell carcinoma and its metastatic counterpart. Furthermore, stromal components such as fibroblasts and endothelial cells also express both XCR1 and hLtn with significant differences between normal and cancerous tissue, which is a novel finding and suggest that hLtn and XCR1 can influence the tumour as well as the microenvironment in OSCC. This is evident as hLtn/XCR1 axis can regulate expression of XCR1 with significant increase in expression after indirect co-culture with cancer-associated fibroblasts. Furthermore, for the first time an alternative technique was employed to produce and purify hLtn variants and tested them on epithelial cells in a working condition. Previously, the protein produced was highly insoluble, using our fusion protein construct, improved the protein solubility. By using the variants, we identified the proliferation, adhesion and migration of oral cancer cell lines in association with XCR1 expression. These findings suggest that the hLtn/XCR1 system may play an important role in oral cancer progression. Researching the behaviour of metamorphic protein can be vital to provide more insight in developing future treatments

6.2 General Discussion

In Chapter 2, chemokines particularly hLtn and its receptor XCR1 were discussed not to only be involved in localisation and trafficking of lymphocytes but also play a pivotal role in cancer growth and dissemination. Mainly in oral epithelial cells and carcinoma where they mediated various effects such as cell migration and invasion, as well as influencing their behaviour. These implications are thought to facilitate tumour invasion and metastasis to lymph nodes *in vivo*.

The first ever study of XCR1 and hLtn in oral squamous cell carcinoma was by Khurram *et al.* (2010). Their study showed expression of chemokine receptor (XCR1) in oral epithelial cells for the first time. Prior to this study, it was only reported to be expressed on lymphocytes, neutrophils and NK cells (Huang *et al.*, 2001), rheumatoid synovium by mononuclear cells (Wang *et al.*, 2004) and by fibroblast-like synoviocytes (Blaschke *et al.*, 2003). Since then more studies have shown expression of XCR1 in dendritic cells as part of antigen-presentation (Ohta *et al.*, 2016) and overexpression in cancer such as in breast (Yang *et al.*, 2017), lung (T. Wang *et al.*, 2015), and ovary (Kim

et al., 2012). Yet none of them reported positive XCR1 expression in normal epithelial cells.

Immunohistochemistry showed XCR1 expression in the basal normal oral epithelium, oral squamous cell carcinoma (OSCC) and its metastatic counterparts (refer **Chapter 2**). Fibroblasts, endothelial cells and lymphocytes were also demonstrated to express XCR1 receptor in normal and diseased tissue, with greater expression in the latter, and similar to what was reported by Khurram *et al.* (2010). Additionally, it was observed that XCR1 and hLtn were strongly expressed in the cervical lymph in the peripheral cortex, subcapsular sinus and germinal centre. Others have reported dendritic cells (DC)-expressing XCR1 in spleen localizing in the T cell zone, marginal zone and the red pulp in mouse (Bachem *et al.*, 2012). One report has stated sparse XCR1 expression in DCs in T-cell zone proximal to B-cell follicles or medullary regions with enriched high endothelial venules (HEV) (Kitano *et al.*, 2016).

Strong and diffuse expression of XCR1 and hLtn was observed in metastatic tumour as well as lymphocytes in cervical lymph nodes, although the sample size was minimal (n=5). The presence of strong XCR1 and hLtn staining by fibroblasts in the reactive stroma of the metastatic node also supports this idea. Results confirms similar to those informed by Khurram *et al.* (2010) although it extends this significantly by using of paired metastatic tissue from the same patient. This suggests a correlation between the modulation of hLtn/XCR1 axis with the spread of metastatic OSCC in the lymph node.

Chapter 3 showed the regulation of XCR1 in various oral cancer cell lines (OCCL) through its activation by hLtn. This can be either mediated through autocrine or paracrine signalling as the same cells i.e. epithelial and stromal cells expressed both the ligand and receptor. Autocrine regulation has been seen by other chemokine receptors in skin after wounding (Kroeze *et al.*, 2012) and in systemic sclerosis by dermal fibroblasts (Carulli *et al.*, 2005). Conditioned media (CM) influences the expression of XCR1 and hLtn mRNA in OCCLs, where cancer-associated fibroblast (CAF) to increase their level of expression. Moreover, their expression was downregulated by myofibroblast and senescence-induced NOF CM. These are novel and interesting findings suggesting a role for hLtn/XCR1 in the tumour microenvironment although further investigations are required to determine the significance of these findings (**Figure 6.1**).

The hLtn variants (WT, CC3 and W55D mutant) were observed to modulate the behaviour of OCCLs in the final experimental chapter. The key difference between the CC3 and W55D mutant is that the former is the monomer form while the latter is the

dimer form of hLtn. Functionally, the dimer has no ability to induce chemotaxis and calcium flux in XCR1-transfected (human embryonic kidney) HEK cells. The function of each variants was first demonstrated in cancer here by the oral cancer cell lines expressing XCR1. These are novel experiments and findings in cancer as previous studies more focus on the structural biology of the variants instead of its physiological or pathological consequences. Understanding its effect in cancer will enable better understanding of its function, thus can be used a tool of drug discovery.

Almost all the previous published work has been performed on either Jurkat cells, immortalized T cell lymphocytes or XCR1-transfected HEK cells. The initial assumption, at the start of the project, was that the dimeric form of hLtn does not activate XCR1, hence acting as antagonist of the receptor. Proliferation assays showed hLtn/XCR1 involvement in the process, where the canonical fold (WT and CC3 mutant) appeared to influence OCCL growth as previously described by Khurram *et al.* (2010). However, the dimeric form still induces proliferation of OCCLs comparable to other variant forms. Due to complexity of chemokine receptors mechanism, there are several possible explanations, such as 1) tissue bias where the hLtn/XCR1 activation and transduction is different from other tissue (Steen *et al.*, 2014); 2) the homo-dimerization or hetero-dimerization of chemokine receptor allows receptor activation by the dimeric ligand such as seen by CXCR4 (Rodríguez-Frade, Mellado and Martínez-A, 2001; Springael, Urizar and Parmentier, 2005; Rodríguez-Frade *et al.*, 2009; Salanga, O'Hayre and Handel, 2009; Kleist *et al.*, 2016); or 3) the W55D hLtn dimer populates the unfolding form, the transitional state between the monomer and dimer as mentioned by Fox *et al.* (2016), thus having some activity on the XCR1 receptor.

Biomarkers can be defined as distinct quantifiable characteristics to indicate biological processes describing normal or pathological state, pathogen process, or pharmacological responses to predict the outcome of incidence, leading to therapeutic intervention (Goossens *et al.*, 2015). Salivary biomarkers have been used as an early-stage detection biomarker for several types cancer such as lung, pancreatic, breast and stomach using transcriptome, proteomic biomarkers, miRNA microarray and exosomes (Wang, Kaczor-Urbanowicz and Wong, 2017). Chemokines such as CCL2, CCL3, CCL4, CXCL1, CXCL8 and CXCL12 have been shown as strong candidates as biomarkers for pre-cancerous cervical lesions based on analysing the protein sample extracted by liquid based cytology using proteomic array technology with high sensitivity and specificity (Bhatia *et al.*, 2018). ELISA data for analysis of CXCL8, CXCL10, and CXCL14 levels in oral fluid indicated their elevation in cancer patients. The levels was not affected by

periodontitis thus indicating their potential as cancer biomarkers (Michiels *et al.*, 2009). Unfortunately, there is less research focusing on salivary biomarker for oral cancer compared to other types of cancer.

Preclinically, the data suggest that XCR1 and hLtn can be used as diagnostic biomarkers for oral cancer detection. High expression of hLtn can be seen in the tissue samples. It would be interesting to investigate if there any differences in the content of hLtn in the serum, saliva or ascitic fluid in normal compared to disease in terms of developing a non-invasive clinical test. Moreover, XCR1 can also be a prognostic biomarker for as it can be a good indicator of OSCC progression.

In clinical sense, XCR1 can be used as target as a diagnostic biomarker as it is highly expressed by OSCC. Currently, there is no drug targeting specifically for oral cancer. All of them are chemotherapy drugs where targeting highly proliferative cells such as cisplatin and carboplatin. Antibody-based drug for cancer therapy has been introduced for clinical trials in human where it is targeting CXCR4, CCR2 and CCR4 (Vela *et al.*, 2015). This review paper stated that most of the studies on CCR2 were in Phase II clinical trial while only in Phase I for CXCR4. Treatment for lymphoma targeting CCR4 was in Phase III clinical trial. Additionally, other chemokine receptors such as CXCR2, CXCR5, CCR7, CCR9 and ACKR3 are still in pre-clinical assay for cancer treatment (Vela *et al.*, 2015). More study on XCR1 and hLtn on its behaviour in *in vivo* metastasis is required to proceed to the next step, where the XCR1 receptor can be used as a target in oral cancer.

The ligand, hLtn can be used for tool development for drug discovery. hLtn dimer has the capability to prevent early HIV infection. Due to uniqueness of hLtn, being able to metamorphose into two distinct protein fold. By using protein engineering, this capability can be exploit on improving future drug treatment. Our understanding on its capability in cancer perspective is still in its infancy. There are discrepancies in the literature how the ligand behaves as well as lack of understanding on the variants behaviour (chemokine or chemokine receptor dimerization interaction) especially in disease.

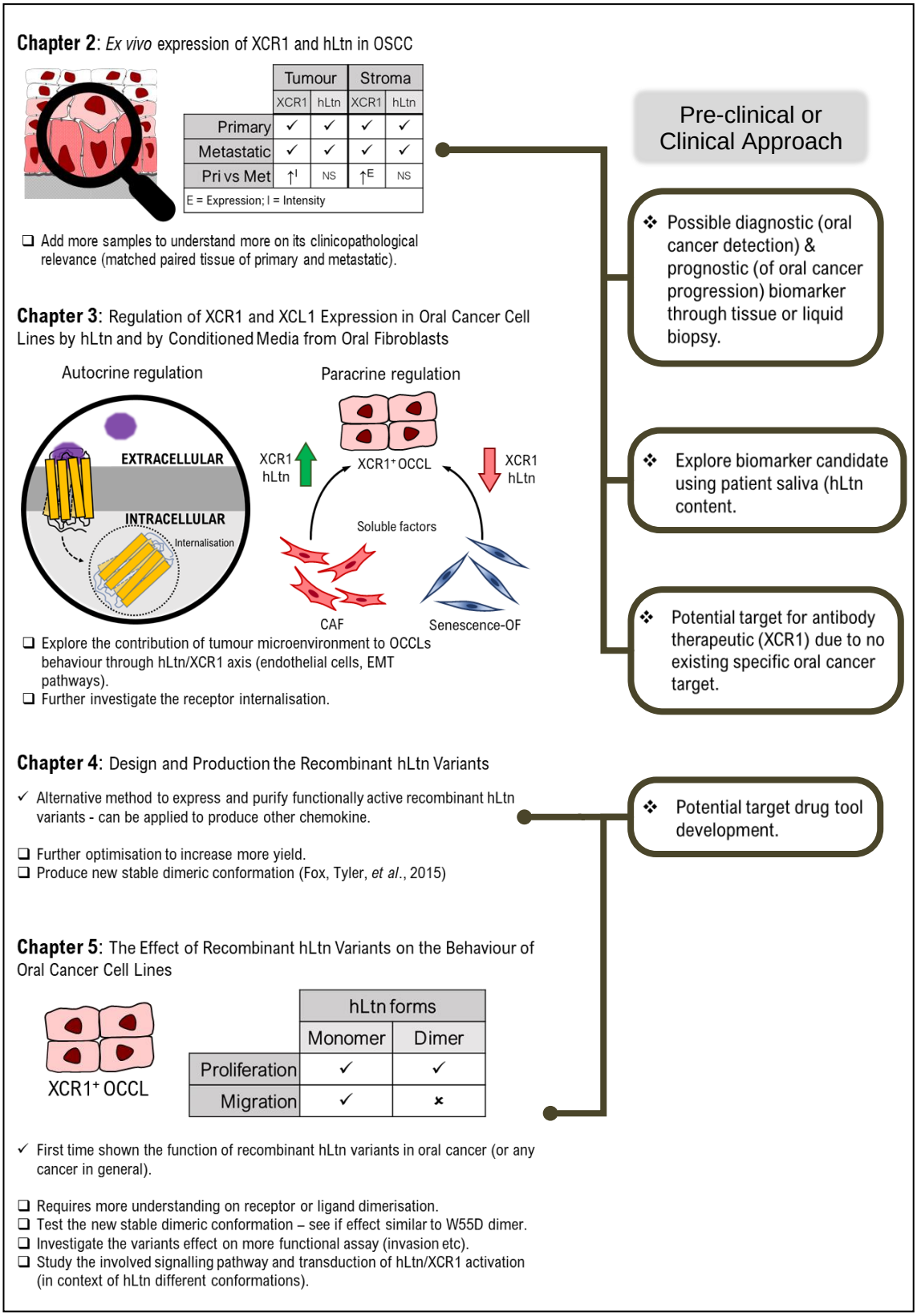

Figure 6.1: Summary of main thesis findings and their significance. *Annotation:* Cancer-associated fibroblast (CAF), oral fibroblast (OF); endothelial-mesenchymal transition (EMT).

6.3 Future Perspectives

Our findings addressed several research questions to understand XCR1 and hLtn role, regulation and mechanism precisely in the OSCC pathogenesis. Additionally, the metamorphic ligand adds another layer of complexity to the receptor activation. Several future investigations should be performed to improve our understanding in the role of hLtn and XCR1 in OSCC progression.

1) **Further immunohistochemistry**

   It would be useful to perform immunohistochemistry on a bigger cohort to establish the findings (XCR1 and hLtn role in OSCC metastasis) and correlate it with clinicopathological variables such as tumour size, depth, recurrence and survival.

2) **Invasion assays using 3D model or tissue-engineered oral mucosa (TEOM).**

   Although monolayer or 2D assay are widely used for studying invasion, it does not really give a similar indication due to its minimal interaction and lack of tissue complexity. Using a 3D model or TEOM will give a better understanding OSCC invasion into the underlying connective tissue in response to chemokine (particularly hLtn) to mimic *in vivo* conditions.

3) **siRNA or CRISPR knockdown of XCR1 and hLtn in OCCLs.**

   XCR1 gene knockdown in cancer cells can be performed using siRNA or CRISPR technique. Functional assays (migration, proliferation, adhesion etc.) can be repeated to better understand the role of XCR1 in cancer cell regulation. More functional assay can also be included such as invasion assay etc.

4) **Contribution of tumour microenvironment to OCCLs behaviour through hLtn/XCR1 axis.**

   Investigate the effect of hLtn on endothelial cell (lymphatic and vascular) by studying proliferation and tubule formation by using hLtn variants. The expression in stroma and role in epithelial-mesenchymal transition (EMT), such as expression of E- and N-cadherin, ZEB-1, SLUG, SNAIL etc. by OCCL could be studied after exposure of hLtn variants.

5) **Post-translational modification (PTM) identification of XCR1 receptor using mass spectrometry (LC-MS/MS).**

Glycosylation of protein is important especially in mammalian system. Some of the interaction between receptor/ligand axis is highly influenced by protein glycosylation. Therefore, it is interesting to investigate whether the glycosylation of XCR1 receptor in normal and OSCC has different glycosylation profile. The result might allow us to better understand the importance of (PTM) in cancer.

6) **Signalling pathway and transduction of hLtn/XCR1 activation (in context of hLtn different conformations).**

ERK1/2 pathway has been demonstrated to be involved in hLtn/XCR1 axis (Khurram *et al.*, 2010). Since, hLtn/XCR1 activation increases adhesion, it will be in interesting to study involvement of focal adhesion kinase (FAK), as well as integrins molecules. α9β1 has been shown to modulate epithelial behaviour and its expression pattern is somewhat similar to what we found by XCR1 *ex vivo* (Roy *et al.*, 2011). Also, hLtn has been shown to enhance α9 integrin-dependent cell migration *in vitro* and *in vivo* in autoimmune disease, which is interesting to investigate similar fashion in OSCC. Furthermore, as migration appeared to be correlated to hLtn variant conformation, F-actin polymerisation could be investigated as XCR1 was observed to be synonymous with OSCC metastasis. Similarly, adhesion to other extracellular matrix molecules could be investigated as well. Additionally, pertussis toxin (PTX) can be used in the assay as to understand XCR1 relation with its G-protein coupled receptor (GPCR) as the toxin abrogates its activity.

7) **New and stable dimeric hLtn conformation.**

Creating the restricted dimeric four-stranded β-sheet fold (CC5 mutant) can further understand the full function of the dimer state of hLtn function in cancer pathology. This engineered mutant forms a stable form compared to $XCL1_{dim}$ than WT-XCL1 or W55D as determined by hydrogen-deuterium exchange (HDX) (Fox, Tyler, *et al.*, 2015). This can further improve our understanding of the role of each conformation better in cancer pathogenesis.

8) ***In vivo* study using orthotropic xenograft mouse models.**

It will be interesting to study the effect of hLtn and its variants *in vivo* using orthotropic xenograft mouse models and compare primary tumour cells as well as lymph node metastases.

REFERENCES

Aboussekhra, A. (2011) 'Role of cancer-associated fibroblasts in breast cancer development and prognosis', *The International Journal of Developmental Biology*, 55(7-8–9), pp. 841–849. doi: 10.1387/ijdb.113362aa.

Acharyya, S., Oskarsson, T., Vanharanta, S., Malladi, S., Kim, J., Morris, P. G., Manova-Todorova, K., Leversha, M., Hogg, N., Seshan, V. E., Norton, L., Brogi, E. and Massagué, J. (2012) 'A CXCL1 Paracrine Network Links Cancer Chemoresistance and Metastasis', *Cell*. NIH Public Access, 150(1), pp. 165–178. doi: 10.1016/j.cell.2012.04.042.

Acosta, J. C., O'Loghlen, A., Banito, A., Guijarro, M. V., Augert, A., Raguz, S., Fumagalli, M., Da Costa, M., Brown, C., Popov, N., Takatsu, Y., Melamed, J., d'Adda di Fagagna, F., Bernard, D., Hernando, E. and Gil, J. (2008) 'Chemokine Signaling via the CXCR2 Receptor Reinforces Senescence', *Cell*, 133(6), pp. 1006–1018. doi: 10.1016/j.cell.2008.03.038.

von Ahrens, D., Bhagat, T. D., Nagrath, D., Maitra, A. and Verma, A. (2017) 'The role of stromal cancer-associated fibroblasts in pancreatic cancer', *Journal of Hematology & Oncology*. BioMed Central, 10(1), p. 76. doi: 10.1186/s13045-017-0448-5.

Al-Jokhadar, M., Al-Mandily, A., Zaid, K. and Maalouf, E. A. (2017) 'CCR7 and CXCR4 Expression in Primary Head and Neck Squamous Cell Carcinomas and Nodal Metastases – a Clinical and Immunohistochemical Study', *doi.org*. Asian Pacific Organization for Cancer Prevention, 18(4), pp. 1093–1104. doi: 10.22034/APJCP.2017.18.4.1093.

Alexandre, Y. O., Ghilas, S., Sanchez, C., Le Bon, A., Crozat, K. and Dalod, M. (2016) 'XCR1 $^{+}$ dendritic cells promote memory CD8 $^{+}$ T cell recall upon secondary infections with *Listeria monocytogenes* or certain viruses', *The Journal of Experimental Medicine*, 213(1), pp. 75–92. doi: 10.1084/jem.20142350.

Alitalo, A. and Detmar, M. (2012) 'Interaction of tumor cells and lymphatic vessels in cancer progression', *Oncogene*. Nature Publishing Group, 31(42), pp. 4499–4508. doi: 10.1038/onc.2011.602.

Alonso, L. and Fuchs, E. (2003) 'Stem cells of the skin epithelium.', *Proceedings of the National Academy of Sciences of the United States of America*. National Academy of Sciences, 100 Suppl 1(suppl 1), pp. 11830–11835. doi: 10.1073/pnas.1734203100.

Althubiti, M., Lezina, L., Carrera, S., Jukes-Jones, R., Giblett, S. M., Antonov, A., Barlev, N., Saldanha, G. S., Pritchard, C. A., Cain, K. and Macip, S. (2014) 'Characterization of novel markers of senescence and their prognostic potential in cancer', *Cell Death & Disease*. Nature Publishing Group, 5(11), pp. e1528–e1528. doi: 10.1038/cddis.2014.489.

Antonelli, A., Ferrari, S. M., Corrado, A., Ferrannini, E. and Fallahi, P. (2014) 'CXCR3, CXCL10 and type 1 diabetes', *Cytokine & Growth Factor Reviews*, 25(1), pp. 57–65. doi: 10.1016/j.cytogfr.2014.01.006.

Antonelli, A., Ferrari, S. M., Giuggioli, D., Ferrannini, E., Ferri, C. and Fallahi, P. (2014)

'Chemokine (C-X-C motif) ligand (CXCL)10 in autoimmune diseases', *Autoimmunity Reviews*, 13(3), pp. 272–280. doi: 10.1016/j.autrev.2013.10.010.

Araujo, J. M., Gomez, A. C., Aguilar, A., Salgado, R., Balko, J. M., Bravo, L., Doimi, F., Bretel, D., Morante, Z., Flores, C., Gomez, H. L. and Pinto, J. A. (2018) 'Effect of CCL5 expression in the recruitment of immune cells in triple negative breast cancer', *Scientific Reports*. Nature Publishing Group, 8(1), p. 4899. doi: 10.1038/s41598-018-23099-7.

Arigami, T., Natsugoe, S., Uenosono, Y., Yanagita, S., Arima, H., Hirata, M., Ishigami, S. and Aikou, T. (2009) 'CCR7 and CXCR4 expression predicts lymph node status including micrometastasis in gastric cancer.', *International journal of oncology*, 35(1), pp. 19–24. Available at: http://www.ncbi.nlm.nih.gov/pubmed/19513547 (Accessed: 9 August 2018).

Ayache, S., Panelli, M. C., Byrne, K. M., Slezak, S., Leitman, S. F., Marincola, F. M. and Stroncek, D. F. (2006) 'Comparison of proteomic profiles of serum, plasma, and modified media supplements used for cell culture and expansion.', *Journal of translational medicine*. BioMed Central, 4, p. 40. doi: 10.1186/1479-5876-4-40.

Bachem, A., Güttler, S., Hartung, E., Ebstein, F., Schaefer, M., Tannert, A., Salama, A., Movassaghi, K., Opitz, C., Mages, H. W., Henn, V., Kloetzel, P.-M., Gurka, S. and Kroczek, R. A. (2010) 'Superior antigen cross-presentation and XCR1 expression define human CD11c+CD141+ cells as homologues of mouse CD8+ dendritic cells.', *The Journal of experimental medicine*. The Rockefeller University Press, 207(6), pp. 1273–81. doi: 10.1084/jem.20100348.

Bachem, A., Hartung, E., Güttler, S., Mora, A., Zhou, X., Hegemann, A., Plantinga, M., Mazzini, E., Stoitzner, P., Gurka, S., Henn, V., Mages, H. W. and Kroczek, R. A. (2012) 'Expression of XCR1 characterizes the Batf3-dependent lineage of dendritic cells capable of antigen cross-presentation', *Frontiers in Immunology*, 3(JUL).

Badr, G., Ebaid, H., Mohany, M. and Abuelsaad, A. S. (2012) 'Modulation of immune cell proliferation and chemotaxis towards CC chemokine ligand (CCL)-21 and CXC chemokine ligand (CXCL)-12 in undenatured whey protein-treated mice', *The Journal of Nutritional Biochemistry*, 23(12), pp. 1640–1646. doi: 10.1016/j.jnutbio.2011.11.006.

Baeshen, N. A., Baeshen, M. N., Sheikh, A., Bora, R. S., Ahmed, M. M. M., Ramadan, H. A. I., Saini, K. S. and Redwan, E. M. (2014) 'Cell factories for insulin production', *Microbial Cell Factories*, 13(1), p. 141. doi: 10.1186/s12934-014-0141-0.

Bailey, S. and Macardle, P. J. (2006) 'A flow cytometric comparison of Indo-1 to fluo-3 and Fura Red excited with low power lasers for detecting Ca2+ flux', *Journal of Immunological Methods*, 311(1–2), pp. 220–225. doi: 10.1016/j.jim.2006.02.005.

Balkwill, F. (2004a) 'Cancer and the chemokine network', *Nature Reviews Cancer*, 4(7), pp. 540–550. doi: 10.1038/nrc1388.

Balkwill, F. (2004b) 'The significance of cancer cell expression of the chemokine receptor CXCR4', *Seminars in Cancer Biology*, 14(3), pp. 171–179. doi: 10.1016/j.semcancer.2003.10.003.

Balkwill, F. R. (2012) 'The chemokine system and cancer', *Journal of Pathology*, 226(2), pp. 148–157. doi: 10.1002/path.3029.

Bartlow, P., Uechi, G. T., Cardamone, J. J., Sultana, T., Fruchtl, M., Beitle, R. R. and Ataai, M. M. (2011) 'Identification of native Escherichia coli BL21 (DE3) proteins that bind to immobilized metal affinity chromatography under high imidazole conditions and use of 2D-DIGE to evaluate contamination pools with respect to recombinant protein expression level', *Protein Expression and Purification*, 78(2), pp. 216–224. doi: 10.1016/j.pep.2011.04.021.

Baxter, E., Windloch, K., Gannon, F. and Lee, J. S. (2014) 'Epigenetic regulation in cancer progression.', *Cell & bioscience*. BioMed Central, 4, p. 45. doi: 10.1186/2045-3701-4-45.

Bazan, J. F., Bacon, K. B., Hardiman, G., Wang, W., Soo, K., Rossi, D., Greaves, D. R., Zlotnik, A. and Schall, T. J. (1997) 'A new class of membrane-bound chemokine with a CX3C motif', *Nature*, 385(6617), pp. 640–644. doi: 10.1038/385640a0.

Bennett, L. D., Fox, J. M. and Signoret, N. (2011) 'Mechanisms regulating chemokine receptor activity.', *Immunology*. Wiley-Blackwell, 134(3), pp. 246–56. doi: 10.1111/j.1365-2567.2011.03485.x.

Bhatia, R., Kavanagh, K., Stewart, J., Moncur, S., Serrano, I., Cong, D., Cubie, H. A., Haas, J. G., Busby-Earle, C., Williams, A. R. W., Howie, S. E. M. and Cuschieri, K. (2018) 'Host chemokine signature as a biomarker for the detection of pre-cancerous cervical lesions.', *Oncotarget*. Impact Journals, LLC, 9(26), pp. 18548–18558. doi: 10.18632/oncotarget.24946.

Bi, M. M., Shang, B., Wang, Z. and Chen, G. (2017) 'Expression of CXCR4 and VEGF-C is correlated with lymph node metastasis in non-small cell lung cancer.', *Thoracic cancer*. Wiley-Blackwell, 8(6), pp. 634–641. doi: 10.1111/1759-7714.12500.

Bian, L., Sun, X., Jin, K. and He, Y. (2012) 'Oral cancer-associated fibroblasts inhibit heat-induced apoptosis in Tca8113 cells through upregulated expression of Bcl-2 through the Mig/CXCR3 axis', *Oncology Reports*, 28(6), pp. 2063–2068. doi: 10.3892/or.2012.2019.

Blaschke, S., Middel, P., Dorner, B. G., Blaschke, V., Hummel, K. M., Kroczek, R. A., Reich, K., Benoehr, P., Koziolek, M. and Müller, G. A. (2003) 'Expression of activation-induced, T cell-derived, and chemokine-related cytokine/lymphotactin and its functional role in rheumatoid arthritis', *Arthritis and Rheumatism*, 48(7), pp. 1858–1872. doi: 10.1002/art.11171.

Block, H., Maertens, B., Spriestersbach, A., Brinker, N., Kubicek, J., Fabis, R., Labahn, J. and Schäfer, F. (2009) 'Chapter 27 Immobilized-Metal Affinity Chromatography (IMAC)', in *Methods in enzymology*, pp. 439–473. doi: 10.1016/S0076-6879(09)63027-5.

Bonecchi, R. and Graham, G. J. (2016) 'Atypical Chemokine Receptors and Their Roles

in the Resolution of the Inflammatory Response.', *Frontiers in immunology*. Frontiers Media SA, 7, p. 224. doi: 10.3389/fimmu.2016.00224.

Borroni, E. M., Mantovani, A., Locati, M. and Bonecchi, R. (2010) 'Chemokine receptors intracellular trafficking', *Pharmacology & Therapeutics*, 127(1), pp. 1–8. doi: 10.1016/j.pharmthera.2010.04.006.

van den Bosch, T., Koopmans, A. E., Vaarwater, J., van den Berg, M., de Klein, A. and Verdijk, R. M. (2013) 'Chemokine Receptor CCR7 Expression Predicts Poor Outcome in Uveal Melanoma and Relates to Liver Metastasis Whereas Expression of CXCR4 Is Not of Clinical Relevance', *Investigative Opthalmology & Visual Science*, 54(12), p. 7354. doi: 10.1167/iovs.13-12407.

Bremnes, R. M., Dønnem, T., Al-Saad, S., Al-Shibli, K., Andersen, S., Sirera, R., Camps, C., Marinez, I. and Busund, L.-T. (2011) 'The Role of Tumor Stroma in Cancer Progression and Prognosis: Emphasis on Carcinoma-Associated Fibroblasts and Non-small Cell Lung Cancer', *Journal of Thoracic Oncology*. Elsevier, 6(1), pp. 209–217. doi: 10.1097/JTO.0B013E3181F8A1BD.

Bryan, P. N. and Orban, J. (2010) *Proteins that switch folds*, *Current Opinion in Structural Biology*. doi: 10.1016/j.sbi.2010.06.002.

Busch, S. and Landberg, G. (2015) 'CAF-specific markers: role of the TGFβ pathway.', *Oncoscience*. Impact Journals, LLC, 2(10), pp. 835–6. doi: 10.18632/oncoscience.209.

Buskermolen, J. K., Roffel, S. and Gibbs, S. (2017) 'Stimulation of oral fibroblast chemokine receptors identifies CCR3 and CCR4 as potential wound healing targets', *Journal of Cellular Physiology*, 232(11), pp. 2996–3005. doi: 10.1002/jcp.25946.

Bussmann, J. and Raz, E. (2015) 'Chemokine-guided cell migration and motility in zebrafish development', *The EMBO Journal*, 34(10), pp. 1309–1318. doi: 10.15252/embj.201490105.

Cairns, C. M., Gordon, J. R., Li, F., Baca-Estrada, M. E., Moyana, T. and Xiang, J. (2001) 'Lymphotactin expression by engineered myeloma cells drives tumor regression: mediation by CD4+ and CD8+ T cells and neutrophils expressing XCR1 receptor.', *Journal of immunology (Baltimore, Md. : 1950)*, 167(1), pp. 57–65. Available at: http://www.ncbi.nlm.nih.gov/pubmed/11418632 (Accessed: 23 June 2017).

Calderwood, D. A., Campbell, I. D. and Critchley, D. R. (2013) 'Talins and kindlins: partners in integrin-mediated adhesion.', *Nature reviews. Molecular cell biology*. NIH Public Access, 14(8), pp. 503–17. doi: 10.1038/nrm3624.

de Camargo Cancela, M., Voti, L., Guerra-Yi, M., Chapuis, F. F., Mazuir, M. and Curado, M. P. (2010) 'Oral cavity cancer in developed and in developing countries: Population-based incidence', *Head & Neck*, 32(3), pp. 357–367. doi: 10.1002/hed.21193.

Camilloni, C. and Sutto, L. (2009) 'Lymphotactin: How a protein can adopt two folds', *Journal of Chemical Physics*, 131. doi: 10.1063/1.3276284.

Campisi, J. (2013) 'Aging, cellular senescence, and cancer.', *Annual review of physiology*. NIH Public Access, 75, pp. 685–705. doi: 10.1146/annurev-physiol-030212-183653.

Carulli, M. T., Ong, V. H., Ponticos, M., Shiwen, X., Abraham, D. J., Black, C. M. and Denton, C. P. (2005) 'Chemokine receptor CCR2 expression by systemic sclerosis fibroblasts: Evidence for autocrine regulation of myofibroblast differentiation', *Arthritis & Rheumatism*, 52(12), pp. 3772–3782. doi: 10.1002/art.21396.

Cassier, P. A., Treilleux, I., Bachelot, T., Ray-Coquard, I., Bendriss-Vermare, N., Ménétrier-Caux, C., Trédan, O., Goddard-Léon, S., Pin, J.-J., Mignotte, H., Bathélémy-Dubois, C., Caux, C., Lebecque, S. and Blay, J.-Y. (2011) 'Prognostic value of the expression of C-Chemokine Receptor 6 and 7 and their ligands in non-metastatic breast cancer', *BMC Cancer*, 11(1), p. 213. doi: 10.1186/1471-2407-11-213.

Celesti, G., Di Caro, G., Bianchi, P., Grizzi, F., Marchesi, F., Basso, G., Rahal, D., Delconte, G., Catalano, M., Cappello, P., Roncalli, M., Zerbi, A., Montorsi, M., Novelli, F., Mantovani, A., Allavena, P., Malesci, A. and Laghi, L. (2013) 'Early expression of the fractalkine receptor CX3CR1 in pancreatic carcinogenesis', *British Journal of Cancer*, 109(9), pp. 2424–2433. doi: 10.1038/bjc.2013.565.

Cen, B., Yu, Q., Guo, J., Wu, Y., Ling, K., Cheng, Z., Ma, L. and Pei, G. (2001) 'Direct binding of beta-arrestins to two distinct intracellular domains of the delta opioid receptor.', *Journal of neurochemistry*, 76(6), pp. 1887–94. Available at: http://www.ncbi.nlm.nih.gov/pubmed/11259507 (Accessed: 16 February 2018).

Chang, K.-P., Wu, C.-C., Fang, K.-H., Tsai, C.-Y., Chang, Y.-L., Liu, S.-C. and Kao, H.-K. (2013) 'Serum levels of chemokine (C-X-C motif) ligand 9 (CXCL9) are associated with tumor progression and treatment outcome in patients with oral cavity squamous cell carcinoma', *Oral Oncology*, 49(8), pp. 802–807. doi: 10.1016/j.oraloncology.2013.05.006.

Chaturvedi, A. K., Anderson, W. F., Lortet-Tieulent, J., Curado, M. P., Ferlay, J., Franceschi, S., Rosenberg, P. S., Bray, F., Gillison, M. L., Paula Curado, M., Ferlay, J., Franceschi, S., Rosenberg, P. S., Bray, F. and Gillison, M. L. (2013) 'Worldwide trends in incidence rates for oral cavity and oropharyngeal cancers', *Journal of Clinical Oncology*, 31(36), pp. 4550–4559. doi: 10.1200/JCO.2013.50.3870.

Chaturvedi, A. K., Engels, E. A., Pfeiffer, R. M., Hernandez, B. Y., Xiao, W., Kim, E., Jiang, B., Goodman, M. T., Sibug-Saber, M., Cozen, W., Liu, L., Lynch, C. F., Wentzensen, N., Jordan, R. C., Altekruse, S., Anderson, W. F., Rosenberg, P. S. and Gillison, M. L. (2011) 'Human Papillomavirus and Rising Oropharyngeal Cancer Incidence in the United States', *Journal of Clinical Oncology*, 29(32), pp. 4294–4301. doi: 10.1200/JCO.2011.36.4596.

Chen, B., Zhang, D., Zhou, J., Li, Q., Zhou, L., Li, S.-M., Zhu, L., Chou, K.-Y., Zhou, L., Tao, L. and Lu, L.-M. (2013) 'High CCR6/CCR7 expression and Foxp3+ Treg cell number are positively related to the progression of laryngeal squamous cell carcinoma', *Oncology Reports*, 30(3), pp. 1380–1390. doi: 10.3892/or.2013.2603.

Chen, J.-H., Ozanne, S. E. and Hales, C. N. (2007) 'Methods of Cellular Senescence Induction Using Oxidative Stress', in *Methods in molecular biology (Clifton, N.J.)*, pp. 179–189. doi: 10.1007/978-1-59745-361-5_14.

Chen, R. (2012) 'Bacterial expression systems for recombinant protein production: E. coli and beyond', *Biotechnology Advances*, 30(5), pp. 1102–1107. doi: 10.1016/j.biotechadv.2011.09.013.

Cheng, W.-L., Wang, C.-S., Huang, Y.-H., Tsai, M.-M., Liang, Y. and Lin, K.-H. (2011) 'Overexpression of CXCL1 and its receptor CXCR2 promote tumor invasion in gastric cancer', *Annals of Oncology*, 22(10), pp. 2267–2276. doi: 10.1093/annonc/mdq739.

Cheng, X., Wu, H., Jin, Z.-J., Ma, D., Yuen, S., Jing, X.-Q., Shi, M.-M., Shen, B.-Y., Peng, C.-H., Zhao, R. and Qiu, W.-H. (2017) 'Up-regulation of chemokine receptor CCR4 is associated with Human Hepatocellular Carcinoma malignant behavior.', *Scientific reports*. Nature Publishing Group, 7(1), p. 12362. doi: 10.1038/s41598-017-10267-4.

Cheng, Z.-H., Shi, Y.-X., Yuan, M., Xiong, D., Zheng, J.-H. and Zhang, Z.-Y. (2016) 'Chemokines and their receptors in lung cancer progression and metastasis.', *Journal of Zhejiang University. Science. B*. Zhejiang University Press, 17(5), pp. 342–51. doi: 10.1631/jzus.B1500258.

Childs, B. G., Durik, M., Baker, D. J. and van Deursen, J. M. (2015) 'Cellular senescence in aging and age-related disease: from mechanisms to therapy.', *Nature medicine*. NIH Public Access, 21(12), pp. 1424–35. doi: 10.1038/nm.4000.

Chuang, J.-Y., Yang, W.-H., Chen, H.-T., Huang, C.-Y., Tan, T.-W., Lin, Y.-T., Hsu, C.-J., Fong, Y.-C. and Tang, C.-H. (2009) 'CCL5/CCR5 axis promotes the motility of human oral cancer cells', *Journal of Cellular Physiology*, 220(2), pp. 418–426. doi: 10.1002/jcp.21783.

Coppé, J.-P., Rodier, F., Patil, C. K., Freund, A., Desprez, P.-Y. and Campisi, J. (2011) 'Tumor suppressor and aging biomarker p16(INK4a) induces cellular senescence without the associated inflammatory secretory phenotype.', *The Journal of biological chemistry*. American Society for Biochemistry and Molecular Biology, 286(42), pp. 36396–403. doi: 10.1074/jbc.M111.257071.

Costea, D., Tsinkalovsky, O., Vintermyr, O., Johannessen, A. and Mackenzie, I. (2006) 'Cancer stem cells – new and potentially important targets for the therapy of oral squamous cell carcinoma', *Oral Diseases*, 12(5), pp. 443–454. doi: 10.1111/j.1601-0825.2006.01264.x.

Crola Da Silva, C., Lamerant-Fayel, N., Paprocka, M., Mitterrand, M., Gosset, D., Dus, D. and Kieda, C. (2009) 'Selective human endothelial cell activation by chemokines as a guide to cell homing.', *Immunology*. Wiley-Blackwell, 126(3), pp. 394–404. doi: 10.1111/j.1365-2567.2008.02906.x.

Cukierman, E. and Bassi, D. E. (2012) 'The mesenchymal tumor microenvironment', *Cell Adhesion & Migration*, 6(3), pp. 285–296. doi: 10.4161/cam.20210.

Daber, R., Stayrook, S., Rosenberg, A. and Lewis, M. (2007) 'Structural analysis of lac repressor bound to allosteric effectors.', *Journal of molecular biology*. NIH Public

Access, 370(4), pp. 609–19. doi: 10.1016/j.jmb.2007.04.028.

Dairaghi, D. J., Oldham, E. R., Bacon, K. B. and Schall, T. J. (1997) 'Chemokine receptor CCR3 function is highly dependent on local pH and ionic strength.', *The Journal of biological chemistry*, 272(45), pp. 28206–9. Available at: http://www.ncbi.nlm.nih.gov/pubmed/9353270 (Accessed: 11 February 2018).

Dardel, F., Davis, A. L., Laue, E. D. and Perham, R. N. (1993) 'Three-dimensional structure of the lipoyl domain from Bacillus stearothermophilus pyruvate dehydrogenase multienzyme complex.', *Journal of molecular biology*, 229, pp. 1037–1048.

Das, M., Ithychanda, S., Qin, J. and Plow, E. F. (2014) 'Mechanisms of talin-dependent integrin signaling and crosstalk.', *Biochimica et biophysica acta*. NIH Public Access, 1838(2), pp. 579–88. doi: 10.1016/j.bbamem.2013.07.017.

Das, S., Sarrou, E., Podgrabinska, S., Cassella, M., Mungamuri, S. K., Feirt, N., Gordon, R., Nagi, C. S., Wang, Y., Entenberg, D., Condeelis, J. and Skobe, M. (2013) 'Tumor cell entry into the lymph node is controlled by CCL1 chemokine expressed by lymph node lymphatic sinuses', *The Journal of Experimental Medicine*, 210(8), pp. 1509–1528. doi: 10.1084/jem.20111627.

Debacq-Chainiaux, F., Erusalimsky, J. D., Campisi, J. and Toussaint, O. (2009) 'Protocols to detect senescence-associated beta-galactosidase (SA-betagal) activity, a biomarker of senescent cells in culture and in vivo.', *Nature protocols*, 4(12), pp. 1798–806. doi: 10.1038/nprot.2009.191.

Delilbasi, C. B., Okura, M., Iida, S. and Kogo, M. (2004) 'Investigation of CXCR4 in squamous cell carcinoma of the tongue.', *Oral oncology*, 40(2), pp. 154–157. Available at: http://www.ncbi.nlm.nih.gov/pubmed/14693238 (Accessed: 23 June 2017).

Desgrosellier, J. S. and Cheresh, D. A. (2010) 'Integrins in cancer: biological implications and therapeutic opportunities', *Nature Reviews Cancer*. Nature Publishing Group, 10(12), pp. 890–890. doi: 10.1038/nrc2965.

van Deursen, J. M. (2014) 'The role of senescent cells in ageing.', *Nature*. NIH Public Access, 509(7501), pp. 439–46. doi: 10.1038/nature13193.

Deying, W., Feng, G., Shumei, L., Hui, Z., Ming, L. and Hongqing, W. (2017) 'CAF-derived HGF promotes cell proliferation and drug resistance by up-regulating the c-Met/PI3K/Akt and GRP78 signalling in ovarian cancer cells.', *Bioscience reports*. Portland Press Ltd, 37(2). doi: 10.1042/BSR20160470.

Ding, L., Li, B., Zhao, Y., Fu, Y.-F., Hu, E.-L., Hu, Q.-G., Ni, Y.-H. and Hou, Y.-Y. (2014) 'Serum CCL2 and CCL3 as potential biomarkers for the diagnosis of oral squamous cell carcinoma', *Tumor Biology*, 35(10), pp. 10539–10546. doi: 10.1007/s13277-014-2306-1.

Ding, S., Chen, G., Zhang, W., Xing, C., Xu, X., Xie, H., Lu, A., Chen, K., Guo, H., Ren, Z., Zheng, S. and Zhou, L. (2015) 'MRC-5 fibroblast-conditioned medium influences multiple pathways regulating invasion, migration, proliferation, and apoptosis in hepatocellular carcinoma.', *Journal of translational medicine*. BioMed Central, 13, p. 237. doi: 10.1186/s12967-015-0588-8.

Dirice, E., Kahraman, S., Jiang, W., El Ouaamari, A., De Jesus, D. F., Teo, A. K. K., Hu, J., Kawamori, D., Gaglia, J. L., Mathis, D. and Kulkarni, R. N. (2014) 'Soluble factors secreted by T cells promote β-cell proliferation.', *Diabetes*. American Diabetes Association, 63(1), pp. 188–202. doi: 10.2337/db13-0204.

Dolnik, V. and Gurske, W. A. (2011) 'Chemical modification of proteins to improve the accuracy of their relative molecular mass determination by electrophoresis.', *Electrophoresis*. NIH Public Access, 32(20), pp. 2893–7. doi: 10.1002/elps.201100141.

Dong, C., Chua, A., Ganguly, B., Krensky, A. M. and Clayberger, C. (2005) 'Glycosylated recombinant human XCL1/lymphotactin exhibits enhanced biologic activity', *Journal of Immunological Methods*, 302(1–2), pp. 136–144. doi: 10.1016/j.jim.2005.05.008.

Dorner, B., Müller, S., Entschladen, F., Schröder, J. M., Franke, P., Kraft, R., Friedl, P., Clark-Lewis, I. and Kroczek, R. A. (1997) 'Purification, structural analysis, and function of natural ATAC, a cytokine secreted by CD8+ T cells', *Journal of Biological Chemistry*, 272(13), pp. 8817–8823. doi: 10.1074/jbc.272.13.8817.

Downer, C. S., Watt, F. M. and Speight, P. M. (1993) 'Loss of α6 and β4 integrin subunits coincides with loss of basement membrane components in oral squamous cell carcinomas', *The Journal of Pathology*, 171(3), pp. 183–190. doi: 10.1002/path.1711710306.

Dumon-Seignovert, L., Cariot, G. and Vuillard, L. (2004) 'The toxicity of recombinant proteins in Escherichia coli: a comparison of overexpression in BL21(DE3), C41(DE3), and C43(DE3)', *Protein Expression and Purification*, 37(1), pp. 203–206. doi: 10.1016/j.pep.2004.04.025.

Dumont, N. and Arteaga, C. L. (2000) 'Transforming growth factor-beta and breast cancer: Tumor promoting effects of transforming growth factor-β', *Breast Cancer Research*. BioMed Central, 2(2), p. 125. doi: 10.1186/bcr44.

Dustin, L. B. (2000) 'Ratiometric analysis of calcium mobilization', *Clinical and Applied Immunology Reviews*. Elsevier, 1(1), pp. 5–15. doi: 10.1016/S1529-1049(00)00002-7.

Dvorak, P., Chrast, L., Nikel, P. I., Fedr, R., Soucek, K., Sedlackova, M., Chaloupkova, R., de Lorenzo, V., Prokop, Z. and Damborsky, J. (2015) 'Exacerbation of substrate toxicity by IPTG in Escherichia coli BL21(DE3) carrying a synthetic metabolic pathway.', *Microbial cell factories*. BioMed Central, 14, p. 201. doi: 10.1186/s12934-015-0393-3.

Elad, S., Zadik, Y., Zeevi, I., Miyazaki, A., de Figueiredo, M. A. Z. and Or, R. (2010) 'Oral cancer in patients after hematopoietic stem-cell transplantation: long-term follow-up suggests an increased risk for recurrence.', *Transplantation*, 90(11), pp. 1243–4. doi: 10.1097/TP.0b013e3181f9caaa.

Erdogan, B., Ao, M., White, L. M., Means, A. L., Brewer, B. M., Yang, L., Washington, M. K., Shi, C., Franco, O. E., Weaver, A. M., Hayward, S. W., Li, D. and Webb, D. J. (2017) 'Cancer-associated fibroblasts promote directional cancer cell migration by aligning fibronectin', *J Cell Biol*. Rockefeller University Press, 216(11), p. jcb.201704053. doi: 10.1083/JCB.201704053.

Eyman, D., Damodarasamy, M., Plymate, S. R. and Reed, M. J. (2009) 'CCL5 secreted by senescent aged fibroblasts induces proliferation of prostate epithelial cells and expression of genes that modulate angiogenesis', *Journal of Cellular Physiology*, 220(2), pp. 376–381. doi: 10.1002/jcp.21776.

Feller, L., Altini, M. and Lemmer, J. (2013) 'Inflammation in the context of oral cancer', *Oral Oncology*, 49(9), pp. 887–892. doi: 10.1016/j.oraloncology.2013.07.003.

Ferguson, S. S. (2001) 'Evolving concepts in G protein-coupled receptor endocytosis: the role in receptor desensitization and signaling.', *Pharmacological reviews*, 53(1), pp. 1–24. Available at: http://www.ncbi.nlm.nih.gov/pubmed/11171937 (Accessed: 11 February 2018).

Feuser, K., Thon, K.-P. P., Bischoff, S. C. and Lorentz, A. (2012) 'Human intestinal mast cells are a potent source of multiple chemokines', *Cytokine*. Elsevier Ltd, 58(2), pp. 178–185. doi: 10.1016/j.cyto.2012.01.001.

Fokas, E., Engenhart-Cabillic, R., Daniilidis, K., Rose, F. and An, H.-X. X. (2007) 'Metastasis: The seed and soil theory gains identity', *Cancer and Metastasis Reviews*, 26(3–4), pp. 705–715. doi: 10.1007/s10555-007-9088-5.

Formaneck, M. S., Ma, L. and Cui, Q. (2006) 'Effects of temperature and salt concentration on the structural stability of human lymphotactin: insights from molecular simulations.', *Journal of the American Chemical Society*. NIH Public Access, 128(29), pp. 9506–9517. doi: 10.1021/ja061620o.

Fossum, E., Gr?deland, G., Terhorst, D., Tveita, A. A., Vikse, E., Mjaaland, S., Henri, S., Malissen, B. and Bogen, B. (2015) 'Vaccine molecules targeting Xcr1 on cross-presenting DCs induce protective CD8 $^{+}$ T-cell responses against influenza virus', *European Journal of Immunology*, 45(2), pp. 624–635. doi: 10.1002/eji.201445080.

Fox, J. C., Nakayama, T., Tyler, R. C., Sander, T. L., Yoshie, O. and Volkman, B. F. (2015) 'Structural and agonist properties of XCL2, the other member of the C-chemokine subfamily', *Cytokine*. Elsevier Ltd, 71(2), pp. 302–311. doi: 10.1016/j.cyto.2014.11.010.

Fox, J. C., Tyler, R. C., Guzzo, C., Tuinstra, R. L., Peterson, F. C., Lusso, P. and Volkman, B. F. (2015) 'Engineering Metamorphic Chemokine Lymphotactin/XCL1 into the GAG-Binding, HIV-Inhibitory Dimer Conformation', *ACS Chemical Biology*. American Chemical Society, 10(11), pp. 2580–2588. doi: 10.1021/acschembio.5b00542.

Fox, J. C., Tyler, R. C., Peterson, F. C., Dyer, D. P., Zhang, F., Linhardt, R. J., Handel, T. M. and Volkman, B. F. (2016) 'Examination of Glycosaminoglycan Binding Sites on the XCL1 Dimer', *Biochemistry*. NIH Public Access, 55(8), pp. 1214–1225. doi: 10.1021/acs.biochem.5b01329.

Gantsev, S. K., Umezawa, K., Islamgulov, D. V., Khusnutdinova, E. K., Ishmuratova, R. S., Frolova, V. Y. and Kzyrgalin, S. R. (2013) 'The role of inflammatory chemokines in lymphoid neoorganogenesis in breast cancer', *Biomedicine & Pharmacotherapy*, 67(5), pp. 363–366. doi: 10.1016/j.biopha.2013.03.017.

Gecchele, E., Merlin, M., Brozzetti, A., Falorni, A., Pezzotti, M. and Avesani, L. (2015) 'A

comparative analysis of recombinant protein expression in different biofactories: bacteria, insect cells and plant systems.', *Journal of visualized experiments : JoVE*. MyJoVE Corporation, (97). doi: 10.3791/52459.

German, R. Z. and Palmer, J. B. (2006) 'Anatomy and development of oral cavity and pharynx', *GI Motility online, Published online: 16 May 2006;* | *doi:10.1038/gimo5*. Nature Publishing Group. doi: 10.1038/gimo5.

Geyer, H., Hartung, E., Mages, H. W., Weise, C., Beluzic, R., Vugrek, O., Jonjic, S., Kroczek, R. A. and Voigt, S. (2014) 'Cytomegalovirus Expresses the Chemokine Homologue vXCL1 Capable of Attracting XCR1+ CD4- Dendritic Cells', *Journal of Virology*, 88(1), pp. 292–302. doi: 10.1128/JVI.02330-13.

Girard, J.-P., Moussion, C. and Förster, R. (2012) 'HEVs, lymphatics and homeostatic immune cell trafficking in lymph nodes', *Nature Reviews Immunology*, 12(11), pp. 762–773. doi: 10.1038/nri3298.

Gong, H., Shen, B., Flevaris, P., Chow, C., Lam, S. C.-T., Voyno-Yasenetskaya, T. A., Kozasa, T. and Du, X. (2010) 'G protein subunit Galpha13 binds to integrin alphaIIbbeta3 and mediates integrin "outside-in" signaling.', *Science (New York, N.Y.)*. NIH Public Access, 327(5963), pp. 340–3. doi: 10.1126/science.1174779.

Goossens, N., Nakagawa, S., Sun, X. and Hoshida, Y. (2015) 'Cancer biomarker discovery and validation.', *Translational cancer research*. NIH Public Access, 4(3), pp. 256–269. doi: 10.3978/j.issn.2218-676X.2015.06.04.

Gortz, A., Nibbs, R. J. B., McLean, P., Jarmin, D., Lambie, W., Baird, J. W. and Graham, G. J. (2002) 'The chemokine ESkine/CCL27 displays novel modes of intracrine and paracrine function.', *Journal of immunology (Baltimore, Md. : 1950)*, 169(3), pp. 1387–94. doi: 10.4049/jimmunol.169.3.1387.

Gottesman, S. (1996) 'Proteases and their targets in Escherichia coli', *Annual Review of Genetics*, 30(1), pp. 465–506. doi: 10.1146/annurev.genet.30.1.465.

Guan, Y., Zhu, Q., Huang, D., Zhao, S., Jan Lo, L. and Peng, J. (2015) 'An equation to estimate the difference between theoretically predicted and SDS PAGE-displayed molecular weights for an acidic peptide', *Scientific Reports*. Nature Publishing Group, 5(1), p. 13370. doi: 10.1038/srep13370.

Guo, H., Liu, Z., Xu, B., Hu, H., Wei, Z., Liu, Q., Zhang, X., Ding, X., Wang, Y., Zhao, M., Gong, Y. and Shao, C. (2013) 'Chemokine receptor CXCR2 is transactivated by p53 and induces p38-mediated cellular senescence in response to DNA damage', *Aging Cell*, 12(6), pp. 1110–1121. doi: 10.1111/acel.12138.

Gupta, P., Sharma, P. K., Mir, H., Singh, R., Singh, N., Kloecker, G. H., Lillard, J. W., Singh, S. and Singh, S. (2014) 'CCR9/CCL25 expression in non-small cell lung cancer correlates with aggressive disease and mediates key steps of metastasis.', *Oncotarget*. Impact Journals, LLC, 5(20), pp. 10170–9. doi: 10.18632/oncotarget.2526.

Guzzo, C., Fox, J. C., Miao, H., Volkman, B. F. and Lusso, P. (2015) 'Structural Determinants for the Selective Anti-HIV-1 Activity of the All-β Alternative Conformer of XCL1', *Journal of Virology*. American Society for Microbiology,

89(17), pp. 9061–9067. doi: 10.1128/JVI.01285-15.

Guzzo, C., Fox, J., Lin, Y., Miao, H., Cimbro, R., Volkman, B. F., Fauci, A. S. and Lusso, P. (2013) 'The CD8-Derived Chemokine XCL1/Lymphotactin Is a Conformation-Dependent, Broad-Spectrum Inhibitor of HIV-1', *PLoS Pathogens*. Public Library of Science, 9(12), pp. 1–11. doi: 10.1371/journal.ppat.1003852.

Hadjidakis, D. J. and Androulakis, I. I. (2006) 'Bone remodeling', *Annals of the New York Academy of Sciences*. Blackwell Publishing Inc, 1092(1), pp. 385–396. doi: 10.1196/annals.1365.035.

Haferkamp, S., Scurr, L. L., Becker, T. M., Frausto, M., Kefford, R. F. and Rizos, H. (2009) 'Oncogene-Induced Senescence Does Not Require the p16INK4a or p14ARF Melanoma Tumor Suppressors', *Journal of Investigative Dermatology*. Elsevier, 129(8), pp. 1983–1991. doi: 10.1038/JID.2009.5.

Hagman, Z., Haflidadottir, B. S., Ansari, M., Persson, M., Bjartell, A., Edsjö, A. and Ceder, Y. (2013) 'The tumour suppressor miR-34c targets MET in prostate cancer cells', *British Journal of Cancer*. Nature Publishing Group, 109(5), pp. 1271–1278. doi: 10.1038/bjc.2013.449.

Hannelien, V., Karel, G., Jo, V. D., Sofie, S., Van Damme, J., Jo, V. D., Struyf, S. and Sofie, S. (2012) 'The role of CXC chemokines in the transition of chronic inflammation to esophageal and gastric cancer', *Biochimica et Biophysica Acta (BBA) - Reviews on Cancer*, 1825(1), pp. 117–129. doi: 10.1016/j.bbcan.2011.10.008.

Harwood, N. E. and Batista, F. D. (2010) 'Early Events in B Cell Activation', *Annual Review of Immunology*, 28(1), pp. 185–210. doi: 10.1146/annurev-immunol-030409-101216.

Hashibe, M., Hunt, J., Wei, M., Buys, S., Gren, L. and Lee, Y.-C. A. (2013) 'Tobacco, alcohol, body mass index, physical activity, and the risk of head and neck cancer in the prostate, lung, colorectal, and ovarian (PLCO) cohort', *Head & Neck*, 35(7), pp. 914–922. doi: 10.1002/hed.23052.

Hayashido, Y., Kitano, H., Sakaue, T., Fujii, T., Suematsu, M., Sakurai, S. and Okamoto, T. (2014) 'Overexpression of integrin αv facilitates proliferation and invasion of oral squamous cell carcinoma cells via MEK/ERK signalling pathway that is activated by interaction of integrin αvβ8 with type I collagen', *International Journal of Oncology*, 45(5), pp. 1875–1882. doi: 10.3892/ijo.2014.2642.

Hearnden, V., Lomas, H., MacNeil, S., Thornhill, M., Murdoch, C., Lewis, A., Madsen, J., Blanazs, A., Armes, S. and Battaglia, G. (2009) 'Diffusion Studies of Nanometer Polymersomes Across Tissue Engineered Human Oral Mucosa', *Pharmaceutical Research*, 26(7), pp. 1718–1728. doi: 10.1007/s11095-009-9882-6.

Hedrick, J. A., Saylor, V., Figueroa, D., Mizoue, L., Xu, Y., Menon, S., Abrams, J., Handel, T. and Zlotnik, A. (1997) 'Lymphotactin is produced by NK cells and attracts both NK cells and T cells in vivo', *Journal of Immunology*, 158, pp. 1533–1540.

Heinrich, E. L., Arrington, A. K., Ko, M. E., Luu, C., Lee, W., Lu, J. and Kim, J. (2013) 'Paracrine activation of chemokine receptor CCR9 enhances the invasiveness of

pancreatic cancer cells', *Cancer Microenvironment*, 6(3), pp. 241–245. doi: 10.1007/s12307-013-0130-6.

Herbig, U., Jobling, W. A., Chen, B. P. C., Chen, D. J. and Sedivy, J. M. (2004) 'Telomere shortening triggers senescence of human cells through a pathway involving ATM, p53, and p21(CIP1), but not p16(INK4a).', *Molecular cell*, 14(4), pp. 501–13. Available at: http://www.ncbi.nlm.nih.gov/pubmed/15149599 (Accessed: 24 March 2018).

Hileman, R. E., Fromm, J. R., Weiler, J. M. and Linhardt, R. J. (1998) 'Glycosaminoglycan-protein interactions: definition of consensus sites in glycosaminoglycan binding proteins', *BioEssays*, 20(2), pp. 156–167. doi: 10.1002/(SICI)1521-1878(199802)20:2<156::AID-BIES8>3.0.CO;2-R.

Hillyer, P. and Male, D. (2005) 'Expression of chemokines on the surface of different human endothelia', *Immunology and Cell Biology*, 83(4), pp. 375–382. doi: 10.1111/j.1440-1711.2005.01345.x.

Hoogewerf, A. J., Kuschert, G. S. V., Proudfoot, A. E. I., Borlat, F., Clark-Lewis, I., Power, C. A. and Wells, T. N. C. (1997) 'Glycosaminoglycans mediate cell surface oligomerization of chemokines', *Biochemistry*, 36(44), pp. 13570–13578. doi: 10.1021/bi971125s.

Hosono, M., Koma, Y.-I., Takase, N., Urakawa, N., Higashino, N., Suemune, K., Kodaira, H., Nishio, M., Shigeoka, M., Kakeji, Y. and Yokozaki, H. (2017) 'CXCL8 derived from tumor-associated macrophages and esophageal squamous cell carcinomas contributes to tumor progression by promoting migration and invasion of cancer cells.', *Oncotarget*. Impact Journals, LLC, 8(62), pp. 106071–106088. doi: 10.18632/oncotarget.22526.

Hou, T., Liang, D., Xu, L., Huang, X., Huang, Y. and Zhang, Y. (2013) 'Atypical chemokine receptors predict lymph node metastasis and prognosis in patients with cervical squamous cell cancer', *Gynecologic Oncology*, 130(1), pp. 181–187. doi: 10.1016/j.ygyno.2013.04.015.

Huang, H., Li, F., Cairns, C. M., Gordon, J. R. and Xiang, J. (2001) 'Neutrophils and B cells express XCR1 receptor and chemotactically respond to lymphotactin.', *Biochemical and biophysical research communications*, 281, pp. 378–382. doi: 10.1006/bbrc.2001.4363.

Huma, Z. E., Sanchez, J., Lim, H. D., Bridgford, J. L., Huang, C., Parker, B. J., Pazhamalil, J. G., Porebski, B. T., Pfleger, K. D. G., Lane, J. R., Canals, M. and Stone, M. J. (2017) 'Key determinants of selective binding and activation by the monocyte chemoattractant proteins at the chemokine receptor CCR2', *Science Signaling*, 10(480), p. eaai8529. doi: 10.1126/scisignal.aai8529.

Ishikawa, T., Nakashiro, K.-I., Hara, S., Klosek, S. K., Li, C., Shintani, S. and Hamakawa, H. (2006) 'CXCR4 expression is associated with lymph-node metastasis of oral squamous cell carcinoma.', *International journal of oncology*, 28(1), pp. 61–66. Available at: http://www.ncbi.nlm.nih.gov/pubmed/16327980 (Accessed: 23 June 2017).

Jamieson-Gladney, W. L., Zhang, Y., Fong, A. M., Meucci, O. and Fatatis, A. (2011) 'The chemokine receptor CX_3CR1 is directly involved in the arrest of breast cancer cells

to the skeleton.', *Breast cancer research : BCR*. BioMed Central, 13(5), p. R91. doi: 10.1186/bcr3016.

Janes, S. M. and Watt, F. M. (2006) 'New roles for integrins in squamous-cell carcinoma', *Nature Reviews Cancer*, 6(3), pp. 175–183. doi: 10.1038/nrc1817.

Jensen, P. C. and Rosenkilde, M. M. (2009) 'Chapter 8 Activation Mechanisms of Chemokine Receptors', in *Methods in enzymology*, pp. 171–190. doi: 10.1016/S0076-6879(09)05408-1.

Jia, B. and Jeon, C. O. (2016) 'High-throughput recombinant protein expression in Escherichia coli: current status and future perspectives.', *Open biology*. The Royal Society, 6(8). doi: 10.1098/rsob.160196.

Jiang, Y., Wu, X., Shi, B., Wu, W. and Yin, G. (2006) 'Expression of chemokine CXCL12 and its receptor CXCR4 in human epithelial ovarian cancer: An independent prognostic factor for tumor progression', *Gynecologic Oncology*, 103(1), pp. 226–233. doi: 10.1016/j.ygyno.2006.02.036.

Jokinen, J. *et al.* (2004) 'Integrin-mediated cell adhesion to type I collagen fibrils', *Journal of Biological Chemistry*, 279(30), pp. 31956–31963. doi: 10.1074/jbc.M401409200.

Jones, J., Sugiyama, M., Watt, F. M. and Speight, P. M. (1993) 'Integrin expression in normal, hyperplastic, dysplastic, and malignant oral epithelium', *The Journal of Pathology*, 169(2), pp. 235–243. doi: 10.1002/path.1711690210.

Jones, J., Watt, F. M. and Speight, P. M. (1997) 'Changes in the expression of alphav integrins in oral squamous cell carcinomas', *Journal of Oral Pathology and Medicine*. Blackwell Publishing Ltd, 26(2), pp. 63–68. doi: 10.1111/j.1600-0714.1997.tb00023.x.

Joyce, J. A. and Pollard, J. W. (2009) 'Microenvironmental regulation of metastasis', *Nature Reviews Cancer*, 9(4), pp. 239–252. doi: 10.1038/nrc2618.

Juliano, R. L. and Haskill, S. (1993) 'Signal transduction from the extracellular matrix.', *The Journal of cell biology*, 120(3), pp. 577–585. doi: 10.1083/jcb.120.3.577.

Junttila, M. R. and de Sauvage, F. J. (2013) 'Influence of tumour micro-environment heterogeneity on therapeutic response', *Nature*, 501(7467), pp. 346–354. doi: 10.1038/nature12626.

Kabir, T., Leigh, R., Tasena, H., Mellone, M., Coletta, R., Parkinson, E., Prime, S., Thomas, G., Paterson, I., Zhou, D., McCall, J., Speight, P. and Lambert, D. (2016) 'A miR-335/COX-2/PTEN axis regulates the secretory phenotype of senescent cancer-associated fibroblasts', *Aging*, 8(8), pp. 1608–1635. doi: 10.18632/aging.100987.

Kalluri, R. (2003) 'Angiogenesis: Basement membranes: structure, assembly and role in tumour angiogenesis', *Nature Reviews Cancer*, 3(6), pp. 422–433. doi: 10.1038/nrc1094.

Kalluri, R. (2016) 'The biology and function of fibroblasts in cancer', *Nature Reviews*

Cancer, 16(9), pp. 582–598. doi: 10.1038/nrc.2016.73.

Kalluri, R. and Zeisberg, M. (2006) 'Fibroblasts in cancer', *Nature Reviews Cancer*, 6(5), pp. 392–401. doi: 10.1038/nrc1877.

Karagiannis, G. S., Poutahidis, T., Erdman, S. E., Kirsch, R., Riddell, R. H. and Diamandis, E. P. (2012) 'Cancer-associated fibroblasts drive the progression of metastasis through both paracrine and mechanical pressure on cancer tissue.', *Molecular cancer research : MCR*. NIH Public Access, 10(11), pp. 1403–18. doi: 10.1158/1541-7786.MCR-12-0307.

Karaman, S. and Detmar, M. (2014) 'Review series Mechanisms of lymphatic metastasis', *The Journal of clinical investigation*, 124(3), pp. 922–8. doi: 10.1172/JCI71606.922.

Keeley, E. C., Mehrad, B. and Strieter, R. M. (2011) 'Chemokines as mediators of tumor angiogenesis and neovascularization.', *Experimental cell research*. NIH Public Access, 317(5), pp. 685–690. doi: 10.1016/j.yexcr.2010.10.020.

Kelner, G. S., Kennedy, J., Bacon, K. B., Kleyensteuber, S., Largaespada, D. A., Jenkins, N. A., Copeland, N. G., Bazan, J. F., Moore, K. W. and Schall, T. J. (1994) 'Lymphotactin: a cytokine that represents a new class of chemokine.', *Science (New York, N.Y.)*, 266(5189), pp. 1395–1399. doi: 10.1126/science.7973732.

Kelner, G. S. and Zlotnik, A. (1995) 'Cytokine production profile of early thymocytes and the characterization of a new class of chemokine.', *Journal of leukocyte biology*, 57, pp. 778–781.

Kennedy, J., Kelner, G. S., Kleyensteuber, S., Schall, T. J., Weiss, M. C., Yssel, H., Schneider, P. V, Cocks, B. G., Bacon, K. B. and Zlotnik, A. (1995) 'Molecular cloning and functional characterization of human lymphotactin', *Journal of immunology (Baltimore, Md. : 1950)*, 155(1), pp. 203–209. Available at: http://www.ncbi.nlm.nih.gov/entrez/query.fcgi?cmd=Retrieve&db=PubMed&dopt=Citation&list_uids=7602097 (Accessed: 23 June 2017).

Kennedy, J., Vicari, A. P., Saylor, V., Zurawski, S. M., Copeland, N. G., Gilbert, D. J., Jenkins, N. A. and Zlotnik, A. (2000) 'A molecular analysis of NKT cells: identification of a class-I restricted T cell-associated molecule (CRTAM).', *Journal of leukocyte biology*, 67, pp. 725–734.

Kessenbrock, K., Plaks, V. and Werb, Z. (2010) 'Matrix Metalloproteinases: Regulators of the Tumor Microenvironment', *Cell*, 141(1), pp. 52–67. doi: 10.1016/j.cell.2010.03.015.

Kharaishvili, G., Simkova, D., Bouchalova, K., Gachechiladze, M., Narsia, N. and Bouchal, J. (2014) 'The role of cancer-associated fibroblasts, solid stress and other microenvironmental factors in tumor progression and therapy resistance.', *Cancer cell international*. BioMed Central, 14, p. 41. doi: 10.1186/1475-2867-14-41.

Khurram, S. A., Bingle, L., McCabe, B. M., Farthing, P. M. and Whawell, S. A. (2014) 'The chemokine receptors CXCR1 and CXCR2 regulate oral cancer cell behaviour', *Journal of Oral Pathology and Medicine*, 43(9), pp. 667–674. doi:

10.1111/jop.12191.

Khurram, S. A., Whawell, S. A., Bingle, L., Murdoch, C., McCabe, B. M. and Farthing, P. M. (2010) 'Functional expression of the chemokine receptor XCR1 on oral epithelial cells', *The Journal of pathology*, 221(2), pp. 153–163. doi: 10.1002/path.2695.

Kim, M., Rooper, L., Xie, J., Rayahin, J., Burdette, J. E., Kajdacsy-Balla, A. A. and Barbolina, M. V. (2012) 'The Lymphotactin Receptor Is Expressed in Epithelial Ovarian Carcinoma and Contributes to Cell Migration and Proliferation', *Molecular Cancer Research*, 10(11), pp. 1419–1429. doi: 10.1158/1541-7786.MCR-12-0361.

Kimple, M. E., Brill, A. L. and Pasker, R. L. (2013) 'Overview of affinity tags for protein purification.', *Current protocols in protein science*. NIH Public Access, 73, p. Unit 9.9. doi: 10.1002/0471140864.ps0909s73.

Kitano, M., Yamazaki, C., Takumi, A., Ikeno, T., Hemmi, H., Takahashi, N., Shimizu, K., Fraser, S. E., Hoshino, K., Kaisho, T. and Okada, T. (2016) 'Imaging of the cross-presenting dendritic cell subsets in the skin-draining lymph node', *Proceedings of the National Academy of Sciences*, 113(4), pp. 1044–1049. doi: 10.1073/pnas.1513607113.

Kleinhans, M., Tun-Kyi, A., Gilliet, M., Kadin, M. E., Dummer, R., Burg, G. and Nestle, F. O. (2003) 'Functional expression of the eotaxin receptor CCR3 in CD30+ cutaneous T-cell lymphoma', *Blood*, 101(4), pp. 1487–1493. doi: 10.1182/blood-2002-02-0475.

Kleist, A. B., Getschman, A. E., Ziarek, J. J., Nevins, A. M., Gauthier, P.-A., Chevigné, A., Szpakowska, M. and Volkman, B. F. (2016) 'New paradigms in chemokine receptor signal transduction: Moving beyond the two-site model', *Biochemical Pharmacology*, 114, pp. 53–68. doi: 10.1016/j.bcp.2016.04.007.

Kodama, J., Hasengaowa, Kusumoto, T., Seki, N., Matsuo, T., Ojima, Y., Nakamura, K., Hongo, A. and Hiramatsu, Y. (2006) 'Association of CXCR4 and CCR7 chemokine receptor expression and lymph node metastasis in human cervical cancer', *Annals of Oncology*, 18(1), pp. 70–76. doi: 10.1093/annonc/mdl342.

Koistinen, P. and Heino, J. (2013) *Integrins in Cancer Cell Invasion*, *Landes Bioscience, Austin (TX)*. Landes Bioscience. Available at: https://www.ncbi.nlm.nih.gov/books/NBK6070/?report=reader (Accessed: 23 June 2017).

Kondo, T. (2007) 'Stem cell-like cancer cells in cancer cell lines.', *Cancer biomarkers : section A of Disease markers*, 3(4–5), pp. 245–50. Available at: http://www.ncbi.nlm.nih.gov/pubmed/17917153 (Accessed: 13 March 2018).

Krištić, J. and Lauc, G. (2017) 'Ubiquitous Importance of Protein Glycosylation', in *Methods in molecular biology (Clifton, N.J.)*, pp. 1–12. doi: 10.1007/978-1-4939-6493-2_1.

Kroczek, R. A. and Henn, V. (2012) *The role of XCR1 and its ligand XCL1 in antigen cross-presentation by murine and human dendritic cells*, *Frontiers in Immunology*. doi: 10.3389/fimmu.2012.00014.

Kroeze, K. L., Boink, M. A., Sampat-Sardjoepersad, S. C., Waaijman, T., Scheper, R. J. and Gibbs, S. (2012) 'Autocrine Regulation of Re-Epithelialization After Wounding by Chemokine Receptors CCR1, CCR10, CXCR1, CXCR2, and CXCR3', *Journal of Investigative Dermatology*. Nature Publishing Group, 132(1), pp. 216–225. doi: 10.1038/jid.2011.245.

Krtolica, A., Parrinello, S., Lockett, S., Desprez, P.-Y. and Campisi, J. (2001) 'Senescent fibroblasts promote epithelial cell growth and tumorigenesis: A link between cancer and aging', *Proceedings of the National Academy of Sciences*, 98(21), pp. 12072–12077. doi: 10.1073/pnas.211053698.

Kuloglu, E. S., McCaslin, D. R., Kitabwalla, M., Pauza, C. D., Markley, J. L. and Volkman, B. F. (2001) 'Monomeric solution structure of the prototypical "C" chemokine lymphotactin', *Biochemistry*, 40(42), pp. 12486–12496. doi: 10.1021/bi011106p.

Kuloglu, E. S., McCaslin, D. R., Markley, J. L. and Volkman, B. F. (2002) 'Structural rearrangement of human lymphotactin, a C chemokine, under physiological solution conditions', *Journal of Biological Chemistry*, 277(20), pp. 17863–17870. doi: 10.1074/jbc.M200402200.

Kumai, T., Nagato, T., Kobayashi, H., Komabayashi, Y., Ueda, S., Kishibe, K., Ohkuri, T., Takahara, M., Celis, E. and Harabuchi, Y. (2015) 'CCL17 and CCL22/CCR4 signaling is a strong candidate for novel targeted therapy against nasal natural killer/T-cell lymphoma', *Cancer Immunology, Immunotherapy*. NIH Public Access, 64(6), pp. 697–705. doi: 10.1007/s00262-015-1675-7.

Lakemond, C. M. M., De Jongh, H. H. J., Hessing, M., Gruppen, H. and Voragen, A. G. J. (2000) 'Soy glycinin: Influence of pH and ionic strength on solubility and molecular structure at ambient temperatures', *Journal of Agricultural and Food Chemistry*. American Chemical Society, 48(6), pp. 1985–1990. doi: 10.1021/jf9908695.

Lebendiker, M. and Danieli, T. (2014) 'Production of prone-to-aggregate proteins', *FEBS Letters*, 588(2), pp. 236–246. doi: 10.1016/j.febslet.2013.10.044.

Lecot, P., Alimirah, F., Desprez, P.-Y., Campisi, J. and Wiley, C. (2016) 'Context-dependent effects of cellular senescence in cancer development', *British Journal of Cancer*, 114(11), pp. 1180–1184. doi: 10.1038/bjc.2016.115.

Lee, J. K., Lee, E. H., Yun, Y. P., Kim, K., Kwack, K., Na, D. S., Kwon, B. S. and Lee, C.-K. (2002) 'Truncation of NH_2-terminal Amino Acid Residues Increases Agonistic Potency of Leukotactin-1 on CC Chemokine Receptors 1 and 3', *Journal of Biological Chemistry*, 277(17), pp. 14757–14763. doi: 10.1074/jbc.M109309200.

Levi, F., Pasche, C., La Vecchia, C., Lucchini, F., Franceschi, S. and Monnier, P. (1998) 'Food groups and risk of oral and pharyngeal cancer.', *International journal of cancer*, 77(5), pp. 705–709. Available at: http://www.ncbi.nlm.nih.gov/pubmed/9688303 (Accessed: 23 June 2017).

Li, H., Zhang, J., Chen, S.-W., Liu, L.-L., Li, L., Gao, F., Zhuang, S.-M., Wang, L.-P., Li, Y. and Song, M. (2015) 'Cancer-associated fibroblasts provide a suitable microenvironment for tumor development and progression in oral tongue

squamous cancer.', *Journal of translational medicine*. BioMed Central, 13, p. 198. doi: 10.1186/s12967-015-0551-8.

Lin, H., Sun, S., Lu, X., Chen, P., Chen, C., Liang, W. and Peng, C. (2017) 'CCR10 activation stimulates the invasion and migration of breast cancer cells through the ERK1/2/MMP-7 signaling pathway', *International Immunopharmacology*, 51, pp. 124–130. doi: 10.1016/j.intimp.2017.07.018.

Lin, N.-N., Wang, P., Zhao, D., Zhang, F.-J., Yang, K. and Chen, R. (2017) 'Significance of oral cancer-associated fibroblasts in angiogenesis, lymphangiogenesis, and tumor invasion in oral squamous cell carcinoma', *Journal of Oral Pathology & Medicine*, 46(1), pp. 21–30. doi: 10.1111/jop.12452.

Liu, J., Zhang, F., Li, Y. and Wang, C. (2010) 'The role of chemokine receptor CXCR7 in lung cancer', *Clinical Oncology and Cancer Research*. Tianjin Medical University Cancer Institute and Hospital, 7(6), pp. 342–346. doi: 10.1007/s11805-010-0542-8.

Liu, Y., Ji, R., Li, J., Gu, Q., Zhao, X., Sun, T., Wang, J., Li, J., Du, Q. and Sun, B. (2010) 'Correlation effect of EGFR and CXCR4 and CCR7 chemokine receptors in predicting breast cancer metastasis and prognosis', *Journal of Experimental & Clinical Cancer Research*. BioMed Central, 29(1), p. 16. doi: 10.1186/1756-9966-29-16.

Liu, Y., Wu, B.-Q., Geng, H., Xu, M.-L. and Zhong, H.-H. (2015) 'Association of chemokine and chemokine receptor expression with the invasion and metastasis of lung carcinoma', *Oncology Letters*, 10(3), pp. 1315–1322. doi: 10.3892/ol.2015.3402.

Livak, K. J. and Schmittgen, T. D. (2001) 'Analysis of Relative Gene Expression Data Using Real-Time Quantitative PCR and the 2−ΔΔCT Method', *Methods*, 25(4), pp. 402–408. doi: 10.1006/meth.2001.1262.

Llewellyn, C. D., Linklater, K., Bell, J., Johnson, N. W. and Warnakulasuriya, S. (2004) 'An analysis of risk factors for oral cancer in young people: a case-control study.', *Oral oncology*, 40(3), pp. 304–313. Available at: http://www.ncbi.nlm.nih.gov/pubmed/14747062 (Accessed: 23 June 2017).

Lu, P., Weaver, V. M. and Werb, Z. (2012) 'The extracellular matrix: A dynamic niche in cancer progression', *Journal of Cell Biology*, 196(4), pp. 395–406. doi: 10.1083/jcb.201102147.

Ma, L. and Cui, Q. (2006) 'The temperature dependence of salt-protein association is sequence specific.', *Biochemistry*. NIH Public Access, 45(48), pp. 14466–14472. doi: 10.1021/bi0613067.

Mantovani, A., Savino, B., Locati, M., Zammataro, L., Allavena, P. and Bonecchi, R. (2010) 'The chemokine system in cancer biology and therapy', *Cytokine & Growth Factor Reviews*. Elsevier Ltd, 21(1), pp. 27–39. doi: 10.1016/j.cytogfr.2009.11.007.

Marcaurelle, L. A., Mizoue, L. S., Wilken, J., Oldham, L., Kent, S. B. H., Handel, T. M. and Bertozzi, C. R. (2001) 'Chemical synthesis of lymphotactin: A glycosylated chemokine with a C-terminal mucin-like domain', *Chemistry - A European Journal*.

WILEY-VCH Verlag GmbH, 7(5), pp. 1129–1132. doi: 10.1002/1521-3765(20010302)7:5<1129::AID-CHEM1129>3.0.CO;2-W.

Mashino, K., Sadanaga, N., Yamaguchi, H., Tanaka, F., Ohta, M., Shibuta, K., Inoue, H. and Mori, M. (2002) 'Expression of chemokine receptor CCR7 is associated with lymph node metastasis of gastric carcinoma', *Cancer Research*, 62(10), pp. 2937–2941. doi: 10.1016/j.oraloncology.2008.06.005.

Matsumoto, N., Kon, S., Nakatsuru, T., Miyashita, T., Inui, K., Saitoh, K., Kitai, Y., Muromoto, R., Kashiwakura, J., Uede, T. and Matsuda, T. (2017) 'A Novel α9 Integrin Ligand, XCL1/Lymphotactin, Is Involved in the Development of Murine Models of Autoimmune Diseases', *The Journal of Immunology*, 199(1), pp. 82–90. doi: 10.4049/jimmunol.1601329.

McLaughlin, J. K., Gridley, G., Block, G., Winn, D. M., Preston-Martin, S., Schoenberg, J. B., Greenberg, R. S., Stemhagen, A., Austin, D. F. and Ershow, A. G. (1988) 'Dietary factors in oral and pharyngeal cancer.', *Journal of the National Cancer Institute*, 80(15), pp. 1237–1243. Available at: http://www.ncbi.nlm.nih.gov/pubmed/3418729 (Accessed: 23 June 2017).

Menten, P., Saccani, A., Dillen, C., Wuyts, A., Struyf, S., Proost, P., Mantovani, A., Wang, J. M. and Van Damme, J. (2002) 'Role of the autocrine chemokines MIP-1alpha and MIP-1beta in the metastatic behavior of murine T cell lymphoma', *J Leukoc Biol*, 72(4), p. 780–9. Available at: http://www.ncbi.nlm.nih.gov/pubmed/12377948 (Accessed: 23 June 2017).

Meyer dos Santos, S., Klinkhardt, U., Scholich, K., Nelson, K., Monsefi, N., Deckmyn, H., Kuczka, K., Zorn, A. and Harder, S. (2011) 'The CX3C chemokine fractalkine mediates platelet adhesion via the von Willebrand receptor glycoprotein Ib', *Blood*, 117(18), pp. 4999–5008. doi: 10.1182/blood-2011-02-335471.

Michiels, K., Schutyser, E., Conings, R., Lenaerts, J.-P., Put, W., Nuyts, S., Delaere, P., Jacobs, R., Struyf, S., Proost, P. and Van Damme, J. (2009) 'Carcinoma cell-derived chemokines and their presence in oral fluid', *European Journal of Oral Sciences*, 117(4), pp. 362–368. doi: 10.1111/j.1600-0722.2009.00644.x.

Middleton, J., Patterson, A. M., Gardner, L., Schmutz, C. and Ashton, B. A. (2002) 'Leukocyte extravasation: chemokine transport and presentation by the endothelium', *Blood*, 100(12), pp. 3853–3860. doi: 10.1182/blood.V100.12.3853.

Monnier, J., Lewen, S., O'Hara, E., Huang, K., Tu, H., Butcher, E. C. and Zabel, B. A. (2012) 'Expression, Regulation, and Function of Atypical Chemerin Receptor CCRL2 on Endothelial Cells', *The Journal of Immunology*, 189(2), pp. 956–967. doi: 10.4049/jimmunol.1102871.

Morton, D. L., Thompson, J. F., Cochran, A. J., Mozzillo, N., Elashoff, R., Essner, R., Nieweg, O. E., Roses, D. F., Hoekstra, H. J., Karakousis, C. P., Reintgen, D. S., Coventry, B. J., Glass, E. C., Wang, H.-J. and MSLT Group (2006) 'Sentinel-Node Biopsy or Nodal Observation in Melanoma', *New England Journal of Medicine*, 355(13), pp. 1307–1317. doi: 10.1056/NEJMoa060992.

Müller, A., Homey, B., Soto, H., Ge, N., Catron, D., Buchanan, M. E., McClanahan, T., Murphy, E., Yuan, W., Wagner, S. N., Barrera, J. L., Mohar, A., Verástegui, E. and

Zlotnik, A. (2001) 'Involvement of chemokine receptors in breast cancer metastasis.', *Nature*, 410(6824), pp. 50–56. doi: 10.1038/35065016.

Muller, S. *et al.* (1995) 'Cloning of ATAC, an activation???induced, chemokine???related molecule exclusively expressed in CD8+ T lymphocytes', *European Journal of Immunology*, 25(6), pp. 1744–1748. doi: 10.1002/eji.1830250638.

Murdoch, C., Monk, P. N. and Finn, A. (1999) 'CXC CHEMOKINE RECEPTOR EXPRESSION ON HUMAN ENDOTHELIAL CELLS', *Cytokine*, 11(9), pp. 704–712. doi: 10.1006/cyto.1998.0465.

Nagata, S., Nishiyama, S. and Ikazaki, Y. (2013) 'Bacterial lipopolysaccharides stimulate production of XCL1, a calcium-dependent lipopolysaccharide-binding serum lectin, in Xenopus laevis', *Developmental & Comparative Immunology*, 40(2), pp. 94–102. doi: 10.1016/j.dci.2013.02.008.

Nair, A., Gan, J., Bush-Joseph, C., Verma, N., Tetreault, M. W. W., Saha, K., Margulis, A., Fogg, L. and Scanzello, C. R. R. (2015) 'Synovial chemokine expression and relationship with knee symptoms in patients with meniscal tears', *Osteoarthritis and Cartilage*. Elsevier Ltd, 23(7), pp. 1158–1164. doi: 10.1016/j.joca.2015.02.016.

Nevins, A. M., Subramanian, A., Tapia, J. L., Delgado, D. P., Tyler, R. C., Jensen, D. R., Ouellette, A. J. and Volkman, B. F. (2016) 'A Requirement for Metamorphic Interconversion in the Antimicrobial Activity of Chemokine XCL1', *Biochemistry*, 55(27), pp. 3784–3793. doi: 10.1021/acs.biochem.6b00353.

Nguyen, L. T. and Vogel, H. J. (2012) *Structural perspectives on antimicrobial chemokines*, *Frontiers in Immunology*. Frontiers Media SA. doi: 10.3389/fimmu.2012.00384.

Norton, K.-A., Popel, A. S. and Pandey, N. B. (2015) 'Heterogeneity of chemokine cell-surface receptor expression in triple-negative breast cancer.', *American journal of cancer research*. e-Century Publishing Corporation, 5(4), pp. 1295–307. Available at: http://www.ncbi.nlm.nih.gov/pubmed/26101698 (Accessed: 27 February 2018).

Notohamiprodjo, M., Segerer, S., Huss, R., Hildebrandt, B., Soler, D., Djafarzadeh, R., Buck, W., Nelson, P. J. and von Luettichau, I. (2005) 'CCR10 is expressed in cutaneous T-cell lymphoma', *International Journal of Cancer*, 115(4), pp. 641–647. doi: 10.1002/ijc.20922.

Ogrunc, M. and d'Adda di Fagagna, F. (2011) 'Never-ageing cellular senescence.', *European journal of cancer (Oxford, England : 1990)*. Elsevier, 47(11), pp. 1616–22. doi: 10.1016/j.ejca.2011.04.003.

Ohta, T., Sugiyama, M., Hemmi, H., Yamazaki, C., Okura, S., Sasaki, I., Fukuda, Y., Orimo, T., Ishii, K. J., Hoshino, K., Ginhoux, F. and Kaisho, T. (2016) 'Crucial roles of XCR1-expressing dendritic cells and the XCR1-XCL1 chemokine axis in intestinal immune homeostasis', *Scientific Reports*. Nature Publishing Group, 6(1), p. 23505. doi: 10.1038/srep23505.

Oji, C. and Chukwuneke, F. (2012) 'Poor oral Hygiene may be the Sole Cause of Oral Cancer.', *Journal of maxillofacial and oral surgery*. Springer, 11(4), pp. 379–83.

doi: 10.1007/s12663-012-0359-5.

Okamoto, H., Miyagawa, A., Shiota, T., Tamura, Y. and Endo, T. (2014) 'Intramolecular disulfide bond of Tim22 protein maintains integrity of the TIM22 complex in the mitochondrial inner membrane.', *The Journal of biological chemistry*. American Society for Biochemistry and Molecular Biology, 289(8), pp. 4827–38. doi: 10.1074/jbc.M113.543264.

Panda, S., Padhiary, S. K. and Routray, S. (2016) 'Chemokines accentuating protumoral activities in oral cancer microenvironment possess an imperious stratagem for therapeutic resolutions', *Oral Oncology*, 60, pp. 8–17. doi: 10.1016/j.oraloncology.2016.06.008.

Panicker, G., Meadows, K. S., Lee, D. R., Nisenbaum, R. and Unger, E. R. (2007) 'Effect of storage temperatures on the stability of cytokines in cervical mucous', *Cytokine*, 37(2), pp. 176–179. doi: 10.1016/j.cyto.2007.03.006.

Pankov, R. and Yamada, K. M. (2002) 'Fibronectin at a glance.', *Journal of cell science*, 115(Pt 20), pp. 3861–3. Available at: http://www.ncbi.nlm.nih.gov/pubmed/12244123 (Accessed: 11 December 2017).

Papagerakis, S., Pannone, G., Zheng, L., About, I., Taqi, N., Nguyen, N. P. T., Matossian, M., McAlpin, B., Santoro, A., McHugh, J., Prince, M. E. and Papagerakis, P. (2014) 'Oral epithelial stem cells - implications in normal development and cancer metastasis.', *Experimental cell research*. NIH Public Access, 325(2), pp. 111–29. doi: 10.1016/j.yexcr.2014.04.021.

Park, J. and Bryers, J. D. (2013) 'Chemokine programming dendritic cell antigen response: part II - programming antigen presentation to T lymphocytes by partially maintaining immature dendritic cell phenotype.', *Immunology*. Wiley-Blackwell, 139(1), pp. 88–99. doi: 10.1111/imm.12059.

Peh, S. C., Kim, L. H. and Poppema, S. (2001) 'TARC, a CC chemokine, is frequently expressed in classic Hodgkin's lymphoma but not in NLP Hodgkin's lymphoma, T-cell-rich B-cell lymphoma, and most cases of anaplastic large cell lymphoma.', *The American journal of surgical pathology*, 25(7), pp. 925–9. Available at: http://www.ncbi.nlm.nih.gov/pubmed/11420464 (Accessed: 9 August 2018).

Peterson, F. C., Elgin, E. S., Nelson, T. J., Zhang, F., Hoeger, T. J., Linhardt, R. J. and Volkman, B. F. (2004) 'Identification and Characterization of a Glycosaminoglycan Recognition Element of the C Chemokine Lymphotactin', *Journal of Biological Chemistry*. American Society for Biochemistry and Molecular Biology, 279(13), pp. 12598–12604. doi: 10.1074/jbc.M311633200.

Plow, E. F., Haas, T. A., Zhang, L., Loftus, J. and Smith, J. W. (2000) 'Ligand Binding to Integrins', *Journal of Biological Chemistry*, 275(29), pp. 21785–21788. doi: 10.1074/jbc.R000003200.

Popple, A., Durrant, L. G., Spendlove, I., Rolland, P., Scott, I. V, Deen, S. and Ramage, J. M. (2012) 'The chemokine, CXCL12, is an independent predictor of poor survival in ovarian cancer', *British Journal of Cancer*, 106(7), pp. 1306–1313. doi: 10.1038/bjc.2012.49.

Prajapati, P. and Lambert, D. W. (2016) 'Cancer-associated fibroblasts – Not-so-

innocent bystanders in metastasis to bone?', *Journal of Bone Oncology*. Elsevier, 5(3), pp. 128–131. doi: 10.1016/J.JBO.2016.03.008.

Prasad, G. and McCullough, M. (2013) 'Chemokines and cytokines as salivary biomarkers for the early diagnosis of oral cancer', *Int J Dent*. Hindawi Publishing Corporation, 2013, p. 813756. doi: 10.1155/2013/813756.

Qian, Y., Wang, Y., Li, D.-S., Zhu, Y.-X., Lu, Z.-W., Ji, Q.-H. and Yang, G. (2014) 'The chemokine receptor-CXCR2 plays a critical role in the invasion and metastases of oral squamous cell carcinoma *in vitro* and *in vivo*', *Journal of Oral Pathology & Medicine*, 43(9), pp. 658–666. doi: 10.1111/jop.12189.

Raghuraman, H. and Chattopadhyay, A. (2006) 'Effect of ionic strength on folding and aggregation of the hemolytic peptide melittin in solution', *Biopolymers*, 83(2), pp. 111–121. doi: 10.1002/bip.20536.

Rajagopalan, L. and Rajarathnam, K. (2006) 'Structural basis of chemokine receptor function--a model for binding affinity and ligand selectivity.', *Bioscience reports*. NIH Public Access, 26(5), pp. 325–39. doi: 10.1007/s10540-006-9025-9.

Ram, H., Sarkar, J., Kumar, H., Konwar, R., Bhatt, M. L. B. and Mohammad, S. (2011) 'Oral cancer: risk factors and molecular pathogenesis.', *Journal of maxillofacial and oral surgery*. Springer, 10(2), pp. 132–7. doi: 10.1007/s12663-011-0195-z.

Ramos, C. R. R., Abreu, P. A. E., Nascimento, A. L. T. O. and Ho, P. L. (2004) 'A high-copy T7 Escherichia coli expression vector for the production of recombinant proteins with a minimal N-terminal His-tagged fusion peptide.', *Brazilian journal of medical and biological research = Revista brasileira de pesquisas medicas e biologicas*, 37(8), pp. 1103–9. doi: /S0100-879X2004000800001.

Räsänen, K. and Vaheri, A. (2010) 'Activation of fibroblasts in cancer stroma', *Experimental Cell Research*, 316(17), pp. 2713–2722. doi: 10.1016/j.yexcr.2010.04.032.

Ravindran, A., Sawant, K. V, Sarmiento, J., Navarro, J. and Rajarathnam, K. (2013) 'Chemokine CXCL1 dimer is a potent agonist for the CXCR2 receptor.', *The Journal of biological chemistry*. American Society for Biochemistry and Molecular Biology, 288(17), pp. 12244–52. doi: 10.1074/jbc.M112.443762.

Rehman, A. O. and Wang, C. (2009) 'CXCL12/SDF-1 alpha activates NF-kappaB and promotes oral cancer invasion through the Carma3/Bcl10/Malt1 complex', *International Journal of Oral Science*, 1(3), pp. 105–118. doi: 10.4248/IJOS.09059.

Ricard-Blum, S. (2011) 'The Collagen Family', *Cold Spring Harbor Perspectives in Biology*. Cold Spring Harbor Laboratory Press, 3(1), pp. 1–19. doi: 10.1101/cshperspect.a004978.

Robichon, C., Luo, J., Causey, T. B., Benner, J. S. and Samuelson, J. C. (2011) 'Engineering Escherichia coli BL21(DE3) Derivative Strains To Minimize E. coli Protein Contamination after Purification by Immobilized Metal Affinity Chromatography', *Applied and Environmental Microbiology*, 77(13), pp. 4634–4646. doi: 10.1128/AEM.00119-11.

Robinson, C. R. and Sauer, R. T. (1998) 'Optimizing the stability of single-chain proteins by linker length and composition mutagenesis.', *Proceedings of the National Academy of Sciences of the United States of America*, 95(11), pp. 5929–34. Available at: http://www.ncbi.nlm.nih.gov/pubmed/9600894 (Accessed: 11 August 2017).

Rodier, F. and Campisi, J. (2011) 'Four faces of cellular senescence.', *The Journal of cell biology*. Rockefeller University Press, 192(4), pp. 547–56. doi: 10.1083/jcb.201009094.

Rodríguez-Frade, J. M., Mellado, M. and Martínez-A, C. (2001) 'Chemokine receptor dimerization: two are better than one.', *Trends in immunology*, 22(11), pp. 612–7. Available at: http://www.ncbi.nlm.nih.gov/pubmed/11698222 (Accessed: 10 December 2017).

Rodríguez-Frade, J. M., Muñoz, L. M., Holgado, B. L. and Mellado, M. (2009) 'Chemokine Receptor Dimerization and Chemotaxis', in *Methods in molecular biology (Clifton, N.J.)*, pp. 179–198. doi: 10.1007/978-1-60761-198-1_12.

Rosano, G. L. and Ceccarelli, E. A. (2014) 'Recombinant protein expression in Escherichia coli: advances and challenges.', *Frontiers in microbiology*. Frontiers Media SA, 5, p. 172. doi: 10.3389/fmicb.2014.00172.

Ross, D. J., Strieter, R. M., Fishbein, M. C., Ardehali, A. and Belperio, J. A. (2012) 'Type I immune response cytokine?chemokine cascade is associated with pulmonary arterial hypertension', *The Journal of Heart and Lung Transplantation*, 31(8), pp. 865–873. doi: 10.1016/j.healun.2012.04.008.

Round, J. (2007) 'Calcium flux: Indo-1 loading and sample staining procedure for simultaneous measurement of intracellular Ca2+', *Protocol Exchange*. doi: 10.1038/nprot.2007.66.

Roy, S., Bingle, L., Marshall, J. F., Bass, R., Ellis, V., Speight, P. M. and Whawell, S. A. (2011) 'The role of α9β1 integrin in modulating epithelial cell behaviour', *Journal of Oral Pathology and Medicine*, 40(10), pp. 755–761. doi: 10.1111/j.1600-0714.2011.01050.x.

Rubie, C., Frick, V., Ghadjar, P., Wagner, M., Grimm, H., Vicinus, B., Justinger, C., Graeber, S. and Schilling, M. K. (2010) 'CCL20/CCR6 expression profile in pancreatic cancer', *Journal of Translational Medicine*, 8(1), p. 45. doi: 10.1186/1479-5876-8-45.

Rucci, N. (2008) 'Molecular biology of bone remodelling.', *Clinical cases in mineral and bone metabolism : the official journal of the Italian Society of Osteoporosis, Mineral Metabolism, and Skeletal Diseases*. CIC Edizioni Internazionali, 5(1), pp. 49–56. Available at: http://www.ncbi.nlm.nih.gov/pubmed/22460846 (Accessed: 23 June 2017).

Ruhland, M. K., Loza, A. J., Capietto, A.-H., Luo, X., Knolhoff, B. L., Flanagan, K. C., Belt, B. A., Alspach, E., Leahy, K., Luo, J., Schaffer, A., Edwards, J. R., Longmore, G., Faccio, R., DeNardo, D. G. and Stewart, S. A. (2016) 'Stromal senescence establishes an immunosuppressive microenvironment that drives tumorigenesis', *Nature Communications*. Nature Publishing Group, 7, p. 11762. doi: 10.1038/ncomms11762.

Saccani, A., Saccani, S., Orlando, S., Sironi, M., Bernasconi, S., Ghezzi, P., Mantovani, A. and Sica, A. (2000) 'Redox regulation of chemokine receptor expression.', *Proceedings of the National Academy of Sciences of the United States of America*. National Academy of Sciences, 97(6), pp. 2761–6. Available at: http://www.ncbi.nlm.nih.gov/pubmed/10716998 (Accessed: 11 February 2018).

Sahingur, S. E. and Yeudall, W. A. (2015) 'Chemokine function in periodontal disease and oral cavity cancer', *Frontiers in Immunology*. Frontiers Media SA, 6(MAY), p. 214. doi: 10.3389/fimmu.2015.00214.

Saintigny, P. *et al.* (2013) 'CXCR2 expression in tumor cells is a poor prognostic factor and promotes invasion and metastasis in lung adenocarcinoma.', *Cancer research*. NIH Public Access, 73(2), pp. 571–82. doi: 10.1158/0008-5472.CAN-12-0263.

Salanga, C. L., O'Hayre, M. and Handel, T. (2009) 'Modulation of chemokine receptor activity through dimerization and crosstalk.', *Cellular and molecular life sciences : CMLS*. NIH Public Access, 66(8), pp. 1370–86. doi: 10.1007/s00018-008-8666-1.

Sanchez-Lugo, Y. E., Perez-Trujillo, J. J., Gutierrez-Puente, Y., Garcia-Garcia, A., Rodriguez-Rocha, H., Barboza-Quintana, O., Mu?oz-Maldonado, G. E., Saucedo-Cardenas, O., de Oca-Luna, R. M. and Loera-Arias, M. J. (2015) 'CXCL10/XCL1 fusokine elicits in vitro and in vivo chemotaxis', *Biotechnology Letters*, 37(4), pp. 779–785. doi: 10.1007/s10529-014-1746-4.

Sarvaiya, P. J., Guo, D., Ulasov, I., Gabikian, P. and Lesniak, M. S. (2013) 'Chemokines in tumor progression and metastasis.', *Oncotarget*. Impact Journals, LLC, 4(12), pp. 2171–85. doi: 10.18632/oncotarget.1426.

Sasisekharan, R., Raman, R. and Prabhakar, V. (2006) 'Glycomics Approach To Structure-Function Relationships of Glycosaminoglycans', *Annual Review of Biomedical Engineering*, 8(1), pp. 181–231. doi: 10.1146/annurev.bioeng.8.061505.095745.

Sathiyasekar, A. C., Chandrasekar, P., Pakash, A., Kumar, K. U. G. and Jaishlal, M. S. (2016) 'Overview of immunology of oral squamous cell carcinoma.', *Journal of pharmacy & bioallied sciences*. Wolters Kluwer -- Medknow Publications, 8(Suppl 1), pp. S8–S12. doi: 10.4103/0975-7406.191974.

Sauer, R. T., Cordes, M. H. J., Burton, R. E., Walsh, N. P. and McKnight, C. J. (2000) 'An evolutionary bridge to a new protein fold', *Nature Structural Biology*. Nature Publishing Group, 7(12), pp. 1129–1132. doi: 10.1038/81985.

Scala, S., Ottaiano, A., Ascierto, P. A., Cavalli, M., Simeone, E., Giuliano, P., Napolitano, M., Franco, R., Botti, G. and Castello, G. (2005) 'Expression of CXCR4 Predicts Poor Prognosis in Patients with Malignant Melanoma', *Clinical Cancer Research*, 11(5), pp. 1835–1841. doi: 10.1158/1078-0432.CCR-04-1887.

Schioppa, T., Uranchimeg, B., Saccani, A., Biswas, S. K., Doni, A., Rapisarda, A., Bernasconi, S., Saccani, S., Nebuloni, M., Vago, L., Mantovani, A., Melillo, G. and Sica, A. (2003) 'Regulation of the Chemokine Receptor CXCR4 by Hypoxia', *Journal of Experimental Medicine*. Rockefeller University Press, 198(9), pp. 1391–1402. doi: 10.1084/JEM.20030267.

Schmittgen, T. D. and Livak, K. J. (2008) 'Analyzing real-time PCR data by the comparative CT method', *Nature Protocols*. Nature Publishing Group, 3(6), pp. 1101–1108. doi: 10.1038/nprot.2008.73.

Scholten, D., Canals, M., Wijtmans, M., de Munnik, S., Nguyen, P., Verzijl, D., de Esch, I., Vischer, H., Smit, M. and Leurs, R. (2012) 'Pharmacological characterization of a small-molecule agonist for the chemokine receptor CXCR3', *British Journal of Pharmacology*, 166(3), pp. 898–911. doi: 10.1111/j.1476-5381.2011.01648.x.

Schrevel, M., Karim, R., ter Haar, N. T., van der Burg, S. H., Trimbos, J. B. M. Z., Fleuren, G. J., Gorter, A. and Jordanova, E. S. (2012) 'CXCR7 expression is associated with disease-free and disease-specific survival in cervical cancer patients', *British Journal of Cancer*. Nature Publishing Group, 106(9), pp. 1520–1525. doi: 10.1038/bjc.2012.110.

Segerer, S., Cui, Y., Eitner, F., Goodpaster, T., Hudkins, K. L., Mack, M., Cartron, J.-P. P., Colin, Y., Schlondorff, D. and Alpers, C. E. (2001) 'Expression of chemokines and chemokine receptors during human renal transplant rejection', *American Journal of Kidney Diseases*. National Kidney Foundation, Inc, 37(3), pp. 518–531. doi: 10.1053/ajkd.2001.22076.

Shan, L., Qiao, X., Oldham, E., Catron, D., Kaminski, H., Lundell, D., Zlotnik, A., Gustafson, E. and Hedrick, J. A. (2000) 'Identification of viral macrophage inflammatory protein (vMIP)-II as a ligand for GPR5/XCR1.', *Biochemical and biophysical research communications*, 268(3), pp. 938–941. doi: 10.1006/bbrc.2000.2235.

Shang, Z. J., Liu, K. and Shao, Z. (2009) 'Expression of chemokine receptor CCR7 is associated with cervical lymph node metastasis of oral squamous cell carcinoma', *Oral Oncology*, 45(6), pp. 480–485. doi: 10.1016/j.oraloncology.2008.06.005.

Shanmugam, N., Reddy, M. A., Guha, M. and Natarajan, R. (2003) 'High glucose-induced expression of proinflammatory cytokine and chemokine genes in monocytic cells.', *Diabetes*, 52(5), pp. 1256–1264. Available at: http://www.ncbi.nlm.nih.gov/pubmed/12716761 (Accessed: 23 June 2017).

Shen, B., Delaney, M. K. and Du, X. (2012) 'Inside-out, outside-in, and inside-outside-in: G protein signaling in integrin-mediated cell adhesion, spreading, and retraction.', *Current opinion in cell biology*. NIH Public Access, 24(5), pp. 600–6. doi: 10.1016/j.ceb.2012.08.011.

Shen, Y., Shen, R., Ge, L., Zhu, Q. and Li, F. (2012) 'Fibrillar type I collagen matrices enhance metastasis/invasion of ovarian epithelial cancer via β1 integrin and PTEN signals', *International Journal of Gynecological Cancer*, 22(8), pp. 1316–1324. doi: 10.1097/IGC.0b013e318263ef34.

Sheu, B.-C., Chang, W.-C., Cheng, C.-Y., Lin, H.-H., Chang, D.-Y. and Huang, S.-C. (2008) 'Cytokine regulation networks in the cancer microenvironment.', *Frontiers in bioscience : a journal and virtual library*, 1(12), pp. 6255–6268. Available at: http://www.ncbi.nlm.nih.gov/pubmed/18508658 (Accessed: 23 June 2017).

Shiga, K., Hara, M., Nagasaki, T., Sato, T., Takahashi, H. and Takeyama, H. (2015) 'Cancer-Associated Fibroblasts: Their Characteristics and Their Roles in Tumor Growth.', *Cancers*. Multidisciplinary Digital Publishing Institute (MDPI), 7(4),

pp. 2443–58. doi: 10.3390/cancers7040902.

El Shikh, M. E. M., El Sayed, R. M., Sukumar, S., Szakal, A. K. and Tew, J. G. (2010) 'Activation of B cells by antigens on follicular dendritic cells.', *Trends in immunology*. NIH Public Access, 31(6), pp. 205–11. doi: 10.1016/j.it.2010.03.002.

Shimizu, N., Tanaka, A., Oue, A., Mori, T., Ohtsuki, T., Apichartpiyakul, C., Uchiumi, H., Nojima, Y. and Hoshino, H. (2009) 'Broad usage spectrum of G protein-coupled receptors as coreceptors by primary isolates of HIV', *AIDS*, 27(7), pp. 761–769. doi: 10.1097/QAD.0b013e328326cc0d.

Shimoda, M., Mellody, K. T. and Orimo, A. (2010) 'Carcinoma-associated fibroblasts are a rate-limiting determinant for tumour progression.', *Seminars in cell & developmental biology*. Elsevier, 21(1), pp. 19–25. doi: 10.1016/j.semcdb.2009.10.002.

Shintani, S., Ishikawa, T., Nonaka, T., Li, C., Nakashiro, K., Wong, D. T. W. and Hamakawa, H. (2004) 'Growth-Regulated Oncogene-1 Expression Is Associated with Angiogenesis and Lymph Node Metastasis in Human Oral Cancer', *Oncology*, 66(4), pp. 316–322. doi: 10.1159/000078333.

Shoulders, M. D. and Raines, R. T. (2009) 'Collagen Structure and Stability', *Annual Review of Biochemistry*, 78(1), pp. 929–958. doi: 10.1146/annurev.biochem.77.032207.120833.

Silva, S. D. da, Ferlito, A., Takes, R. P., Brakenhoff, R. H., Valentin, M. D., Woolgar, J. A., Bradford, C. R., Rodrigo, J. P., Rinaldo, A., Hier, M. P. and Kowalski, L. P. (2011) 'Advances and applications of oral cancer basic research', *Oral Oncology*, 47(9), pp. 783–791. doi: 10.1016/j.oraloncology.2011.07.004.

Simonetti, O., Goteri, G., Lucarini, G., Filosa, A., Pieramici, T., Rubini, C., Biagini, G. and Offidani, A. (2006) 'Potential role of CCL27 and CCR10 expression in melanoma progression and immune escape', *European Journal of Cancer*, 42(8), pp. 1181–1187. doi: 10.1016/j.ejca.2006.01.043.

Singh, P., Carraher, C. and Schwarzbauer, J. E. (2010) 'Assembly of Fibronectin Extracellular Matrix', *Annual Review of Cell and Developmental Biology*, 26(1), pp. 397–419. doi: 10.1146/annurev-cellbio-100109-104020.

Slettenaar, V. I. F. F. and Wilson, J. L. (2006) 'The chemokine network: A target in cancer biology?', *Advanced Drug Delivery Reviews*, 58(8), pp. 962–974. doi: 10.1016/j.addr.2006.03.012.

Smith, J. S. and Rajagopal, S. (2016) 'The β-Arrestins: Multifunctional Regulators of G Protein-coupled Receptors', *Journal of Biological Chemistry*, 291(17), pp. 8969–8977. doi: 10.1074/jbc.R115.713313.

Soares, M. Q. S., Mendonça, J. A., Morais, M. O., Leles, C. R., Batista, A. C. and Mendonça, E. F. (2015) 'E-cadherin, β-catenin, and α2β1 and α3β1 integrin expression in primary oral squamous cell carcinoma and its regional metastasis.', *Histology and histopathology*, 30(10), pp. 1213–1222. doi: 10.14670/HH-11-616.

Soltany-Rezaee-Rad, M., Sepehrizadeh, Z., Mottaghi-Dastjerdi, N., Yazdi, M. T. and

Seyatesh, N. (2015) 'Comparison of SYBR Green and TaqMan real-time PCR methods for quantitative detection of residual CHO host-cell DNA in biopharmaceuticals', *Biologicals*. Academic Press, 43(2), pp. 130–135. doi: 10.1016/J.BIOLOGICALS.2014.11.004.

Sørensen, H. P. and Mortensen, K. K. (2005) 'Soluble expression of recombinant proteins in the cytoplasm of Escherichia coli.', *Microbial cell factories*. BioMed Central, 4(1), p. 1. doi: 10.1186/1475-2859-4-1.

Sosa-Costa, A., Isern de Val, S., Sevilla-Movilla, S., Borgman, K. J. E., Manzo, C., Teixidó, J. and Garcia-Parajo, M. F. (2016) 'Lateral Mobility and Nanoscale Spatial Arrangement of Chemokine-activated α4β1 Integrins on T Cells.', *The Journal of biological chemistry*. American Society for Biochemistry and Molecular Biology, 291(40), pp. 21053–21062. doi: 10.1074/jbc.M116.733709.

Speyer, C. L. and Ward, P. A. (2011) 'Role of Endothelial Chemokines and Their Receptors during Inflammation', *Journal of Investigative Surgery*, 24(1), pp. 18–27. doi: 10.3109/08941939.2010.521232.

Springael, J.-Y., Urizar, E. and Parmentier, M. (2005) 'Dimerization of chemokine receptors and its functional consequences', *Cytokine & Growth Factor Reviews*, 16(6), pp. 611–623. doi: 10.1016/j.cytogfr.2005.05.005.

Sriram, G., Bigliardi, P. L. and Bigliardi-Qi, M. (2015) 'Fibroblast heterogeneity and its implications for engineering organotypic skin models in vitro', *European Journal of Cell Biology*. Urban & Fischer, 94(11), pp. 483–512. doi: 10.1016/J.EJCB.2015.08.001.

Steen, A., Larsen, O., Thiele, S. and Rosenkilde, M. M. (2014) 'Biased and g protein-independent signaling of chemokine receptors.', *Frontiers in immunology*. Frontiers Media SA, 5, p. 277. doi: 10.3389/fimmu.2014.00277.

Steinmetz, E. J. and Auldridge, M. E. (2017) 'Screening Fusion Tags for Improved Recombinant Protein Expression in *E. coli* with the Expresso® Solubility and Expression Screening System', in *Current Protocols in Protein Science*. NJ, NJ, USA: John Wiley & Sons, Inc., p. 5.27.1-5.27.20. doi: 10.1002/cpps.39.

Studier, F. W. (2014) 'Stable Expression Clones and Auto-Induction for Protein Production in E. coli', in *Methods in molecular biology (Clifton, N.J.)*, pp. 17–32. doi: 10.1007/978-1-62703-691-7_2.

Sugimoto, H., Mundel, T. M., Kieran, M. W. and Kalluri, R. (2006) 'Identification of fibroblast heterogeneity in the tumor microenvironment.', *Cancer biology & therapy*, 5(12), pp. 1640–6. Available at: http://www.ncbi.nlm.nih.gov/pubmed/17106243 (Accessed: 24 March 2018).

Sun, Q., Tyler, R. C., Volkman, B. F. and Julian, R. R. (2011) 'Dynamic interchanging native states of lymphotactin examined by SNAPP-MS', *Journal of the American Society for Mass Spectrometry*, 22(3), pp. 399–407. doi: 10.1007/s13361-010-0042-3.

Sun, X., Cheng, G., Hao, M., Zheng, J., Zhou, X., Zhang, J., Taichman, R. S., Pienta, K. J. and Wang, J. (2010) 'CXCL12 / CXCR4 / CXCR7 chemokine axis and cancer progression.', *Cancer metastasis reviews*. NIH Public Access, 29(4), pp.

709–22. doi: 10.1007/s10555-010-9256-x.

Sun, Y., Mao, X., Fan, C., Liu, C., Guo, A., Guan, S., Jin, Q., Li, B., Yao, F. and Jin, F. (2014) 'CXCL12-CXCR4 axis promotes the natural selection of breast cancer cell metastasis', *Tumor Biology*, 35(8), pp. 7765–7773. doi: 10.1007/s13277-014-1816-1.

Szpakowska, M., Fievez, V., Arumugan, K., van Nuland, N., Schmit, J.-C. and Chevigné, A. (2012) 'Function, diversity and therapeutic potential of the N-terminal domain of human chemokine receptors', *Biochemical Pharmacology*, 84(10), pp. 1366–1380. doi: 10.1016/j.bcp.2012.08.008.

Tamgüney, G., Van Snick, J. and Fickenscher, H. (2004) 'Autocrine stimulation of rhadinovirus-transformed T cells by the chemokine CCL1/I-309', *Oncogene*, 23(52), pp. 8475–8485. doi: 10.1038/sj.onc.1207903.

Tang, T., Xia, Q. and Xi, M. (2016) 'CXC chemokine receptor 7 expression in cervical intraepithelial neoplasia.', *Biomedical reports*. Spandidos Publications, 4(1), pp. 63–67. doi: 10.3892/br.2015.529.

Teng, F., Tian, W.-Y., Wang, Y.-M., Zhang, Y.-F., Guo, F., Zhao, J., Gao, C. and Xue, F.-X. (2016) 'Cancer-associated fibroblasts promote the progression of endometrial cancer via the SDF-1/CXCR4 axis.', *Journal of hematology & oncology*. BioMed Central, 9, p. 8. doi: 10.1186/s13045-015-0231-4.

Thomas, G. J., Lewis, M. P., Whawell, S. a, Russell, a, Sheppard, D., Hart, I. R., Speight, P. M. and Marshall, J. F. (2001) 'Expression of the alphavbeta6 integrin promotes migration and invasion in squamous carcinoma cells.', *The Journal of investigative dermatology*, 117(1), pp. 67–73. doi: 10.1046/j.0022-202x.2001.01379.x.

Thuwajit, C., Ferraresi, A., Titone, R., Thuwajit, P. and Isidoro, C. (2017) 'The metabolic cross-talk between epithelial cancer cells and stromal fibroblasts in ovarian cancer progression: Autophagy plays a role', *Medicinal Research Reviews*. doi: 10.1002/med.21473.

Todd, J. R., Ryall, K. A., Vyse, S., Wong, J. P., Natrajan, R. C., Yuan, Y., Tan, A.-C. and Huang, P. H. (2016) 'Systematic analysis of tumour cell-extracellular matrix adhesion identifies independent prognostic factors in breast cancer.', *Oncotarget*. Impact Journals, LLC, 7(39), pp. 62939–62953. doi: 10.18632/oncotarget.11307.

Tomasek, J. J., Gabbiani, G., Hinz, B., Chaponnier, C. and Brown, R. A. (2002) 'Myofibroblasts and mechano-regulation of connective tissue remodelling', *Nature Reviews Molecular Cell Biology*, 3(5), pp. 349–363. doi: 10.1038/nrm809.

Tripp, R. A., Jones, L. P., Haynes, L. M., Zheng, H., Murphy, P. M. and Anderson, L. J. (2001) 'CX3C chemokine mimicry by respiratory syncytial virus G glycoprotein.', *Nature Immunology*, 2(8), pp. 732–738. doi: 10.1038/90675.

Tropea, J. E., Cherry, S. and Waugh, D. S. (2009) 'Expression and Purification of Soluble His6-Tagged TEV Protease', in *Methods in molecular biology (Clifton, N.J.)*, pp. 297–307. doi: 10.1007/978-1-59745-196-3_19.

Tshering Vogel, D. W., Zbaeren, P. and Thoeny, H. C. (2010) 'Cancer of the oral cavity

and oropharynx.', *Cancer imaging : the official publication of the International Cancer Imaging Society*. BioMed Central, 10(1), pp. 62–72. doi: 10.1102/1470-7330.2010.0008.

Tsuzuki, H., Takahashi, N., Kojima, A., Narita, N., Sunaga, H., Takabayashi, T. and Fujieda, S. (2006) 'Oral and oropharyngeal squamous cell carcinomas expressing CCR7 have poor prognoses', *Auris Nasus Larynx*. Elsevier, 33(1), pp. 37–42. Available at: http://www.ncbi.nlm.nih.gov/pubmed/16223574 (Accessed: 4 August 2018).

Tuinstra, R. L., Peterson, F. C., Elgin, E. S., Pelzek, A. J. and Volkman, B. F. (2007) 'An engineered second disulfide bond restricts lymphotactin/XCL1 to a chemokine-like conformation with XCR1 agonist activity', *Biochemistry*, 46(10), pp. 2564–2573. doi: 10.1021/bi602365d.

Tuinstra, R. L., Peterson, F. C., Kutlesa, S., Elgin, E. S., Kron, M. A. and Volkman, B. F. (2008) 'Interconversion between two unrelated protein folds in the lymphotactin native state.', *Proceedings of the National Academy of Sciences of the United States of America*, 105(13), pp. 5057–5062. doi: 10.1073/pnas.0709518105.

Tyler, R. C., Murray, N. J., Peterson, F. C. and Volkman, B. F. (2011) 'Native-state interconversion of a metamorphic protein requires global unfolding', *Biochemistry*, 50(33), pp. 7077–7079. doi: 10.1021/bi200750k.

Uchida, D., Begum, N.-M. M., Almofti, A., Nakashiro, K., Kawamata, H., Tateishi, Y., Hamakawa, H., Yoshida, H. and Sato, M. (2003) 'Possible role of stromal-cell-derived factor-1/CXCR4 signaling on lymph node metastasis of oral squamous cell carcinoma', *Experimental Cell Research*, 290(2), pp. 289–302. doi: 10.1016/S0014-4827(03)00344-6.

Vaahtomeri, K., Brown, M., Hauschild, R., De Vries, I., Leithner, A. F., Mehling, M., Kaufmann, W. A. and Sixt, M. (2017) 'Locally Triggered Release of the Chemokine CCL21 Promotes Dendritic Cell Transmigration across Lymphatic Endothelia', *Cell Reports*, 19(5), pp. 902–909. doi: 10.1016/j.celrep.2017.04.027.

Vaheri, A., Enzerink, A., Räsänen, K. and Salmenperä, P. (2009) 'Nemosis, a novel way of fibroblast activation, in inflammation and cancer', *Experimental Cell Research*, 315(10), pp. 1633–1638. doi: 10.1016/j.yexcr.2009.03.005.

Vartanian, J. G., Carvalho, A. L., de Araújo Filho, M. J., Junior, M. H., Magrin, J. and Kowalski, L. P. (2004) 'Predictive factors and distribution of lymph node metastasis in lip cancer patients and their implications on the treatment of the neck.', *Oral oncology*, 40(2), pp. 223–227. Available at: http://www.ncbi.nlm.nih.gov/pubmed/14693248 (Accessed: 23 June 2017).

De Veirman, K., Rao, L., De Bruyne, E., Menu, E., Van Valckenborgh, E., Van Riet, I., Frassanito, M. A., Di Marzo, L., Vacca, A. and Vanderkerken, K. (2014) 'Cancer associated fibroblasts and tumor growth: focus on multiple myeloma.', *Cancers*. Multidisciplinary Digital Publishing Institute (MDPI), 6(3), pp. 1363–81. doi: 10.3390/cancers6031363.

Vela, M., Aris, M., Llorente, M., Garcia-Sanz, J. A. and Kremer, L. (2015) 'Chemokine receptor-specific antibodies in cancer immunotherapy: achievements and challenges.', *Frontiers in immunology*. Frontiers Media SA, 6, p. 12. doi:

10.3389/fimmu.2015.00012.

Velarde, M. C., Demaria, M. and Campisi, J. (2013) 'Senescent cells and their secretory phenotype as targets for cancer therapy.', *Interdisciplinary topics in gerontology*. NIH Public Access, 38, pp. 17–27. doi: 10.1159/000343572.

Vines, C. M., Revankar, C. M., Maestas, D. C., LaRusch, L. L., Cimino, D. F., Kohout, T. A., Lefkowitz, R. J. and Prossnitz, E. R. (2003) '*N* -Formyl Peptide Receptors Internalize but Do Not Recycle in the Absence of Arrestins', *Journal of Biological Chemistry*, 278(43), pp. 41581–41584. doi: 10.1074/jbc.C300291200.

Volkman, B. F., Liu, T. Y. and Peterson, F. C. (2009) *Chapter 3 Lymphotactin Structural Dynamics*, *Methods in Enzymology*. NIH Public Access. doi: 10.1016/S0076-6879(09)05403-2.

Wagner, P. L., Hyjek, E., Vazquez, M. F., Meherally, D., Liu, Y. F., Chadwick, P. A., Rengifo, T., Sica, G. L., Port, J. L., Lee, P. C., Paul, S., Altorki, N. K. and Saqi, A. (2009) 'CXCL12 and CXCR4 in adenocarcinoma of the lung: Association with metastasis and survival', *The Journal of Thoracic and Cardiovascular Surgery*, 137(3), pp. 615–621. doi: 10.1016/j.jtcvs.2008.07.039.

Wang, C.-R. C.-R., Liu, M.-F., Huang, Y.-H. and Chen, H.-C. (2004) 'Up-regulation of XCR1 expression in rheumatoid joints.', *Rheumatology (Oxford, England)*, 43(5), pp. 569–573. doi: 10.1093/rheumatology/keh147.

Wang, J. D., Nonomura, N., Takahara, S., Li, B. S., Azuma, H., Ichimaru, N., Kokado, Y., Matsumiya, K., Miki, T., Suzuki, S. and Okuyama, A. (1998) 'Lymphotactin: A key regulator of lymphocyte trafficking during acute graft rejection', *Immunology*. Wiley-Blackwell, 95(1), pp. 56–61. doi: 10.1046/j.1365-2567.1998.00570.x.

Wang, J., Zhuang, Z.-G., Xu, S.-F., He, Q., Shao, Y.-G., Ji, M., Yang, L. and Bao, W. (2015) 'Expression of CCL2 is significantly different in five breast cancer genotypes and predicts patient outcome.', *International journal of clinical and experimental medicine*. e-Century Publishing Corporation, 8(9), pp. 15684–91. Available at: http://www.ncbi.nlm.nih.gov/pubmed/26629063 (Accessed: 9 August 2018).

Wang, T., Han, S., Wu, Z., Han, Z., Yan, W., Liu, T., Wei, H., Song, D., Zhou, W., Yang, X. and Xiao, J. (2015) 'XCR1 promotes cell growth and migration and is correlated with bone metastasis in non-small cell lung cancer', *Biochemical and Biophysical Research Communications*, 464(2), pp. 635–641. doi: 10.1016/j.bbrc.2015.06.175.

Wang, T., Notta, F., Navab, R., Joseph, J., Ibrahimov, E., Xu, J., Zhu, C.-Q., Borgida, A., Gallinger, S. and Tsao, M.-S. (2017) 'Senescent Carcinoma-Associated Fibroblasts Upregulate IL8 to Enhance Prometastatic Phenotypes', *Molecular Cancer Research*, 15(1), pp. 3–14. doi: 10.1158/1541-7786.MCR-16-0192.

Wang, W.-J., Cai, G.-Y. and Chen, X.-M. (2017) 'Cellular senescence, senescence-associated secretory phenotype, and chronic kidney disease.', *Oncotarget*. Impact Journals, LLC, 8(38), pp. 64520–64533. doi: 10.18632/oncotarget.17327.

Wang, X., Kaczor-Urbanowicz, K. E. and Wong, D. T. W. (2017) 'Salivary biomarkers in

cancer detection.', *Medical oncology (Northwood, London, England)*. NIH Public Access, 34(1), p. 7. doi: 10.1007/s12032-016-0863-4.

Wang, Z., Liu, H., Shen, Z., Wang, X., Zhang, H., Qin, J., Xu, J., Sun, Y. and Qin, X. (2015) 'The prognostic value of CXC-chemokine receptor 2 (CXCR2) in gastric cancer patients', *BMC Cancer*, 15(1), p. 766. doi: 10.1186/s12885-015-1793-9.

Warburton, M., Omar Ali, H., Choon Liong, W., Martin Othusitse, A., Zaki Abdullah Zubir, A., Maddock, S. and Seng Wong, T. (2015) 'OneClick: A Program for Designing Focused Mutagenesis Experiments', *AIMS Bioengineering*, 2(3), pp. 126–143. doi: 10.3934/bioeng.2015.3.126.

Warnakulasuriya, S. (2009) 'Global epidemiology of oral and oropharyngeal cancer', *Oral Oncology*. Elsevier Ltd, 45(4–5), pp. 309–316. doi: 10.1016/j.oraloncology.2008.06.002.

Warner, K. A., Miyazawa, M., Cordeiro, M. M. R., Love, W. J., Pinsky, M. S., Neiva, K. G., Spalding, A. C. and Nör, J. E. (2008) 'Endothelial cells enhance tumor cell invasion through a crosstalk mediated by CXC chemokine signaling.', *Neoplasia (New York, N.Y.)*. Neoplasia Press, 10(2), pp. 131–139. Available at: http://www.ncbi.nlm.nih.gov/pubmed/18283335 (Accessed: 23 June 2017).

Wilen, C. B., Tilton, J. C., Doms, R. W., Walker, B., Mcmichael, A., Wilen, C. B., Tilton, J. C., Doms, R. W., Craigie, R., Bushman, F. D., Shaw, G. M. and Hunter, E. (2012) 'HIV : Cell Binding and Entry', *Cold Spring Harbor Perspectives in Medicine*, 2(8), pp. 1–14. doi: 10.1101/cshperspect.a006866.

Wiley, H. E., Gonzalez, E. B., Maki, W., Wu, M. -t. T. and Hwang, S. T. (2001) 'Expression of CC Chemokine Receptor-7 and Regional Lymph Node Metastasis of B16 Murine Melanoma', *JNCI Journal of the National Cancer Institute*, 93(21), pp. 1638–1643. doi: 10.1093/jnci/93.21.1638.

Wise, E. L., Duchesnes, C., da Fonseca, P. C. A., Allen, R. A., Williams, T. J. and Pease, J. E. (2007) 'Small Molecule Receptor Agonists and Antagonists of CCR3 Provide Insight into Mechanisms of Chemokine Receptor Activation', *Journal of Biological Chemistry*, 282(38), pp. 27935–27943. doi: 10.1074/jbc.M703255200.

Wörnle, M., Schmid, H., Merkle, M. and Banas, B. (2004) 'Effects of chemokines on proliferation and apoptosis of human mesangial cells.', *BMC nephrology*. BioMed Central, 5, p. 8. doi: 10.1186/1471-2369-5-8.

Wu, K., Yu, S., Liu, Q., Bai, X., Zheng, X. and Wu, K. (2017) 'The clinical significance of CXCL5 in non-small cell lung cancer', *OncoTargets and Therapy*, Volume 10, pp. 5561–5573. doi: 10.2147/OTT.S148772.

Xia, J., Chen, N., Hong, Y., Chen, X., Tao, X., Cheng, B. and Huang, Y. (2012) 'Expressions of CXCL12/CXCR4 in oral premalignant and malignant lesions', *Mediators of Inflammation*. Hindawi Publishing Corporation, 2012, p. 516395. doi: 10.1155/2012/516395.

Xia, J., Wang, J., Chen, N., Dai, Y., Hong, Y., Chen, X. and Cheng, B. (2011) 'Expressions of CXCR7/ligands may be involved in oral carcinogenesis', *Journal of Molecular Histology*, 42(2), pp. 175–180. doi: 10.1007/s10735-011-9322-x.

Xu, L. N., Xu, B. N., Cai, J., Yang, J. B. and Lin, N. (2013) 'Tumor-associated fibroblast-conditioned medium promotes tumor cell proliferation and angiogenesis', *Genetics and Molecular Research*, 12(4), pp. 5863–5871. doi: 10.4238/2013.November.22.14.

Yamazaki, C., Sugiyama, M., Ohta, T., Hemmi, H., Hamada, E., Sasaki, I., Fukuda, Y., Yano, T., Nobuoka, M., Hirashima, T., Iizuka, A., Sato, K., Tanaka, T., Hoshino, K. and Kaisho, T. (2013) 'Critical Roles of a Dendritic Cell Subset Expressing a Chemokine Receptor, XCR1', *The Journal of Immunology*, 190(12), pp. 6071–6082. doi: 10.4049/jimmunol.1202798.

Yan, R., Shuai, H., Luo, X., Wang, X. and Guan, B. (2017) 'The clinical and prognostic value of CXCL8 in cervical carcinoma patients: immunohistochemical analysis.', *Bioscience reports*. Portland Press Ltd, 37(5). doi: 10.1042/BSR20171021.

Yang, X. L., Qi, L. G., Lin, F. J. and Ou, Z. L. (2017) 'The role of the chemokine receptor XCR1 in breast cancer cells', *Breast Cancer: Targets and Therapy*, Volume 9, pp. 227–236. doi: 10.2147/BCTT.S126184.

Yang, Y., Du, L., Yang, X., Qu, A., Zhang, X., Zhou, C. and Wang, C. (2015) 'Aberrant CCR4 Expression Is Involved in Tumor Invasion of Lymph Node-Negative Human Gastric Cancer', *PLOS ONE*. Edited by C.-H. Tang, 10(3), p. e0120059. doi: 10.1371/journal.pone.0120059.

Yanru, W., Zhenyu, B., Zhengchuan, N., Qi, Q., Chunmin, L. and Weiqiang, Y. (2018) 'Transcriptomic analyses of chemokines reveal that down-regulation of XCR1 is associated with advanced hepatocellular carcinoma', *Biochemical and Biophysical Research Communications*, 496(4), pp. 1314–1321. doi: 10.1016/j.bbrc.2018.02.008.

Yao, L., Herlea-Pana, O., Heuser-Baker, J., Chen, Y. and Barlic-Dicen, J. (2014) 'Roles of the chemokine system in development of obesity, insulin resistance, and cardiovascular disease', *Journal of Immunology Research*. Hindawi Publishing Corporation, 2014(181450), pp. 1–11. doi: 10.1155/2014/181450.

Ying, J., Xu, Q., Zhang, G., Liu, B. and Zhu, L. (2012) 'The expression of CXCL12 and CXCR4 in gastric cancer and their correlation to lymph node metastasis', *Medical Oncology*, 29(3), pp. 1716–1722. doi: 10.1007/s12032-011-9990-0.

Yoshida, T., Imai, T., Kakizaki, M., Nishimura, M., Takagi, S. and Yoshie, O. (1998) 'Identification of single C motif-1/lymphotactin receptor XCR1', *Journal of Biological Chemistry*, 273(26), pp. 16551–16554. doi: 10.1074/jbc.273.26.16551.

Yoshida, T., Ishikawa, I., Ono, Y., Imai, T., Suzuki, R. and Yoshie, O. (1999) 'An activation-responsive element in single C motif-1/lymphotactin promoter is a site of constitutive and inducible DNA-protein interactions involving nuclear factor of activated T cell.', *Journal of immunology (Baltimore, Md. : 1950)*, 163, pp. 3295–3303.

Yoshie, O., Yoshida, T., Imai, T., Kakizaki, M., Nishimura, M. and Yoshie, O. (1995) 'Molecular cloning of a novel C or ?? type chemokine, SCM-1', *FEBS Letters*, 360(2), pp. 155–159. doi: 10.1016/0014-5793(95)00093-O.

You, J. S. and Jones, P. A. (2012) 'Cancer genetics and epigenetics: two sides of the same coin?', *Cancer cell*. NIH Public Access, 22(1), pp. 9–20. doi: 10.1016/j.ccr.2012.06.008.

Yu, J., Tao, S., Hu, P., Wang, R., Fang, C., Xu, Y., Qi, D., Wei, Z., Zhang, J. and Tan, Q. (2017) 'CCR7 promote lymph node metastasis via regulating VEGF-C/D-R3 pathway in lung adenocarcinoma.', *Journal of Cancer*. Ivyspring International Publisher, 8(11), pp. 2060–2068. doi: 10.7150/jca.19069.

Yuan, C., Liu, Z., Zou, N., Wang, Y. and Chen, Z. (2017) 'Relationship between expression of CXCR7 and NF-κB in breast cancer tissue and occurrence of breast cancer and lymphatic metastasis', *Saudi Journal of Biological Sciences*. Elsevier, 24(8), pp. 1767–1770. doi: 10.1016/J.SJBS.2017.11.009.

Yue, B. (2014) 'Biology of the extracellular matrix: an overview.', *Journal of glaucoma*. NIH Public Access, 23(8 Suppl 1), pp. S20-3. doi: 10.1097/IJG.0000000000000108.

Zhang, J., Liu, C., Mo, X., Shi, H. and Li, S. (2017) 'Mechanisms by which CXCR4/CXCL12 cause metastatic behavior in pancreatic cancer', *Oncology Letters*, 15(2), pp. 1771–1776. doi: 10.3892/ol.2017.7512.

Zhang, X., Qin, X., Qin, C. Y., Yin, Y., Chen, Y. and Zhu, H. (2013) 'Expression of monocyte chemoattractant protein-1 and CC chemokine receptor 2 in non-small cell lung cancer and its significance', *Cancer Immunology, Immunotherapy*, 62(3), pp. 563–570. doi: 10.1007/s00262-012-1361-y.

Zhang, X., Wang, Y., Cao, Y., Zhang, X. and Zhao, H. (2017) 'Increased CCL19 expression is associated with progression in cervical cancer.', *Oncotarget*. Impact Journals, LLC, 8(43), pp. 73817–73825. doi: 10.18632/oncotarget.17982.

Zhou, X., Fragala, M. S., McElhaney, J. E. and Kuchel, G. A. (2010) 'Conceptual and methodological issues relevant to cytokine and inflammatory marker measurements in clinical research', *Current Opinion in Clinical Nutrition and Metabolic Care*, 13(5), pp. 541–547. doi: 10.1097/MCO.0b013e32833cf3bc.

van Zijl, F., Krupitza, G. and Mikulits, W. (2011) 'Initial steps of metastasis: Cell invasion and endothelial transmigration', *Mutation Research/Reviews in Mutation Research*, 728(1–2), pp. 23–34. doi: 10.1016/j.mrrev.2011.05.002.

Zlotnik, A., Burkhardt, A. M. and Homey, B. (2011) 'Homeostatic chemokine receptors and organ-specific metastasis', *Nature Reviews Immunology*, 11(9), pp. 597–606. doi: 10.1038/nri3049.

Zlotnik, A. and Yoshie, O. (2012) 'The Chemokine Superfamily Revisited', *Immunity*, 36(5), pp. 705–716. doi: 10.1016/j.immuni.2012.05.008.

Zlotnik, A., Yoshie, O. and Nomiyama, H. (2006) 'The chemokine and chemokine receptor superfamilies and their molecular evolution.', *Genome biology*. BioMed Central, 7(12), p. 243. doi: 10.1186/gb-2006-7-12-243.

Zweemer, A. J. M., Toraskar, J., Heitman, L. H. and IJzerman, A. P. (2014) 'Bias in chemokine receptor signalling', *Trends in Immunology*, 35(6), pp. 243–252.

doi: 10.1016/j.it.2014.02.004.

APPENDICES

Appendix 1: List of reagents

List of Reagent	Catalogue #; Manufacturer details
1 kb DNA Ladder	Cat#: N3232L; New England Biolabs, Hitchin, UK
Adenine	Cat#: A8626; Sigma-Aldrich, Dorset, UK
Amphotericin B solution	Cat#: A2942; Sigma-Aldrich, Dorset, UK
Anti-alpha smooth muscle actin (α-SMA) [1A4] (FITC-conjugated)	Cat#: ab8211; Abcam, Cambridge, UK
Anti-XCR1 human antibody (extracellular domain) IHC-plus™ LS-A158 (human anti-rabbit)	Cat#: LS-A158-50; LifeSpan Bioscience Inc., WA, USA
Anti-XCL1/Lymphotactin antibody (clone 1E1) IHC-plus™ LS-B5938 (human anti-mouse)	Cat#: LS-B5938-50; LifeSpan Bioscience Inc., WA, USA
B2M probe (TaqMan Gene Expression Assays) [sequence not available]	Cat#:4331182; Life Technologies, Paisley, UK
CellTiter 96® Aqueous One Solution Cell Proliferation Reagent	Cat#: G3582; Promega, South Hampton, UK
Cholera toxin	Cat#: C8052; Sigma-Aldrich, Dorset, UK
Collagen Type IV from human cell culture	Cat#: C6745; Sigma-Aldrich®, Dorset, UK
Collagen, Type I solution from rat tail	Cat#: C3867; Sigma-Aldrich®, Dorset, UK
Dimethyl sulfoxide	Cat#: D8418; Sigma-Aldrich, Dorset, UK
Dulbecco's Modified Eagle Media (DMEM)	Cat#: D5546; Sigma-Aldrich, Dorset, UK
Dulbecco's Phosphate Buffered Saline with $MgCl_2$ and $CaCl_2$	Cat#: D8552; Sigma-Aldrich, Dorset, UK
Fibronectin bovine plasma	Cat#: F1141; Sigma-Aldrich®, Dorset, UK
Foetal Bovine Serum (FBS)	Cat#: F9665, Sigma-Aldrich, Dorset, UK
Goat anti-rabbit IgG (H+L) secondary antibody, Alexa Fluor® 488 conjugate	Cat#: A-11008; Life Technologies Ltd, Paisley, UK
Goat serum donor herd	Cat#:G6767; Sigma-Aldrich, Dorset, UK
Ham's Nutrient Mixture F12 (HAMS-F12)	Cat#: N6013, Sigma-Aldrich, Dorset, UK)
His-Pur™ Ni-NTA Resin	Cat#: 88221; ThermoFisher Scientific, Paisley, UK
Horse serum donor herd	Cat#:H1270; Sigma-Aldrich, Dorset, UK
Human epidermal growth factor (hEGF)	Cat#: E9644; Sigma-Aldrich, Dorset, UK
Hydrocortisone	Cat#: H4001; Sigma-Aldrich, Dorset, UK

Hydrogen peroxide 30% (w/v) (100 volumes), Extra Pure SLR	Cat#: 10687022; Fisher Chemical, Loughborough, UK
Hydrogen peroxide 30% (w/v) (100 volumes), Extra Pure SLR	Cat#: 10687022; Fisher Chemical, Loughborough, UK
Indo-1, AM	Cat#: 21030, AAT Bioquest (by Stratech), Suffolk
Insulin	Cat#: 91077C; Sigma-Aldrich, Dorset, UK
Isopropanol	Cat#: 10674732; Fisher Chemical, Loughborough, UK
L-Glutamine	Cat#: G7513; Sigma-Aldrich, Dorset, UK
Methanol	Cat#: 10598240; Fisher Chemical, Loughborough, UK
Minimum Essential Medium Eagle (EMEM)	Cat#: M2279; Sigma-Aldrich, Dorset, UK
Mitomycin C	Cat#: ab120797; Abcam, Cambridge, UK
Nuclease-free water	
Nuclease-free water	Cat#:AM9914G; Life Technologies, Paisley, UK
Penicillin-Streptomycin	Cat#: P4333; Sigma-Aldrich, Dorset, UK
Penta.His HRP Conjugate Kit	Cat#: 34460; QIAGEN, Manchester, UK
Phosphate Buffered Saline (PBS)	Cat#: D8537; Sigma-Aldrich, Dorset, UK
Pierce™ Protease Inhibitor Mini Tablets	Cat#: 88665; Thermo Fisher Scientific, Paisley, UK
Propan-2-ol	Cat#: 11428782; Fisher Chemical, Loughborough, UK
QIAprep Spin Miniprep Kit	Cat#: 27106; Qiagen, Manchester, UK
Recombinant human lymphotactin (XCL1)	Cat#:300-20; Peprotech, London, UK
Recombinant Transforming Growth Factor-beta 1(TGF-β1) Protein	Cat#: 240-B-010; R&D System, Abingdon, UK
Senescence Detection Kit	Cat#: ab65351; Abcam, Cambridge, UK
SYBR™ Green PCR Master Mix	Cat#: 4309155; ThermoFisher Scientific, Paisley, UK
TaqMan Gene Expression Master Mix	Cat#:4369016; Life Technologies, Paisley, UK
Trypan blue solution 0.4%	Cat#: T8154; Sigma-Aldrich, Dorset, UK
Trypsin-EDTA solution	Cat#: T3924; Sigma-Aldrich, Dorset, UK
VECTASTAIN® Elite® ABC-HRP kit (peroxidase, Mouse IgM)	Cat#: PK-6102; Vector Laboratories Ltd, Peterborough, UK
VECTASTAIN® Elite® ABC-HRP kit (peroxidase, Rabbit IgG)	Cat#: PK-6101; Vector Laboratories Ltd, Peterborough, UK

VECTOR NovaRED peroxidase substrate kit	Cat#: SK-4800; Vector Laboratories Ltd, Peterborough, UK
XCR1 probe (TaqMan Gene Expression Assays)	Cat#:4331182; Life Technologies, Paisley, UK
XCL1 probe (TaqMan Gene Expression Assays)	Cat#:4331182; Life Technologies, Paisley, UK
Xylene, Extra Pure, SLR	Cat#: 10784001; Fisher Chemical, Loughborough, UK

Appendix 2: List of kit

List of Kit	**Catalogue #; Manufacturer details**
High Capacity cDNA Reverse Transcription Kit	Cat#: 4368814; Life Technologies Ltd, Paisley, UK
ISOLATE II RNA Mini Kit	Cat#: BIO-52072; Bioline Reagents Limited, London, UK
Pierce™ BCA Protein Assay Kit	Cat#: 23225; ThermoFisher Scientific, Paisley, UK
QIAprep Spin Miniprep Kit	Cat #: 27106, QIAGEN, Manchester, UK.
QIAquick Gel Extraction Kit	Cat #: 28706, QIAGEN, Manchester, UK.
QIAquick PCR Purification Kit	Cat #: 28106, QIAGEN, Manchester, UK.

Appendix 3: List of equipment

List of Equipment	**Details**
BD™ FACSCalibur	BD Bioscience, Oxford, UK
BD™ LSRII	BD Bioscience, Oxford, UK
DNA Engine Dyad® Peltier Thermal Cycler	Bio-Rad Laboratories Ltd., Hertfordshire, UK
Infinite® M200 Pro Series	Tecan UK Ltd, Reading, UK
Olympus BX51-P polarising microscope	KeyMed Ltd., Essex, UK
Spectrafuge™ 24D Digital Microcentrifuge	Labnet International Inc., NJ, USA

Appendix 4: List of software

List of Software	Details
FlowJo v10	FlowJo, LCC, USA
GraphPad Prism	GraphPad Software, CA, USA
Magellan™ Data Analysis Software	Tecan UK Ltd, Reading, UK
Mendeley	Elsevier, Amsterdam, Netherlands
Pymol	Schrödinger, LLC, NY, USA

Appendix 5: List of miscellaneous

List of Miscellaneous	Catalogue #; Manufacturer details
96 well PCR plate, Semi-Skirted	Cat#: 1402-9700; STARLAB (UK) Ltd, Milton Keynes, UK
Advanced Polyolefin StarSeal Film	Cat#: E2796-9795; STARLAB (UK) Ltd, Milton Keynes, UK
Corning® 6.5 mm Transwell® with 8.0 µm polycarbonate membrane cell culture inserts, TC-treated, sterile, 48/cs	Cat#: CLS3422-48EA; Sigma-Aldrich, Dorset, UK
Corning® Costar® tissue-culture treated multiple well plates	Cat#: CL3516; Sigma-Aldrich, Dorset, UK
SuperFrost® Plus microscope slide	Cat#: 4951PLUS4, ThermoFisher Scientific, Paisley, UK
T25 suspension culture flask with filter cap	Cat#: 658190; Greiner Bio-One Ltd, UK
T75 suspension culture flask with filter cap	Cat#: 690195; Greiner Bio-One Ltd, UK
X-cell II Blot Module	Cat#: EI9051; ThermoFisher Scientific, Paisley, UK

Appendix 6: HistoQuest settings

Haematoxylin settings	
Various Shape 2.0	
Nuclei size	5
Remove small-sized objects	1
Remove weakly stained objects	1
Automatic background threshold	Yes
Threshold range	[5, 255]
Use Merging rules:	
Max combined area	10,000 µm^2
Max involved compactness	0.9
Group max	6
Min resulted compactness	0.6

NovaRed settings	
Various Shape 2.0	
Ring mask	Yes
Interior radius	-0.28 µM
Exterior radius	+0.28 µM
Use identified cell mask	Outside
Max growing steps	2.2 µM
Use nuclei mask	No

(A) H&E (100×)

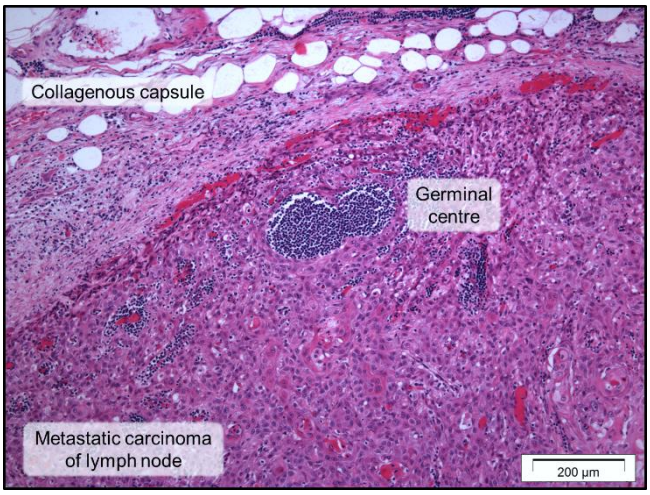

(B) XCR1 (100×)

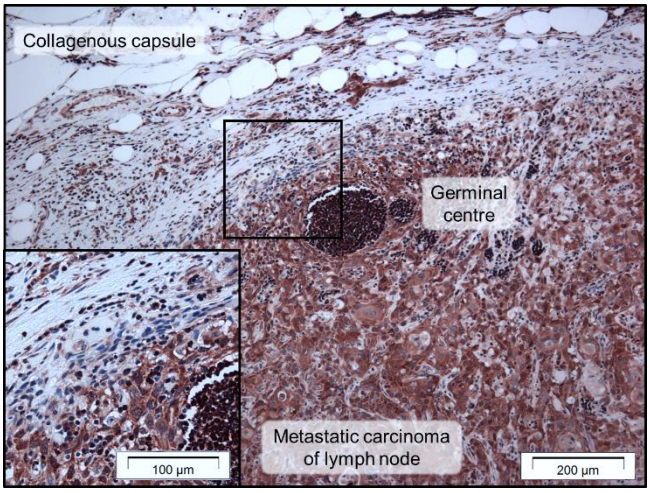

(C) XCR1 (400×)

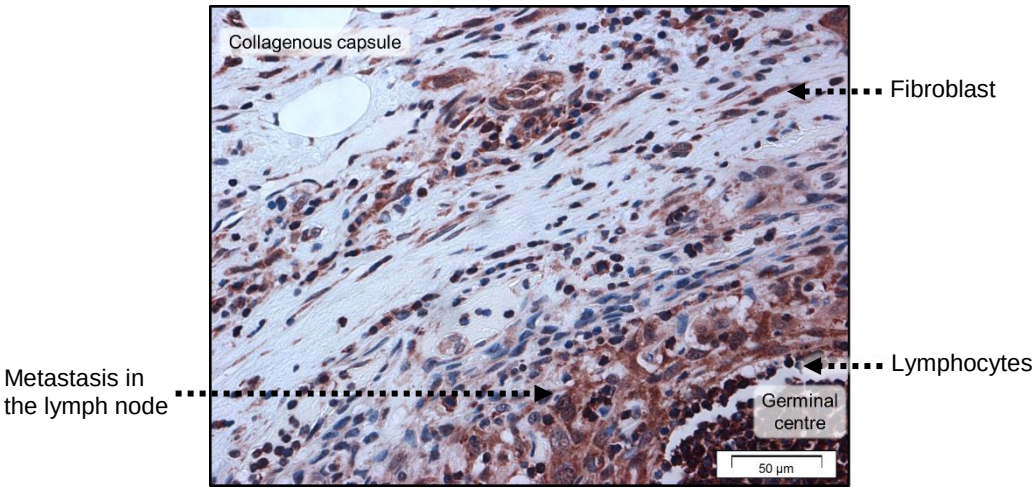

(D) hLtn (100×)

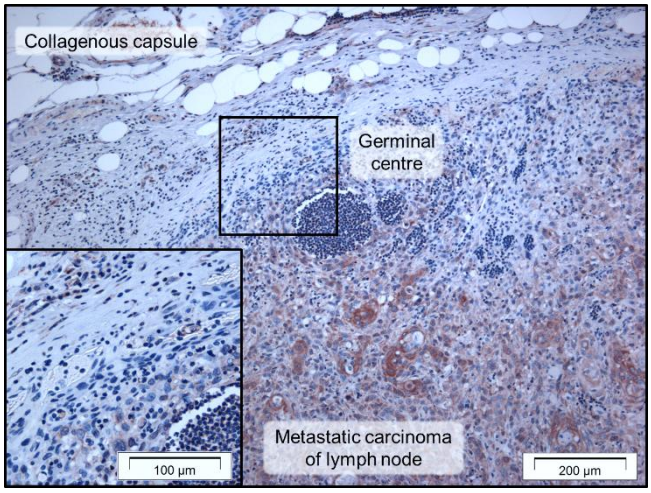

(E) hLtn (400×)

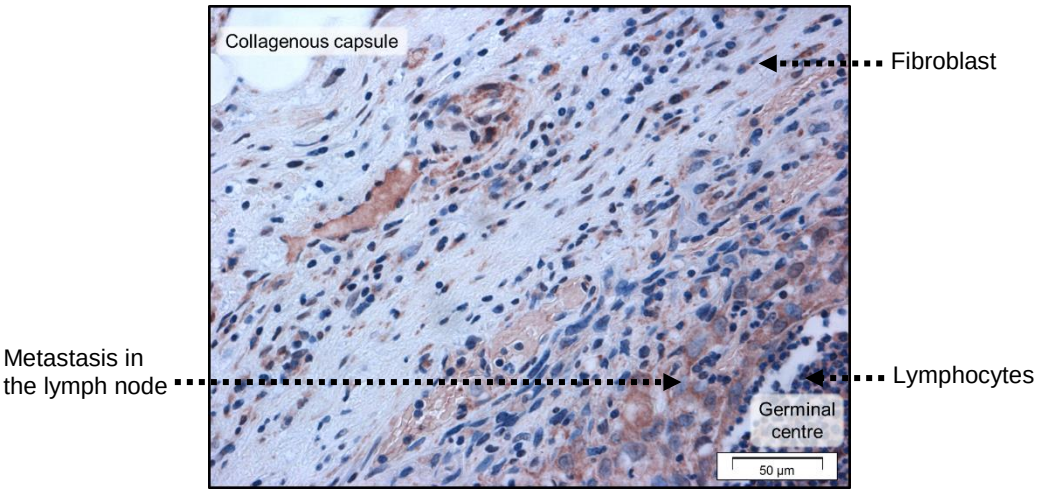

Appendix 7: Metastatic OSCC in a lymph node (representative photomicrograph). **(A)** H&E staining at 100× magnification, **(B, C)** XCR1 staining at 100× and 400× magnification respectively, and **(D, E)** hLtn staining at 100× and 400× magnification respectively. XCR1 staining is seen throughout the tumour cells and in lymphocytes. Scattered fibroblasts are also positive. In contrast, hLtn stain is weaker but still seen in the metastatic carcinoma, lymphocytes and fibroblasts in the reactive stroma.

Appendix 8: Keratinocytes grown (KGM) media preparation

Keratinocytes Growth Media (KGM)

Material: 335mL Dulbecco's Modified Eagle Medium (DMEM), 115mL F12, 50mL Serum (either fetal calf serum (FCS) or fetal bovine serum (FBS)), 5mL Penicillin/Streptomycin (P/S), 5mL Antifungal, 5mL L-Glutamine, 5mL Adenine, 2mL Hydrocortisone, 500µL Cholera Toxin, 250µL Insulin and 500µL epithelial growth factor (EGF).

EGF: 0.2mg Vial adds 10mL DMEM containing 10% FCS aliquot into 0.5mL (10µg/mL) and store at -20ºC.
Final concentration 10ng/mL

Hydrocortisone: Make 10X concentrate first. Weigh out 40mg and add 4mL 100% ethanol and agitate. Add 36mL DMEM. This 10X concentrate is filtered and can be stored in 5mL aliquots at-20ºC 0- label well. Each aliquot can be added to 45mL DMEM and 2mL aliquots stored at -20ºC (100µg/mL)
Final Concentration 0.5µg/mL

Insulin: 10mL sterile water add 100µL glacial acetic acid add to vial of insulin (100mg) resulting in 10mg/mL conc. Aliquot into 250µL and store at 4ºC
Final concentration 5µg/mL

Adenine: Weigh out 330mg add 100 mL 0.1HCl, agitate to mix well, filter and aliquot into 5mLs store at -20ºC (1.8×10^{-2}M stock)
Final Concentration 1.8×10^{-4}

Cholera toxin: Add 1.67mL distilled sterile water into vial (0.5mg) half of this into 50mL sterile water (10^{-7}M stock). Keep at 4ºC
Final Concentration 10^{-10}

Appendix 9: Melting curve of α-SMA and U6-snRNA primers.

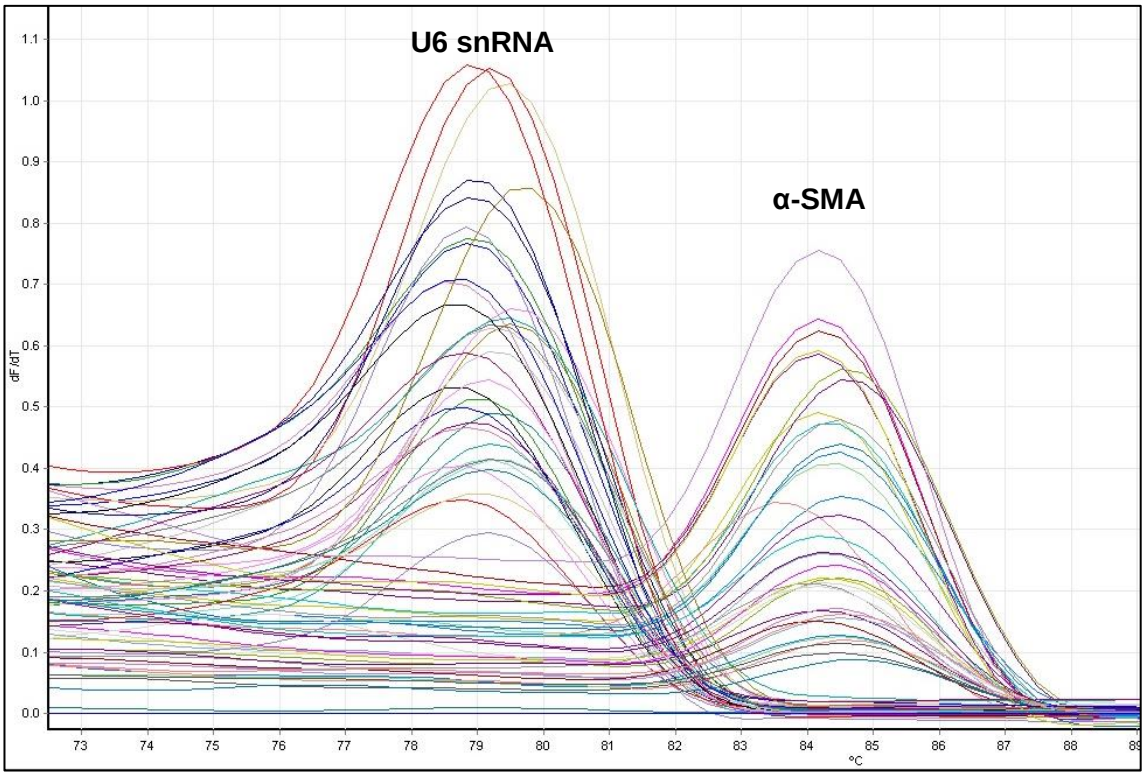

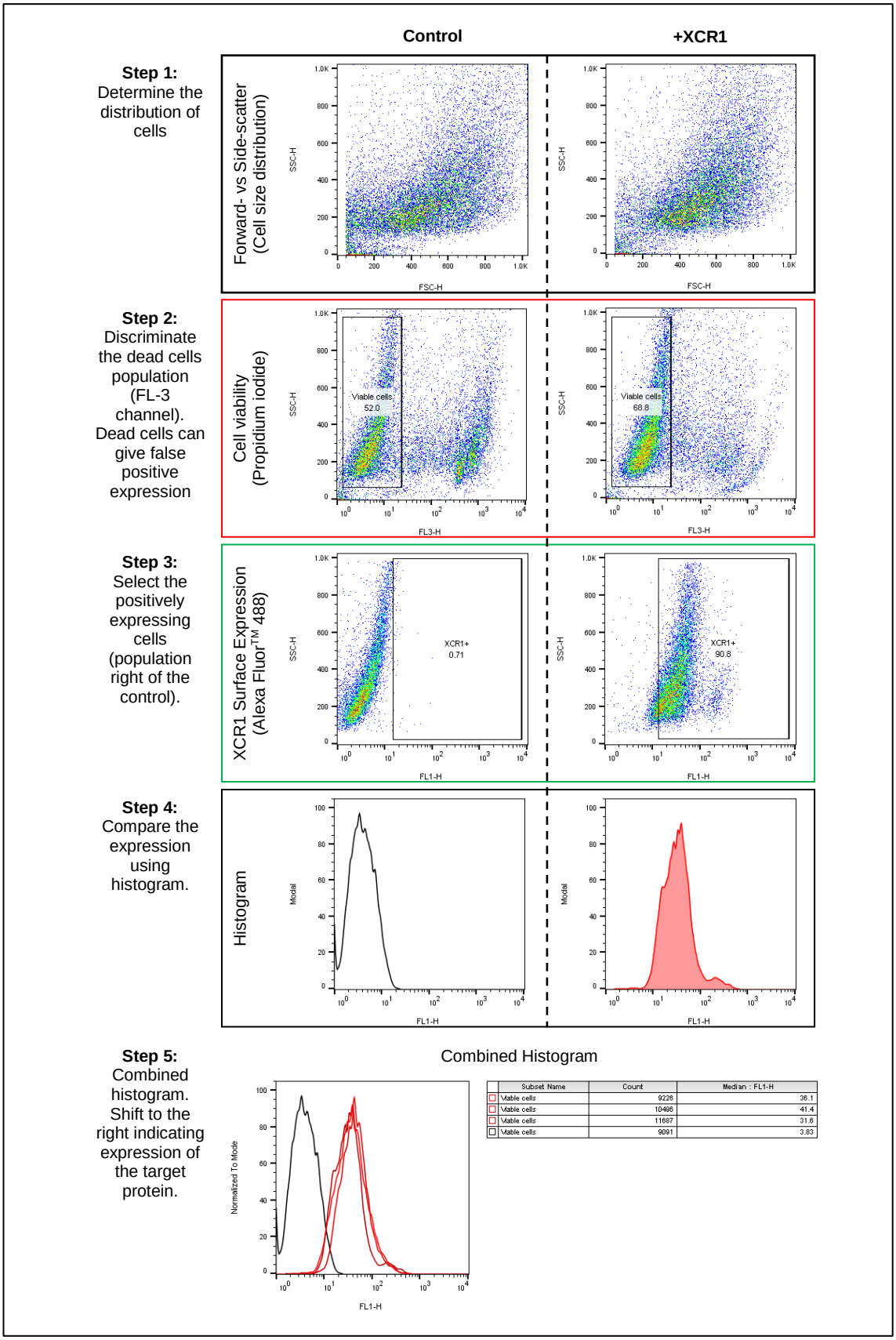

Appendix 10: Example for XCR1 surface receptor analysis of SCC4 cell using FlowJo software.

```
CATATG
 NdeI

        10         20         30         40         50         60
CATCATCATCATCATCACTCGGGTGCTTTTGAATTTAAACTGCCGGACATTGGCGAAGGT
 H  H  H  H  H  H  S  G  A  F  E  F  K  L  P  D  I  G  E  G

        70         80         90        100        110        120
ATCCACGAAGGCGAAATTGTGAAATGGTTTGTGAAACCGGGTGATGAAGTTAACGAAGAT
 I  H  E  G  E  I  V  K  W  F  V  K  P  G  D  E  V  N  E  D

       130        140        150        160        170        180
GACGTGCTGTGCGAAGTTCAGAATGACAAAGCGGTGGTTGAAATTCCGAGTCCGGTCAAG
 D  V  L  C  E  V  Q  N  D  K  A  V  V  E  I  P  S  P  V  K

       190        200        210        220        230        240
GGTAAAGTGCTGGAAATCCTGGTGCCGGAGGGTACGGTTGCAACCGTCGGCCAAACGCTG
 G  K  V  L  E  I  L  V  P  E  G  T  V  A  T  V  G  Q  T  L

       250        260        270        280        290        300
ATTACCCTGGATGCTCCGGGCTATGAAAACATGACGTTTGGCGGTGGCAGTGGTGGCGGT
 I  T  L  D  A  P  G  Y  E  N  M  T  F  G  G  G  S  G  G  G

       310        320        330        340        350        360
TCCGGCGGTGGCACCGGTGGCGGATCCGGCGGTGGCATTGAAGGTCGTGTTGGCAGCGAA
 S  G  G  G  T  G  G  G  S  G  G  G  I  E  G  R  V  G  S  E

       370        380        390        400        410        420
GTCTCTGACAAACGTACCTGTGTCAGCCTGACCACCCAGCGTCTGCCGGTTTCTCGTATT
 V  S  D  K  R  T  C  V  S  L  T  T  Q  R  L  P  V  S  R  I

       430        440        450        460        470        480
AAAACCTACACGATCACCGAAGGTAGCCTGCGCGCAGTGATTTTCATCACGAAACGTGGC
 K  T  Y  T  I  T  E  G  S  L  R  A  V  I  F  I  T  K  R  G

       490        500        510        520        530        540
CTGAAAGTGTGTGCCGATCCGCAGGCCACCTGGGTTCGTGATGTCGTGCGCTCAATGGAC
 L  K  V  C  A  D  P  Q  A  T  W  V  R  D  V  V  R  S  M  D

       550        560        570        580        590        600
CGTAAATCGAATACCCGCAACAATATGATCCAAACGAAACCGACGGGCACGCAACAATCC
 R  K  S  N  T  R  N  N  M  I  Q  T  K  P  T  G  T  Q  Q  S

       610        620
ACCAACACCGCAGTGACGCTGACGGGT
 T  N  T  A  V  T  L  T  G

TAATGAATTC
    EcoRI

START CODON; HIS-TAG; PROTEIN LINKER; LIPOYL DOMAIN; FACTOR XA;
MATURE LYMPHOTACTIN SEQUENCE; STOP CODON;
```

Appendix 11: Optimized codon sequence of the designed recombinant fusion protein HL-IEGR.hLtn (WT).

Appendix 12: Flow cytometer settings and preparation.

Instrument settings: The BD LSRII (BD Bioscience, Oxford, UK) was used to measure to emission of bound or unbound Indo-1 dye. The violet laser was turned off by using the in-line rocker-type switch. This is critical as stray violet laser light may cause interference in the violet channel of the UV trigon for Indo-1. Importantly, the waste tank was ensured to be empty and the sheath tank was filled to the maximum level allowed. The filter configuration on the UV trigon was verified as follows: “B” PMT: the 450 /50 filter was removed and replaced with 405 /20 for Indo-1 violet (calcium-bound); and “A” PMT: the 505 DLP was removed and replaced with 450 DLP filter for Indo-1 blue (calcium-unbound).

Instrument setting optimization: 1) It is critical that the cells should be acquired on “LO” setting with the flow rate adjusted to approximately 200 – 300 cells/seconds; 2) Ensure the Indo-1 only sample was installed; 3) The FSC and SSC voltages, and FSC threshold were adjusted; 4) A linear bivariate dot blot of blue and violet was created, ensuring the ‘blue’ on the y-axis and ‘violet’ on the x-axis; 5) The voltages and gains on the blue and violet parameters were adjusted so that the population that appears forms along an imaginary line from the vertex at 0/0 and 70° from the x-axis; and 6) A ‘time vs ratio’ dot plot was created. During the run, unbound loaded cells should fill the bottom part of the plot and when the Indo-1 dye binds to the calcium (violet) due to stimulation, it causes a shift in the ratio resulting in the changes of the observed histogram due to shift in population ratio.

Appendix 13: DNA sequence identification for W55D site-directed mutagenesis from pCMV6-Entry-hLtn (WT) DNA sequence.

Original sequence:

```
atcagtaccgaggagatctgcgccgcgatcgccatgagacttctcatcctggccctcctt
 I  S  T  E  E  I  C  A  A  I  A  M  R  L  L  I  L  A  L  L
ggcatctgctctctcactgcatacattgtggaaggtgtagggagtgaagtctcagataag
 G  I  C  S  L  T  A  Y  I  V  E  G  V  G  S  E  V  S  D  K
aggacctgtgtgagcctcactacccagcgactgccggttagcagaatcaagacctacacc
 R  T  C  V  S  L  T  T  Q  R  L  P  V  S  R  I  K  T  Y  T
atcacggaaggctccttgagagcagtaatttttattaccaaacgtggcctaaaagtctgt
 I  T  E  G  S  L  R  A  V  I  F  I  T  K  R  G  L  K  V  C
gctgatccacaagccacatgggtgagagacgtggtcaggagcatggacaggaaatccaac
 A  D  P  Q  A  T  W  V  R  D  V  V  R  S  M  D  R  K  S  N
accagaaataacatgatccagaccaagccaacaggaacccagcaatcgaccaatacagct
 T  R  N  N  M  I  Q  T  K  P  T  G  T  Q  Q  S  T  N  T  A
gtgactctgactggctagacgcgtacgcggccgctcgagcagaaactcatctcagaagag
 V  T  L  T  G  -  T  R  T  R  P  L  E  Q  K  L  I  S  E  E
gatctggcagcaaatgatatcctggattacaaggatgacgacgataaggtttaaacggcc
 D  L  A  A  N  D  I  L  D  Y  K  D  D  D  D  K  V  -  T  A
ggccgcggtcatagctgtttcctgaacagatcccgggtggcatccctgtgacccctcccc
 G  R  G  H  S  C  F  L  N  R  S  R  V  A  S  L  -  P  L  P
agtgcctctcctggccctggaagttgccactccagtgcccaccagccttgtcctaataaa
 S  A  S  P  G  P  G  S  C  H  S  S  A  H  Q  P  C  P  N  K
attaagttgcatcatttgtctgactaggtgtccttctataatattatggggtggaaggg
 I  K  L  H  H  F  V  -  L  G  V  L  L  -  Y  Y  G  V  E  G
ggggtgggt
 G  V  G
```

After mutagenesis:

```
atcagtaccgaggagatctgcgccgcgatcgccatgagacttctcatcctggccctcctt
 I  S  T  E  E  I  C  A  A  I  A  M  R  L  L  I  L  A  L  L
ggcatctgctctctcactgcatacattgtggaaggtgtagggagtgaagtctcagataag
 G  I  C  S  L  T  A  Y  I  V  E  G  V  G  S  E  V  S  D  K
aggacctgtgtgagcctcactacccagcgactgccggttagcagaatcaagacctacacc
 R  T  C  V  S  L  T  T  Q  R  L  P  V  S  R  I  K  T  Y  T
atcacggaaggctccttgagagcagtaatttttattaccaaacgtggcctaaaagtctgt
 I  T  E  G  S  L  R  A  V  I  F  I  T  K  R  G  L  K  V  C
gctgatccacaagccacagacgtgagagacgtggtcaggagcatggacaggaaatccaac
 A  D  P  Q  A  T  D  V  R  D  V  V  R  S  M  D  R  K  S  N
accagaaataacatgatccagaccaagccaacaggaacccagcaatcgaccaatacagct
 T  R  N  N  M  I  Q  T  K  P  T  G  T  Q  Q  S  T  N  T  A
gtgactctgactggctagacgcgtacgcggccgctcgagcagaaactcatctcagaagag
 V  T  L  T  G  -  T  R  T  R  P  L  E  Q  K  L  I  S  E  E
gatctggcagcaaatgatatcctggattacaaggatgacgacgataaggtttaaacggcc
 D  L  A  A  N  D  I  L  D  Y  K  D  D  D  D  K  V  -  T  A
ggccgcggtcatagctgtttcctgaacagatcccgggtggcatccctgtgacccctcccc
 G  R  G  H  S  C  F  L  N  R  S  R  V  A  S  L  -  P  L  P
agtgcctctcctggccctggaagttgccactccagtgcccaccagccttgtcctaataaa
 S  A  S  P  G  P  G  S  C  H  S  S  A  H  Q  P  C  P  N  K
attaagttgcatcatttgtctgactaggtgtccttctataatattatggggtggagggg
 I  K  L  H  H  F  V  -  L  G  V  L  L  -  Y  Y  G  V  E  G
ggggtgggtttg
 G  V  G  L
```

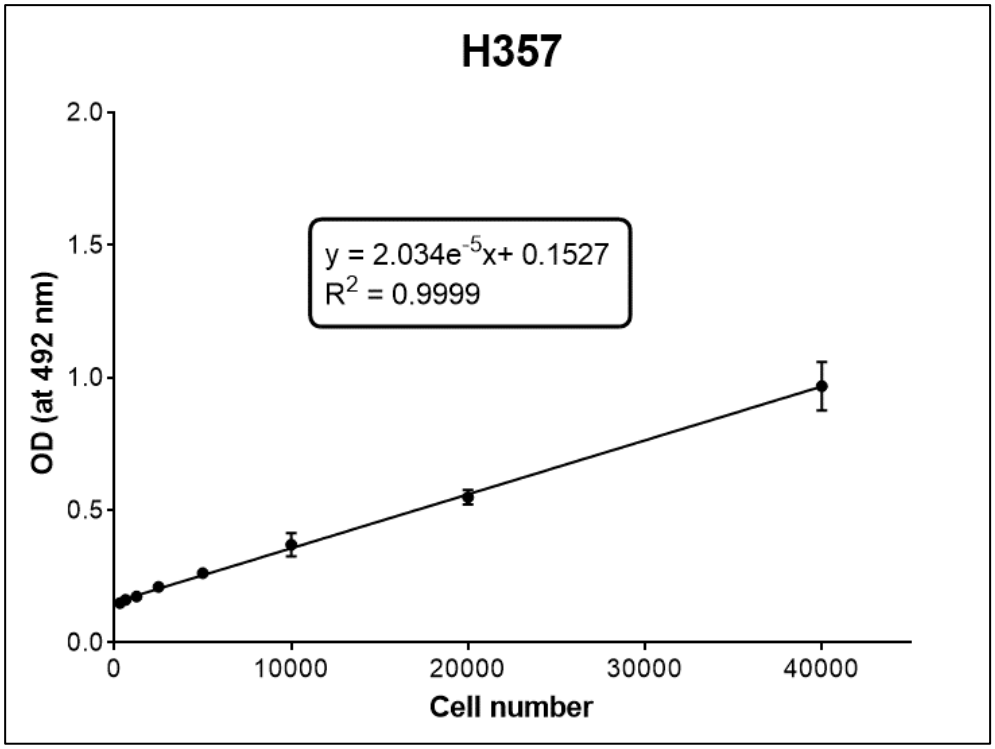

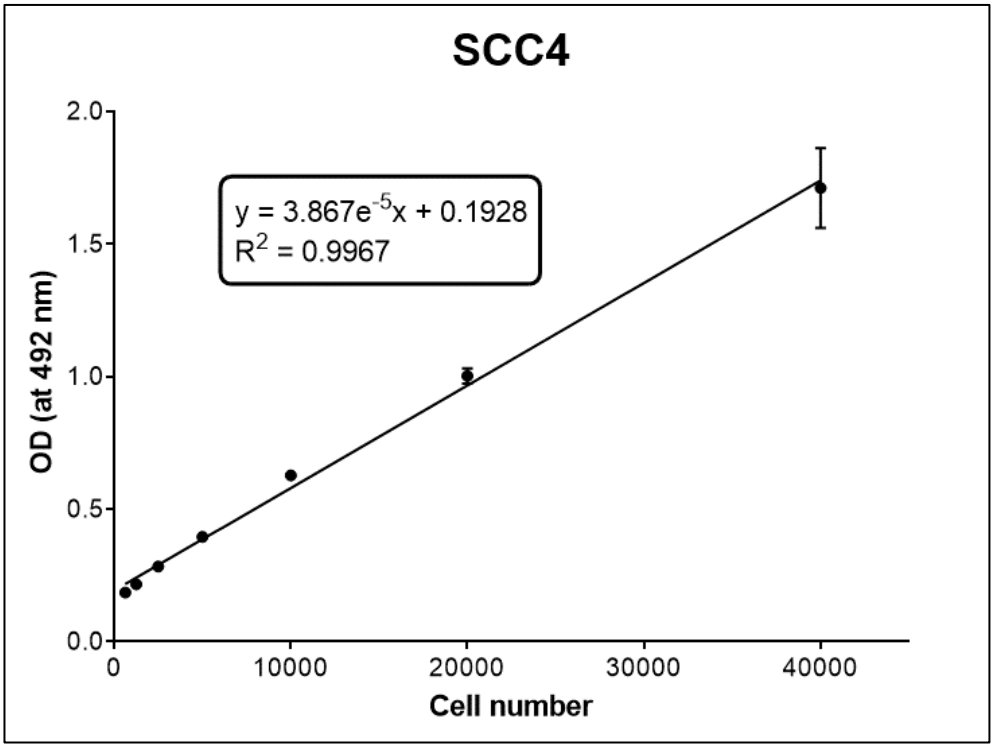

Appendix 14: Linear regression of OCCLs

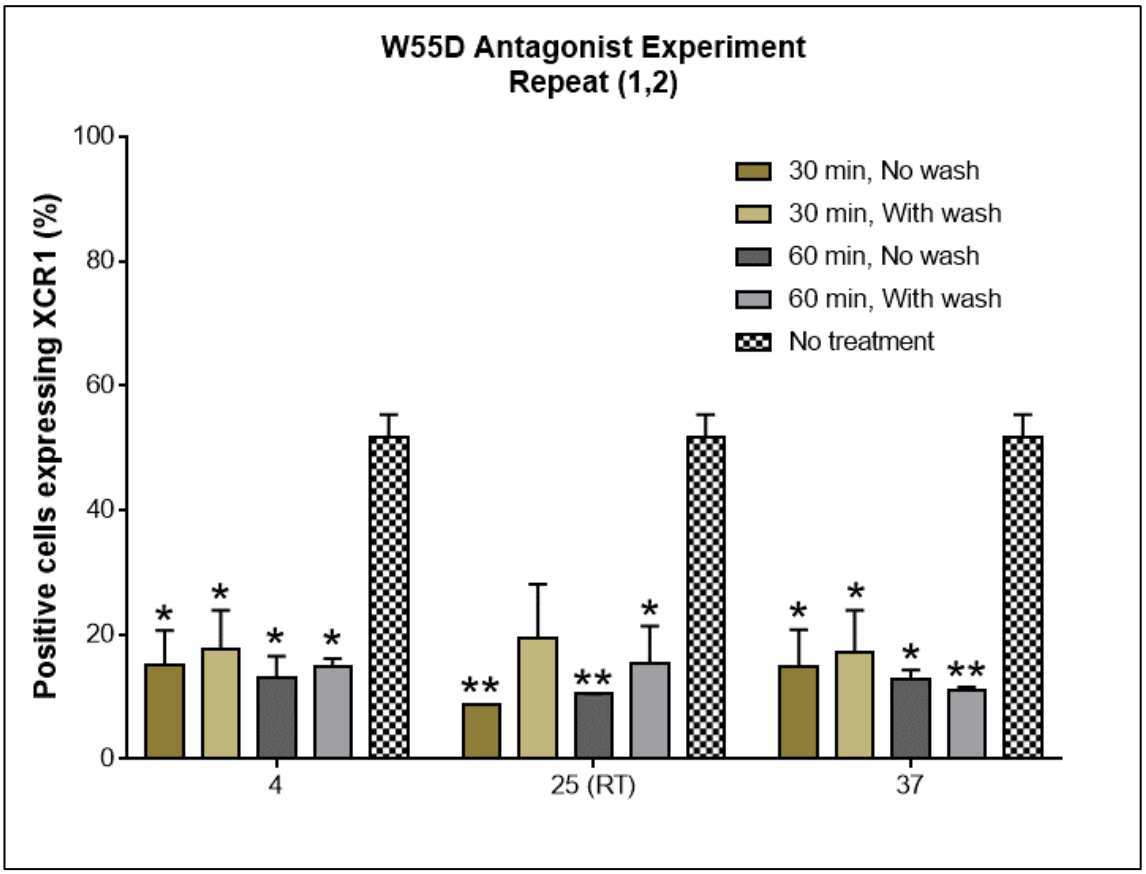

Appendix 15: XCR1 dimer form (hLtn W55D mutant) capable of binding to the XCR1 receptor or blocking the antibody attachment. Similar trend observed amongst the variables (temperature, duration and washing) suggesting that the W55D dimer variant able to attach to the receptor by blocking the anti-XCR1 antibody, impairing its capability to bind to the third extracellular loop of the receptor.

Appendix 16: List of amino acids and its abbreviation

	Amino Acid	3-Letter	1-Letter		Amino Acid	3-Letter	1-Letter
	Alanine	Ala	A		Leucine	Leu	L
	Arginine	Arg	R		Lysine	Lys	K
	Asparagine	Asn	N		Methionine	Met	M
	Aspartic acid	Asp	D		Phenylalanine	Phe	F
	Cysteine	Cys	C		Proline	Pro	P
	Glutamic acid	Glu	E		Serine	Ser	S
	Glutamine	Gln	Q		Threonine	Thr	T
	Glycine	Gly	G		Tryptophan	Trp	W
	Histidine	His	H		Tyrosine	Tyr	Y
	Isoleucine	Ile	I		Valine	Val	V
	Selenocysteine	Sec	U				

Side chain properties:

	Basic (positively charged)
	Acidic (negatively charged)
	Polar (uncharged)
	Hydrophobic
	Special cases